University of Southampton

Faculty of Engineering, Science & Mathematics

School of Chemistry

X-Ray Absorption Spectroscopy for the Study of a Homogeneous Catalysis System based upon Chromium

By Jerome Olivier MOULIN

A Thesis Submitted for the Degree of Doctor of Philosophy

October 2006

UNIVERSITY OF SOUTHAMPTON

ABSTRACT

FACULTY OF ENGINEERING, SCIENCE & MATHEMATICS
SCHOOL OF CHEMISTRY

Doctor of Philosophy

"X-Ray Absorption Spectroscopy for the Study of a Homogeneous Catalysis System based upon Chromium"

by Jerome Olivier Moulin

The selective trimerisation and tetramerisation of ethene to 1-hexene and 1-octene is of great interest due to the importance of these co-monomers in the production of linear low-density polyethylene. A route based upon a cyclic trimerisation and using a chromium catalyst has achieved extremely high selectivity for a trimer. This mechanism is thought to be the basis of newer reactions based upon Cr(III) precursors, using methylaluminoxane (MAO) as a co-catalyst. The auxiliary ligand on Cr(III) is generally a tridentate ligand with group 15 or 16 donor atoms. Due to the paramagnetic nature of these complexes, characterisation is usually undertaken using EXAFS techniques. As yet the mechanism by which halide ligands are stripped off to create and support vacant sites allowing oligomerisation by cyclisation is not understood.

The body of this work was commenced by investigating the nature of the active species when the chromium(III) complex $[CrCl_3\{HN(CH_2CH_2SC_{10}H_{21})_2\}]$, known to trimerise ethylene to 1-hexene, is treated with an aluminium reagent. Studies were carried out via a wide range of techniques, such as UV/visible and EPR spectroscopy as well as X-ray absorption spectroscopy, to validate or otherwise the first species of the catalytic cycle. Similar investigations were carried out on the chromium(III) complex $[CrCl_3\{PNP\}(THF)]$, known to tetramerise ethylene to 1-octene.

The work was then focused on the synthesis of novel S-, N- and O-donor tridentate ligands with three geometries; the open-chains $S(CH_2CH_2SC_{10}H_{21})_2$, $O(CH_2CH_2SC_{10}H_{21})_2$, the tripods $MeC(CH_2SC_4H_9)_3$, $MeC(CH_2SC_{10}H_{21})_3$ and the macrocycles $(C_{10}H_{21})[9]aneN_3$, $(C_{10}H_{21})_3[9]aneN_3$. Their coordination chemistry with Cr(III) is investigated via spectroscopic methods and the ability of these complexes to trimerise, oligomerise and polymerise is studied with catalytic testings. Partial structure of the active species is proposed after analysis of EXAFS data.

The coordination chemistry of N- and S-donor ligands $S(CH_2CH_2SCH_3)_2$, $MeC(CH_2SCH_3)_3$, $[9]aneS_3$, $[9]aneN_3$, $Me_3[9]aneN_3$ and $(isoPr)_2[9]aneN_3$ with Cr(III) is investigated. The coordination modes adopted by the ligands have been probed by UV/visible, infra-red and EPR spectroscopy as well as X-ray absorption spectroscopy.

Table of Contents

List of Figures

List of Tables

List of Schemes

Acknowledgements

I would like to thank my supervisors Professor John Evans and Professor Gill Reid for their support, help and advice during the course of this research. I would also like to thank Dr. Moniek Tromp for her assistance with the XAFS measurements and the data analysis. She is a constant source of advice. Thank you to my advisor Professor Bill Levason and to all the people who gave me advice during the group meetings.

Thanks are also due to SASOL Technology (UK) Ltd and SASOL Technology (Pty) Ltd for the financial support and to all the people involved in the project and who helped me with the catalysis work and gave me useful guidance throughout the project: Dr. Robert Tooze, Dr. Dave McGuinness, Dr. Adam Rucklidge, Dr. John T. Dixon and Dr. Martin Hanton.

I thank the EPSRC EPR National Service in Manchester University and Dr. Eric McInnes and Dr. Joanna Wolowska for their help in the measurements and interpretations of the EPR spectra.

I would like to acknowledge the ESRF for provision of synchrotron radiation facilities and Serge Nikitenko for assistance in using BM26A (DUBBLE).
I thank Mr Andrew Lobo for the synthesis of the ligand $O(CH_2CH_2SC_{10}H_{21})$ and his help for the cyclic voltammetry and UV/visible measurements.

Thank you to Miss Lorna Nichols for her kind help with the X-ray crystallography and the solving of my crystal structure.

I would like to thank the members of my group, past and present, for their constant support and advice.

Finally, I would like to thank my family for all their encouragement.

Abbreviations

Techniques

CV	Cyclic Voltammetry
EI	Electron Impact
EPR	Electron Paramagnetic Resonance
ES^+	Positive Ion Electrospray
EXAFS	Extended X-ray Absorption Fine Structure
NMR	Nuclear Magnetic Resonance
UV/Vis	Ultra Violet / Visible Spectroscopy
XANES	X-ray Absorption Near Edge Structure

Solvents

DCM	Dichloromethane
DMF	N,N-dimethyl formamide
Pet. Ether	Petroleum Ether
THF	Tetrahydrofuran

Ligand and Complexes

M	Metal
L	Ligand
X	Halide
R	Aryl or Alkyl substituent
Cp	Cyclopentadienyl
SNS	$HN(CH_2CH_2SC_{10}H_{21})_2$
PNP	$isoPrN(PPh_2)_2$

General

ν	Vibrational Frequency
λ	Wavelength
υ	Wavelength
Å	Angstrom (10^{-10} m)
ε	Molar extinction coefficient

m/z	Mass to Charge Ratio
Hz	Hertz
$\{^1H\}$	Proton Decoupled
δ	Chemical Shift
ppm	Parts per Million
RT	Room Temperature
s	Singlet
d	Doublet
t	Triplet
m	Multiplet
fac	Facial
mer	Meridional
Me	Methyl
Ph	Phenyl
o-	Ortho-
p-	Para-
MAO	Methylaluminoxane
MMAO	Modified Methylaluminoxane

Nomenclature

A standard form of nomenclature has been used for the macrocyclic compounds in this thesis:

R_x[N]aneA_y

Where R = substituent on donor atom; N = number of atoms in the ring; A = donor atom type; x and y = integers, denoting the number of substituent and donor atoms.

Chapter 1

Introduction

1.1. General Principles of Transition Metal Chemistry

Transition metals are usually defined as elements which possess incompletely filled *d* orbitals in the ground state. In one or more of its common oxidation states, all of these metals form organometallic derivatives. A *d*-block metal ion has nine valence shell orbitals in which to accommodate its valence electrons which help to form molecular orbitals in bonding with other groups. Depending upon the nature of the ligand, these valence orbitals can form both σ, and π bonds with other ligands.

Most commonly, coordination numbers of four and six are encountered. The ability of a transition metal to accommodate several different ligands in its coordination sphere is clearly important if it is to catalyse reaction between one or more substrates. However, of equal importance to being able to adopt different coordination numbers, and consequently different stereochemistries, is the ability to rapidly change between them.

The ability to form stable complexes with the metal in a variety of oxidation states is common among the transition elements. On one hand, metals in low oxidation states are largely preferred by π-accepting ligands such as CO and tertiary phosphines. On the other hand, metals in high oxidation states are preferred by σ-bonding ionic ligands such as F^- and O^{2-}. Oxides can also be good π-donor groups.

However, perhaps more important than this access is the ability to readily interchange between oxidation states during the course of a chemical/catalytic reaction. This ability to readily enter into redox cycles is especially marked for the group VIII metals. Such a cycle has been reported for the palladium-catalysed Heck reaction [1]. The ability of transition metal catalysts to accommodate both participative and non-participative ligands within their coordination sphere offers us the possibility of directing the course of a reaction between participative ligands, by modifying the structural/electronic properties of the non-participative ligands. Formally, a ligand can influence the behaviour of a transition metal catalyst by modifying the steric or electronic environment at the active site.

1.2. Metal-Ligand Bonding

The bonding between a transition metal centre and a ligand varies markedly depending upon both the nature and oxidation state of the metal and the type of ligand.

1.2.1. Metal-Phosphine Bonding

Ligands of the type PR_3, where R = halide, alkyl, Ph, etc, are capable of π- and/or σ-bonding. The bonding model proposed by Chatt [2] states that there is a σ donation from the lone pair on P to an appropriate empty *d* orbital on the metal, and secondly π-back donation from a filled metal $d\pi$ orbital into an empty 3*d* orbital on the P. In low oxidation state compounds, tertiary phosphines use both σ- and π-bonding, the latter involving empty $d\pi$ orbitals on the P atom. The Lewis basicity of PR_3 ligands varies according to R. There is a synergistic balance between σ donor and π acceptor behaviour in the M-PR_3 bond [3].

In 1985 Orpen and Connelly [4] proposed an alternative and preferred model in which the P-E σ^* orbital (E = H, CH_3, F) accepts electron density from the metal. The advantage of this model is that the new acceptor orbital retains the *e* symmetry required for π-back donation but is lower in energy than the P *3d* orbitals. It has been shown that increasing the metal oxidation state increased the M-P distance but reduced the P-E distance [4]. It is therefore widely accepted that σ bonding provides the main component of M-P bonding, the π component becoming more significant with electronegative substituents.

At least as important as the electronic properties of particular PR_3 ligands are steric factors. The steric requirement of a particular PR_3 ligand is usually expressed by *Tolman's cone angle* θ (Figure 1.1) [5]. The cone is one that can just enclose the Van der Waals surface of all the ligand atoms over all rotational orientations about the M-P bond. An increase in cone angle in PR_3 tends to favour lower coordination numbers in complexes, the formation of less sterically crowded isomers, and increased rates and equilibria in dissociative reactions. However, cone angles can only be used as a relative measure as real ligands are not rigid cones (Table 1.1).

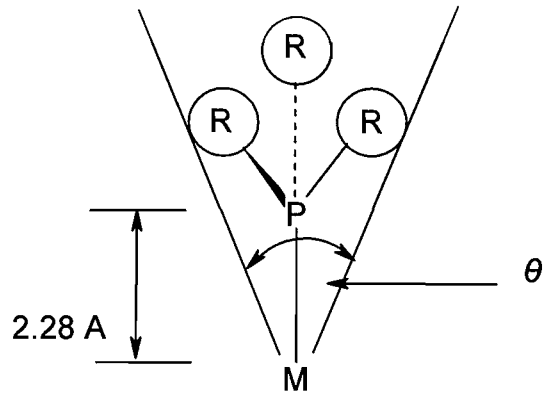

Figure 1.1. Representation of Tolman's cone angle, setting M-P at 2.28 Å (based on Ni-P) [3]

Ligand	θ / °
PF_3	104
$P(OMe)_3$	107
$P(OEt)_3$	109
PMe_3	118
PPh_3	145

Table 1.1. Cone angle values for some ligands [3]

1.2.2. Metal-Thioether Bonding

In contrast with phosphine ligands, a group 16 atom carries only two R substituents, steric effects are then less important [6]. However, interdonor linkages and resulting ring-sizes in multidentate and macrocyclic thioethers will affect coordination in the same way as with phosphines. The configuration for thioethers is often described as the sp^3 hybridised sulfur with two lone pairs. One is used for σ bonding. The second lone pair can either remain non-bonding, in which case there may be significant π repulsion between the lone pair and electron rich centres [7], or it may be involved in π donation to a suitable metal *d* orbital, although there is little good evidence for this. SR_2 could also behave as a π acceptor ligand, accepting electron density into the empty *3d* orbital as in the original Chatt model [2], or perhaps more likely into the S-C(σ^*) orbitals as proposed by Orpen and Connelly for the PR_3 system [4].

Thioethers are relatively poor σ donors due to the high electronegativity of S ($\chi_p = 2.58$). The mode of molecular vibration known as inversion exists, in principle, for all non-planar molecular species. However, the term is normally restricted to the spontaneous inversion of configuration of an atom bonded to three substituents in a pyramidal geometry and possessing one lone pair of electrons. Coordination of SR_1R_2 to a metal generates chiral centres at S and leads to a thioether inversion. This inversion involves the displacement of the lone pair of S used in the M-L bond by the lone pair not involved in bonding (Figure 1.2).

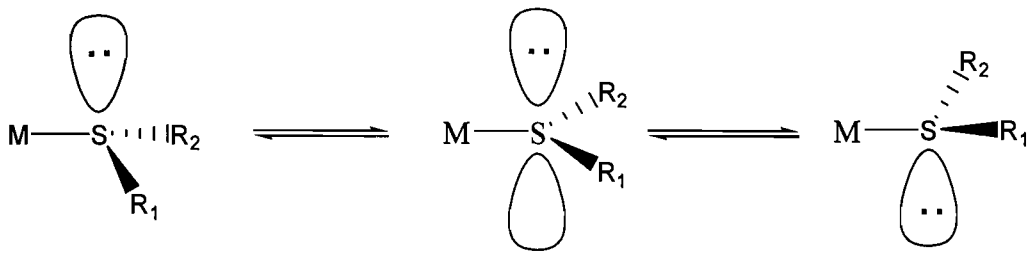

Figure 1.2. Pyramidal inversion at sulfur

Coordination of bidentate RS—SR to a metal generates chiral centres at S leading to diastereoisomers which can interconvert by pyramidal inversion at the group 16 atom (Figure 1.3).

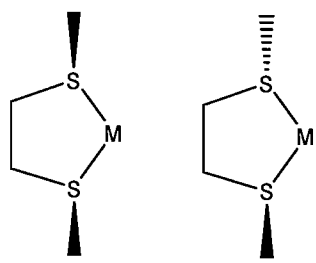

Figure 1.3. Representation of the diastereoisomers

1.2.3. Metal-Amine Bonding

The interaction of the lone pair on the nitrogen atom of an amine with a metal ion spans a considerable range from the very weak "template assisted" association of alkali and alkaline earth cation to the very robust Co^{III} and Ru^{III} metal nitrogen bonds. It is perhaps convenient to classify complexes with nitrogen donors into "labile" and

"inert" systems, with "inert" being defined as systems which allow geometric isomers. Another attempt at classification is the hard acid / soft base concept [8, 9] with the N atom being considered as a hard centre as it binds strongly to protons and thus expected to bind strongly to hard metal centres, like Cr(III).

1.2.4. Metal-Carbonyl Bonding

Carbon monoxide is an excellent example of a π-acceptor ligand. There are two types of bonding. The first is a σ donor interaction from the CO carbon lone pair into an empty metal orbital. The π orbital of CO is filled but it is the empty π^* orbitals which are of interest here. The π^* orbitals are of correct symmetry to overlap with the metal t_{2g} orbitals in an octahedral complex. The interaction between the metal t_{2g} orbitals and linear combinations of the CO π^* orbitals effectively means that there is a flow of electron density from the metal to the ligand. This donation from the metal to the ligand is referred to as "back-bonding" (Figure 1.4).

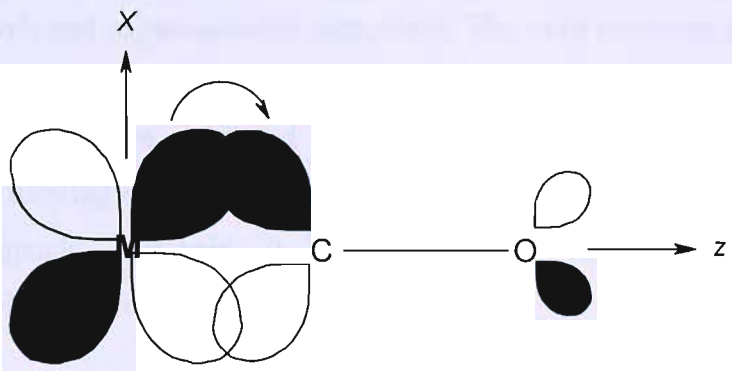

Figure 1.4. Donation of metal d_{xz} electron density into the π_x^* molecular orbital of CO. An analogous process may be drawn in the *yz* plane.

1.2.5. Metal-Ether Bonding

Metal-ether bonding is *via* σ donation from the lone pair on the oxygen atom. Oxygen is a hard donor ligand and therefore preferentially binds to hard metal centre such as transition metals in high oxidation states or more usually group 1 or group 2 cations.

1.3. Chromium Chemistry

Discovered in 1797 by the French chemist Louis N. Vauquelin, it was named chromium (Greek chroma, "colour") because of the many different colours characteristic of its compounds. Chromium is the 21st most abundant element in the Earth's crust and the 6th most abundant transition metal [10].

Chromium has the outer electronic configuration $3d^5\ 4s^1$ and is known to exist in every oxidation state between and including –IV and +VI, the latter corresponding to a complete loss of all *d*-orbital electrons. The compounds exhibit a wide range of geometries including square planar, tetrahedral, octahedral, and various distorted geometries. Chromium is found in nature principally as the chromite ore $FeCr_2O_4$ in which chromium is in the +III state.

The extremely low oxidation states are stabilized by π-acceptor ligands; therefore, the –IV to +I states are formal oxidation states held by chromium compounds such as carbonyl nitrosyls and organometallic complexes. The most common oxidation states of chromium in inorganic compounds are +II, +III, and +VI. Coordination numbers from three to seven are exhibited by chromium(II), although it is commonly six-coordinate, forming complexes which are high-spin ($t_{2g}^3 e_g^1$ configuration) or, with strong-field ligands, low-spin (t_{2g}^4 configuration). Chromium(II) complexes, especially in solution, are rapidly oxidised by air.

The most stable oxidation state of the element is +III and so the largest number of its coordination compounds exist in this state. Octahedral complexes of chromium(III) are kinetically inert and this, combined with ease of synthesis, is why so many have been isolated. Chromium(III) complexes have well-characterised electronic spectra and extensive photochemistry. The complexes of chromium(III) are almost exclusively six-coordinate with an octahedral disposition of the ligands: $[CrBr_2\{NH_3\}_4]Br$ [11], $[Cr\{acac\}_3]$ [12], $[CrCl_3\{SMe_2\}_3]$ [13]. Many are monomeric, although hydroxyl-bridged and other polynuclear complexes are known in which spins on neighbouring chromiums are coupled [14]. Chromium(III) is a hard Lewis acid and many stable complexes are formed with oxygen donor ligands.

The oxidation states +IV and +V are relatively rare [15]. The few compounds that have been isolated rapidly disproportionate to chromium(III) and chromium(VI) compounds (Scheme 1.1).

$$3Cr^{IV} \longrightarrow 2Cr^{III} + Cr^{VI}$$

Scheme 1.1. Disproportionation of chromium(IV)

Chromium(IV) and chromium(V) species are, however, important in chromium(VI) induced oxidations, since they always occur as transient intermediates. In its highest oxidation state (+VI) chromium forms compounds which are, for the majority, oxo compounds, but the number of coordination compounds representing it is rather limited. Hexavalent chromium [16] is a powerful oxidant and the use of chromium based oxidants in organic synthesis [17] goes back well over a century.

1.4. Hard and Soft Acids and Bases

When considering Lewis acids and bases, we must allow for a great variety of acceptors and hence more factors that influence the interactions between electron pair donors and acceptors in general. The classification of substances as "hard" and "soft" acids and bases was introduced by Pearson [8, 9]. It is a generalisation of the distinction between two types of behaviour which originally were named "class a" and "class b" respectively, by Ahrland, Chatt, and Davies [18, 19].
The two classes are identified empirically by the opposite order of strengths (as measured by the equilibrium constant, K_f, for the formation of the complex) with which they form complexes with the halide ion bases:

- Hard acids bond in the order: $I^- < Br^- < Cl^- < F^-$
- Soft acids bond in the order: $F^- < Cl^- < Br^- < I^-$

In general, acids are identified as hard or soft by the thermodynamic stability of the complexes they form, as set out for the halide ions above and for other species as follows:

- Hard acids bond in the order: $R_3P << R_3N$, $R_2S << R_2O$
- Soft acids bond in the order: $R_2O << R_2S$, $R_3N << R_3P$

It follows by definition of hardness that hard acids tend to bind to hard bases and soft acids tend to bind to soft bases (Table 1.2).
Hard acids (electron-pair acceptors) have no low lying unfilled orbitals and therefore do not readily form covalent bonds with bases. Hard bases (electron-pair donor) have no high-lying orbitals and also do not readily form covalent bonds to acids, but since the acids and bases are usually positively and negatively charged respectively, they tend to bond strongly to each other through ionic interactions. Soft acids do tend to have low-energy unfilled orbitals, which will readily form covalent bonds, and soft bases tend to have high-energy filled orbitals, forming covalent bonds.

	Hard	Borderline	Soft
Acids	H^+, Li^+, Na^+, K^+, Cr^{2+}, Cr^{3+}	Fe^{2+}, Co^{2+}, Ni^{2+}, Cu^{2+}, SO_2	Cu^+, Ag^+, all *d*-block metals in zero oxidation state
Bases	F^-, OH^-, H_2O, NH_3, O^{2-}, NO_3^-, NR_3	Br^-, N_2, N_3^-, NH_2Ph	H^-, R_2S, R_3P, R^-, CO, SR^-, C_2H_4

Table 1.2. A selection of hard, soft and borderline acids and bases

1.5. Macrocyclic Chemistry

For the purpose of this work, a macrocycle compound is conveniently defined throughout the following material as a carbocyclic compound with nine or more members and with three or more donor atoms allowing the macrocycle to bind a metal centre [20]. A few scattered reports of synthetic macrocycles were made prior to 1960. In the 1950s, Linstead, Elvidge and co-workers reported the synthesis of a variety of

macrocyclic compounds, some of which are potential tri- and tetradentate ligands [21, 22].

In 1967 a new series of macrocyclic compounds which have the ability to function as complexing agents was reported by Pedersen [23], who synthesised a number of cyclic polyether compounds with a variety of ring sizes, a varying number of ether oxygens, and substituent groups. The properties and behaviour of a macrocycle are usually dictated by the number and type of donor atom (*e.g.* N, S), the size of the macrocyclic cavity, the degree of alkylation of donor atoms, the degree of alkylation of the backbone and the degree of unsaturation/conjugation. Many systems have been studied and reported [20, 24-30].

1.5.1. The Macrocyclic Effect

The term macrocyclic effect was first used by Cabbiness and Margerum [31] to describe the greater thermodynamic stability observed for the complexes of cyclic ligands over those of open-chain ligands of similar structure and denticity [31]. The macrocyclic effect can also be defined as an extrapolation of the chelate effect, which was first reported in 1920 by Morgan and Drew [32]. The chelate effect refers to the enhanced stability of a complex containing chelating ligands when compared to that of a similar system containing monodentate ligands. A further investigation on the nature of the macrocyclic effect has been reported in 1975 [33] and states that both enthalpy and entropy terms are involved.

$$\Delta G^0 = \Delta H^0 - T\Delta S^0 \qquad \textbf{Equation 1.1}$$

$$\Delta G^0 = -RT\ln\beta \qquad \textbf{Equation 1.2}$$

With G = Gibbs free energy, H = enthalpy, S = entropy, T = temperature, R = gas constant, β = formation / stability constant.

A large and negative value for ΔG^0 results in a favourable reaction. This arises from making the enthalpy ΔH^0 more negative or by making the entropy ΔS^0 more positive.

a) The Entropic Contribution

Macrocyclic ligands have less rotational and translational freedom than their open-chain analogues. This is mainly due to the ring structure of the macrocycle. For the macrocycle, which is compact and relatively rigid in its free form, coordination to a metal ion only leads to a small reduction in the rotational and vibrational degrees of freedom. However, the open-chain analogue exhibits greater configurational entropy in the free form than in the coordinated form. Thus, there is a net gain in entropy upon release of the acyclic ligand into solution. Moreover, the equilibrium lies substantially to the right hard side:

$$ML_{(oc)} + L_{(mac)} \rightleftharpoons ML_{(mac)} + L_{(oc)}$$

$L_{(oc)}$ and $L_{(mac)}$ indicate the open-chain and macrocyclic ligands respectively.

b) The Enthalpic Contribution

The magnitude of the enthalpic term is determined by a variety of factors including the ring size, metal ion and donor atom types [34, 35]. The different solvation energies of the open-chain and macrocyclic ligands may play a crucial role in determining the enthalpic contribution. Solvation occurs more readily for the open-chain ligand compared to the analogous macrocycle, which in its uncoordinated form is more rigid and compact. The variability of the enthalpy term appears to reflect a number of influences. An important concern is any difference in the energy of the bonds between the metal ions and their respective ligands. For complexation to occur, less enthalpic energy is required to break hydrogen bonds with the solvent.

c) Kinetic Effect

In addition to the enhanced thermodynamic stability exhibited by many macrocyclic complexes, these are also usually kinetically inert to dissociation [36]. The reaction of metal cations with macrocyclic ligands in solution can be summarised as the following equation:

$$M^{x+} + L \underset{k_d}{\overset{k_f}{\rightleftharpoons}} ML^{x+}$$

Equation 1.3

$$K = k_f/k_d$$

Macrocyclic complexes have very high kinetic stability, greater than that of the analogous open-chain ligand complexes. The rates of formation and dissociation (k_f and k_d respectively) are both much smaller for the macrocycle species compared to open-chain complexes. For simple ligand complexes, the formation rate is often controlled by the solvent exchange rate of the solvated metal ion. This can be ascribed to the differences in flexibility of the coordinative bonds in the two systems. Dissociation requires elongation and cleavage of the M-L bonds, which is inhibited in the macrocycle complex since M-L cleavage leads to a distortion throughout the whole ring. In contrast, M-L cleavage in an open-chain polychelate is much easier, involving an "unzipping mechanism" [37].

d) Preorganisation

The study of structure and conformation of large molecules has been a topic of interest for a number of years among workers in various areas of chemistry for equally various reasons. The nature of macrocyclic species with the potential to coordinate metal ions has been an area of detailed study. The conformation adopted by many crown thioethers studied by X-ray crystallographic methods is one in which all the sulfur atoms are directed out of the cavity, adopting *exo*-conformations (Figure 1.5) [38]. In contrast to these results, coordination to a metal within the cavity assumes the conformation in which the sulfur atoms are directed towards the centre of the ring, adopting *endo*-conformations (Figure 1.5) [39]. The *exo*- and *endo*-conformations, although connected by a complex kinetic process, usually involve relatively small energy differences. Studies of the crystal structure of $[Mo(CO)_3\{[9]aneS_3\}]$ proved that the torsion angle for S-C-C'-S is 48° whereas the torsion angle for the uncomplexed $[9]aneS_3$ is 58°. The reduction in this torsion angle is likely to be the result of stabilisation provided by the formation of metal-sulfur bonds, which partly overcomes the repulsion between the sulfur lone pairs [40]. Similarly, 1,4,7-triazacyclononane, the nitrogen analogue of $[9]aneS_3$, adopts a *facial*

configuration when coordinated to a metal [41]. [9]aneN$_3$ and [9]aneS$_3$ have been recognised as being strong tridentate *facially* chelating ligands [42].

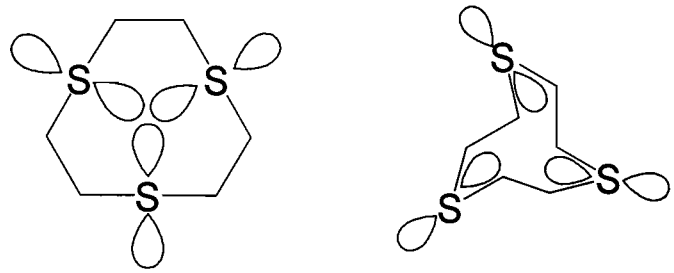

Figure 1.5. Representation of the "free" [9]aneS$_3$ displaying the orientation of the lone pairs

1.5.2. Macrocycle Synthesis

There are a variety of methods used for synthesising macrocycles, such as direct synthesis, template reaction, self-assembly and depolymerisation. However, the published cyclisations can be broadly subdivided into two major categories [37].

a) High-Dilution Synthesis

A typical direct synthetic procedure involves the reaction, in equimolar concentrations, of two precursor species incorporating the required fragments for the target macrocycle such that a 1:1 condensation occurs (Scheme 1.2). Such reactions are frequently performed under high-dilution conditions which tend to favour cyclisation by enhancing the prospect of the "half-condensed" moiety reacting with itself "head-to-head" rather than undergoing an intermolecular condensation with another molecule in the reaction solution, the initial step of a polymerisation process [43]. Such a synthesis is depicted in the following scheme [44].

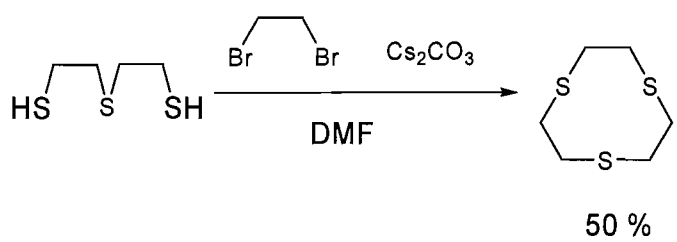

Scheme 1.2. Synthetic route to the cyclic thioether [9]aneS$_3$ – high-dilution process

b) Metal-Ion Template Synthesis

The effect of metal ions in promoting certain cyclisation reactions has been recognised for a very long time. Three possible roles for the metal ion in a template reaction have been delineated. First, the metal ion may sequester the cyclic product from an equilibrium mixture such as, for example, between products and reagents (thermodynamic template effect). The formation of the macrocycle is then promoted as its metal complex. Secondly, the metal ion may direct the steric course of a condensation such that the formation of the required cyclic product is facilitated (kinetic template effect). Finally, the equilibrium template effect, which is a combination of the previous two effects. The reactants react reversibly to form an intermediate that can form a stable complex with the metal ion (Scheme 1.3) [37, 45, 46].

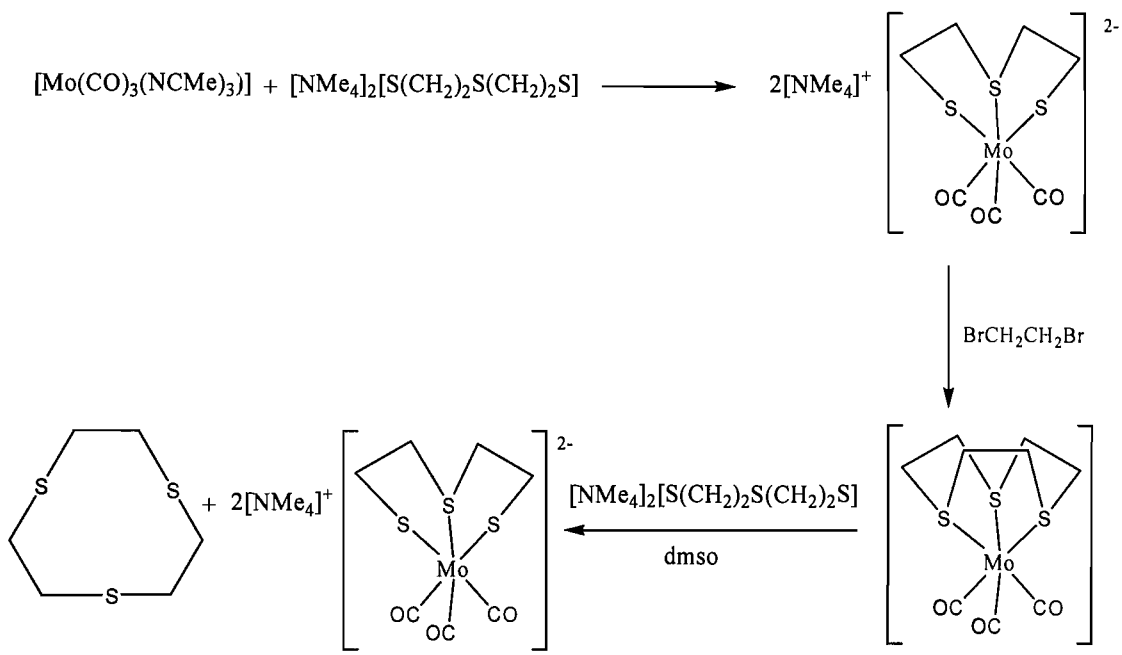

Scheme 1.3. Synthetic route to the cyclic thioether [9]aneS$_3$ *via* a metal-ion template process

1.6. Catalysis

Exactly how catalysts are able to speed up reactions without changing the free energy of either reactants or products remained a mystery for many years. Elucidation of mechanistic pathways involving catalysts has been possible in the last few decades. The catalyst will change form during the catalytic process, and in any side reactions. If any of the side reactions are not completely reversible then the catalyst will decompose. It is now clear that catalysts interact with reactants to provide a reaction pathway with a significantly lower free energy of activation than the corresponding uncatalysed pathway [47]. Usually the change in the activation entropy becomes more negative, because the transition metal assembles the reagents stepwise. If alternative routes exist, a catalyst can enhance product selectivity by enhancing just one of the competing reaction sequences.

The requirements for a successful catalytic process [48]:

- The reaction must be thermodynamically favourable.
- The reaction must run at a reasonable rate.
- The catalyst must have an appropriate selectivity towards the desired product.
- The catalyst must have a lifetime long enough to be economical.

Catalysts are used extensively in many branches of chemistry and are a vital constituent of many natural processes. They find wide application throughout the chemical industry where they assist in the production of several million tonnes of chemicals each year [49]. A catalyst is defined as a substance that changes the rate of a chemical reaction without itself being consumed in the reaction.

Homogeneous catalysis is among the most important areas of chemistry and chemical technology. New applications of transition metals as central atoms of ligand-modified complexes open novel routes to new compounds, together with new possibilities for reaction control. In homogeneous catalysis both the reactants and the catalysts are in the same phase, generally liquid/liquid. It provides a good mechanistic understanding of its microscopic processes ("catalytic cycles") and the possibility of influencing steric and electronic properties of these molecularly defined catalysts. With a homogeneous transition metal catalyst, there is generally only one type of active site

to the reactants. Higher activity is also observed in homogeneous catalysis as these catalysts are discrete soluble transition metal complexes implying a greater ease of mixing with the reactants and a greater contact area between catalysts and reactants. Ligand variation can make the homogeneous catalyst tailor-made so high specificity is achieved and the reaction can often be carried out at low temperatures and pressures [50].

The major disadvantage of homogeneous catalysis is the difficulty of separation and recycling. This is necessary as the transition metals used are usually expensive and environmentally damaging. There are however ways of overcoming this problem and higher reaction temperatures or polymer supported catalysts could be used.

1.6.1. Trimerisation of Ethylene to 1-Hexene

The efficient conversion of small organic and inorganic molecules into more complex species in commercial demand is an important aspect of the development of the chemical industry. Transition metal-catalysed alkene oligomerisations usually yield mixtures of alkenes in the C_4-C_{26} range. The separation of such mixtures into pure compounds can require expensive and energy demanding techniques (distillation, etc). Subsequently, much effort has been devoted to the search for more efficient catalysts that will produce terminal alkenes of specific lengths [51].

The trimerisation of ethylene to 1-hexene is an area of much recent interest due to the importance of this co-monomer in the production of linear low-density polyethylene (LLDPE) [52]. A large number of methods for the trimerisation of ethylene by a wide variety of catalysts has already been reported, most of them being based on early transition metals such as titanium, tantalum or, more commonly chromium [53].

The first selective formation of 1-hexene from ethylene was reported by Manyik *et al.* in 1977 (Scheme 1.4) [54]. At that time, 1-hexene was detected as an oligomeric by-product in the ethylene polymerisation system with Cr-based catalysts [55].

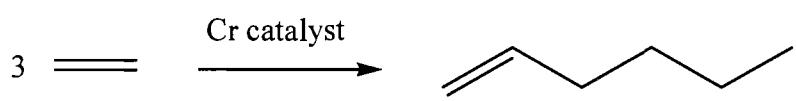

Scheme 1.4. Ethylene trimerisation

Hessen and co-workers recently reported a highly selective method to produce 1-hexene as a main product with the use of a titanium complex with a hemi-labile ancillary ligand (η^5-$C_5H_4CMe_2R$) and methylalumoxane (MAO) as co-catalyst [56]. In the same way, Sen and co-workers [57] discovered that [$TaCl_3R_2$], generated *in situ* by the reaction of $TaCl_5$ with alkyl metal compounds such as CH_3Li or $Zn(CH_3)_2$, can also function as trimerisation catalysts under mild conditions and give 96-99% selectivity for 1-hexene. Moreover, the activation of nickel complexes by alkylaluminium co-catalysts is a well established method of producing homogeneous catalysts for the oligomerisation of alkenes into higher α-olefins [58].

While some ethylene trimerisation catalysts are based on titanium and tantalum [57, 59], chromium-based systems generally display higher activity, selectivity, and thermal stability. Despite the industrial importance of chromium-based catalysts for the production of ethylene oligomers such as 1-hexene, well-defined homogeneous model systems were limited and exploration of such catalysts has been started only recently [60]. Hence, an important investigation has been undertaken using homogeneous Cr catalysts for the reaction of trimerisation. Chromium has been used in a number of different polymerisation studies, employing Cp-type ligands, non-Cp ligands possessing heteroatom donor sets and various mixed systems (Figure 1.6) [61].

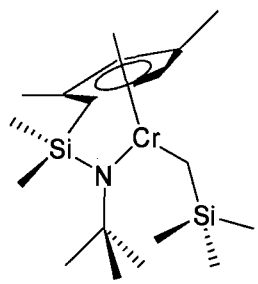

A

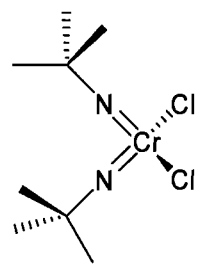

B

Figure 1.6. Selected examples of homogeneous chromium-based polymerisation catalysts

Many of these complexes require an alkylating co-catalyst in order to achieve activation. Methylaluminoxane (MAO) is commonly used as a co-catalyst for the trimerisation reaction.

One of the most promising results in homogeneous chromium catalysts was recently reported by Jolly (Figure 1.7) [62-64], who disclosed that by changing the well-known "constrained geometry" ligand's anionic amido ligand to a neutral amine, highly active cationic chromium(III) catalysts could be produced upon activation with MAO.

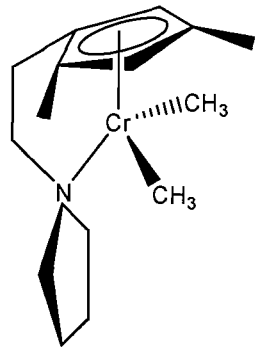

Figure 1.7. Jolly's complex for the trimerisation of ethylene

A recent communication describes a catalyst, generated in situ by treating Cr(III) salts with MAO in the presence of the diphosphine PNP^{OMe} (PNP^{OMe} = $(o\text{-MeO-}C_6H_4)_2PN(Me)P(o\text{-MeO-}C_6H_4)_2$), that trimerises ethylene to 1-hexene with unprecedented selectivity and productivity [65] following a proposed catalytic cycle (Scheme 1.5).

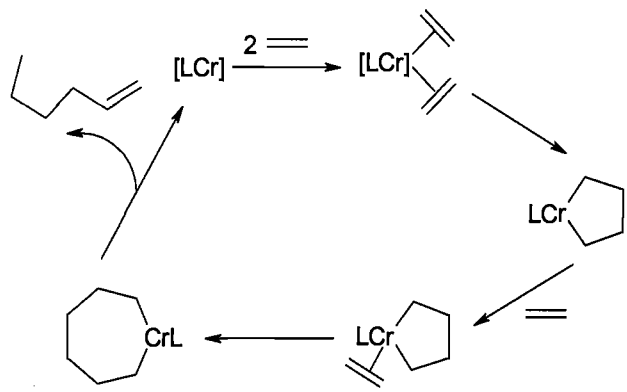

Scheme 1.5. Proposed catalytic cycle for the selective trimerisation of ethylene to 1-hexene [66]

1.6.2. Trimerisation and Tetramerisation Studies by SASOL

a) Selective Trimerisation of Ethylene to 1-Hexene.

In the course of investigations on alternative catalysts for ethylene trimerisation, SASOL became interested in tridentate PNP ligands of the type $HN(CH_2CH_2PR_2)_2$ in combination with Cr as precatalysts for this reaction (Scheme 1.6) [53, 67]. The outcome of this study was the preparation of Cr(III)-PNP complexes which, when activated with methylaluminoxane, were evaluated as catalysts for ethylene trimerisation, with several giving high activity and excellent selectivity towards 1-hexene [53, 67].

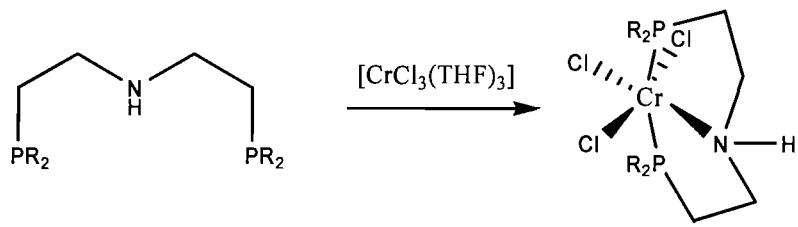

R = phenyl, cyclohexyl, ethyl

Scheme 1.6. Synthesis of *mer*-Cr(III)-PNP complexes

Under mild conditions of temperature and pressure and in the presence of a large amount of MAO (680 equiv.), it appeared that compact diethylphosphino substituents led to a very high activity with excellent selectivity towards 1-hexene. Sterically demanding dicyclohexylphosphino substituents however, led to a dramatic decrease in activity. Increasing the amount of MAO beyond this did not significantly further increase the activity of the complex. Finally, a reasonable activity and good selectivity towards 1-hexene were observed with the diphenylphosphino substituents. Given the structural similarities of the two bulky phosphine derivatives, it is difficult to reconcile the remarkable differences in activity that each provides. However the X-ray crystal structures only represent that of the precatalyst, and it is possible that in the active catalyst the ligand is coordinated in a manner that is more sensitive to greater steric bulk phosphine [53].

However, the high cost of secondary alkyl phosphine precursors for the synthesis of the ligands make their use in a potential industrial process difficult. Along with this, the toxicity and sensitivity towards oxidation represent serious drawbacks for phosphine-containing systems. To increase the attractiveness of this system, interest was in alternatives that could replace the phosphorus donors while maintaining the attributes of the donor set. In the Cr(III)-PNP system, it was thought that phosphines operate as soft donor, capable of facile association-dissociation equilibria [68, 69]. From this respect, soft thioether groups should have similar donor properties. SNS-type ligands were then prepared and tested for catalysis (Scheme 1.7) [69].

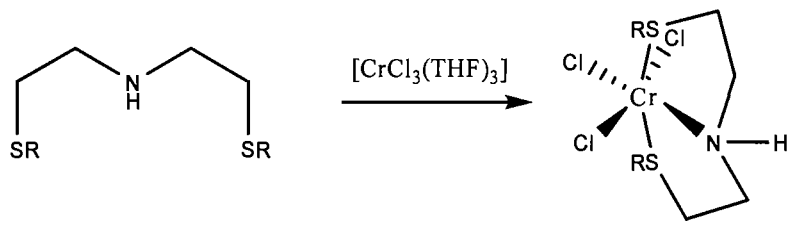

R = methyl, ethyl, ^{n}butyl, ^{n}decyl

Scheme 1.7. Synthesis of *mer*-Cr(III)-SNS complexes

Along with MAO as co-catalyst for the trimerisation of ethylene to 1-hexene, all complexes gave rise to highly active and selective catalysts. Using low amount of MAO and mild temperature and pressure conditions, best results were observed with the more soluble ^{n}decyl derivative. This may in part be due to the enhanced solubility in toluene that the longer alkyl chain affords. It was concluded that thioether groups can make effective substitutes for phosphines and can lead to highly active and excellent selective catalysts. On the whole, thioether ligands have received very little attention with respect to catalytic studies and can be valuable for such a catalysis process.

Recent investigations on both PNP and SNS systems concluded that the effect of placing alkyl groups on the central nitrogen atom shows that H-substitution is an essential attribute of this ligand class for high activity [67]. However, the role of the MAO co-catalyst, the mode of ligand binding and the oxidation state of the metal during catalysis remain unclear. The mechanism of ethylene trimerisation is thought to follow a metallacycle route involving oxidative addition of two ethylene molecules to

and reduce the chromium metal centre to facilitate cation generation. Studies led to suggest a Cr(II)-Cr(IV) mechanistic process. However, there is at present little evidence to support these proposals [67, 71].

b) Selective Tetramerisation of Ethylene to 1-Octene

The selective trimerisation of ethylene to 1-hexene is a well-known process. However, until recently, a corresponding selective tetramerisation reaction of ethylene to 1-octene was unknown and the common belief was that the process was improbable. The discovery of the first catalyst capable of this transformation with selectivities up to 70% has recently been reported [66]. The observed selectivity in ethylene trimerisation reaction is thought to be a consequence of the unusual metallacycle mechanism in operation (Chapter 3). Until recently, it was thought unlikely that further ethylene insertion (*i.e.* more than two ethylene molecules) to give a metallacycle could compete with 1-hexene elimination or that elimination of 1-octene from such a species would take place. Bollman *et al* [66] recently discovered that the selective tetramerisation of ethylene is also possible by using a chromium catalyst (comprising a chromium source and a $(Ph_2P)_2NR$ ligand) and MAO-based activator (Figure 1.8) [66] .

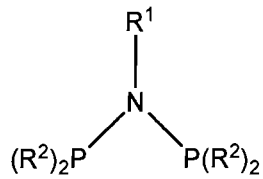

1: R^1 = Me, R^2 = Ph
2: R^1 = Pentyl, R^2 = Ph
3: R^1 = Cyclohexyl, R^2 = Ph
4: R^1 = ^{iso}Propyl, R^2 = Ph
5: R^1 = Ph, R^2 = Ph

Figure 1.8. Selected examples of PNP ligands for the tetramerisation of ethylene to 1-octene

By using a number of N-substituted bis(diphenylphosphino)amine PNP donor ligands, it has been possible to show that significant selectivity control is possible for the tetramerisation [72]. Deuterium labelling studies supported the suggestion that this reaction in fact involves metallacyclic intermediates. Ligand variation experiments also revealed that the selectivity between 1-hexene and 1-octene could be switched by

modifications at the P-Ar moiety of the PNP ligand backbone [72]. The possibility that the reaction mechanism may proceed *via* an initial reduction to the divalent state and that the catalytic process is performed by the Cr(II)/Cr(IV) redox couple has been contemplated in the literature [67]. Different redox couples such as Cr(I)/Cr(III) [64, 73] and even Cr(III)/Cr(V) [70, 74-76] have been envisaged. A recent study shows that a cationic Cr(II) complex has been isolated by reaction of $[CrCl_3\{PNP\}]_2$ (with PNP = $RN(PPh_2)_2$; R = Cy) with trimethylaluminum [71]. However its isolation and characterisation do not provide definite answers to the important question about the actual catalytically active species.

1.7. Aim of Research

The main aim of this work is the preparation and investigation of Cr(III) complexes for the catalytic process of trimerisation of ethylene to 1-hexene. The series of ligands will probe geometric control (macrocyclic, tripodal and facultative geometries) and ligand donor effects (sulfur, nitrogen, phosphorus and oxygen) on the ability of the associated chromium complexes to promote the selective trimerisation of ethylene to 1-hexene. Initial tests to probe the activity of the complexes were carried out and investigation of the active species formed upon addition of an aluminium reagent to the complex in solution was followed using spectroscopic techniques such as infra-red, UV/visible and EPR spectroscopy as well as X-ray absorption spectroscopy (Chapter 2). The effects of the addition of a co-catalyst were also evaluated using similar techniques.

Chapter 3 is concerned primarily with the Cr(III)-SNS system and describes the preparation and characterisation of the ligand and the complex as well as its partial structure using X-ray absorption spectroscopy. Cyclic voltammetry was also used to investigate the oxidation/reduction properties associated to the ligand donor set. The reaction between the complex and trimethylaluminum was investigated in order to give evidence of the suggested roles of MAO.

Chapter 4 is mostly dedicated to the study of the Cr(III)-PNP(THF) system for the selective tetramerisation of ethylene to 1-octene. Similar experiments as the ones used in Chapter 3 are carried out in an attempt to characterise the active species and validate or otherwise the involvement of a Cr(I)-Cr(III) couple for the catalytic process.

In Chapter 5, the effects of ligand structure on activity and selectivity are studied. The series of ligands probe geometric control and ligand donor effects on the ability of the chromium(III) complexes to allow trimerisation and oligomerisation of ethylene. Characterisation of the active species and the effects of the addition of trimethylaluminum to the precatalysts are carried out *via* spectroscopic methods similar to the ones used in Chapters 3 and 4.

Chapter 6 describes the coordination chemistry of chromium(III) complexes containing cyclic and acyclic N- and S-donor ligands and their characterisation using X-ray absorption spectroscopy.

1.8. References

1. Evans, J.; O'Neill, L.; Kambhampati, V. L.; Rayner, G.; Turin, S.; Genge, A.; Dent, A. J. and Neisius, T.; *J. Chem. Soc., Dalton Trans.*, (2002), 2207.
2. Chatt, J. and Williams, A. A.; *J. Chem. Soc.*, (1951), 3061.
3. McCleverty, J.; *Chemistry of the First-row Transition Metals*, (1999), Oxford, Oxford University Press.
4. Orpen, A. G. and Connelly, N. G.; *J. Chem. Soc., Chem. Commun.*, (1985), 1310.
5. Tolman, C. A.; *Chem. Rev.*, (1977), **77**, 313.
6. Levason, W. and Reid, G.; *Comprehensive Coordination Chemistry II*, (2004), Amsterdam : London, Elsevier Pergamon, **1**, 391.
7. Murray, S. G. and Hartley, F. R.; *Chem. Rev.*, (1981), **81**, 365.
8. Pearson, R. G.; *J. Chem. Ed.*, (1968), **45**, 581.
9. Pearson, R. G.; *Coord. Chem. Rev.*, (1990), **100**, 403.
10. Barnhart, J.; *Reg. Toxi. Pharma.*, (1997), **26**, S3.
11. Jackson, W. G.; Coronas, J. M. and Ferrer, M.; *Inorg. Chim. Acta*, (1976), **16**, 47.
12. Lowery, A. H.; George, C.; D'Antonio, P. and Karle, J.; *J. Am. Chem. Soc.*, (1971), **93**, 6399.
13. Clark, R. J. M. and Natile, G.; *Inorg. Chim. Acta*, (1970), **4**, 533.
14. Wieghardt, K.; Chaudhuri, P.; Nuber, B. and Weiss, J.; *Inorg. Chem.*, (1982), **21**, 3086.
15. Mitewa, M. and Bontchev, P. R.; *Coord. Chem. Rev.*, (1985), **61**, 241.
16. Salt, J. E.; Girolami, G. S.; Wilkinson, G.; Motevalli, M.; Thornton-Pett, M. and Hursthouse, M. B.; *J. Chem. Soc., Dalton Trans.*, (1985), 685.
17. Badanyan, S. O.; Minasyan, T. T. and Vardapetyan, S. K.; *Russ. Chem. Rev.*, (1987), **56**, 740.
18. Lewis, G. N.; *J. Am. Chem. Soc.*, (1913), **35**, 1448.
19. Ahrland, S.; Chatt, J. and Davies, N. R.; *Q. Rev. Chem. Soc.*, (1958), **12**, 265.
20. Melson, G. A.; *Coordination Chemistry of Macrocyclic Compounds*, (1979), New York, Plenum Press.
21. Eldvidge, J. A. and Linstead, R. P.; *J. Chem. Soc.*, (1952), 5008.
22. Linstead, R. P. and Whalley, W.; *J. Chem. Soc.*, (1952), 4839.

23. Pedersen, C. J.; *J. Am. Chem. Soc.*, (1967), **89**, 2495.
24. Pedersen, C. J.; *J. Am. Chem. Soc.*, (1967), **89**, 7017.
25. Shoham, G.; Lipscomb, W. N. and Olsher, U.; *J. Am. Chem. Soc.*, (1983), **105**, 1247.
26. Bush, M. A. and Truter, M. R.; *J. Chem. Soc., Perkin Trans. II*, (1972), 341.
27. Mallison, P. R. and Truter, M. R.; *J. Chem. Soc., Perkin Trans. II*, (1972), 1818.
28. Zuchman, S. A.; Freeman, G. M.; Troutner, D. E.; Volkert, W. A.; Holmes, R. A.; VanDerveer, D. G. and Barefield, E. K.; *Inorg. Chem.*, (1981), **20**, 2386.
29. Chaudhuri, P. and Wieghardt, K.; *Prog. Inorg. Chem.*, (1987), **35**, 329.
30. Blake, A. J. and Schroder, M., *Adv. Inorg. Chem.*, Vol. 35, (1990), New York, Academic Press.
31. Cabbiness, D. K. and Margerum, D. W.; *J. Am. Chem. Soc.*, (1969), **91**, 6540.
32. Morgan, G. T. and Drew, H. D. K.; *J. Chem. Soc., Trans.*, (1920), **117**, 1456.
33. Dei, A. and Gori, R.; *Inorg. Chim. Acta*, (1975), **14**, 157.
34. Myers, R. T.; *Inorg. Chem.*, (1978), **17**, 952.
35. Hancock, R. D. and Thom, V. J.; *J. Am. Chem. Soc.*, (1982), **104**, 291.
36. Hinz, F. P. and Margerum, D. W.; *Inorg. Chem.*, (1974), **13**, 2941.
37. Lindoy, L. F., *The Chemistry of Macrocyclic Ligand Complexes*, (1989), Cambridge, Cambridge University Press.
38. DeSimone, R. E. and Glick, M. D.; *J. Am. Chem. Soc.*, (1976), **98**, 762.
39. Glass, R. S.; Wilson, G. S. and Setzer, W. N.; *J. Am. Chem. Soc.*, (1980), **102**, 5068.
40. Ashby, M. T. and Lichtenberger, D. L.; *Inorg. Chem.*, (1985), **24**, 636.
41. Chaudhuri, P.; Wieghardt, K.; Tsai, Y. H. and Kruger, C.; *Inorg. Chem.*, (1984), **23**, 427.
42. Yang, R. and Zompa, L.; *Inorg. Chem.*, (1976), **15**, 1499.
43. Rosen, W. and Bush, D. H.; *J. Am. Chem. Soc.*, (1969), **91**, 4694.
44. Blower, P. J. and Cooper, S. R.; *Inorg. Chem.*, (1987), **26**, 2009.
45. Curtis, N. F.; *J. Chem. Soc.*, (1960), 4409.
46. Curtis, N. F. and House, D. A.; *Chem. and Ind.*, (1961), 1708.
47. Spessard, G. O. and Miessler, G. L., *Organometallic Chemistry*, (1997), New York, Prenctice Hall.

48. Shriver, D.; Atkins, P. and Langford, C.; *Inorganic Chemistry, 3rd Edition*, (1992), Oxford, Oxford University Press.

49. Arnold, L. A.; Cloke, F. G.; Geldbach, T. and Hitchcock, P. B.; *Organometallics*, (1999), **18**, 3228.

50. Elschenbroich, C. and Slazer, A., *Organometallics, 2nd Edition*, (1992), New York, VCH Publisher Inc.

51. Yu, Z. and Houk, K. N.; *Angew. Chem. Int. Ed.*, (2003), **42**, 808.

52. Small, B. L. and Brookhart, M.; *J. Am. Chem. Soc.*, (1998), **120**, 7143.

53. McGuinness, D. S.; Wasserscheid, P.; W, W. Keim; Hu, C.; Englert, U.; Dixon, J. T. and Grove, C.; *J. Chem. Soc., Chem. Commun.*, (2003), 334.

54. Manyik, R. M.; Walker, W. E. and Wilson, T. P.; *J. Catal.*, (1977), **47**, 197.

55. Yang, Y.; Kim, H.; Lee, J.; Paik, H. and Jang, H. G.; *Appl. Catal. A: Gen.*, (2000), **193**, 29.

56. DeBruin, T. J. M.; Magna, L.; Raybaud, P. and Toulhoat, H.; *Organometallics*, (2003), **22**, 3404.

57. Andes, C.; Harkins, S. B.; Murtuza, S.; Oyler, K. and Sen, A.; *J. Am. Chem. Soc.*, (2001), **123**, 7423.

58. Andrews, P.; Corker, J. M.; Evans, J. and Webster, M.; *J. Chem. Soc., Dalton Trans.*, (1994), 1337.

59. Deckers, P. J. W.; Hessen, B. and Teuben, J. H.; *Angew. Chem. Int. Ed.*, (2001), **40**, 2516.

60. Ruther, T.; Braussaud, N. and Cavell, K. J.; *Organometallics*, (2001), **20**, 1247.

61. Small, B. L.; Carney, M. J.; Holman, D. M.; O'Rourke, C. E. and Halfen, J. A.; *Macromolecules*, (2004), **37**, 4375.

62. Jensen, V. R.; Angermund, K. and Jolly, P. W.; *Organometallics*, (2000), **19**, 403.

63. Dohring, A.; Gohre, J.; Jolly, P. W.; Kryger, B.; Rust, J. and Verhovnik, G. P. J.; *Organometallics*, (2000), **19**, 388.

64. Emrich, R.; Heinemann, O.; Jolly, P. W.; Kruger, C. and Verhovnik, G. P. J.; *Organometallics*, (1997), **16**, 1511.

65. Carter, A.; Cohen, S. A.; Cooley, N. A.; Murphy, A.; Scutt, J. and Wass, D. F.; *Chem. Commun.*, (2000), 858.

66. Bollmann, A.; Blann, K.; Dixon, J. T.; Hess, F. M.; Killian, E.; Maumela, H.; McGuinness, D. S.; Morgan, D. H.; Neveling, A.; Otto, S.; Overett, M.; Slawin, A. M. Z.; Wasserscheid, P. and Kuhlmann, S.; *J. Am. Chem. Soc.*, (2004), **126**, 14712.

67. McGuinness, D. S.; Brown, D. B.; Tooze, R. P.; Hess, F. M.; Dixon, J. T. and Slawin, A. M. Z.; *Organometallics*, (2006), **25**, 3605.

68. McGuinness, D. S.; Wasserscheid, P.; Morgan, D. H. and Dixon, J. T.; *Organometallics*, (2005), **24**, 552.

69. McGuinness, D. S.; Wasserscheid, P.; Keim, W.; Morgan, D.; Dixon, J. T.; Bollmann, A.; Maumela, H.; Hess, F. and Englert, U.; *J. Am. Chem. Soc.*, (2003), **125**, 5272.

70. Agapie, T.; Schofer, S. J.; Labinger, J. A. and Bercaw, J. E.; *J. Am. Chem. Soc.*, (2004), **126**, 1304.

71. Jabri, A.; Crewdson, P.; Gambarotta, S.; Korobkov, I. and Duchateau, R.; *Organometallics*, (2006), **25**, 715.

72. Overett, M. J.; Blann, K.; Bollmann, A.; Dixon, J. T.; Haasbroek, D.; Maumela, H.; McGuinness, D. S. and Morgan, D. H.; *J. Am. Chem. Soc.*, (2005), **127**, 10723.

73. Kohn, R. D.; Haufe, M.; Kociok-Kohn, G.; Grim, S.; Wasserscheid, P. and Keim, W.; *Angew. Chem. Int. Ed.*, (2000), **39**, 4337.

74. Meijboom, N.; Schaverien, C. J. and Orpen, A. G.; *Organometallics*, (1990), **9**, 774.

75. Fang, Y.; Liu, Y.; Ke, Y.; Cuo, C.; Zhu, N.; Mi, X.; Ma, Z. and Hu, Y.; *Appl. Catal. A: Gen.*, (2002), **235**, 33.

76. Kohn, R. D.; Haufe, M.; Mihan, S. and Lilge, D.; *Chem. Commun.*, (2000), 1927.

Chapter 2

Experimental Techniques

2.1. Introduction

The paramagnetic nature of the chromium(III) complexes make them unsuitable for usual analysis techniques such as NMR spectroscopy. Characterisations were then focused on techniques such as X-ray absorption and electron paramagnetic resonance spectroscopy, UV/visible and infra-red spectroscopy and cyclic voltammetry.

2.2. X-Ray Absorption Fine Structure (XAFS)

XAFS spectroscopy is the only spectroscopic technique that provides information on the electronic and structural properties of catalysts under reaction conditions and in the presence of reactants. XAFS is used to study the local structure up to 5 Å from the absorbing atom. It is element specific and gives a picture of the average local coordination. The material to be studied can be presented to the X-ray in any form, as crystalline solids, amorphous solids, solutions or gases [1]. For the purpose of this project, only solid and solution states will be considered.

2.2.1. XAFS Theory [2]

In X-ray absorption spectroscopy, a sample is exposed to X-rays produced by a synchrotron. When a beam of X-ray photons passes through a material, the incident intensity I_0 will be decreased by an amount determined by the absorption characteristics of the irradiated material. The incident X-ray beam with intensity I_0 is attenuated by the sample, following Lambert's law (Figure 2.1):

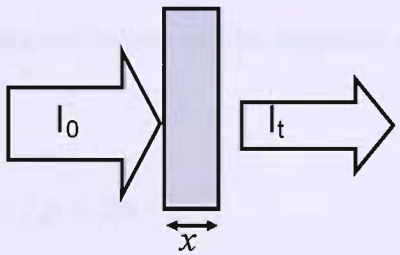

Figure 2.1. Attenuation of an X-ray beam by an absorbing sample; Lambert's law

$$I_t = I_0 e^{-\mu(E)x} \qquad \textbf{Equation 2.1}$$

Where I_t is the intensity of the transmitted photons, $\mu(E)$ the linear absorption coefficient (function of the photon energy) and x the thickness of the sample.

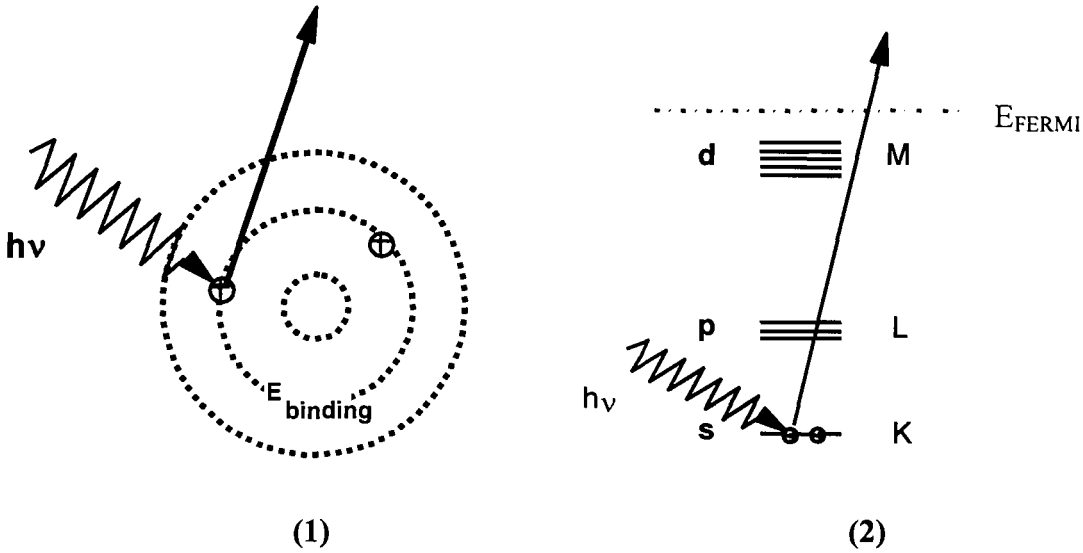

Figure 2.2. Schematic illustration of the photoelectric effect in term of excitation of the orbital **(1)** or different energy levels **(2)** [2]

When the energy of the incoming photons is large enough to excite a core electron to a vacant excited state or to the continuum (Figure 2.2), a strong increase in absorption intensity is observed (Figure 2.3). This sharp rise is the absorption edge. The absorption edge being correlated to the binding energy E_0 of an electron, hence the absorption edge is element specific. At the absorption edge, E_{edge}, the kinetic energy of the electron E_{kin} is defined to be equal to E_0. For any energy above this, the photoelectron kinetic energy is given by:

$$E_{kin} = h\upsilon - E_0 \qquad \textbf{Equation 2.2}$$

The photoelectron can be regarded as a wave with the wavelength λ being determined by:

$$\lambda = h / p = 2\pi / k \qquad \textbf{Equation 2.3}$$

Where p is the momentum of the photoelectron, k is the wave vector and h is the Planck's constant. As a photoelectron is energetic enough to be treated as a free electron, k can be defined as:

$$k = \sqrt{\left(\frac{8\pi^2 m}{h^2}\right)\left(h\nu + E_0 - E_{edge}\right)} \qquad \textbf{Equation 2.4}$$

With m the electron mass and h Planck's constant.

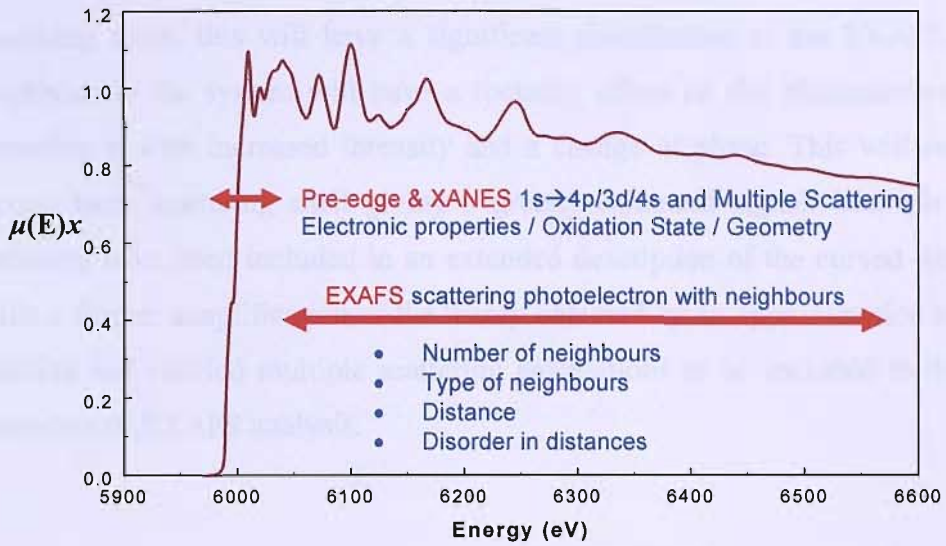

Figure 2.3. Typical X-ray absorption spectrum of a Cr foil, showing the pre-edge and X-ray absorption near edge region (XANES) and the extended X-ray absorption fine structure (EXAFS) region

2.2.2. X-Ray Absorption Near Edge Structure (XANES)

The XANES part of the absorption spectrum (Figure 2.3) is determined by the empty density of states, itself probed by multiple scattering of the outgoing electron [3]. Below an energy of ~60 eV, the ejected electron can occupy resonant states that correspond to antibonding orbitals arising from the linear combination of atomic orbitals forming the bonds surrounding the central atom. It is these states that give rise to XANES features. Their source is physically distinct to EXAFS and yields different information. XANES information is predominantly due to electronic structure rather than physical structure.

2.2.3. Multiple Scattering Effects

Multiple scattering effects can yield some angular information about the atoms adjacent to the absorbing atom [4]. The phenomenon of multiple scattering occurs if the emitted photoelectron encounters more than one backscattering atom before returning to the absorber (Figure 2.4). If one atom is behind another, relative to the absorbing atom, this will have a significant contribution to the EXAFS. The first neighbour in the system will have a focusing effect on the photoelectron, forward scattering it with increased intensity and a change of phase. This will result in the second back scattering shell giving a greatly enhanced signal. Multiple scattering pathways have been included in an extended description of the curved wave theory, while a further simplification of the theory obtained by an approximation to the wave function has enabled multiple scattering calculations to be included in the iterative procedure of EXAFS analysis.

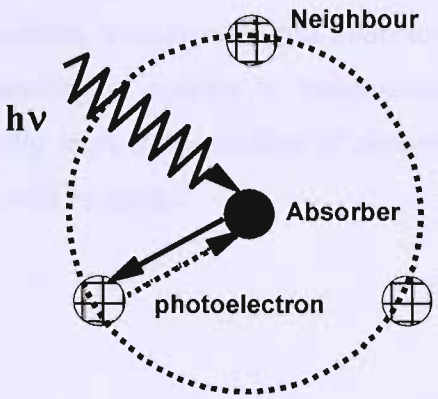

Figure 2.4. Illustration of neighbouring shells of atoms about the absorber [2]

2.2.4. Data Acquisition

EXAFS is a weak phenomenon, so requires high X-ray flux to produce sufficiently intense, collimated radiation over a range of energies. All XAFS spectra presented in this work have been recorded at the European Synchrotron Radiation Facility (ESRF) in Grenoble, France, station BM26-DUBBLE (Figure 2.5).

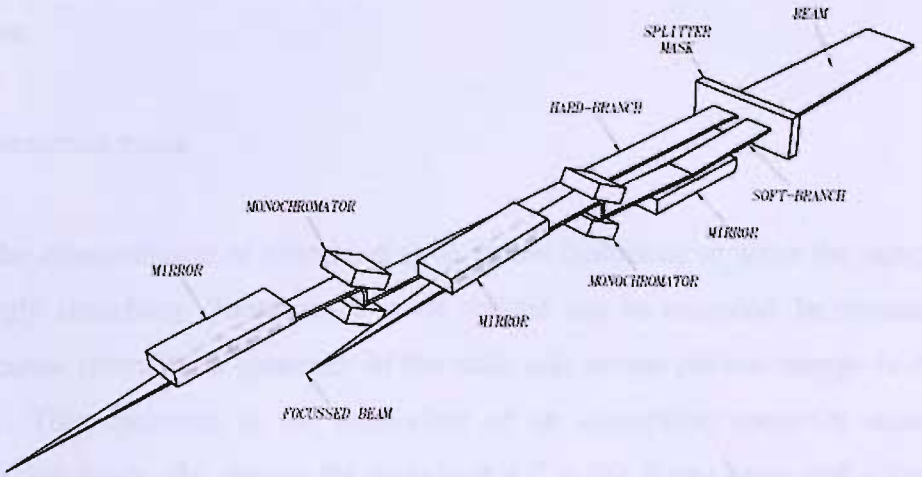

Figure 2.5. Schematic layout of the optical components of BM26, displaying the two branches SAXS/WAXS and XAS

Two modes of data acquisition, transmission and fluorescence, were used in recording XAFS spectra. The recording of spectra in transmission mode normally requires samples with a sufficiently high concentration of absorbing atom. If this is not the case, fluorescence mode will be used.

a) Transmission mode

In EXAFS spectroscopy, μ, the absorption coefficient, is defined by the equation

$$I_t = I_0 e^{-\mu(E)x} \qquad \textbf{Equation 2.5}$$

where I_t is the intensity of the transmitted photons, $\mu(E)$ the linear absorption coefficient (function of the photon energy) and x the thickness of the sample. Solid samples were ground to a fine homogeneous powder and diluted with some boron nitride. When possible, pellets were made for the non-sensitive compounds and placed into an aluminium cell fitted with Kapton windows. The sensitive compounds were loaded under inert atmosphere. The design of the airtight cell consists of two

aluminium plates with a Teflon plate placed between them and fitted with Kapton windows.

b) Fluorescence mode

When the concentration of absorbing atom is low (solution) or when the sample used is strongly absorbing, fluorescence mode spectra can be recorded. In measuring the fluorescence intensity, a spectrum of the ratio I_f/I_0 *versus* photon energy is obtained directly. This spectrum is the equivalent of an absorption spectrum recorded in transmission mode. By placing the sample at 45° to the X-ray beam and a detector at 90°, the fluorescence yield, *versus* scattered radiation, is maximised improving the signal to noise ratio. The design of the solution cell consists of three stainless steel plates with a 25 mm drilled hole in the middle to allow the passage of the X-ray beam. These three plates are screwed together with a Kalrez 'O' ring and a Kapton film (0.025 mm thickness) placed between each of the plates. The cell is also equipped with an inlet and an outlet on the top of each cell which are sealed with NMR suba seals to allow the purging with N_2 and the injection of the solution (Figure 2.6). The cells are mounted onto a motorised jack which can be remotely moved in the x, y and z directions (Figure 2.7).

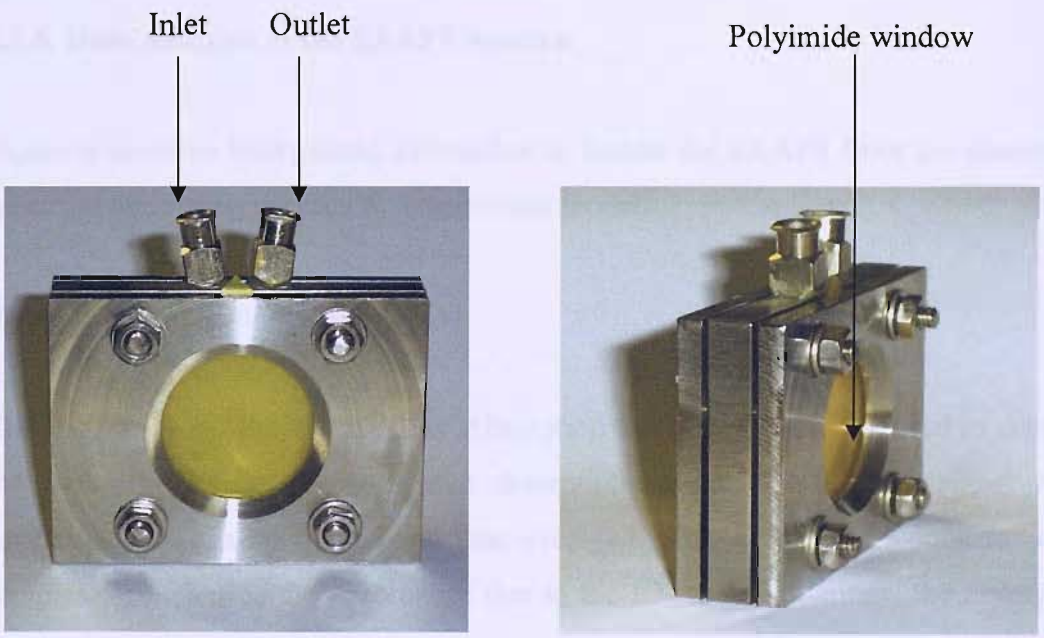

Figure 2.6. Picture of the fluorescence cell

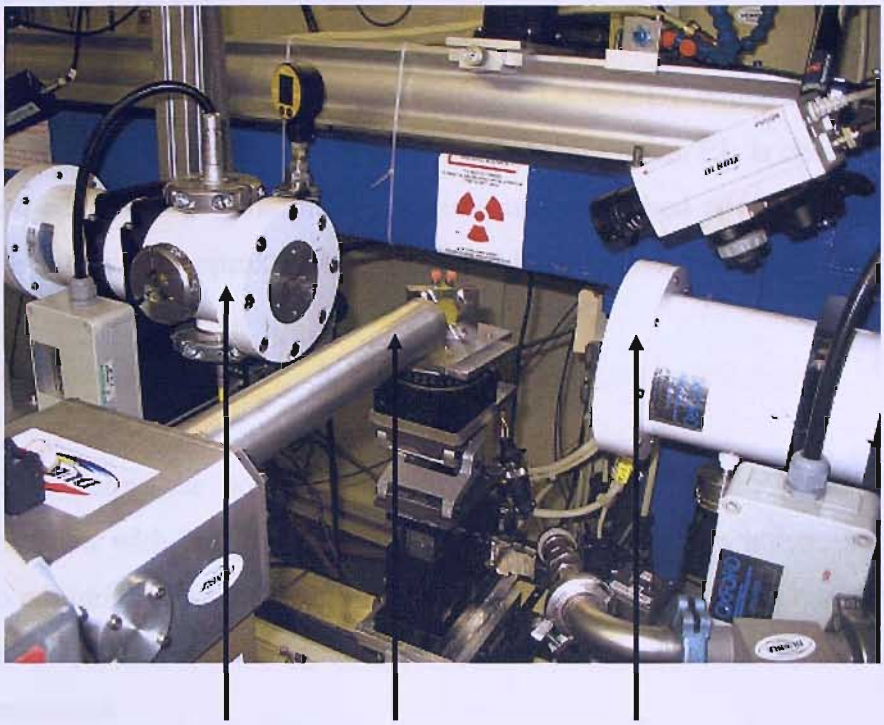

Figure 2.7. Picture of fluorescence EXAFS set up at the Beamline (BM26-DUBBLE, ESRF, Grenoble, France)

2.2.5. Data Analysis of the EXAFS Spectra

Analysis involves background subtraction to isolate the EXAFS from the absorption spectrum and fitting the data to a theoretical model.

Background subtraction, PAXAS [5]

The Program for Analysis of X-ray Absorption Spectra (PAXAS) is used to subtract the background from the calibrated absorption spectra. To improve signal ratio, several spectra can be aligned and then averaged. This is commonly done for weak samples. To examine the absorbance due to the EXAFS oscillations, the absorption due to the spectrometer and the sample matrix are removed by respective subtraction of the pre- and post-edge background.

a) Pre-edge subtraction

The program defines polynomial by two points, L1 and U1 which are found at the beginning and end of the pre-edge region; whilst a third point, P1, is chosen at the end of the post-edge region. This third point is usually weighed and its y-coordinate is adjusted to achieve an approximately horizontal background subtracted absorption.

b) Post-edge subtraction

Three points define the post-edge background subtraction, L2, P2 and U2. These points are fitted with high order polynomials of 6, 7 or 8. The polynomial order is chosen to minimise unwanted features below distances of 1 Å in the Fourier transform spectrum. Only shells containing the structural information are therefore selected and back transformed.

c) Model fitting

The model fitting program EXCURVE 9.27 [6] uses curved wave theory and computationally fast algorithms to theoretically model the oscillations in the EXAFS and to determine structural information.

- Phaseshifts

The phaseshifts corresponding to the photoelectron wave associated with the central atom and potential surrounding atoms are calculated by *ab initio* methods, using Hedin-Lundqvist potentials and muffin tin radii potentials. Central atom phaseshifts include the effects of a 1*s* core hole such as using the wave function of the atomic number of the absorber +1, the calculations treat the outer-electrons as being fully relaxed.

- Fitting procedure

A number of structural dependent parameters are used to generate a theoretical spectrum. The fit between the theoretical and the experimental spectra is then improved by refining these parameters by least squares iteration.

- Cn, the number of atoms in the shell (coordination number).
- Tn, the type of atom in the shell.
- An, the Debye-Waller factor for the shell defined as $2\sigma^2$, where σ is the mean square variation in interatomic distances.
- Rn, the distance of the n^{th} shell from the central atom.
- Ef, the difference calculated between the calculated Fermi level energy and the known values for the element, typically -15 to 5 eV.
- Lmax, the maximum angular momentum used in calculating the phaseshifts.
- Emin, the minimum energy to calculate the theoretical spectrum.
- Emax, the maximum energy to calculate the theoretical spectrum.
- afac, the energy amplitude factor which accounts for the reduction in amplitude to multiple excitations occurring at the central atom.

- Fitting parameters

The fit between the experimental and theoretical spectra is given by the fit index (FI). In a k^3-weighted EXAFS, FI is calculated following the equation:

$$\text{FI (EXAFS)} = \sum i \, [(\chi^T - \chi^E)k_i^3]^2 \qquad \textbf{Equation 2.6}$$

The sum of the square of the differences between the theoretical and experimental data points has to be below 5×10^{-4} to produce a good fit. However, FIs of less than 8×10^{-4} are acceptable.

A second parameter, the R-factor, is calculated to estimate the quality of the fit and is given by the equation [4, 7]:

$$\text{R(EXAFS)} = [\int(\chi^T - \chi^E)k^3 \, dk / \int \chi^E k^3 \, dk] \times 100 \qquad \textbf{Equation 2.7}$$

The R-factor is a percentage calculating the total sum of all the errors between the data points. An R-factor below 30% constitutes a good fit. However, for dilute samples, a value of 45% is acceptable.

- Sine transform

The *k* weighted data can be shown as a sine transform rather than as the Fourier transform. This appears more complex, but can be useful to determine which atom is in a shell, especially if the atoms are similar in size. The Fourier transform is the square root of the sine transform squared, which ensures that the amplitude is always positive in the transform, but can cause some phase information to be lost.

2.3. UV/visible Spectroscopy

Absorption spectra are obtained using a spectrophotometer which usually plots the absorption, A, *versus* wavelength or, preferably, wave number. A UV/visible spectrum is usually represented with increasing wavelength running from left to right, so that the UV region is on the left of the visible and the near IR is on the right.

2.3.1 *d-d* Spectra

A d^3 ion such as Cr(III) has a ^4F ground state configuration. In this case, the strong field ground state is $(t_{2g})^3$ whose term symbol can be shown by direct product to be $^4A_{2g}$. In an octahedron, the $^4A_{2g}$ level will lie at -12*Dq* (3 x -4Dq). The first excited state $(t_{2g})^2(e_g)^1$ gives rise to $^4T_{1g}$ + $^4T_{2g}$ (plus doublet state) and lies at -2*Dq* ((2 x -4*Dq*) + 6*Dq*), and the second excited state $(t_{2g})^1(e_g)^2$ yields $^4T_{1g}$, at + 8*Dq*. Three spin allowed transitions are expected from $^4A_{2g}$ to the three excited quartets [8]:

$$^4A_{2g} \rightarrow {}^4T_{2g}\ (\upsilon_1);$$
$$^4A_{2g} \rightarrow {}^4T_{1g}(F)(\upsilon_2);$$
$$^4A_{2g} \rightarrow {}^4T_{1g}(P)(\upsilon_3).$$

However the last of these transitions is usually obscured due to an intense ligand-metal charge transfer bands. As the name suggests, these transitions involve a re-distribution of electronic charges within the molecule and are usually strongly Laporte allowed, being from ligand to metal orbital or *vice versa*.

For complexes with C_{3v} symmetry, Figure 2.8 displays the energy level diagram for a d^3 ion in octahedral and trigonal environments.

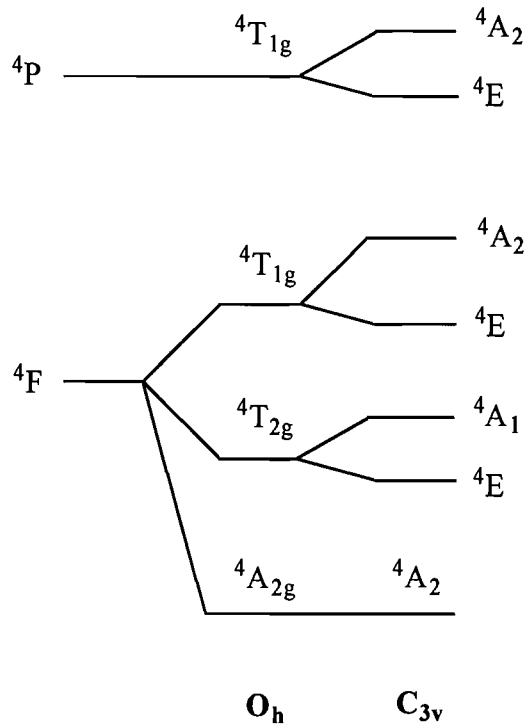

Figure 2.8. Energy level diagram for a d^3 ion in octahedral and trigonal (C_{3v}) environments [8]

The number of spin allowed transitions increases for this reduced symmetry and in theory, splitting of the three bands, resulting from the octahedral symmetry, should be observed. However, in practice the trigonal species only gives two broad bands with no evidence of splitting. These two bands are assigned υ_1 and υ_2 with a possible third band υ_3 usually obscured by more intense charge transfer bands. UV/visible spectra were recorded as either diffuse reflectance (30% $BaSO_4$ in sample) or toluene or CH_2Cl_2 solutions. Both bands υ_1 and υ_2 were observed for all the chromium(III)

complexes studied and from the first transition band υ_1, the ligand field parameter *Dq* was calculated.

It is thought that amongst others, the factors contributing to *Dq* include electrostatic perturbations, the strength of the metal-ligand σ bond and the strength of the metal-ligand π bonding. π donor ligands tend to decrease *Dq* whilst π acceptors result in an increase in *Dq*. For a given metal in a given oxidation state, the magnitude of *Dq* is found to vary with the nature of the ligand.

2.4. Infra-red Spectroscopy

In an infra-red absorption process, a photon of infra-red radiation of frequency ν is absorbed and the molecule or solid is promoted to a higher vibrational state. For this absorption process to occur the energy of the photon must match the separation of vibrational states in the sample.

Infra-red spectroscopy was used extensively in this work to provide evidence for the identity of the products. Principally, the spectra were analysed in the far infra-red region (500-180 cm^{-1}), for the identification of metal-halogen stretching modes and possible structural deductions.

2.4.1. The 500-180 cm^{-1} region (far infra-red region)

In this region, direct metal-ligand vibrations are excited and, in particular, a study of the position and number of metal-halogen vibrations is useful in the assignment of a possible stereochemistry to a complex compound.

In order to find the number of IR active bands to be expected, the reduction formula is applied to the reducible representation of symmetry operations within the molecules.

$$n_i = 1/h \times \Sigma g_i \chi_I \chi_r \qquad \textbf{Equation 2.8 [9]}$$

h = number of operations in the group

g_i = number of symmetry operations in the class

χ_I = character of the irreducible representation

χ_r = character of the reducible representation

For an octahedral complex compound of the type MX_3E_3 (X = Cl, E = S, N, O, P), theory predicts three infra-red active metal-halogen stretches for *mer* isomers ($2A_1 + B_1$) and two for *fac* ($A_1 + E$), based upon local symmetry (Figure 2.9). It is thus possible to distinguish between *fac* and *mer* MX_3E_3 complexes by examination of their low frequency infra-red spectra which should show two or three peaks respectively, attributable to metal-halogen stretching vibrations [9, 10]. In this project, we will go through three different point groups: C_S showing three infra-red active bands (2A' + A"), C_{3V} showing two infra-red active bands ($A_1 + E$) and C_{2V} showing three infra-red active bands ($2A_1 + B_1$).

meridional isomer *facial* isomer

with X = Cl
and E = S-,N-,O-,P-

Figure 2.9. Representation of the *facial* and *meridional* isomers for an octahedral compound of the form ME_3X_3

We should however note that chromium-thioether or chromium-phosphorus stretching modes would also be expected in the far infra-red region and definitive assignments to chromium-chlorine stretches were not possible.

The spectra of the complexes are usually run as Nujol mulls. Unless a good mull is prepared, the metal-halogen bands will be invariably broad and poorly resolved. Their number may not be diagnostic of the stereochemistry of the complex.

2.5. Cyclic Voltammetry

Cyclic voltammetry is a useful tool for studying electrochemical reactions. It is used either to elucidate reaction mechanisms or to carry out quantitative analysis. It is generally applied to evaluate the effects of ligands on the oxidation/reduction potential of the central metal ion in complexes and multinuclear clusters. The technique consists of carrying the electrode potential in a linear fashion between two limits: the initial electrode potential E_i and the final electrode potential E_f [11, 12]. The potential of the working electrode is controlled *versus* a reference electrode such as a saturated calomel electrode (SCE). The controlling potential which is applied across the two electrodes can be considered as an excitation signal.

For a reduction, we usually start from an electrode potential value where no reduction takes place and sweep, on the backward scan, the electrode potential to more negative values [13]:

$$E(t) = E_i - vt \qquad \textbf{Equation 2.9}$$

After reaching the final value, the electrode potential is scanned back to the initial value:

$$E(t) = E_f + vt \qquad \textbf{Equation 2.10}$$

With v, the sweep rate (or scan rate)

It is common practice to report the average of the backward and return peak potentials as the formal reduction potential for the redox couple. For a reversible process, the equilibrium ratio between the concentration of the oxidised and reduced forms at a given potential is given by the Nernst equation:

$$E = E^0 - (RT/nF)\ln([R]/[O])_{x=0} \qquad \textbf{Equation 2.11}$$

With O is the oxidised form and R is the reduced form, *n* the number of electrons transferred per molecule, R is the universal gas constant, T is the Kelvin temperature and F is the Faraday constant.

There are some cases in which the peaks are so widely separated that no parts of the two peaks overlap on the potential axis at all. These are generally known as irreversible systems. A subset of this class are those reactions that yield products that can not be recycled electrochemically to give back the original reactants (*e.g.* loss of substituents to solution). These are chemically irreversible reactions, and many yield no return peak at all [13].

A typical cell usually consists of a glass container with a cap having holes for introducing electrodes and argon. Provision is made for oxygen removal from solution by bubbling with argon gas. The cell is then maintained oxygen free by passing argon over the solution. The reference electrode is typically a saturated calomel electrode. The auxiliary electrode is usually a platinum wire that is placed directly into the solution (Figure 2.10). The cell could also be thermostated for the most exact work.

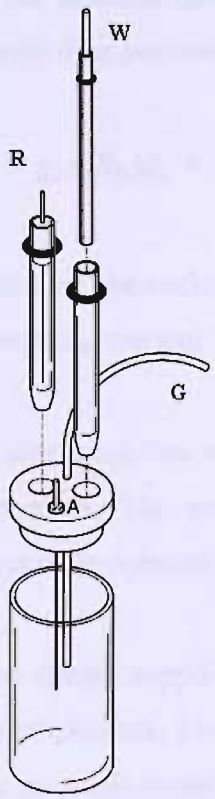

With W = working electrode
R = reference electrode
G = inert gas inlet
A = auxiliary electrode

Figure 2.10. Electrochemical cell for voltammetry

2.6. Electron Paramagnetic Resonance Spectroscopy

Electron paramagnetic resonance (EPR) was first detected by Zavoisky in 1945 [14]. The technique can be applied to species having one or more unpaired electrons. This covers a wide range of substances, including free radicals, biradicals and other triplet states, and many transition metal compounds. EPR is frequently considered to be in the microwave branch of spectroscopy whereas nuclear magnetic resonance (NMR) is usually classified in radiofrequency spectroscopy [15]. The spin of an electron and its associated magnetic moment are the basis of EPR spectroscopy. In the presence of a magnetic field, B_0, a molecule or ion having one unpaired electron has two spin energy levels, given by [16]:

$$E = \boldsymbol{g}\mu_B B_0 M_S \qquad \textbf{Equation 2.12}$$

With μ_B, the Bohr magneton; M_S, the electron spin quantum number (± ½) and $\boldsymbol{g}$ is a proportionality factor, equal to 2.00232 for a free electron [16].

If the electron can interact with a neighbouring nuclear magnetic dipole, the energy levels then become [16]:

$$E = \boldsymbol{g}\mu_B B_0 M_S + a M_S m_I \qquad \textbf{Equation 2.13}$$

With m_I, the nuclear spin quantum for the neighbouring nucleus and a is the hyperfine coupling constant.

A single nucleus with spin ½ will split each level into two and two transitions can be observed. The energy difference between these two transitions is equal to the hyperfine constant (Figure 2.11).

The energy supplied during an EPR experiment is transferred from the spin system to its neighbours. This process is called spin-lattice relaxation. Relaxation can also occur by spin-spin transfer. If the relaxation time is long, the population of the upper state will increase and the signal will saturate or decrease in intensity. If the relaxation time

is short, as this is the case for transition metal complexes, then by the Uncertainty Principle the resonance lines must be wide and measuring at low temperature could allow the observation of a spectrum.

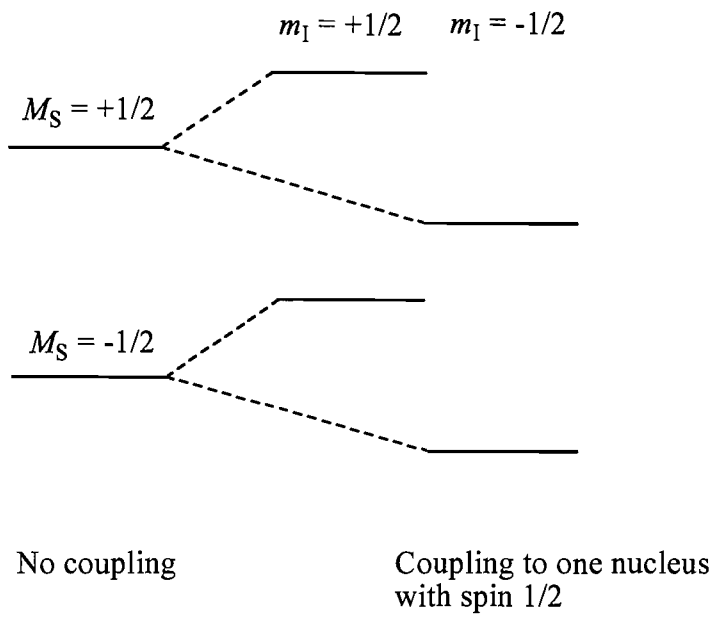

Figure 2.11. Energy levels and transitions for a single unpaired electron in an external magnetic field [16]

For transition metal compounds spin-orbit coupling and zero-field splitting can lead to major variations in ***g*** values. Using appropriate frequencies for the study of the transitions between energy levels is required and those usually correspond to 9.4 GHz (X-band), 24.0 GHz (K-band) or 34.0 GHz (Q-band).

2.6.1. Quartet States and Cr^{3+} in an Octahedral Field, ^4F, L = 3, S = 3/2 [17, 18]

An ion with three unpaired electrons and a total spin S = 3/2 is said to be in a quartet state, with four components in which the M_S quantum number is allowed to take the values Ms = +3/2, +1/2, -1/2, -3/2. However, these four states are not usually degenerate, even in zero-field. The principal mechanism of the splitting involves spin-orbit coupling combined with deviations from regular symmetry, and the EPR spectra can usually be interpreted in terms of the spin Hamiltonian:

$$\mathcal{H} = \beta H \,.\, \boldsymbol{g} \,.\, \hat{S} + D(\hat{S}_z^2 - 5/4) + E(\hat{S}_x^2 - \hat{S}_y^2) \qquad \textbf{Equation 2.14}$$

With E = 0 if the ion is axially symmetric.

There are three allowed $\Delta M_S = \pm 1$ transitions, and provided the zero-field splitting is not too large, three absorption bands are observable. If the zero-field splitting is much greater than the energy *hv*, one transition (+1/2 ↔ +3/2) will not be accessible and another (-1/2 ↔ -3/2) will only be observable in very high magnetic fields. The transition between +1/2 and –1/2 is always seen, no matter how large the zero-field splitting (Figure 2.12). Distorted octahedral Cr(III) complexes usually show small zero-field splittings since the ground electron configuration is t_{2g}^3 and the nearest excited states involve promotion of an electron from the t_{2g} to the e_g. A distortion from octahedral symmetry splits this excited orbital triplet state and the splitting reacts back through the spin-orbit coupling to remove the degeneracy of the ground spin state. The resonance spectrum observed in the ground state is generally that expected for a spin quadruplet, with a ***g*** value close to that of a free electron spin. ***g*** is found to be about 1.98 with a wide resonance line (Figure 2.12).

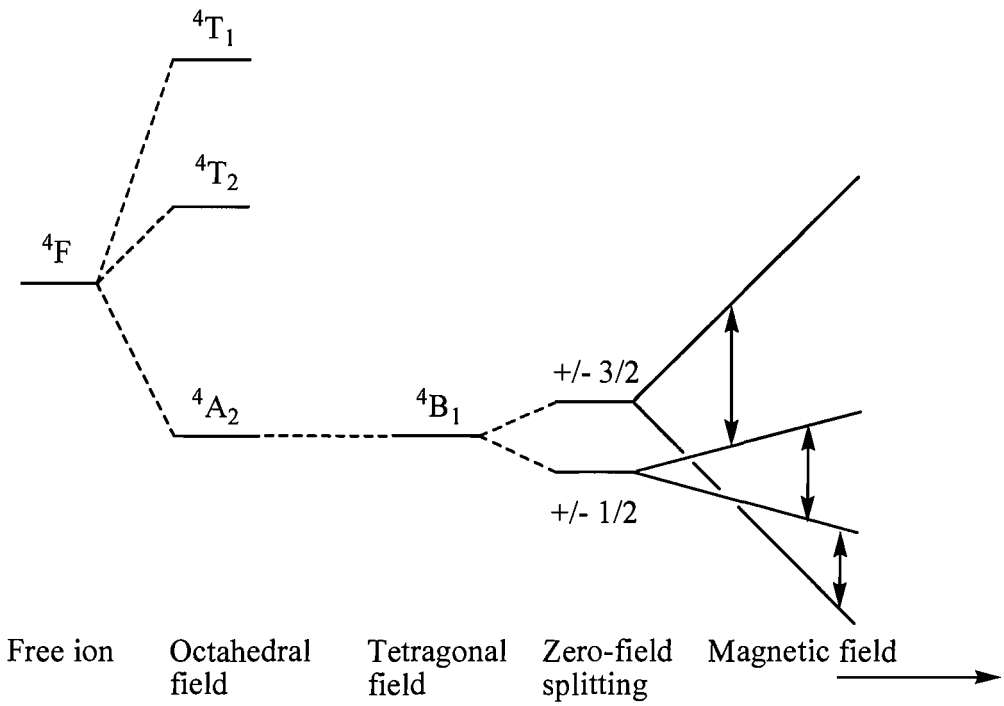

Figure 2.12. Splitting of the ^4F ground state of a d^3 ion by octahedral and tetragonal fields, showing effects of zero-field and magnetic field splittings [16]

2.6.2. Quintet States, Cr^{2+} in an Octahedral Field, ^5D, L = 2, S = 2 [17, 18]

An ion with four unpaired electrons has spin S = 2 and M_S can therefore take the values +2, +1, 0, -1, -2. In fields of low symmetry the degeneracy of these five spin states is completely removed and the resonance spectrum is quite complicated. Since there is an even number of electrons in a d^4 species there is no Kramers' degeneracy for such an ion and resonance absorption may be impossible if the zero-field splitting is large enough, which is usually the case for Cr(II) complexes. Although one of the few salts of this ion in which resonance has been observed is $CrSO_4,5H_2O$, results of Ono, Koide, Sekiyama and Abe in 1954 [19].

2.6.3. Triplet State, Cr^{4+} in an Octahedral Field, ^3F, L = 3, S = 1 [17, 18]

This ion is chemically rather unstable, and there is little experimental information. The spectra for transition metal ions with triplet ground states are invariably interpreted in terms of the spin Hamiltonian (with additional terms involving nuclear spin if necessary).

$$\mathcal{H} = \beta H \,.\, \boldsymbol{g} \,.\, \hat{S} + D(\hat{S}_z^2 - 2/3) + E(\hat{S}_x^2 - \hat{S}_y^2) \qquad \textbf{Equation 2.15}$$

The zero-field splitting in metal ions usually arises because of spin-orbit coupling and in some cases can be too large to permit the observation of electron resonance absorption.

Although the EPR spectra of transition metals can be very difficult to interpret, for the purpose of this work we will only be interested in the ***g*** value of the chromium(III) complexes and in the overall line shape of the spectra. We will moreover assume that a strong and broad signal is expected for Cr(III) ions whereas no signal should be seen for Cr(II) and Cr(IV) species.

2.7. References

1. Corker, J. M.; Evans, J.; Leach, H. and Levason, W.; *J. Chem. Soc., Chem. Commun.*, (1989), 181.
2. Koningsberger, D. C.; Mojet, B. L.; Van Dorssen, G. E. and Ramaker, D. E.; *Topics in Catal.*, (2000), **10**, 143.
3. Koningsberger, D. C. and Prins, R.; *X-ray Absorption, Principles, Application, Techniques of EXAFS, SEXAFS and XANES*, (1988), New York, Wiley Interscience.
4. Binsted, N.; Cook, S. L.; Evans, J.; Greaves, G. N. and Price, R. J.; *J. Am. Chem. Soc.*, (1987), **109**, 3669.
5. Binsted, N.; *PAXAS, Program for the Analysis of X-ray Absorption Spectra*, (1988), University of Southampton.
6. Binsted, N.; *EXCURV98*, (1992), SERC Daresbury Laboratory Program.
7. Joyner, R. W.; Martin, K. J. and Meeham, P.; *J. Phys. C: Solid State Phys.*, (1987), **20**, 4005.
8. Lever, A. B. P.; *Inorganic Electronic Spectroscopy, 2nd Edition*, (1984), Amsterdam, Elsevier Science Publisher.
9. Vincent, A.; *Molecular Symmetry and Group Theory*, (1977), London, John Wiley & Sons.
10. Ogden, J. S.; *Introduction to Molecular Symmetry*, (2001), Oxford, Oxford University Press.
11. Mabbott, G. A.; *J. Chem. Educ.*, (1983), **60**, 697.
12. Kissinger, P. T. and Heineman, W. R.; *J. Chem. Educ.*, (1983), **60**, 702.
13. Girault, H. H.; *Analytical and Physical Electrochemistry*, (2004), Lausanne, EPFL Press.
14. Zavoisky, E.; *J. Phys. USSR*, (1945), **9**, 211.
15. Poole, C. P.; *Electron Spin Resonance*, (1967), New York, John Wiley & Sons.
16. Ebsworth, E. A. V.; Rankin, D. W. H. and Cradock, S.; *Structural Methods in Inorganic Chemistry*, (1987), London, Blackwell Scientific Publications.
17. Carrington, A. and McLachlan, A. D.; *Introduction to Magnetic Resonance*, (1969), New York, Harper & Row.

18. Marshall, W. and Wilkinson, D. H.; *Electron Paramagnetic Resonance of Transition Ions*, (1970), Oxford, Clarendon Press.

19. Ono, K.; Koide, S.; Sekiyama, H. and Abe, H.; *Phys. Rev.*, (1954), **96**, 38.

Chapter 3

Homogeneous Chromium Catalysed Trimerisation of Ethylene with $[CrCl_3\{HN(CH_2CH_2SC_{10}H_{21})_2\}]$: Effect of Ligand Structure, Metal Oxidation State and Role of Activator on Catalysis

3.1. Introduction

Ethylene oligomerisation and polymerisation have been the subject of many studies over the past decade [1-5]. Increasing interest has been focused on the development of homogeneous transition metal catalysts. The conventional oligomerisation of ethylene typically leads to a broad range of linear α-olefins (C_6-C_{20}); catalytic systems that are selective for specific desirable alkenes would be of great interest. Linear α-olefins such as 1-hexene and 1-octene are used, amongst other applications, as co-monomers in the production of linear low-density polyethylene (LLDPE). The trimerisation route largely avoids the production of undesired olefins that usual olefin oligomerisation processes produce. Of the systems known to trimerise ethylene, the majority are based on chromium catalysts, although several catalysts are based on titanium [6, 7] and tantalum [8]. Along with complexes of neutral phosphorus containing ligands of the type $Ar_2PN(Me)PAr_2$ (Ar = *o*-methoxy-substituted aryl group) [9, 10], pyrrolyl-Cr complexes appeared to be among the most successful Cr-based systems to trimerise ethylene [11]. Neutral tridentate NNN ligands have also been used for the trimerisation of some α-olefins [4, 12, 13] (Figure 3.1).

Moreover, chromium(III) complexes of tridentate PNP-donor ligands (Figure 3.1) have been studied and evaluated as catalysts for ethylene trimerisation, with several giving high activity and excellent selectivity towards 1-hexene when activated with MAO [14].

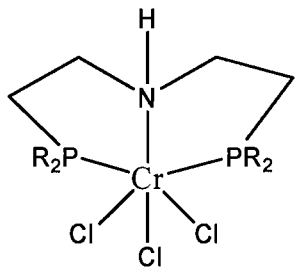

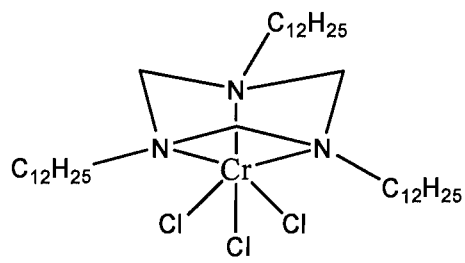

with R = phenyl, cyclohexyl, ethyl

Figure 3.1. Selected examples of homogeneous chromium-based polymerisation catalyst precursors [3, 14]

A number of mechanistic studies point towards a mechanism involving metallacycle formation and growth for the ethylene trimerisation reaction [1, 15, 16]. The generally accepted metallacycle for selective trimerisation of ethylene is shown in the Scheme 3.1[17]:

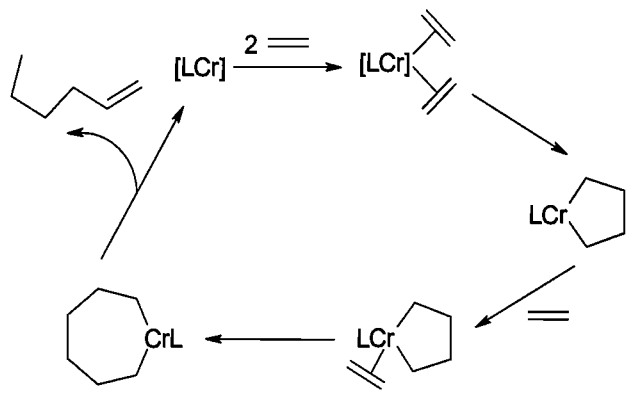

Scheme 3.1. Proposed catalytic cycle for the trimerisation of ethylene to 1-hexene

The mechanism involves oxidative coupling of two ethylene molecules to the metal, followed by insertion of another to yield a metallacycloheptane, although conclusive experimental evidence for this is limited. Jolly has isolated a chromacycloheptane species that liberates 1-hexene upon thermolysis [18]. Following the same idea, Bercaw used deuterium-labelled ethylene to probe this mechanism, while the exact nature of the active catalytic species remains unknown [19].

The application of thioether sulfur based ligands in homogeneous catalysis has recently been reviewed with McGuinness and co-workers reporting the use of a mixed donor ligand $HN(CH_2CH_2SR)_2$ (R = Me, Et, ^{n}Bu, ^{n}decyl) which, when reacted with $[CrCl_3(THF)_3]$ and activated with MAO, gives rise to a highly active and selective catalyst for the trimerisation of ethylene to 1-hexene [20, 21]. The complex of $HN(CH_2CH_2SC_{10}H_{21})_2$ appeared to be the best catalyst for the trimerisation reaction. Requiring only mild temperature and ethylene pressure (90°C and 30-50 bar), the activated catalyst could achieve high activity in the presence of a relatively low amount of MAO (30-100 molar equivalents). These results may be partly due to the enhanced solubility of the complex in toluene that the longer alkyl chain affords. Trimerisation pre-catalysts of the SNS ligand have previously been based on Cr(III), due mainly to the ready availability of the complex precursor, $[CrCl_3(THF)_3]$. It is

however possible that this oxidation state is not maintained during the activation with MAO and a reduction to lower oxidation state or oxidation to higher oxidation state may be envisaged. In order to study the effects of starting from a lower oxidation state, a Cr(II) complex, $[CrCl_2\{HN(CH_2CH_2S^tBu)_2\}]$ was prepared and tested for catalysis. The Cr(II) complex showed broadly similar activity to that obtained with the Cr(III) analogue, although the selectivity towards C_6 was somewhat lower. Assuming that MAO does not oxidise the Cr(II) precatalyst, this suggests that, during activation, the Cr(III) complex is reduced to an oxidation state of II or lower [21].

It has also been shown from this study that a secondary amine donor is essential to activity and it is thought that during activation, the ligand is deprotonated, yielding a monoanionic species. Evidence for the deprotonation has been presented by observing the disappearance of the strong N-H band at 3182 cm^{-1}, in a characteristic region of the N-H stretching mode, after treatment of $[CrCl_3\{HN(CH_2CH_2SC_{10}H_{21})_2\}]$ with the better defined (than MAO) base $LiCH_2SiMe_3$ (Figure 3.2). It has been proposed that MAO or Me_3Al act in the same way and deprotonate the secondary amine from the ligand.

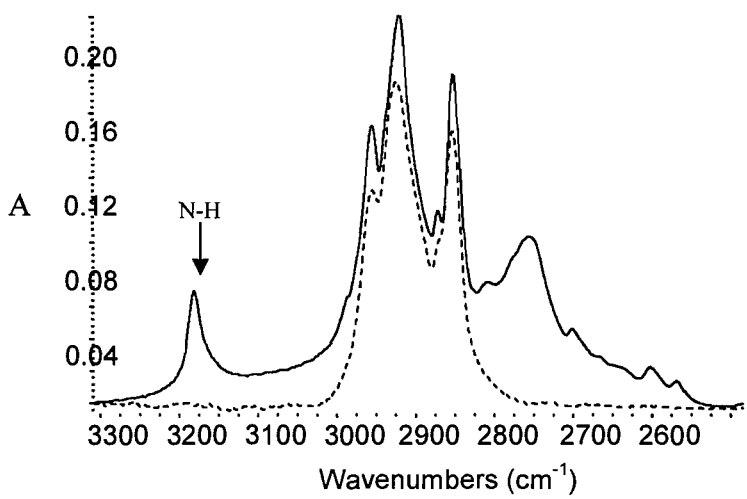

Figure 3.2. Infra-red absorbance spectrum (KBr disk) in the v(NH) region of $[CrCl_3\{HN(CH_2CH_2SC_{10}H_{21})_2\}]$ before (—) and after (---) treatment with $LiCH_2SiMe_3$ [21]

Given the above evidence, two possible mechanisms for the trimerisation could be envisaged. A cycle made up of the formal oxidation state Cr(I)→Cr(III) [22],

involving neutral species, or the couple Cr(II)→Cr(IV) [23, 24] which would necessitate formally cationic active species (Scheme 3.2).

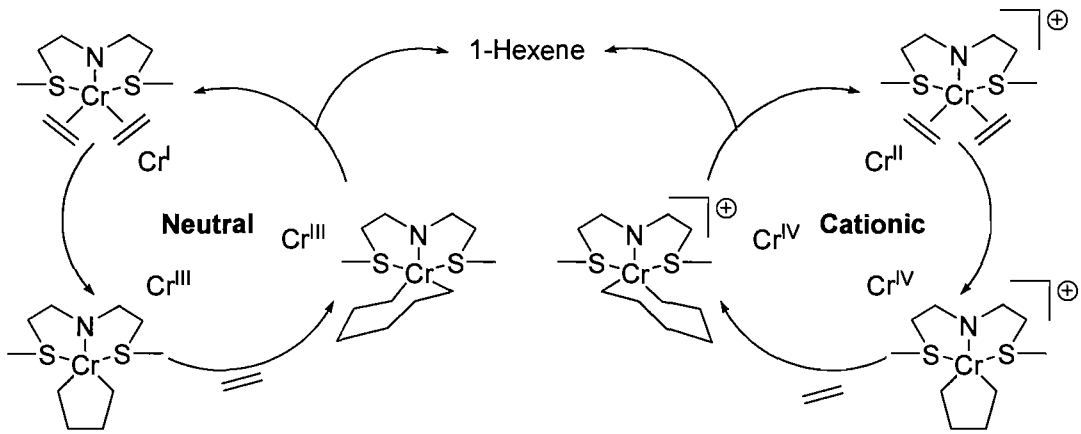

Scheme 3.2. Possible mechanistic cycles with $[CrCl_3\{HN(CH_2CH_2SC_{10}H_{21})_2\}]$: Neutral (Cr(I)→Cr(III)) and Cationic (Cr(II)→Cr(IV)) [21]

McGuinness' work on the SNS-donor system led to an interesting suggestion. The complex can be activated with $AlEt_3$ followed by treatment with the alkyl abstracting agent $B(C_6F_5)_3$, suggesting that a formally cationic active species is responsible for the trimerisation of ethylene to 1-hexene. This suggests a Cr(II)-Cr(IV) mechanistic cycle. The roles of the MAO are then to deprotonate the secondary amine, reduce the metal centre and facilitate cation generation. However, there are little direct evidence to support these conclusions and the involvement of a couple Cr(II)/Cr(IV) is still only a suggestion for the trimerisation mechanism.

3.2. Aims

In this chapter, the chromium(III) complex $[CrCl_3\{HN(CH_2CH_2SC_{10}H_{21})_2\}]$ is synthesised and characterised using a wide range of techniques such as IR and UV/visible spectroscopy, cyclic voltammetry and chromium K-edge studies. Since MAO is not a single chemical entity, its role in the catalytic process is difficult to establish with precision hence, the reaction of the complex $[CrCl_3\{HN(CH_2CH_2SC_{10}H_{21})_2\}]$ with the well defined aluminium reagent Me_3Al is investigated using UV/visible and EPR spectroscopy. The structure of the activated species is studied *via* EXAFS measurements to validate or otherwise outline the structures of the first steps of the "accepted" reaction mechanism scheme (Scheme 3.1). The second part of the chapter is dedicated to the use of additional co-catalyst for the trimerisation of ethylene to 1-hexene. Similar studies (UV/visible, EPR and EXAFS) are applied to study the catalytic system composed of a toluene solution of the complex $[CrCl_3\{HN(CH_2CH_2SC_{10}H_{21})_2\}]$ treated with the aluminium reagent and in the presence of a co-catalyst. Finally, analysis of XANES spectra gives information regarding the oxidation state of the chromium metal centre in the active species.

3.3. Results and Discussion

3.3.1. Synthesis of the Ligand $HN(CH_2CH_2SC_{10}H_{21})_2$

The tridentate ligand $HN(CH_2CH_2SC_{10}H_{21})_2$, hereafter referred as the SNS ligand, was synthesised *via* literature procedures [25] (Scheme 3.3). The preparation consisted of adding a solution of NaOH and decanethiol to a solution of bis(2-chloroethyl)amine hydrochloride in ethanol at 0°C. After stirring for two hours at room temperature, the white solid was filtered off and the filtrate evaporated to dryness. The residue was taken up in diethyl ether and, after evaporation of the solvent, the product was obtained as a yellow oil (yield 76%). The obtained compound was characterised by spectroscopic methods and elemental analysis. From the ^1H NMR spectrum, five different signals can be identified with resonances at δ 0.87 (6H, t, $C\underline{H}_3C_9H_{18}$), 1.25-1.4 (28H, m, $CH_3C_7\underline{H}_{14}C_2H_4S$), 1.52-1.63 (4H, m, $C_8H_{17}C\underline{H}_2CH_2S$), 2.5 (4H, t, $C_9H_{19}C\underline{H}_2S$), 2.6 (4H, t, $C_{10}H_{21}SC\underline{H}_2$), 2.81 (4H, t, $C\underline{H}_2N$) ppm. $^{13}C\{^1H\}$ NMR spectrum shows ten signals out of the twelve expected at 14.1 ($\underline{C}H_3C_9H_{18}S$), 22.6, 28.9, 29.2, 29.5, 29.7, 31.9, 32.1, 32.4 ($CH_3\underline{C}_9H_{18}S\underline{C}H_2$), 48.4 ($\underline{C}H_2N$) ppm. Evidence of the nature of the ligand has been probed by mass spectrometry with a *m/z* value of 418 corresponding to $(HN(CH_2CH_2SC_{10}H_{21})_2 + H)^+$. An infra-red spectrum was recorded and showed the N-H stretching at 3301 cm^{-1}. Elemental analysis confirmed the purity of the desired ligand.

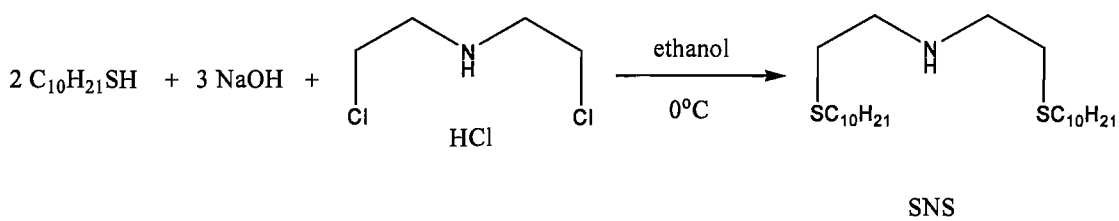

Scheme 3.3. Synthesis of $HN(CH_2CH_2SC_{10}H_{21})_2$

3.3.2. Synthesis of the Chromium(III) Complex $[CrCl_3\{HN(CH_2CH_2SC_{10}H_{21})_2\}]$

The distorted octahedral $[CrCl_3\{HN(CH_2CH_2SC_{10}H_{21})_2\}]$ complex, hereafter referred as the $[CrCl_3\{SNS\}]$ complex, was prepared by reaction of $[CrCl_3(THF)_3]$ [26] with one molar equivalent of the SNS ligand in anhydrous CH_2Cl_2 [27]. The product was isolated as a green solid after evaporation of the solvent to dryness (Scheme 3.4). It has been found that in order to promote coordination through the S- and N-donor atoms it was necessary to remove the THF from the reaction mixture, otherwise the harder O-donor ligand tends to compete for coordination [28]. Table 3.1 summarises the elemental analysis data supporting the nature of the complex synthesised.

$$[CrCl_3(THF)_3] + SNS \xrightarrow[-\ 3\ THF]{CH_2Cl_2} [CrCl_3\{SNS\}]$$

Scheme 3.4. Synthesis of $[CrCl_3\{HN(CH_2CH_2SC_{10}H_{21})_2\}]$

	Elemental Analysis		Exp. (theor.)
Complex	% C	% H	% N
$[CrCl_3\{SNS\}]$	49.93 (50.03)	8.87 (8.92)	2.37 (2.43)

Table 3.1. Elemental analysis data for $[CrCl_3\{SNS\}]$

3.3.3. Characterisation of the $[CrCl_3\{SNS\}]$ Complex

3.3.3.1. UV/visible and Infra-red Spectroscopy

An octahedral d^3 system is expected to exhibit three quartet excited states and show three spin-allowed *d-d* transitions in a UV/visible spectrum: $^4A_{2g} \rightarrow {}^4T_{2g}$ (υ_1); $^4A_{2g} \rightarrow {}^4T_{1g}$ (F) (υ_2); $^4A_{2g} \rightarrow {}^4T_{1g}$ (P) (υ_3) [29]. However, the last of these is usually obscured due to a more intense ligand-metal charge transfer band. The UV/visible spectrum of $[CrCl_3\{SNS\}]$ in toluene solution is displayed in Figure 3.3 and the spectroscopic data are presented in Table 3.2. From the spectra the ligand-field

splitting *Dq* is obtained directly from υ_1. The complex [$CrCl_3${SNS}] exhibits a *Dq* value of 1 520 cm^{-1}. Literature reports *Dq* values of 1 433 cm^{-1} for [$CrCl_3${[9]aneS_3}] [30], 1 449 cm^{-1} for [$CrCl_3${$S(CH_3)_2$}$_3$] [31]. Chapter 6 reports values for [$CrCl_3${$S(CH_2CH_2SC_{10}H_{21})_2$}] where *Dq* = 1 430 cm^{-1} and [$CrCl_3${$O(CH_2CH_2SC_{10}H_{21})_2$}] where *Dq* = 1 390 cm^{-1}. The value obtained for [$CrCl_3${SNS}] here is slightly higher than the value expected for similar chromium(III) complexes studied but the difference is not statistically significant. We can however note that the presence of a nitrogen atom in the mixed donor SNS increases the ligand-field splitting term.

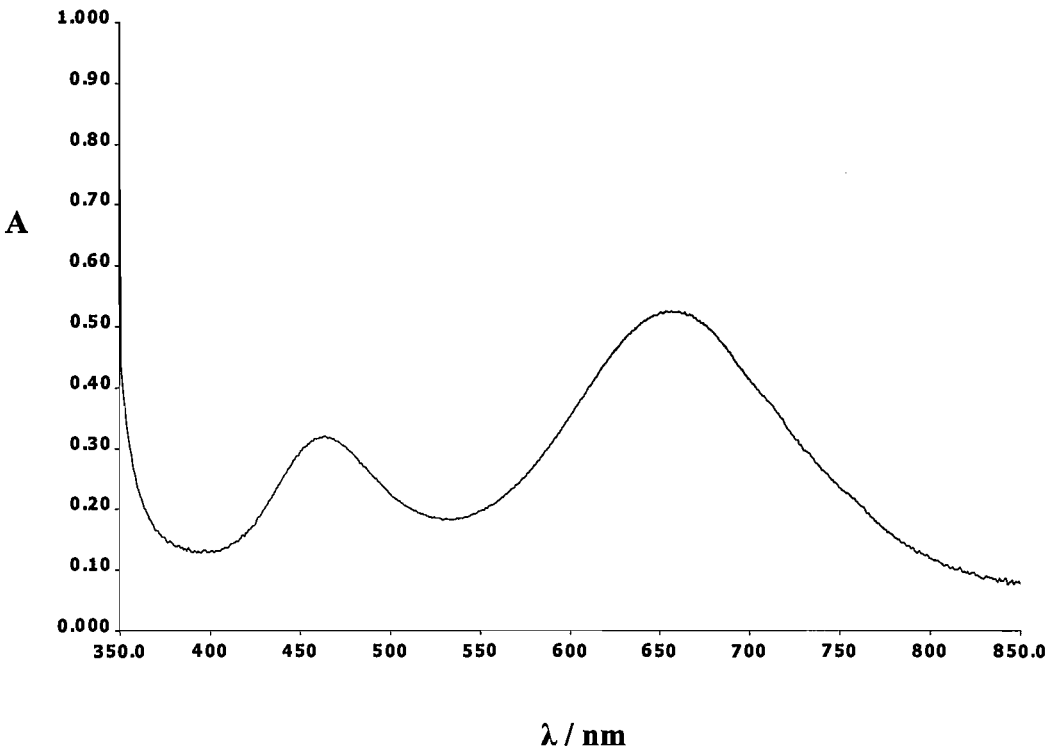

Figure 3.3. UV/visible spectrum for a 5 mM toluene solution of [$CrCl_3${SNS}]

Evidence of the coordination of the ligand to the metal centre however can be confirmed by the shift of the N-H stretching peak to 3191 cm^{-1}. The extensive literature on chromium complexes shows that usually one isomer is preferred [32]. It is instructive to compare the ligand bonding parameters of [$CrCl_3${SNS}] with those of the closely related trimerisation catalysts [$CrCl_3${$HN(CH_2CH_2SC_2H_5)_2$}] [33] and [$CrCl_3${$HN(CH_2CH_2PPh_2)_2$}] [14] where X-ray structures are available. In both complexes, the chromium centre displays the expected octahedral coordination

geometry, with the tridentate ligand coordinated in a *meridional* fashion. The properties of those complexes allow us to suggest the *meridional* geometry of the [$CrCl_3${SNS}] complex. The point group theory predicts three infra-red active bands for the *meridional* [$CrCl_3${SNS}] (C_{2V}). The infra-red spectrum of the chromium(III) complex [$CrCl_3${SNS}] exhibits three peaks at 348, 335 and 324 cm^{-1} which might be assigned tentatively to the Cr-Cl stretching mode (Table 3.2). Given that in some cases these peaks are rather weak, and the Cr-S stretching modes are also expected in this region, definitive assignments are not possible.

Complex	υ_1/cm^{-1}	υ_2/cm^{-1}	Dq/cm^{-1}	ε_1, $\varepsilon_2/dm^3.mol^{-1}.cm^{-1}$	v (Cr-Cl)/cm^{-1}
[$CrCl_3${SNS}]	15,270	21,600	1 520	212, 136	348, 335, 324

UV/visible spectra recorded in toluene solution. Infra-red spectra recorded as nujol mulls

Table 3.2. Spectroscopic data for [$CrCl_3${SNS}]

3.3.3.2. Cyclic Voltammetry for the [$CrCl_3${SNS}] Complex

A cyclic voltammogram was recorded to investigate the oxidation/reduction properties of the [$CrCl_3${SNS}] complex (Figure 3.4). Cyclic voltammetry (CV) is a useful technique to evaluate the effects of ligands on the oxidation/reduction potential of the central metal ion. The effectiveness of CV results from its capability for rapidly observing the redox behaviour over a wide potential range [34, 35]. Electrochemical data were recorded at room temperature under an N_2 atmosphere and with a scan rate of 100 mV/s over a range of 1.5 to -1.5V. A 0.2 M [Bu^n_4N]BF_4 electrolyte in anhydrous CH_2Cl_2 was employed with a double platinum working and counter electrode and a standard calomel electrode. Table 3.3 summarises the potential obtained for [$CrCl_3${SNS}] along with two similar chromium(III) complexes (Chapter 5) to allow a comparison.

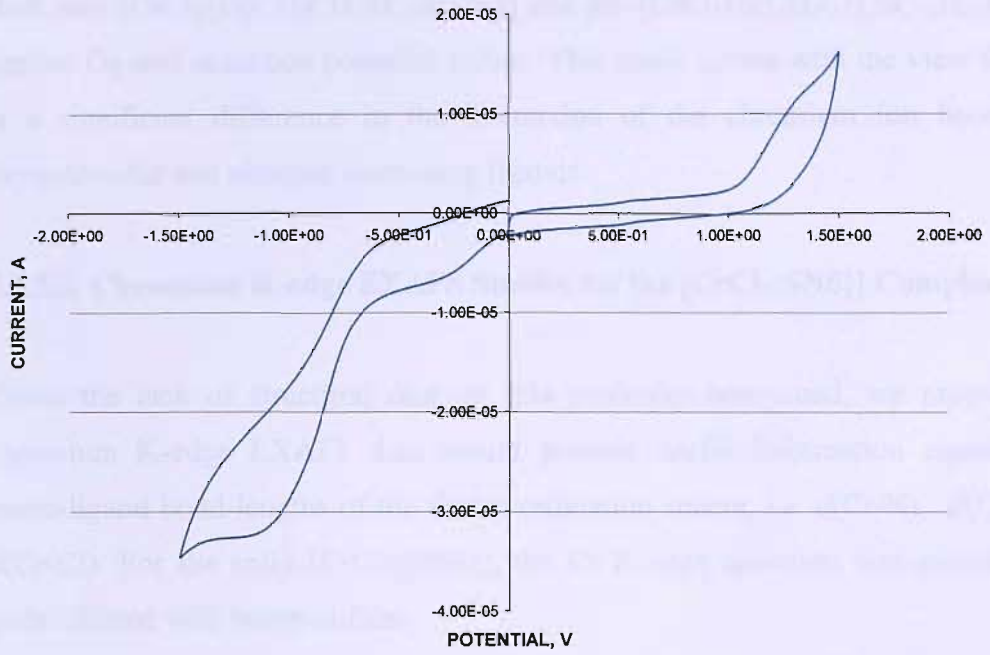

Figure 3.4. Cyclic voltammogram for $[CrCl_3\{SNS\}]$ in 0.2 M $[Bu^n_4N]BF_4$ in CH_2Cl_2, scan rate = 100 mV/s

Complex	E_{PC} *vs* ferrocene/ferrocenium (V)	Dq/cm^{-1}
$[CrCl_3\{HN(CH_2CH_2SC_{10}H_{21})_2\}]$	-1.77	1 520
$[CrCl_3\{O(CH_2CH_2SC_{10}H_{21})_2\}]$	-1.25	1 390
$[CrCl_3\{S(CH_2CH_2SC_{10}H_{21})_2\}]$	-1.28	1 430

Table 3.3. Electrochemical data and *Dq* values for the $[CrCl_3\{SNS\}]$ complex and for similar chromium(III) complexes in 0.2 M $[Bu^n_4N]BF_4$ in CH_2Cl_2, scan rate = 100 mV/s , E_{PC} = reduction potential

The chromium (III) complex $[CrCl_3\{SNS\}]$ showed only an irreversible reduction process (Figure 3.4). The reduction is ill defined. This could be due to a slow structural rearrangement in the complex in comparison to the electron kinetics of the reaction or an irreversible loss of chlorine atoms. Of note are the reduction potential values of the three compounds *mer*-$[CrCl_3\{HN(CH_2CH_2SC_{10}H_{21})_2\}]$, *mer*-$[CrCl_3\{O(CH_2CH_2SC_{10}H_{21})_2\}]$ and *fac*-$[CrCl_3\{S(CH_2CH_2SC_{10}H_{21})_2\}]$, complexes that differ by only one heteroatom (nitrogen, oxygen or sulfur) as mentioned before. The difference in reduction potential mirrors the difference in *Dq*.

Both *mer*-[$CrCl_3\{O(CH_2CH_2SC_{10}H_{21})_2\}$] and *fac*-[$CrCl_3\{S(CH_2CH_2SC_{10}H_{21})_2\}$] have similar *Dq* and reduction potential values. This result agrees with the view that there is a significant difference in the interaction of the chromium ion between the oxygen/sulfur and nitrogen containing ligands.

3.3.3.3. Chromium K-edge EXAFS Studies for the [$CrCl_3\{SNS\}$] Complex

Given the lack of structural data on this particular compound, we proposed that chromium K-edge EXAFS data would provide useful information regarding the metal-ligand bond lengths of the first coordination sphere, *i.e.* *d*(Cr-N), *d*(Cr-S) and *d*(Cr-Cl). For the solid [$CrCl_3\{SNS\}$], the Cr K-edge spectrum was recorded on a pellet diluted with boron nitride.

Figure 3.5 depicts the raw and theoretical EXAFS data for the solid [$CrCl_3\{HN(CH_2CH_2SC_{10}H_{21})_2\}$]. The theory fits the $k^3.\chi\ (k)$, Fourier transform and sine transform well (FI = 7.2) to a simple model of three shells. The model proposed has refined coordination numbers close to the expected values of one nitrogen, three chlorine and two sulfur atoms with 0.8, 2.8 and 1.9 atoms respectively. The model proposed gives us *d*(Cr-N) = 2.15(2), *d*(Cr-Cl) = 2.27(4) and *d*(Cr-S) = 2.41(6) Å. The bond lengths (within the errors) are similar to X-ray crystallography data available in the literature for similar compounds. A crystal structure for the chromium(III) complex [$CrCl_3\{HN(CH_2CH_2SC_2H_5)_2\}$] reports Cr-S distances of 2.4508(7) and 2.4556(7) Å, Cr-Cl distances of 2.2985(8) and 2.3167(7) Å and a Cr-N distance of 2.1059(18) Å [33]. The Debye-Waller terms give sensible values even if the chromium-sulfur and chromium-chlorine shells are difficult to distinguish due to their similar backscattering amplitudes. The chromium(III) complex displays the expected octahedral coordination geometry, with the tridentate ligand coordinated in a *meridional* fashion [14, 33].

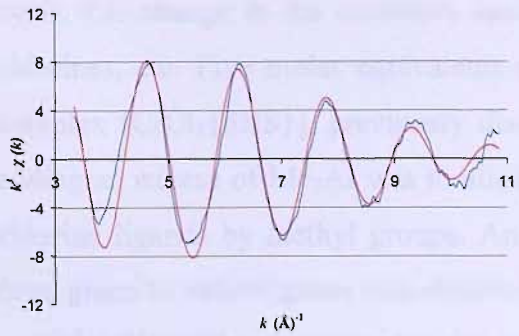

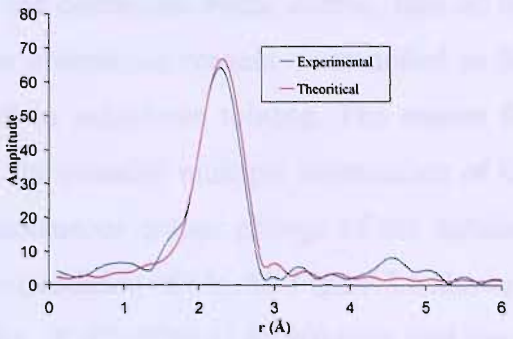

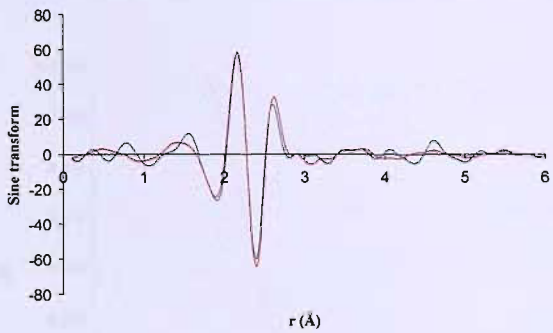

Ef = -7.4(6) eV

R = 23.9 %

Atom	C.N.	R / Å	$2\sigma^2$ / Å^2
N	0.8(7)	2.15(2)	0.015(5)
Cl	2.8(4)	2.27(4)	0.014(1)
S	1.9(3)	2.41(6)	0.005(9)

Figure 3.5. The chromium K-edge k^3-weighted EXAFS, Fourier transform and sine transform for a solid pellet of [$CrCl_3${SNS}] / boron nitride

3.3.4. Study of the [$CrCl_3${SNS}] Complex Activated by Addition of Me_3Al

3.3.4.1. UV/visible Studies

Recent papers report that a change in the oxidation state of the chromium metal centre occurs upon treatment with an aluminium reagent [20, 21]. In an attempt to investigate the nature of the active catalyst it was decided to probe the catalytic species present in solution after addition of Me_3Al by UV/visible spectroscopy. It was anticipated that this reaction between the complex and the aluminium reagent will lead to a better understanding of what is occurring in the first stages of the catalytic

cycle, *i.e.* change in the oxidation state of the chromium metal centre, loss of the chlorines, etc. Five molar equivalents of the aluminium reagent were added to the complex [$CrCl_3${SNS}], previously dissolved in anhydrous toluene. The reason for adding an excess of Me_3Al was to allow for the possible multiple substitution of the chlorine ligands by methyl groups. An instantaneous colour change of the solution from green to yellow/green was observed upon addition of Me_3Al. Figure 3.6 shows a typical UV/visible spectrum for the complex [$CrCl_3${SNS}] in solution and upon activation with five molar equivalents of Me_3Al.

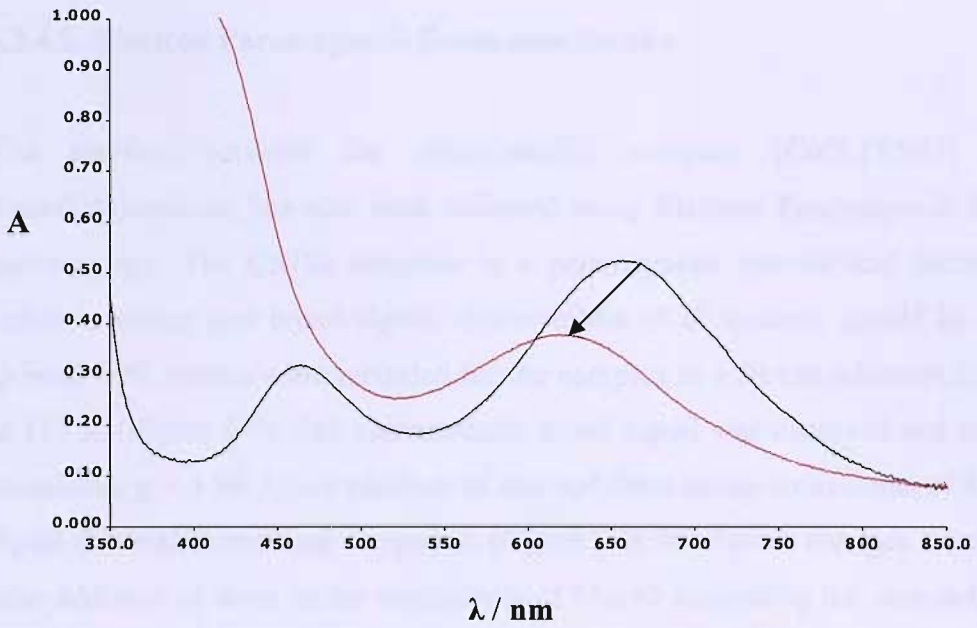

Figure 3.6. UV/visible spectra of a 5 mM toluene solution of [$CrCl_3${SNS}] before (black) and after (red) treatment with 5 molar equivalents of Me_3Al

It is clear that a considerable change is observed in the UV/visible spectrum upon addition of the aluminium reagent. After activation, only one transition is observed and at a different energy (Table 3.4). Either a blue shift is occurring and the peak corresponding to υ_2 is obscured by the charge transfer bands or a change in oxidation state is occurring, leading to a different electronic configuration of the chromium centre hence a different UV/visible spectrum. From a mechanistic point of view, UV/visible spectra displaying a blue-shift are consistent with a ligand exchange of chlorine(s) with methyl groups. Moreover, it is more likely that a change in the

oxidation state occurs upon addition of Me_3Al and in order to have a confirmation of this change, it was decided to investigate the reaction using EPR spectroscopy.

Complex	$\upsilon_1{}^a/cm^{-1}$	$\upsilon_1{}^b/cm^{-1}$
$[CrCl_3\{SNS\}]$	15,270	16,180

Table 3.4. Spectroscopic data for a 5 mM toluene solution of $[CrCl_3\{SNS\}]$ compound [a]before, [b]after treatment with Me_3Al

3.3.4.2. Electron Paramagnetic Resonance Studies

The reaction between the chromium(III) complex $[CrCl_3\{SNS\}]$ and the trimethylaluminum has also been followed using Electron Paramagnetic Resonance spectroscopy. The Cr(III) complex is a paramagnetic species and therefore EPR active; a strong and broad signal, characteristic of d^3 systems should be observed. Q-band EPR spectra were recorded for the complex in a frozen toluene/CH_2Cl_2 glass at 115 K (Figure 3.7). The characteristic broad signal was observed and the g value calculated, $g = 1.99$. Upon addition of one and three molar equivalents of Me_3Al, the signal diminishes and then disappears (Figure 3.6). No further changes are observable after addition of three molar equivalents of Me_3Al suggesting the completion of the reaction. The disappearance of the signal is indicative of a change in the oxidation state of the chromium metal from Cr(III), paramagnetic and EPR active, to Cr(II) or Cr(IV), EPR inactive. The g value of 1.99 stays the same throughout the reaction process indicating that the initial chromium(III) species is gradually oxidised to Cr(IV) or reduced to Cr(II). Thus, these changes, together with the UV/visible spectroscopic data, provide strong evidence for a change in oxidation state upon addition of Me_3Al to $[CrCl_3\{SNS\}]$ in toluene solution.

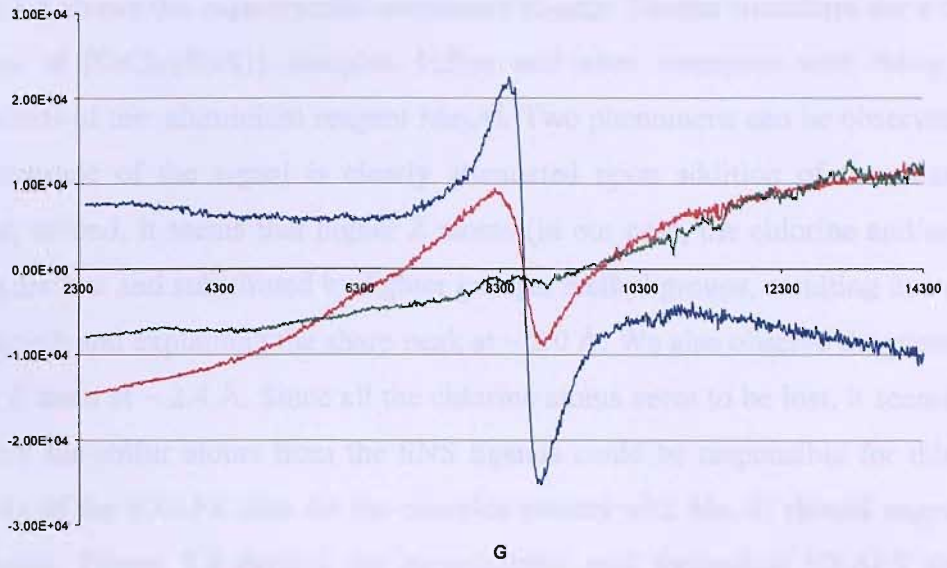

Figure 3.7. EPR spectra of $[CrCl_3\{SNS\}]$ in toluene/CH_2Cl_2 (blue line) treated with 1 molar equivalent of Me_3Al (red) and with 3 molar equivalents of Me_3Al (green), g = 1.99; recorded as a frozen glass at T = 115 K

In order to probe further changes occurring upon addition of Me_3Al to $[CrCl_3\{SNS\}]$ and to obtain structural data on the resulting chromium species, it was decided to follow the reaction using X-ray absorption spectroscopy.

3.3.4.3. Chromium K-edge EXAFS Studies – $[CrCl_3\{SNS\}]$ upon Treatment with Me_3Al

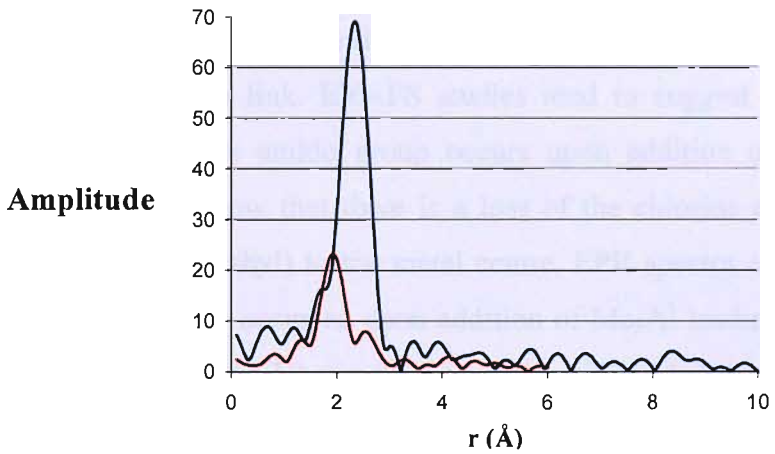

Figure 3.8. The chromium K-edge Fourier transform for a 5 mM toluene solution of $[CrCl_3\{SNS\}]$; before (blue) and after treatment with Me_3Al (red)

Figure 3.8 shows the experimental chromium K-edge Fourier transform for a toluene solution of [$CrCl_3${SNS}] complex before and after treatment with thirty molar equivalents of the aluminium reagent Me_3Al. Two phenomena can be observed; first, the amplitude of the signal is clearly attenuated upon addition of the aluminium reagent; second, it seems that higher Z atoms (in our case, the chlorine and/or sulfur atoms) are lost and substituted by lighter groups, methyl groups, resulting in a shorter bond length and explaining the sharp peak at ~ 2.0 Å. We also observe the presence of a high Z atom at ~ 2.4 Å. Since all the chlorine atoms seem to be lost, it seems likely that only the sulfur atoms from the SNS ligands could be responsible for this peak. Analysis of the EXAFS data for the complex treated with Me_3Al should support this hypothesis. Figure 3.9 depicts the experimental and theoretical EXAFS data for [$CrCl_3${SNS}] treated with an excess of Me_3Al. The model proposed shows a sensible fit with two shells containing 4.0(2) carbon or nitrogen atoms and 0.8(5) sulfur atoms. The atomic radius of a carbon atom and that of a nitrogen atom are in the same range (71 and 73 pm respectively) and therefore can not be readily discriminated within the model. The coordination number of 4.0(2) for the first shell may be interpreted as due to three Cr-C bonds and one Cr-N bond with an average bond length of 2.03(9) Å. We saw above that the X-ray crystal structure of the complex [$CrCl_3${$HN(CH_2CH_2SC_2H_5)_2$}] gave a Cr-N distance of 2.1059(18) Å whereas a Cr-C_{alkyl} bond ranges from 2.042 to 2.151 Å [36, 37].

Based upon all the data obtained from the UV/visible and EPR spectroscopy along with the EXAFS studies, we have evidence of the process occurring when the chromium(III) complex is treated with the aluminium reagent, Me_3Al. The presence of strong bases is known to deprotonate the central nitrogen of the ligand, resulting in a stable Cr-amido link. EXAFS studies tend to suggest that deprotonation of the amine to form the amido group occurs upon addition of Me_3Al. UV/visible and EXAFS results show that there is a loss of the chlorine atoms and coordination of lighter groups (methyl) to the metal centre. EPR spectra confirmed that a change in the oxidation state occurred upon addition of Me_3Al leading to EPR inactive species such as Cr(II) or Cr(IV) species. Having established the deprotonation of the amine, we propose that the species formed is a chromium centre coordinated to three methyl groups, one nitrogen atom *via* a strong double bond and one sulfur atom. Based on these results, it is much more likely to have a Cr(IV) species. Since we have evidence for the retention of the Cr-N bond and the maintenance of one of the Cr-S links it is

likely that the stable amido link anchors the ligand which is also coordinated by one of the two sulfur arms, the affinity of Cr(IV) for thioethers being expected to be low. Figure 3.10 is a representation of the neutral species obtained after activation of the $[CrCl_3\{SNS\}]$ compound by Me_3Al.

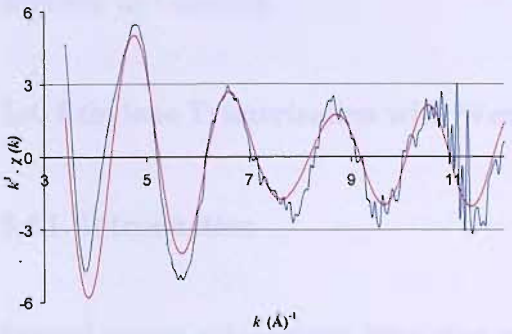

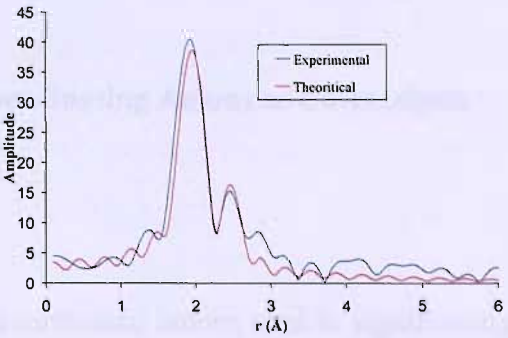

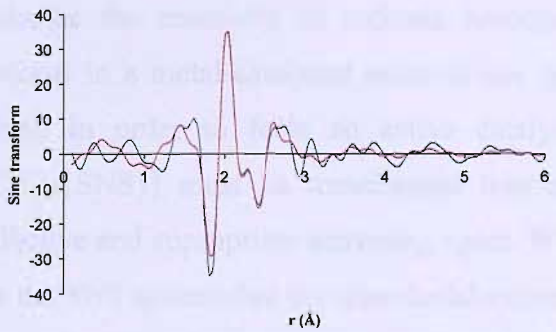

Atom	C.N.	R / Å	$2\sigma^2$ / Å^2
C / N	4.0(2)	2.03(9)	0.008(4)
S	0.8(5)	2.37(8)	0.010(8)

Ef = -5.5(3) eV, R = 36.4 %

Figure 3.9. The chromium K-edge k^3-weighted EXAFS, Fourier transform and sine transform for a 5 mM toluene solution of $[CrCl_3\{SNS\}]$ treated with 30 molar equivalents of Me_3Al

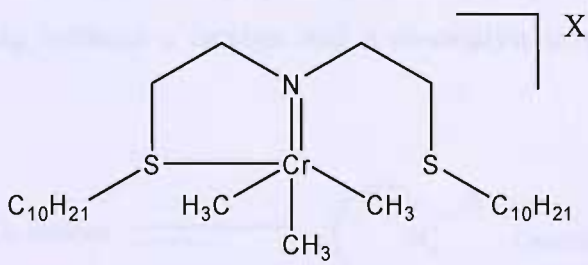

Figure 3.10. Proposed partial structure for the species produced when $[CrCl_3\{SNS\}]$ is treated with an excess of Me_3Al

Spectroscopic techniques provided evidence of a change in the oxidation state of the chromium centre and the retention of the Cr-N bond upon addition of an aluminium reagent. EXAFS studies presumed the presence of a Cr-amido link and confirmed the

presence of three methyl groups and the absence of chlorine atoms, suggesting a substitution of chlorine atoms by methyl groups. A structural model of the species formed after addition of Me_3Al has then been proposed and seems to be one of the first intermediate species involved in the catalytic cycle of the trimerisation of ethylene to 1-hexene.

3.4. Ethylene Trimerisation with Weakly Coordinating Anions as Co-catalysts

3.4.1. Introduction

Several recent publications show that weakly coordinated anions tend to significantly enhance the reactivity of cationic homogeneous catalysts [38-40]. The catalytic process in a metal-catalysed reaction can be analysed and divided into three major steps. In order to form an active catalyst, the catalyst precursor, in our case [$CrCl_3${SNS}] must be transformed into an active catalyst *via* reaction with an effective and appropriate activating agent. We already know from the work performed on the SNS system that the trimethylaluminum reagent is an efficient species for such a reaction. In order to promote a successful activation process, a co-catalyst precursor is required for kinetic/thermodynamic considerations. Finally, the co-catalyst, becoming an anion during the activation process, can play a vital part within the catalytically active cation-anion ion pair and then may significantly influence polymerisation characteristics and polymer properties [40]. Scheme 3.5 depicts the relationship existing between a catalyst and a co-catalyst in metal-catalysed olefin polymerisation.

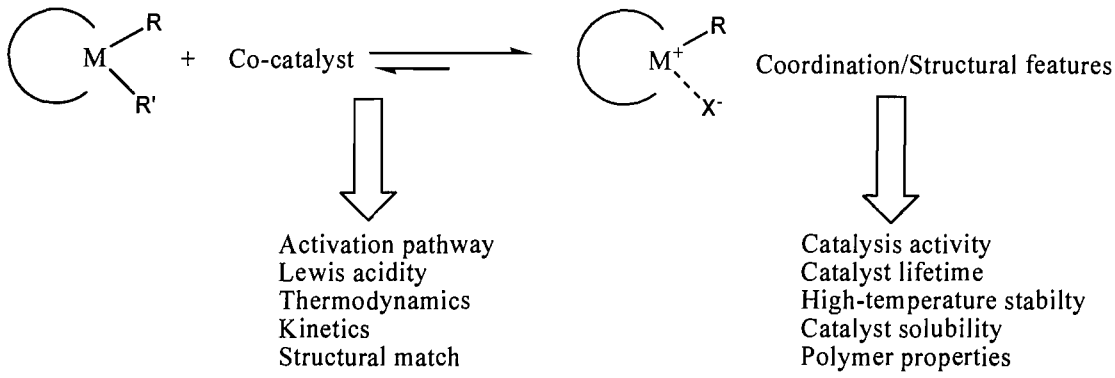

Scheme 3.5. Relationships between catalyst and co-catalyst in metal-catalysed polymerisation [40]

Alkylaluminoxanes, such as MAO, have been known to be active for promoting the polymerisation of monomers since the early 1960s and their role as alkylating agents and Lewis acids has been intensively investigated [40]. Along with MAO, perfluoroaryl boranes (*e.g.* $B(C_6F_5)_3$) appear to be strong Lewis acid, promoting highly efficient olefin polymerisation [40]. The use of the well known alkyl abstracting agents $B(C_6F_5)_3$ and $[Ph_3C][B(C_6F_5)_4]$ in ethylene trimerisation and tetramerisation shows a surprising shift in catalyst properties that these co-catalysts can produce. It has been shown that fluorinated borane and borate co-catalysts, in combination with an alkylating agent, give rise to active trimerisation and tetramerisation. However, productivities are much reduced and a higher proportion of polymer is formed [40]. The choice of the co-catalyst seems to play a relatively important role in the catalytic process. In this project, we have investigated the use of a (*per*-)-fluorinated alkoxy species, $[Ph_3C][Al\{OC(CF_3)_3\}_4]$ [41, 42], and its role in the trimerisation of ethylene to 1-hexene [43].

3.5. Results and Discussion

3.5.1. Synthesis of the Aluminate $[Ph_3C][Al\{OC(CF_3)_3\}_4]$

The aluminate $[Ph_3C][Al\{OC(CF_3)_3\}_4]$, thereafter referred as $[Ph_3C][Al(ORf)_4]$ was synthesised *via* a reported method [41, 42]. The synthesis is a two-step process. The first stage being the preparation of the salt $Li[Al(ORf)_4]$ *via* the reaction between $LiAlH_4$ and the appropriate alcohol $HOC(CF_3)_3$. It has been shown that in order to obtain the lithium aluminate in a relatively good yield, the $LiAlH_4$ needs to be previously purified by dissolution in Et_2O, filtration and removal of all volatiles at 80°C and 5×10^{-3} mbar, until a constant weight is obtained [41]. This purified $LiAlH_4$ was then treated with four molar equivalents of $HOC(CF_3)_3$ by heating the suspension under reflux in anhydrous toluene and under a nitrogen atmosphere (Scheme 3.6).

$$LiAlH_4 + 4\,HOC(CF_3)_3 \xrightarrow[\text{reflux}]{\text{toluene}} Li[Al\{OC(CF_3)_3\}_4] + 4\,H_2$$

Scheme 3.6. Synthesis of $Li[Al\{OC(CF_3)_3\}_4]$ [41]

Scheme 3.7 illustrates the second stage of the process corresponding to the synthesis of the yellow trityl salt $[Ph_3C][Al\{OC(CF_3)_3\}_4]$ [42]. The compound was prepared by addition of Ph_3CCl to one molar equivalent of the lithium salt $Li[Al\{OC(CF_3)_3\}_4]$ in anhydrous CH_2Cl_2. The resulting yellow solid was filtered and washed with anhydrous *n*-pentane. The solid was successfully characterised with spectroscopic methods and elemental analysis.

$$Li[Al\{OC(CF_3)_3\}_4] + Ph_3CCl \xrightarrow{CH_2Cl_2} [Ph_3C][Al\{OC(CF_3)_3\}_4] + LiCl$$

Scheme 3.7. Synthesis of $[Ph_3C][Al\{OC(CF_3)_3\}_4]$ [42]

3.5.2. Catalysis

Table 3.5 shows the results for the trimerisation reaction of ethylene to 1-hexene. Along with one hundred molar equivalents of $AlEt_3$ as activator, one and a half molar equivalent of the aluminate $[Ph_3C][Al(ORf)_4]$ was added to the chromium(III) complex $[CrCl_3\{SNS\}]$ in toluene. After a period of 30 minutes, the catalytic run was stopped and results revealed a high proportion of C_6 (97%) with a selectivity towards 1-C_6 of 99.4%. Results of a similar reported run in the absence of the aluminate and with one hundred molar equivalents of MAO are also presented in the table to allow comparison between the two catalytic systems. Studies [33] showed that the amount of aluminium reagent used along with a co-catalyst has a pronounced effect on productivity.

Complex	T(°C)	C_6(wt %)	1-C_6(wt %)	Productivity[c]	PE (wt %)
$[CrCl_3\{SNS\}]$[a]	80	97	99.4	20 550	0.56
$[CrCl_3\{SNS\}]$[b]	80	97.6	99.7	142 035	0.30

[a] 10 µmol $[CrCl_3\{SNS\}]$, 100 equiv. Et_3Al, 1.5 equiv. aluminate, 100 mL toluene as solvent, 30 min, 45 bars

[b] 12 µmol $[CrCl_3\{SNS\}]$, 100 equiv. MAO, 100 mL toluene as solvent, 30 min, 45 bar [33]

[c] Productivity expressed in g(total product)/g(Cr)

Table 3.5. Ethylene trimerisation

We know from previous studies that ligands with a low steric demand group on the donor atoms lead to the most active catalysts when coordinated to chromium(III) [17]. Catalysis results for the complex treated with MAO in the absence of the aluminate $[Ph_3C][Al(ORf)_4]$ show selectivity towards C_6 of 97.6% of which 99.7% was 1-hexene. This system showed a high activity with a measured productivity of 142 035 g/g(Cr). The recorded run for the same complex treated with Et_3Al and in the presence of the aluminate showed similar results regarding the selectivity towards C_6 (97%) and 1-C_6 (99.4%).

To get better insights of the nature of the active species formed upon addition of an aluminium reagent, Me_3Al, along with $[Ph_3C][Al(ORf)_4]$, spectroscopic methods (UV/visible, EPR and EXAFS) were employed.

3.5.3. Study of $[CrCl_3\{SNS\}]$ Complex Treated with Me_3Al and $[Ph_3C][Al(ORf)_4]$

3.5.3.1. UV/visible Studies

The reaction between the complex $[CrCl_3\{SNS\}]$ (5 mM toluene solution), the aluminium reagent Me_3Al and one molar equivalent of the aluminate $[Ph_3C][Al(ORf)_4]$ has been followed by UV/visible spectroscopy (Figure 3.11). The results are presented in Table 3.6. A similar result as for the treatment of $[CrCl_3\{SNS\}]$ with Me_3Al is observed *i.e.* disappearance of the υ_2 band and shift of the υ_1 band. The shifted transition at 16,140 cm^{-1} is very similar to the band at 16,180 cm^{-1} observed for the complex treated with Me_3Al only. These results tend to confirm that a change in the electronic configuration of the chromium metal centre occurs upon treatment with the aluminum reagent. The role of the aluminate, however, could not be determined since no significant changes are noticed when we compare the UV/visible spectra and the values for the band υ_1 in the absence or in the presence of the aluminate.

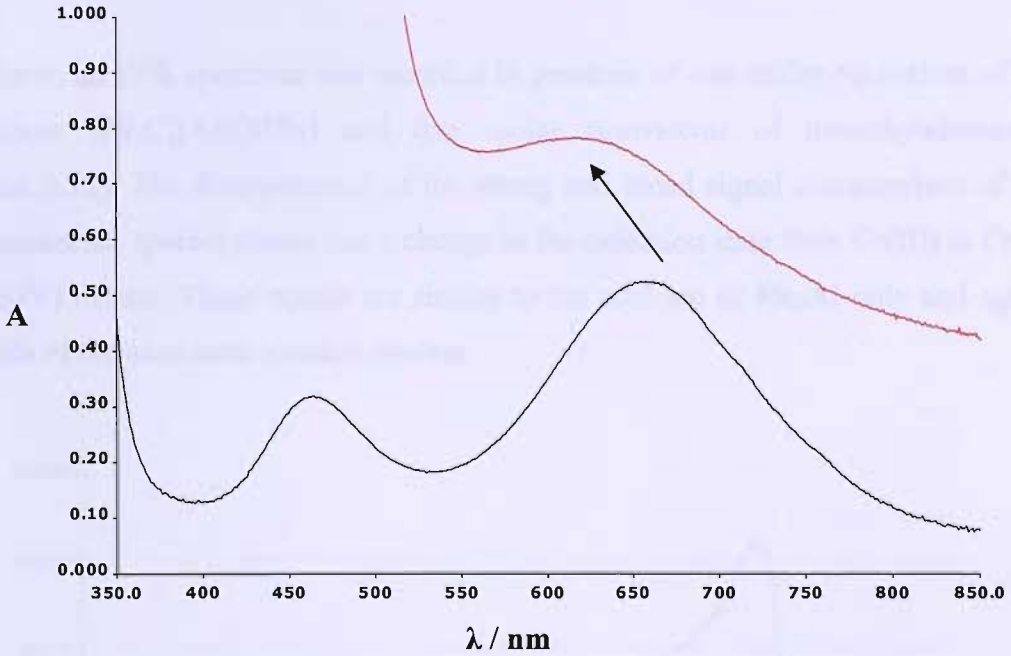

Figure 3.11. UV/visible spectra for a 5 mM toluene solution of $[CrCl_3\{SNS\}]$ before (black) and after (red) treatment with 5 equivalents of Me_3Al and 1 equivalent of $[Ph_3C][Al(ORf)_4]$

Complex	$\upsilon_1{}^a/cm^{-1}$	$\upsilon_1{}^b/cm^{-1}$	$\upsilon_1{}^c/cm^{-1}$
$[CrCl_3\{SNS\}]$	15,270	16,180	16,140

Table 3.6. Spectroscopic data for a 5 mM toluene solution of $[CrCl_3\{SNS\}]$ [a]before, [b]after treatment with 5 equivalents of Me_3Al and with 1 equivalent of $[Ph_3C][Al(ORf)_4]$ [c]

3.5.3.2. Electron Paramagnetic Resonance Studies

Similarly, an EPR spectrum was recorded in presence of one molar equivalent of the aluminate $[Ph_3C][Al(ORf)_4]$ and five molar equivalents of trimethylaluminum (Figure 3.12). The disappearance of the strong and broad signal characteristic of the chromium(III) species shows that a change in the oxidation state from Cr(III) to Cr(II) or Cr(IV) occurs. Those results are similar to the addition of Me_3Al only and again, the role of the aluminate remains unclear.

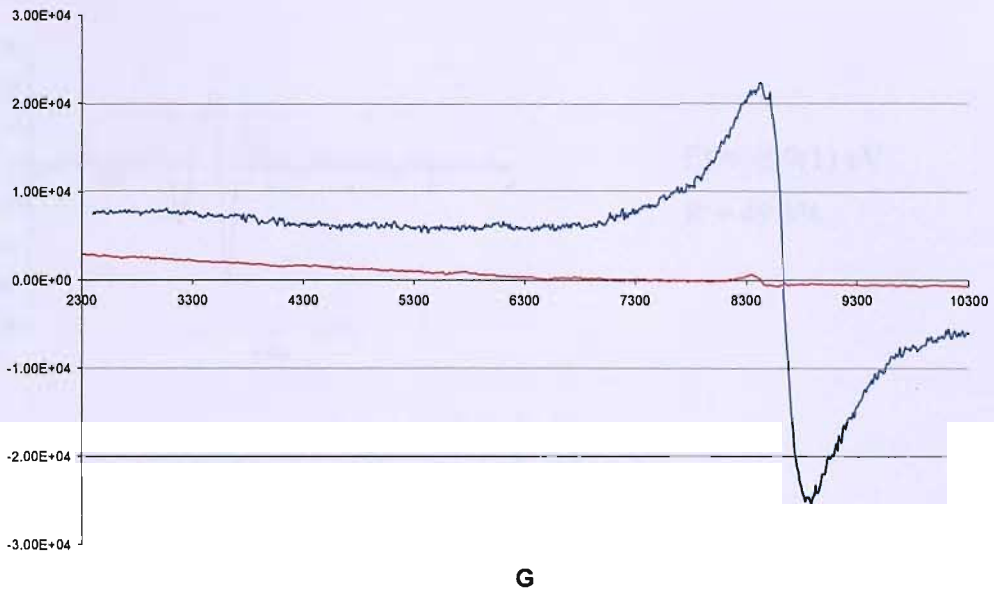

Figure 3.12. EPR spectrum $[CrCl_3\{SNS\}]$ in toluene/CH_2Cl_2 (blue) treated with 5 equivalents of Me_3Al (red) and 1 equivalent of $[Ph_3C][Al(ORf)_4]$, g = 1.99; recorded as a frozen glass at T = 115 K

3.5.3.3. Chromium K-edge EXAFS Studies

Two different measurements involving the use of the aluminate $[Ph_3C][Al(ORf)_4]$ have been recorded. The first one consisted of a mixture of a 5 mM toluene solution of the complex $[CrCl_3\{SNS\}]$ treated with thirty molar equivalents of Me_3Al and one molar equivalent of the aluminate in anhydrous toluene. Figure 3.13 displays the EXAFS data obtained for this reaction system.

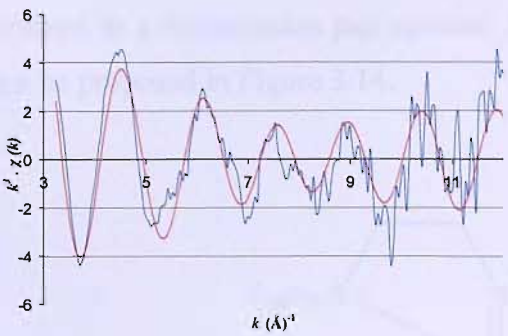

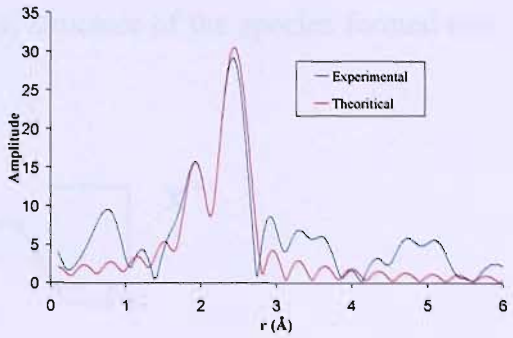

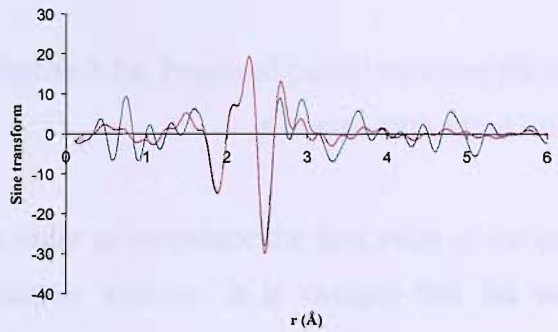

Ef = -5.9(1) eV

R = 49.3%

Atom	C.N.	R / Å	$2\sigma^2$ / Å^2
C / N	2.7(8)	2.12(4)	0.015(3)
S	1.0(3)	2.43(5)	0.003(5)

Figure 3.13. The chromium K-edge k^3-weighted EXAFS, Fourier transform and sine transform for a 5 mM toluene solution of $[CrCl_3\{SNS\}]$ treated with Me_3Al and 1 equivalent of $[Ph_3C][Al(ORf)_4]$

The spectra fit to a model of a carbon/nitrogen shell and a sulfur shell. As for the complex treated with Me_3Al only, one sulfur atom remains coordinated to the chromium metal centre with a bond length of 2.43(5) Å, consistent with X-ray data available. The second shell consists of 2.7(8) carbon/nitrogen atoms. If we consider a deprotonation of the amine to form an amido bond with the chromium metal centre, we then have two Cr-C bonds for the species present in the EXAFS cell. If we consider the substitution of the chlorine atoms by methyl groups, two

chromium-methyl bonds could explain those results. The aluminate is probably involved in a cation-anion pair species. A partial structure of the species formed can then be proposed in Figure 3.14.

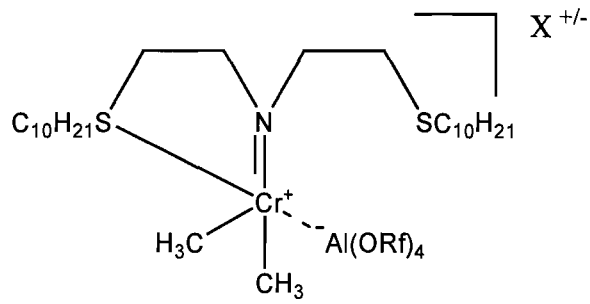

Figure 3.14. Proposed partial structure for the species produced when $[CrCl_3\{SNS\}]$ is treated with Me_3Al and $[Ph_3C][Al(ORf)_4]$

In order to reproduce the first steps of the catalytic cycle, an alkene was added to the reaction mixture. It is thought that the presence of ethylene molecules helps in stabilising the active species by, as described earlier, forming a metallacycle coordinated to the chromium metal centre, avoiding a possible decomposition of the active species. The second measurement was then performed in the presence of 1-hexene (10% in toluene). Figure 3.15 depicts the EXAFS data for a 5 mM toluene/1-hexene solution of $[CrCl_3\{SNS\}]$ treated with thirty molar equivalents of Me_3Al and one equivalent of the aluminate $[Ph_3C][Al(ORf)_4]$. The spectra fit the $k^3.\chi(k)$, Fourier transform and sine transform well (FI = 10.6 and R = 35.8 %) to a simple model of two shells, three carbon/nitrogen at 2.14(3) Å and one sulfur at 2.43(8) Å. The data are very similar to the data obtained for the complex treated in the absence of 1-hexene and a similar partial structure as Figure 3.14 was proposed.

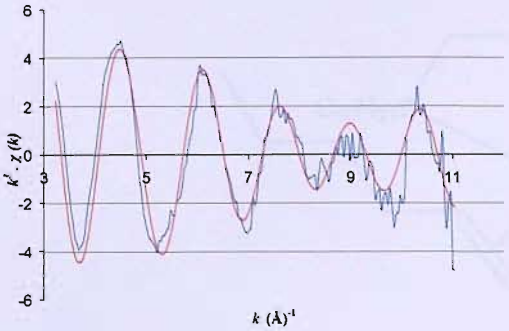

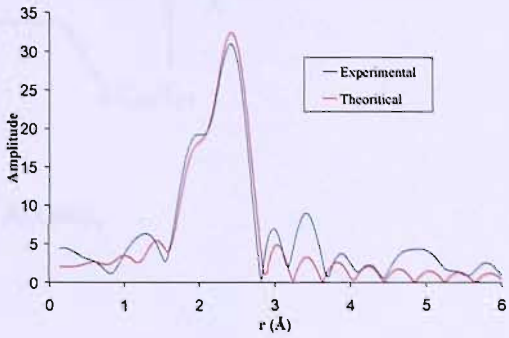

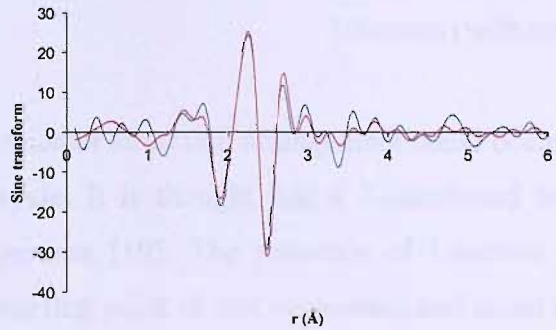

Ef = -3.8(8) eV

R = 35.8 %

Atom	C.N.	R / Å	$2\sigma^2$ / Å^2
C / N	2.8(8)	2.14(3)	0.008(5)
S	1.1(2)	2.43(8)	0.002(5)

Figure 3.15. The chromium K-edge k^3-weighted EXAFS, Fourier transform and sine transform for a 5 mM toluene/1-hexene solution of [$CrCl_3${SNS}] treated with Me_3Al and 1 equivalent of [Ph_3C][$Al(ORf)_4$]

Another possible model is depicted in Figure 3.16. The new structure involves the coordination of the alkene to the chromium *via* the double bond. This hypothesis would however involve the absence of methyl groups in this new active species.

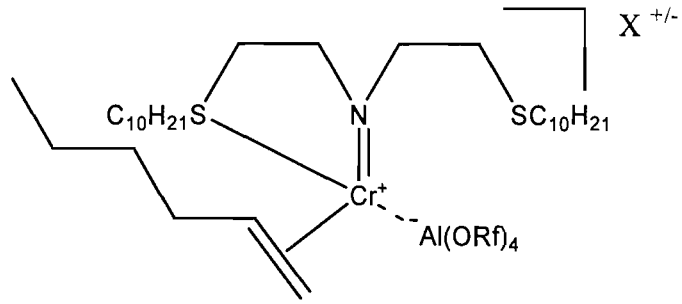

Figure 3.16. Second proposed partial structure for the species produced when $[CrCl_3\{SNS\}]$ is treated with Me_3Al and $[Ph_3C][Al(ORf)_4]$ in the presence of 1-hexene (with coordinated alkene)

Another structural arrangement could occur and confirm the first steps of the catalytic cycle. It is thought that a 7-membered metallacycle is formed during the catalytic process [19]. The presence of 1-hexene within the reaction mixture may be the starting point of this cyclisation and could explain the presence of two Cr-C bonds. A postulated structure of the catalytically active cation-anion ion pair is given in Figure 3.17.

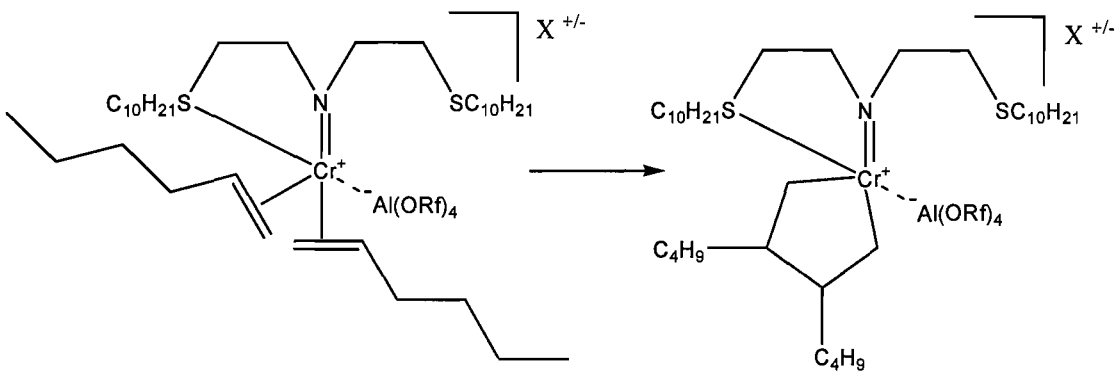

Figure 3.17. Third proposed partial structure for the species produced when $[CrCl_3\{SNS\}]$ is treated with Me_3Al and $[Ph_3C][Al(ORf)_4]$ in the presence of 1-hexene (formation of a metallacycle)

3.6. Chromium K-edge XANES Studies

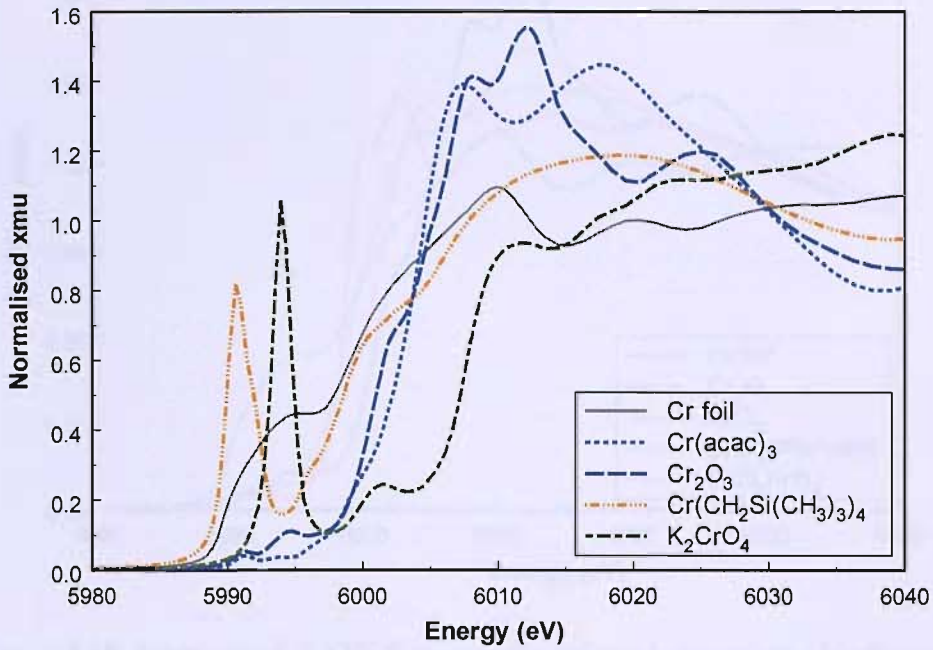

Figure 3.18. Normalised XANES spectra for selected chromium reference compounds (solid pellets)

Figure 3.18 shows the normalised XANES for a few selected reference compounds. The XANES displays a large number of pre-edge features and significant energy shifts of the absorption edge. For this specific series the energy of the absorption edge increases with increasing Cr oxidation state.

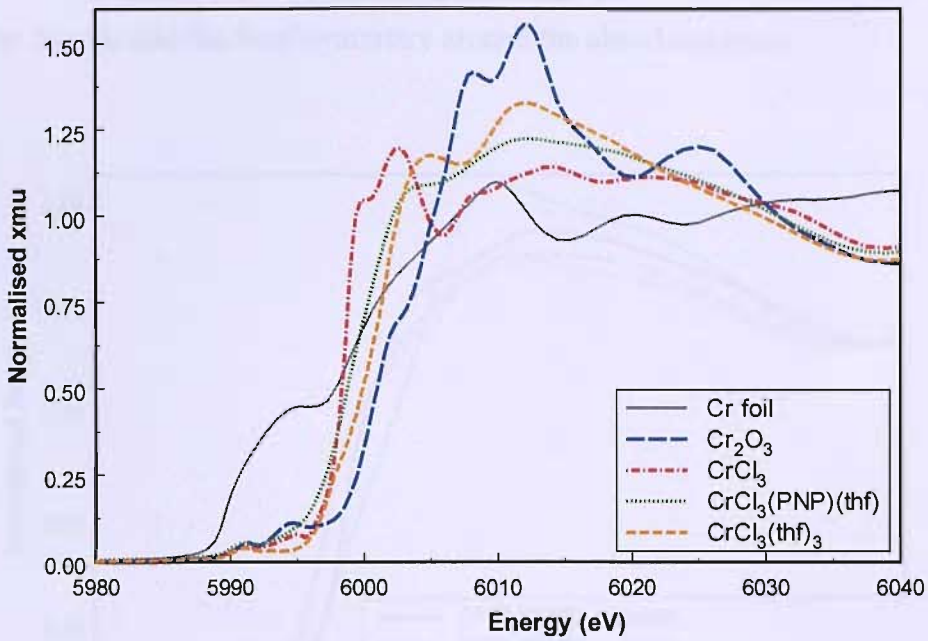

Figure 3.19. Normalised XANES spectra for selected chromium chloride reference compounds (solid pellets)

The ligand system, however, has a large influence on the position of the Cr absorption edge. Although the formal oxidation state of the chlorine complexes, as displayed in Figure 3.19, is +III and thus similar to Cr_2O_3 and $Cr(acac)_3$, the edge now shifts to lower energy in comparison to Cr(0) foil.

The energy of the metal X-ray absorption edge is determined by the difference between the energy of the initial state, that is, the core level energy from which the electron is ejected, and the final state, that is, the valence level at energy that accepts the electron in the final state. If the final state is localised on the metal, the energy of the adsorption edge decreases with increasing metal oxidation state. However, if the final state is localized on the ligand, the absorption edge energy will increase [44]. The electronegativity of the ligand, *i.e.* in this case from Cl^- to O^{2-}, is an important factor for the edge energy difference between the $CrCl_3$ and Cr_2O_3 [45]. Additionally, it is shown that the geometry of the ligand can govern the position of the absorption edge, as shown for a series of $CrCl_3\{L\}$ [45].

It is thus important to note that it is not possible to determine the oxidation state of unknown complexes by simply scaling their edge position, as they are very dependent on the ligands and the local symmetry around the absorbing atom.

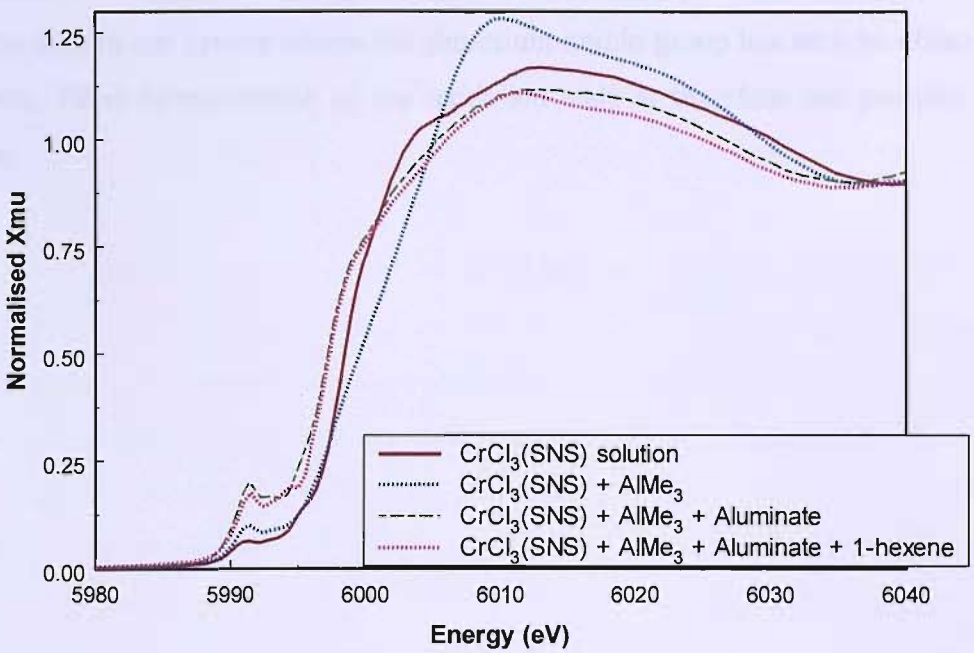

Figure 3.20. Normalised XANES spectra for a 5 mM toluene solution of $[CrCl_3\{SNS\}]$ treated with $AlMe_3$ and $AlMe_3/[Ph_3C][Al(ORf)_4]$ /1-hexene

The XANES spectrum for the complex in solution treated with thirty molar equivalents of Me_3Al shows a shift of the edge to higher energy, from 6003 eV to 6008 eV (Figure 3.20). When compared to some chromium complexes references (Figure 3.18), the edge of a chromium(IV) species with C/O ligand systems and without chlorine atoms, $Cr(CH_2Si(CH_3)_3)_4$, is at 6008 eV. Providing that the species formed is not a dimer, which is confirmed by EXAFS analysis, we can conclude that the oxidation state of the metal centre is expected to be +IV. This result is also supported by the EPR measurements.

When the complex is treated with the aluminium reagent and in the presence of the aluminate, the edge of the spectrum shifts to lower energy. The XANES spectra obtained for the species formed in the presence or absence of 1-hexene are identical. The edge shifts from 6003 eV for the complex $[CrCl_3\{SNS\}]$ to 5999 eV when treated with Me_3Al/aluminate and with or without 1-hexene. We know, from EPR studies,

that the species formed is probably a Cr(II) or Cr(IV) species, both being EPR inactive. XANES studies tend to support that +IV is unlikely to be the oxidation state of the metal centre. This is notably shown by the position of the edge when compared to references [45]. The edge position at low energy could be explained by the presence of a ligand with a large charge transfer to chromium. This does not seem to be the case in our system unless the chromium-amido group has such an effect on the system. Final determination of the oxidation state is therefore not possible at this stage.

3.7. Conclusions

In this chapter, we have probed the reaction between the complex $[CrCl_3\{HN(CH_2CH_2SC_{10}H_{21})_2\}]$ and an aluminium reagent, Me_3Al, using UV/visible, EPR and EXAFS spectroscopy and cyclic voltammetry. UV/visible results revealed that a change in the coordination sphere of the chromium metal centre occurs upon addition of the aluminium reagent involving a substitution of some or all chlorine groups by methyl groups. This was borne out by the disappearance of the υ_2 and the shift of the υ_1 UV/visible bands.

The change in the oxidation state, as proposed several times in the literature, was confirmed by EPR spectroscopy. The disappearance of the strong and broad signal characteristic of d^3 systems such as the Cr(III)-SNS system upon addition of Me_3Al indicated an oxidation to Cr(IV) or reduction to Cr(II). EPR spectroscopy data did not enable us to determine what chromium species was obtained after activation of the complex $[CrCl_3\{SNS\}]$.

Chromium K-edge studies on the $[CrCl_3\{SNS\}]/Me_3Al$ system confirmed the loss of the chlorine groups and analysis of the EXAFS data revealed the presence three Cr-C bonds, supporting the coordination of methyl groups to the chromium centre. Moreover, the Cr-N bond remains in the model proposed after treatment with the aluminium reagent. These results suggest the deprotonation of the amine upon addition of the aluminium reagent, to form an amide strongly bonded to the chromium, as suggested in the literature and avoiding further "unzipping mechanism" of the ligand. We also noticed that one Cr-S bond remains present, suggesting that the sulfur centres are not completely dissociated, as this is the case with the $[CrCl_3\{S(CH_2CH_2SC_{10}H_{21})_2\}]$ complex (Chapter 5). XANES spectra tend to support a Cr(IV) species.

The second part of this chapter was dedicated to the investigation of the role of the aluminate $[Ph_3C][Al(ORf)_4]$. The system was tested for catalysis, with a high selectivity towards 1-hexene and investigation of the active species was carried out. Similar results to the Cr(III)-SNS/Me_3Al system were obtained for the UV and EPR and could not enable us to differentiate the active species with and without the aluminate. Analyses of the EXAFS data showed that a cationic-anionic species is probably formed in the presence of the aluminate and several partial structures

(with and without 1-hexene) were proposed. Definite determination of the oxidation state of this active species was however very difficult and will require further calculations.

3.8. Experimental

The ligand $HN(CH_2CH_2SC_{10}H_{21})_2$, the chromium(III) complex $[CrCl_3\{HN(CH_2CH_2SC_{10}H_{21})_2\}]$ and the co-catalyst $[Ph_3C][Al\{OC(CF_3)_3\}_4]$ were prepared by literature methods.

Bis(2-chloroethyl)amine hydrochloride, decanethiol and $LiAlH_4$ were purchased from Aldrich and used as received. Perfluoro *tert*-butanol was purchased from Fluorochem and used as received.

Synthesis of $HN(CH_2CH_2SC_{10}H_{21})_2$ [25]: A solution of bis(2-chloroethyl)amine hydrochloride (21.0 g, 0.117 mol) in ethanol (150 mL) was added to a solution of NaOH (14.4 g, 0.36 mol) and decanethiol (50 ml, 0.24 mol) in ethanol at 0°C. The mixture was stirred at room temperature for 2 hours and the filtrate evaporated to dryness. The residue was taken up in Et_2O (3 x 30 ml) and filtered again. After evaporation of the solvent *in vacuo*, the product remained as a yellow oil. Yield: 37 g, 89 mmol (76%). ^1H NMR ($CDCl_3$): δ 0.87 (t, 6H, $C\underline{H}_3C_9H_{18}$), 1.25-1.4 (m, 28H, $CH_3C_7\underline{H}_{14}C_2H_4S$), 1.52-1.63 (m, 4H, $C_8H_{17}C\underline{H}_2CH_2S$), 2.5 (t, 4H, $C_9H_{19}C\underline{H}_2S$), 2.6 (t, 4H, $C_{10}H_{21}SC\underline{H}_2$), 2.81 (t, 4H, $C\underline{H}_2N$) ppm. $^{13}C\{^1H\}$ NMR ($CDCl_3$): δ 14.2 ($\underline{C}H_3C_9H_{18}S$), 22.8 ($CH_3\underline{C}H_2C_8H_{16}S$), 28.7, 29.0, 29.4, 29.6, 29.7, 29.9, 32.0 ($C_2H_5\underline{C}_7H_{14}CH_2S$), 32.2 ($C_{10}H_{21}S\underline{C}H_2$), 32.5 ($CH_3C_8H_{16}\underline{C}H_2S$), 48.5 ($\underline{C}H_2N$). Positive electrospray (CH_2Cl_2) *m/z*: 418 $(HN(CH_2CH_2SC_{10}H_{21})_2 + H)^+$.

Synthesis of $[CrCl_3\{HN(CH_2CH_2SC_{10}H_{21})_2\}]$ [27]: The procedure was to add the SNS ligand (0.28 g, 6.67 x 10^{-4} mol) previously dissolved in a minimum volume of CH_2Cl_2 to a solution of $[CrCl_3\{THF\}_3]$ (0.25 g, 6.67 x 10^{-4}mol) in dried and degassed THF (15 mL). The resulting mixture was stirred at room temperature under nitrogen overnight. The volume of CH_2Cl_2 was then concentrated to 1 mL *in vacuo* and diethyl ether (5 mL) was added. The mixture was pumped to dryness to give a green solid. Yield: 0.19 g, 3.34 x 10^{-4} mol (50%). UV/visible (diffuse reflectance): 655, 463 nm. Infra-red (N-H stretch) Nujol mull: 3191 cm^{-1}.

Synthesis of $LiAl[OC(CF_3)_3]_4$ [41]: A solution of $LiAlH_4$ in Et_2O (0.76 g, 20 mmol) was transferred into a Schlenk vessel. All volatiles were removed *in vacuo* until a constant weight was achieved (80°C overnight). This purified $LiAlH_4$ was suspended in toluene (70 mL) and perfluoro *tert*-butanol (19.36 g, 0.082 mmol) was added at 0°C temperature over one hour (gas evolution). The mixture was heated to reflux for 30 hours when a clear solution had formed. Cooling this solution for one hour to -20°C lead to the precipitation of colourless $LiAl[OC(CF_3)_3]_4$. The supernatant solution was decanted and all the volatiles of the remaining white solid were removed *in vacuo* to give a white solid. Yield: 2.10 g, 55 mmol (67%). ^{27}Al NMR (D_2O): δ 33.95 ppm. ^{7}Li NMR (D_2O): δ -0.92 ppm. $C_{16}AlO_4F_{36}Li$ requires C, 19.73 %, Found C, 19.73 %.

Synthesis of $[Ph_3C][Al\{OC(CF_3)_3\}_4]$ [42]: $LiAl[OC(CF_3)_3]_4$ (2.1 g, 55 mmol) and Ph_3CCl (19.35 g, 82 mmol) were weighed into a Schlenk vessel (yellow colouring). Upon addition of CH_2Cl_2 (15 mL) a yellow solution over little colourless precipitate had formed. After stirring the mixture overnight the suspension was filtered, all volatiles were removed from the filtrate *in vacuo* and the remaining yellow material was washed with three portions of *n*-pentane (5 mL). Yield: ^{1}H NMR ($CDCl_3$): δ 7.64 (6H, d, Ph), 7.88 (6H, t, Ph), 8.27 (3H, t, Ph) ppm. ^{13}C {^{1}H} NMR ($CDCl_3$): δ 125.0 (q, $\underline{C}F_3$), 130.7, 139.9, 142.3, 143.7 (Ph), 211.1 ($Ph_3\underline{C}^+$) ppm. ^{27}Al NMR ($CDCl_3$): δ 33.95 ppm. $C_{35}H_{15}AlO_4F_{36}$ requires C, 34.73; H, 1.25 %, Found C, 34.77; H, 1.25 %.

3.9. References

1. Manyik, R. M.; Walker, W. E. and Wilson, T. P.; *J. Catal.*, (1977), **47**, 197.
2. Kohn, R. D.; Haufe, M.; Mihan, S. and Lilge, D.; *Chem. Commun.*, (2000), 1927.
3. Small, B. L.; Carney, M. J.; Holman, D. M.; O'Rourke, C. E. and Halfen, J. A.; *Macromolecules*, (2004), **37**, 4375.
4. Zhang, W.; Sun, W.; Zhang, S.; Hou, J.; Wedeking, K.; Schultz, S.; Frohlich, R. and Song, H.; *Organometallics*, (2006), **25**, 1961.
5. Small, B. L. and Brookhart, M.; *J. Am. Chem. Soc.*, (1998), **120**, 7143.
6. Deckers, P. J. W.; Hessen, B. and Teuben, J. H.; *Angew. Chem. Int. Ed.*, (2001), **40**, 2516.
7. Blok, A. N. J.; M.Budzelaar, P. H. and Gal, A. W.; *Organometallics*, (2003), **22**, 2564.
8. Andes, C.; Harkins, S. B.; Murtuza, S.; Oyler, K. and Sen, A.; *J. Am. Chem. Soc.*, (2001), **123**, 7423.
9. Carter, A.; Cohen, S. A.; Cooley, N. A.; Murphy, A.; Scutt, J. and Wass, D. F.; *J. Chem. Soc., Chem. Comm.*, (2000), 858.
10. Wu, F. J.; *US 5811618, EP 0622347B1*, (1998), Amoco.
11. Lashier, M. E.; *EP 0780353A1*, (1998), Phillips Petroleum.
12. Wasserscheid, P.; Grimm, S.; Kohn, R. D. and Haufe, M.; *Adv. Synth. Catal.*, (2001), **343**, 814.
13. Tomov, A. K.; Chirinos, J. J.; Long, R. J.; Gibson, V. C. and Elsegood, M. R. J.; *J. Am. Chem. Soc.*, (2006), *Advanced article*.
14. McGuinness, D. S.; Wasserscheid, P.; W, W. Keim; Hu, C.; Englert, U.; Dixon, J. T. and Grove, C.; *J. Chem. Soc., Chem. Commun.*, (2003), 334.
15. Yu, Z. and Houk, K. N.; *Angew. Chem. Int. Ed.*, (2003), **42**, 808.
16. DeBruin, T. J. M.; Magna, L.; Raybaud, P. and Toulhoat, H.; *Organometallics*, (2003), **22**, 3404.
17. Bollmann, A.; Blann, K.; Dixon, J. T.; Hess, F. M.; Killian, E.; Maumela, H.; McGuinness, D. S.; Morgan, D. H.; Neveling, A.; Otto, S.; Overett, M.; Slawin, A. M. Z.; Wasserscheid, P. and Kuhlmann, S.; *J. Am. Chem. Soc.*, (2004), **126**, 14712.

18. Emrich, R.; Heinemann, O.; Jolly, P. W.; Kruger, C. and Verhovnik, G. P. J.; *Organometallics*, (1997), **16**, 1511.

19. Agapie, T.; Schofer, S. J.; Labinger, J. A. and Bercaw, J. E.; *J. Am. Chem. Soc.*, (2004), **126**, 1304.

20. McGuinness, D. S.; Wasserscheid, P.; Morgan, D. H. and Dixon, J. T.; *Organometallics*, (2005), **24**, 552.

21. McGuinness, D. S.; Brown, D. B.; Tooze, R. P.; Hess, F. M.; Dixon, J. T. and Slawin, A. M. Z.; *Organometallics*, (2006), **25**, 3605.

22. Kohn, R. D.; Smith, D.; Mahon, M. F.; Prinz, M.; Mihan, S. and Kociok-Kohn, G.; *J. Organomet. Chem.*, (2003), **683**, 200.

23. Morgan, D. H.; Schwikkard, S. L.; Dixon, J. T.; Nair, J. J. and Hunter, R.; *Adv. Synth. Catal.*, (2003), **345**, 1.

24. Rensburg, W. Janse van; Grove, C.; Steynberg, J. P.; Stark, K. B. and Huyser, J. J.; *Organometallics*, (2004), **23**, 1207.

25. Konrad, M.; Meyer, F.; Heinze, K. and Zsolnai, L.; *J. Chem. Soc., Dalton Trans.*, (1998), 199.

26. Herwig, W. and Zeiss, H.; *J. Organomet. Chem.*, (1958), **23**, 1404.

27. Pope, S. J. A.; Champness, N. R. and Reid, G.; *J. Chem. Soc., Dalton Trans.*, (1997), 1639.

28. Gray, L. R.; Hale, A. L.; Levason, W.; McCullough, F. P. and Webster, M.; *J. Chem. Soc., Dalton Trans.*, (1984), 47.

29. Lever, A. B. P.; *Inorganic Electronic Spectroscopy, 2nd Edition,* (1984), Amsterdam: Elsevier Science Publisher.

30. Grant, G. J.; Rogers, K. E.; Setzer, W. N. and VanDerveer, D. G.; *Inorg. Chim. Acta*, (1995), **234**, 35.

31. Kuppers, H. J. and Wieghardt, K.; *Polyhedron*, (1989), **8**, 1770.

32. House, D. A. and Garner, C. S.; *Transition Met. Chem.*, (1970), **6**, 1.

33. McGuinness, D. S.; Wasserscheid, P.; Keim, W.; Morgan, D.; Dixon, J. T.; Bollmann, A.; Maumela, H.; Hess, F. and Englert, U.; *J. Am. Chem. Soc.*, (2003), **125**, 5272.

34. Mabbott, G. A.; *J. Chem. Educ.*, (1983), **60**, 697.

35. Kissinger, P. T. and Heineman, W. R.; *J. Chem. Educ.*, (1983), **60**, 702.

36. Gibson, V. C.; Newton, C.; Redshaw, C.; Solan, G. A.; White, A. J. P. and Williams, D. J.; *Eur. J. Inorg. Chem.*, (2001), 1895.

37. Fryzuk, M. D.; Leznoff, D. B. and Retting, S. J.; *Organometallics*, (1995), **14**, 5193.

38. Krossing, I.; *J. Am. Chem. Soc.*, (2001), **123**, 4603.

39. Reed, C.; *Acc. Chem. Res.*, (1998), **31**, 133.

40. Chen, E. Y. X. and Marks, T. J.; *Chem. Rev.*, (2000), **100**, 1391.

41. Krossing, I.; *Chem. Eur. J.*, (2001), **7**, 490.

42. Krossing, I.; Brands, H.; Feuerhake, R. and Koening, S.; *J. Fluor. Chem.*, (2001), **112**, 83.

43. McGuinness, D. S. and Rucklidge, A. J.; *IPN PCT/IB2006/0053494*, (2006), Sasol Technology UK

44. Tromp, M.; Van Bokhoven J. A.; Van Strijdonck, G. P. F.; Van Leeuwen, P. W. N. M.; Koningsberger, D. C. and Ramaker, D. E.; *J. Am. Chem. Soc.*, (2005), **127**, 777.

45. Tromp, M.; Moulin J.; Reid G. and Evans J.; AIP Conference Proceedings, Proceedings of the 13th International Conference on X-ray Absorption Fine Structure Spectroscopy, Stanford, 9-13 July 2006, *Accepted for publication.*

Chapter 4

Homogeneous Chromium Catalysed Tetramerisation of Ethylene with $[CrCl_3\{isoPrN(PPh_2)_2\}(THF)]$: Investigation for the Production of 1-Octene

4.1. Introduction

Linear α-olefins such as 1-hexene and 1-octene are used, amongst other applications, as co-monomers in the production of linear low density polyethylene (LLDPE). The oligomerisation of ethylene typically leads to a broad range of α-olefins and catalyst systems that are selective for specific desirable alkenes would be of great interest. A number of chromium based catalysts have been studied and developed for the trimerisation reaction of ethylene to 1-hexene, including the Phillips pyrrolide system [1], the Sasol mixed heteroatomic systems [2-4] and the BP diphosphine system [5, 6]. An analogous ethylene tetramerisation route to 1-octene remained unknown for years, despite being highly desirable. The common belief was that ethylene tetramerisation was, on a mechanistic point of view, improbable. If ethylene tetramerisation were to proceed *via* a similar mechanism route to the one proposed for the ethylene trimerisation (Chapter 3), it would imply the formation of a 9-membered metallacycle intermediate [7, 8]. Until very recently, studies showed that this process was unlikely to occur since the 9-membered ring is disfavoured relative to the 7-membered ring [8]. The energy barrier for the insertion of further ethylene molecules in a 7-membered metallacycle would indeed be too high compared to the facile reductive elimination to yield 1-hexene [9].

The selective tetramerisation of ethylene to 1-octene was successfully demonstrated using a chromium source, a diphosphinoamine ligand of the general structure R-N(PPh_2)$_2$ (Figure 4.1) and a methylaluminoxane-based activator [10]. Subsequently, it was shown that the methylaluminoxane activator could be successfully replaced by a combination of trialkylaluminium and non-coordinating anion source [11].

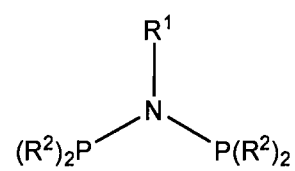

1: R^1 = Me, R^2 = Ph
2: R^1 = Pentyl, R^2 = Ph
3: R^1 = Cyclohexyl, R^2 = Ph
4: R^1 = iPropyl, R^2 = Ph
5: R^1 = Ph, R^2 = Ph

Figure 4.1. Ligands for ethylene tetramerisation [10]

Overett *et al* showed that the nature, position and number of aryl-substituents on diphosphinoamine ligands play an important role on the selectivity of chromium catalysed ethylene oligomerisation [12]. The key to switch between tetramerisation and trimerisation selectivity was the *ortho*-substitution at the diphosphinoamine aryl rings (Figure 4.2). This can be mediated by either steric crowding around the catalytic centre or by pendant coordination of a donor substituent.

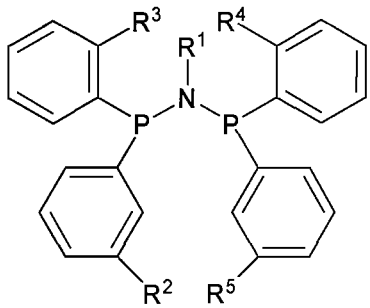

1: R^1 = Me, R^2 = R^3 = R^4 = R^5 = OMe
2: R^1 = Me, R^2 = R^3 = R^4 = R^5 = H
3: R^1 = iPr, R^2 = R^3 = R^4 = R^5 = H
4: R^1 = iPr, R^2 = R^5 = OMe, R^3 = R4 = H
5: R^1 = iPr, R^2 = OMe, R^3 = R^4 = R^5 = H
6: R^1 = iPr, R^2 = Et, R^3 = R^4 = R^5 = H

Figure 4.2. Selected polar-substituted diphosphinoamine ligands [12]

Recent studies also show that the substituent attached to the N-atom of the ligand backbone can play a significant role for the selective tetramerisation of ethylene to 1-octene [12]. The catalysts investigated displayed good activity and selectivity towards 1-octene and 1-hexene, with the best results obtained with ligands containing cyclopentyl or cyclohexyl moieties. Increase in steric bulk with a substitution at the 2-position of the cyclohexyl skeleton led to a drastic reduction of the side products (Scheme 4.1) [9].

In order to have a better insight of the catalytic mechanism, extensive deuterium studies suggested that long-chain linear alpha olefins could be formed by means of a metallacycle mechanism and hence yield the desired 1-octene [13]. Studies demonstrated that the formation of 1-octene from a C_2H_4/C_2D_4 mixture involved no H/D-scrambling, which is in accordance with mechanism based on a metallacycle contribution, as opposed to a Cossee-Arlman mechanism (Scheme 4.1) [13].

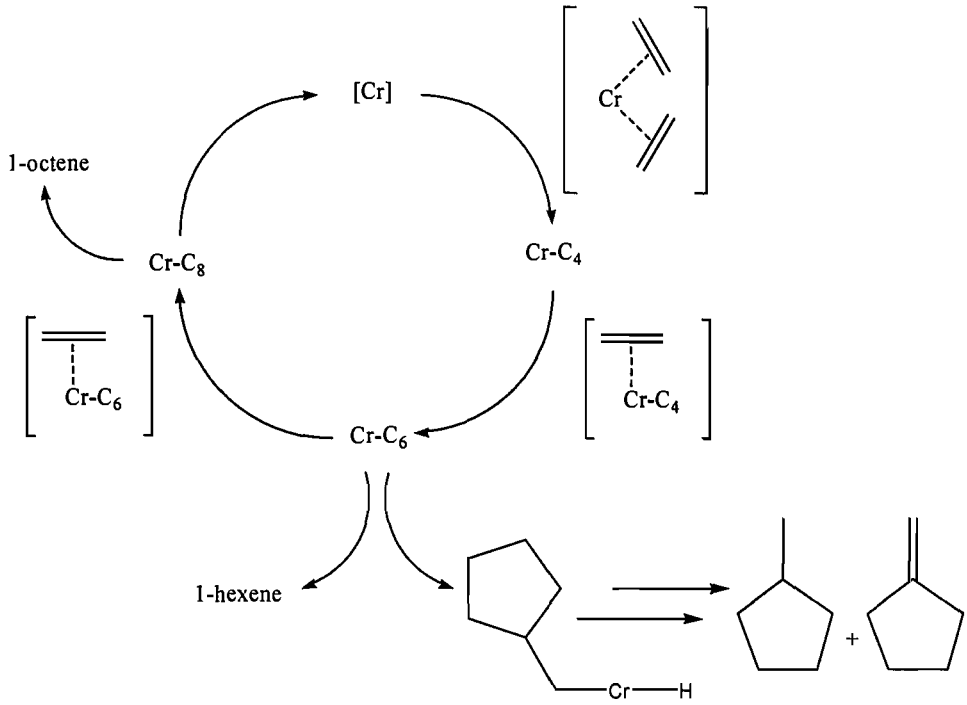

Scheme 4.1. Metallacycle mechanism proposed for the selective tetramerisation of ethylene [9]

Latest studies on the tetramerisation of ethylene were focused on the role played by the temperature and the pressure [9]. It was demonstrated that the insertion of ethylene into the metallacycloheptane species is surprisingly slightly, if not, pressure dependent. However, the reaction temperature seems to be a determinant factor to determine whether 1-hexene is eliminated or if further ethylene molecule is incorporated to form a larger metallacycle and, ultimately 1-octene. Hence an increase in the temperature leads to an increase in the formation of 1-C_6 along with a decrease in the formation of C_8 products [9].

4.2. Aims

In this chapter, the chromium(III) complex $[CrCl_3\{isoPrN(PPh_2)_2\}(THF)]$ is characterised using a wide range of techniques such as IR and UV/visible spectroscopy, cyclic voltammetry and chromium K-edge studies. The reaction of the complex $[CrCl_3\{isoPrN(PPh_2)_2\}(THF)]$ with the aluminium reagent Me_3Al is then investigated using UV/visible and EPR spectroscopy. Studies on the structure of the activated species are carried out *via* EXAFS measurements and a partial structure of the active species is proposed. The reaction between the complex and the aluminium reagent in the presence of the (*per*-)fluorinated alkoxy species, $[Ph_3C][Al\{OC(CF_3)_3\}_4]$, is also investigated using similar spectroscopic methods. Analysis of the XANES spectra of the activated complex gives an insight of the oxidation state of the species formed after addition of the aluminium reagent.

4.3. Results and Discussion

4.3.1. Synthesis of the Ligand (isoPr)N(PPh$_2$)$_2$

The bidentate ligand (isoPr)N(PPh$_2$)$_2$, thereafter referred as the PNP ligand was prepared *via* modification of a reported method (Scheme 4.2) [10]. A mixture of bis(phenyl)phosphorus chloride, triethylamine and isopropylamine in dry degassed toluene was stirred for thirty hours under nitrogen. After an aqueous work-up, the organic extracts were dried over $MgSO_4$, filtered and reduced *in vacuo*. Recrystallisation from methanol afforded a white solid (72% yield). The compound was characterised by NMR spectroscopy. ^{1}H NMR spectrum showed three resonances at δ 1.1 (6H, d, C**H**$_3$), 3.70 (1H, m, C**H**), 7.35 (Ar.) ppm. ^{13}C{^{1}H} NMR showed seven signals which can easily be attributed: δ 24.36 (**C**H$_3$); 51.94 (**C**H); 127.96, 128.04, 128.53, 132.74, 133.02 (Ar.) ppm. Finally, a ^{31}P{^{1}H} NMR spectrum showed a broad and strong peak at 48.9 ppm. Elemental analysis confirmed the nature of the PNP ligand.

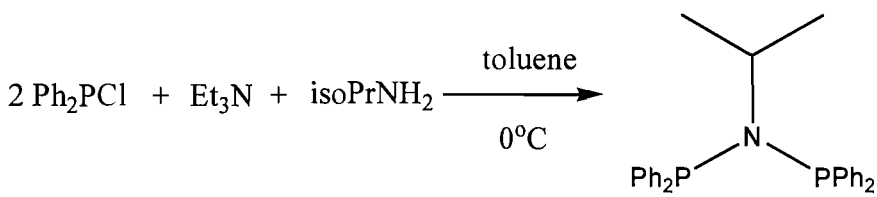

Scheme 4.2. Synthesis of (isoPr)N(PPh$_2$)$_2$ [10]

4.3.2. Synthesis of the Chromium(III) Complex [CrCl$_3${(isoPr)N(PPh$_2$)$_2$}(THF)]

The distorted octahedral [CrCl$_3${(isoPr)N(PPh$_2$)$_2$}(THF)] complex, thereafter referred as [CrCl$_3${PNP}(THF)], was prepared by reaction of [CrCl$_3$(THF)$_3$] with one molar equivalent of the PNP ligand in anhydrous CH_2Cl_2. The product was isolated as a blue solid after evaporation of the solvent to dryness (63% yield) (Scheme 4.3) [14]. Table 4.1 summarises the elemental analysis data supporting the nature of the complex synthesised.

$$[CrCl_3(THF)_3] + PNP \xrightarrow[-\ 2\ THF]{CH_2Cl_2} [CrCl_3\{PNP\}(THF)]$$

Scheme 4.3. Synthesis of $[CrCl_3\{PNP\}(THF)]$

Complex	Elemental Analysis		Exp. (theor.)
	% C	% H	% N
$[CrCl_3\{PNP\}(THF)]$	56.49 (56.59)	5.38 (5.36)	2.09 (2.13)

Table 4.1. Elemental analysis data for $[CrCl_3\{PNP\}(THF)]$

4.3.3. Characterisation of the $[CrCl_3\{PNP\}(THF)]$ Complex

4.3.3.1. UV/visible and Infra-red Spectroscopy

Two low energy *d-d* transitions are observed for the chromium(III) complex studied at 14,260 and 19,910 cm^{-1}, and from the low energy transition, *Dq* can be obtained. The complex $[CrCl_3\{PNP\}(THF)]$ has a *Dq* value of 1 475 cm^{-1}. This value is identical to the one obtained for the dimer PNP complex analogue $[CrCl_3\{PNP\}]_2$ with a *Dq* value of 1 480 cm^{-1}. For chromium(III) complexes with other phosphorus donor sets, the *Dq* values compare generally well, *e.g.* for $[CrCl_3\{MeC(CH_2PPh_2)_3\}]$ where *Dq* = 1 600 cm^{-1} [15]. The *Dq* value is also very similar to well known chromium(III)-thioether species, *e.g.* $[CrCl_3\{MeC(CH_2SMe)_3\}]$ (*Dq* = 1 470 cm^{-1}), $[CrCl_3\{[9]aneS_3\}]$ (*Dq* = 1 445 cm^{-1}) [14] and other Cr(III) complexes (Chapter 6). The molar absorption coefficient ε was also calculated for a 5 mM toluene solution of $[CrCl_3\{PNP\}(THF)]$. Finally, an infra-red spectrum was recorded for a nujol mull of the complex. The spectrum obtained showed transmissions at 1012 cm^{-1} and broad bands in the region of 860 and 1060 cm^{-1} which can be assigned to the THF (855, 1018 and 1042 cm^{-1} for the starting material $[CrCl_3(THF)_3]$) [16]. Moreover, three bands at 372, 350 and 323 cm^{-1} can be tentatively assigned to Cr-Cl stretching modes for a distorted octahedral compound presenting a C_S geometry (2A' + A") [17]. The spectroscopic data for the $[CrCl_3\{PNP\}(THF)]$ adduct are presented in

Table 4.2 and a UV/visible spectrum of the complex in toluene solution is presented in Figure 4.3.

Complex	υ_1/cm^{-1}	υ_2/cm^{-1}	Dq/cm^{-1}	$\varepsilon_1,\varepsilon_2/dm^3.mol^{-1}.cm^{-1}$	ν(Cr-Cl)/cm^{-1}
$[CrCl_3\{PNP\}(THF)]$	14,750	19,910	1,420	300, 233	372, 345, 315

UV/visible recorded in toluene solution; Infra-red spectrum recorded as a nujol mull.

Table 4.2. Spectroscopic data for $[CrCl_3\{PNP\}(THF)]$

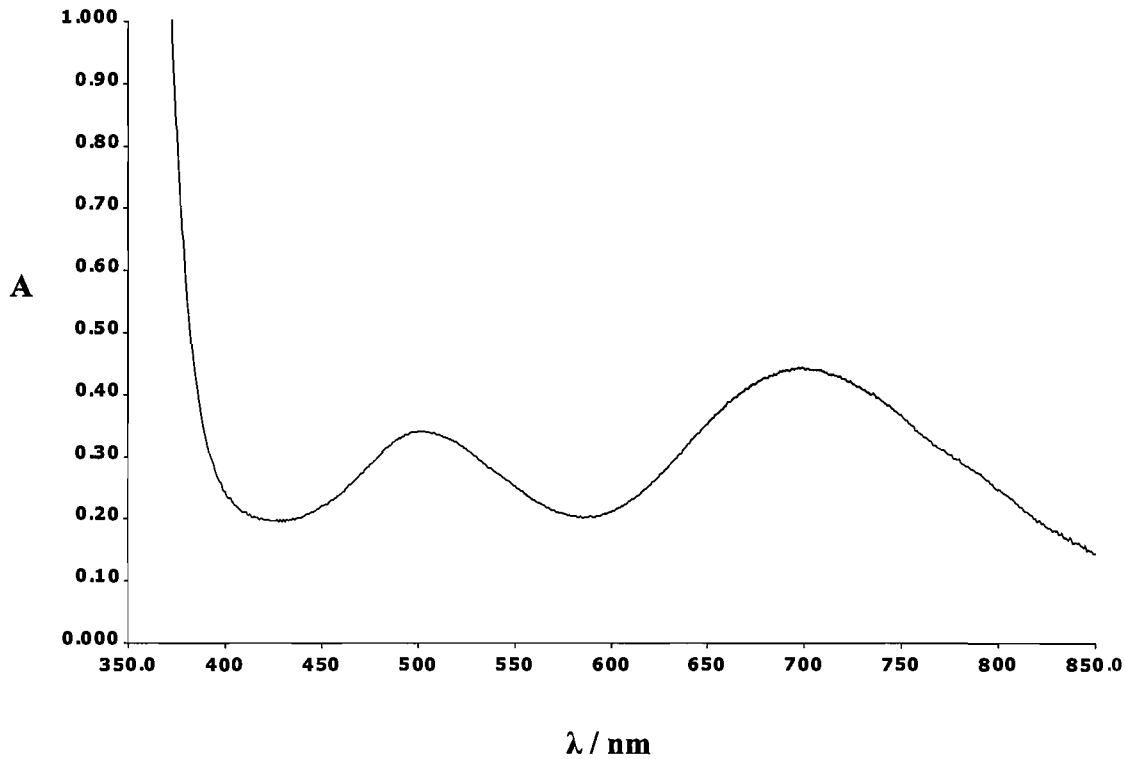

Figure 4.3. UV/visible spectrum for a 5 mM toluene solution of $[CrCl_3\{PNP\}(THF)]$

4.3.3.2. Cyclic voltammetry for the $[CrCl_3\{PNP\}(THF)]$ Complex

A cyclic voltammogram was recorded to investigate the oxidation/reduction properties of the complex $[CrCl_3\{PNP\}(THF)]$ (Figure 4.4). Electrochemical data were recorded at room temperature under an N_2 atmosphere and with a scan rate of 100 mV/s over a range of 1.5 to -1.5V. A 0.2 M $[Bu^n_4N]BF_4$ electrolyte in anhydrous CH_2Cl_2 was employed with a double platinum working and counter electrode and a

standard calomel electrode. Table 4.3 summarises the potential obtained for $[CrCl_3\{PNP\}(THF)]$.

Complex	E_{PC} *vs* ferrocene/ferrocenium(V)
$[CrCl_3\{PNP\}(THF)]$	-1.55

Table 4.3. Electrochemical data for the $[CrCl_3\{PNP\}(THF)]$ complex in 0.2 M $[Bu^n{}_4N]BF_4$ in CH_2Cl_2, scan rate = 100 mV/s , E_{PC} = reduction potential

As seen for the complex $[CrCl_3\{SNS\}]$ in Chapter 3 and for all the chromium(III) complexes studied in Chapter 5, the $[CrCl_3\{PNP\}(THF)\}]$ showed only irreversible reduction. This irreversible reduction process is supported by cyclic voltammetry studies on a series of chromium(III) trichloride complexes with phosphine ligands [18]

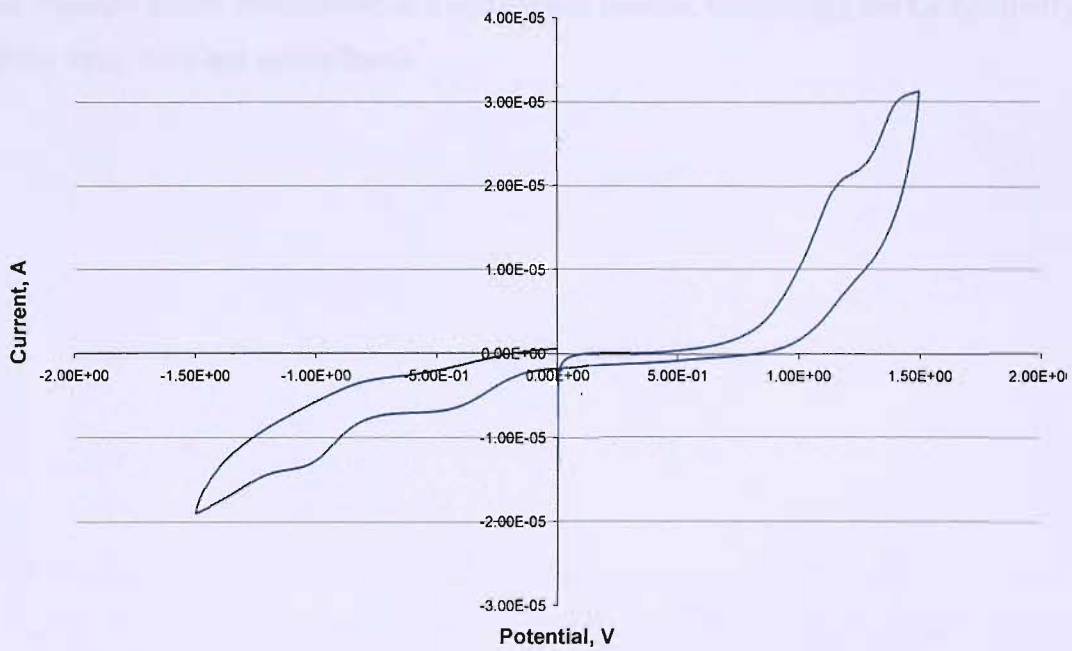

Figure 4.4. Cyclic voltammogram for $[CrCl_3\{PNP\}(THF)]$ in 0.2 M $[Bu^n{}_4N]BF_4$ in CH_2Cl_2, scan rate = 100 mV/s

4.3.3.3. Chromium K-edge EXAFS studies for the [$CrCl_3${PNP}(THF)] Complex

Figure 4.5 depicts the raw and theoretical EXAFS data for the solid [$CrCl_3${PNP}(THF)]. The theory fits the $k^3.\chi(k)$, Fourier transform and sine transform to a simple model of three shells. The model proposed has refined coordination numbers close to the expected values of one oxygen, three chlorine and two phosphorus atoms with 0.9, 3.0 and 2.2 atoms respectively. The model proposed gives d(Cr-O) = 1.95(3), d(Cr-Cl) = 2.29(8) and d(Cr-P) = 2.39(8) Å. The bond lengths are consistent with X-ray crystallography data available in the literature. A crystal structure for the chromium(III) dimer complex [Cr{PNP}$Cl_2(\mu$-Cl)]$_2$ reports a Cr-P distance of 2.419(2) Å and Cr-Cl (non-bridged) distances of 2.280(2) and 2.265(2) Å [10]. The X-ray crystal data for [$CrCl_3(THF)_3$] [19], where Cr-O = 1.994(4), 2.027(4) and 2.077(4) Å, also gives consistent data for the Cr-O (THF) bond. Based on the infra-red data obtained, the chromium(III) complex [$CrCl_3${PNP}(THF)] displays the expected octahedral coordination geometry, with the three chlorine atoms coordinated in a *meridional* fashion, confirming the C_S symmetry and the three infra-red active bands.

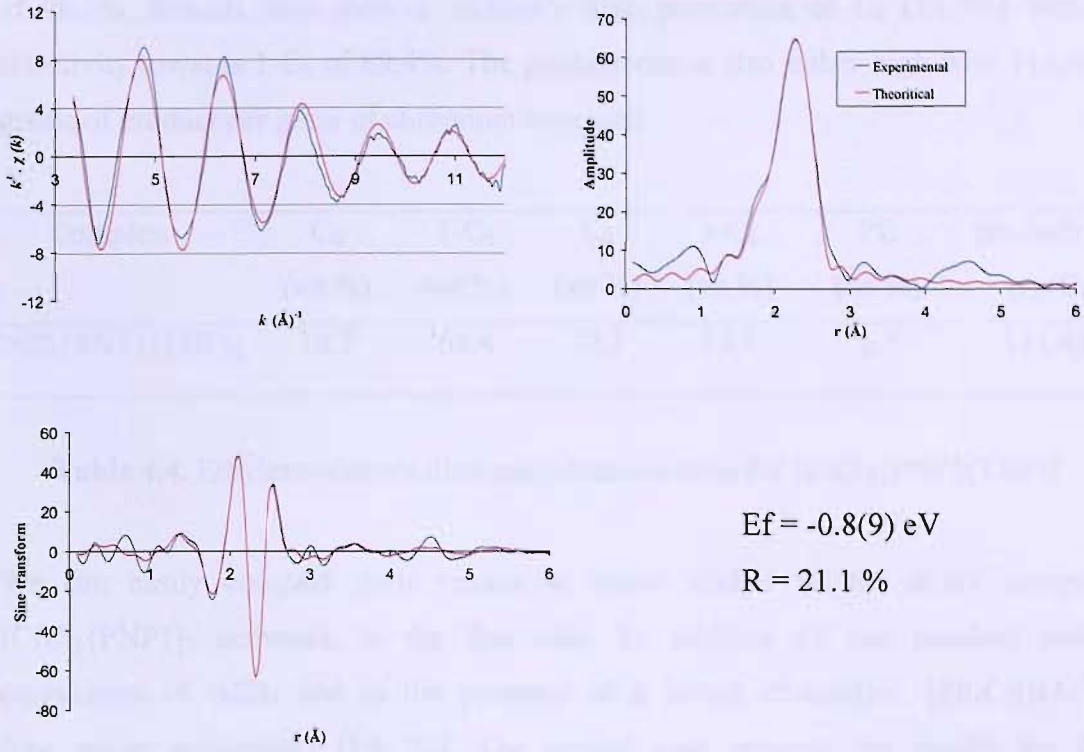

Atom	C.N.	R / Å	$2\sigma^2$ / Å^2
O	0.9(2)	1.95(3)	0.011(4)
Cl	3.0(1)	2.29(8)	0.014(3)
P	2.2(2)	2.39(8)	0.008(3)

Figure 4.5. The chromium K-edge k^3-weighted EXAFS, Fourier transform and sine transform for a solid pellet of [$CrCl_3${PNP}(THF)] / boron nitride

4.3.4. Ethylene Tetramerisation

Table 4.4 shows the results for the tetramerisation reaction of ethylene to 1-octene. A similar catalysis test to the one run for the [$CrCl_3${SNS}] (Chapter 3) was performed. The chromium(III) complex (10 μmol) in toluene was activated upon addition of one hundred molar equivalents of $AlEt_3$, followed by the addition of one and a half molar equivalent of the aluminate $[Ph_3C][Al(ORf)_4]$. The temperature and pressure conditions (45^{0}C and 40 bar) were chosen to match the catalytic conditions of similar systems [10]. After a period of 60 minutes, the catalytic run was stopped and results revealed a high proportion of C_8 (72.1%) with a selectivity towards 1-C_8

of 98.7%. Results also show a relatively high proportion of C_6 (16.7%) with a selectivity towards 1-C_6 of 69.4%. The productivity is also rather high with 114,481 grams of product per gram of chromium complex.

Complex	C_6 (wt %)	1-C_6 (wt %)	C_8 (wt %)	1-C_8 (wt %)	PE (wt %)	productivity g/g(Cr)
$[CrCl_3\{PNP\}(THF)]$	16.7	69.4	72.1	98.7	1.7	114,481

Table 4.4. Ethylene trimerisation and tetramerisation for $[CrCl_3\{PNP\}(THF)]$

We can easily compare these results to recent studies on the dimer complex $[CrCl_3\{PNP\}]_2$ activated, in the first case, by addition of one hundred molar equivalents of $AlEt_3$ and in the presence of a borate co-catalyst, $[Ph_3C][BAr^F{}_4]$ (one molar equivalent) [10, 20]. The second case presents the results for the tetramerisation of ethylene to 1-octene with the dimer in presence of three hundred molar equivalents of MAO [10, 20]. The results of these studies are presented in Table 4.5.

Complex	PE (wt %)	C_6 (wt %)	1-C_6 (wt %)	C_8 (wt %)	1-C_8 (wt %)	productivity g/g(Cr)
[a] $[CrCl_3\{PNP\}]_2$	trace	19.6	69.2	70.8	98.3	2 540
[b] $[CrCl_3\{PNP\}]_2$	1.1	16.9	70.3	68.3	98.8	272, 400

[a] 10 μmol $[CrCl_3(THF)_3]$, 12 μmol PNP, 100 equiv. $AlEt_3$,
1 equiv. co-catalyst,
100 mL toluene as solvent, 45^{0}C, 30 min.

[b] 33 μmol $[Cr(acac)_3]$, 66 μmol PNP, 300 equiv. MAO,
100 mL toluene as solvent, 45^{0}C, 30 min.

Table 4.5. Ethylene trimerisation and tetramerisation [10]

Table 4.5 displays the results for the above-mentioned systems. 1-octene and 1-hexene are clearly the main products under the same temperature and pressure

conditions and show a selectivity towards 1-C_8 of ~ 98 %. The combined C_6 and C_8 fractions correspond to ~ 90 % of the liquid products in both cases. These results compares well with our system, $[CrCl_3\{PNP\}(THF)]$ / $AlEt_3$ / $[Ph_3C][Al(ORf)_4]$ with a selectivity towards 1-C_8 of 98.7 % and a C_6/C_8 fraction of 88.8 % of the liquid products. We can also note that the productivity of our system is relatively high when compared to the system with $[Ph_3C][BAr^F{}_4]$ as a co-catalyst. This implies that the choice of the co-catalyst is a determinant factor for the productivity. All these results enable us to say that the complex $[CrCl_3\{PNP\}(THF)]$ is efficient for the selective tetramerisation of ethylene to 1-hexene.

4.3.5. Study of the $[CrCl_3\{PNP\}(THF)]$ Complex Activated by Addition of Me_3Al and $[Ph_3C][Al(ORf)_4]$

4.3.5.1. UV/visible Studies

To get more insight of the reaction between the complex $[CrCl_3\{PNP\}(THF)]$ and an aluminium reagent, Me_3Al, in the presence and in the absence of one molar equivalent of the aluminate $[Ph_3C][Al(ORf)_4]$, the activation reaction was followed by UV/visible spectroscopy. A spectrum for a 5 mM solution of the complex in toluene was recorded and five molar equivalents of the trimethylaluminum were added. The blue solution turned yellow upon addition of the aluminium reagent. The new spectrum displayed a shift of the low energy *d-d* transition band along with the disappearance of the high energy band (Figure 4.6). The same features were observed with the $[CrCl_3\{SNS\}]$ complex and the chromium(III) complexes studied in Chapter 5 upon addition of an excess of Me_3Al. The change observed is then probably due to the same reason, *i.e.* a ligand exchange of chlorine(s) with methyl groups and a change in the oxidation state of the chromium metal centre is also very likely to occur. No significant difference could be observed when the chromium(III) complex was activated in the absence or in the presence of the aluminate (Figure 4.7), with a blue shift of ~120 cm^{-1} for the activated complex in solution and in the presence of $[Ph_3C][Al(ORf)_4]$. The bands being relatively broad, an accurate value of υ_1 could not be given. Table 4.6 presents the spectroscopic data for a 5 mM solution of $[CrCl_3\{PNP\}(THF)]$ activated with five molar equivalents of Me_3Al and in the presence of the aluminate $[Ph_3C][Al(ORf)_4]$. In order to confirm the suggested change

in the oxidation state, it was decided to repeat the above experiments using EPR spectroscopy.

Complex	$\upsilon 1^{a}/cm^{-1}$	$\upsilon_1{}^{b}/cm^{-1}$	$\upsilon_1{}^{c}/cm^{-1}$
$[CrCl_3\{PNP\}(THF)]$	14,750	15,190	15,310

Table 4.6. Spectroscopic data for a 5 mM toluene solution of $[CrCl_3\{PNP\}(THF)]$ [a]before, [b]after treatment with Me_3Al, [c]and in the presence of $[Ph_3C][Al(ORf)_4]$

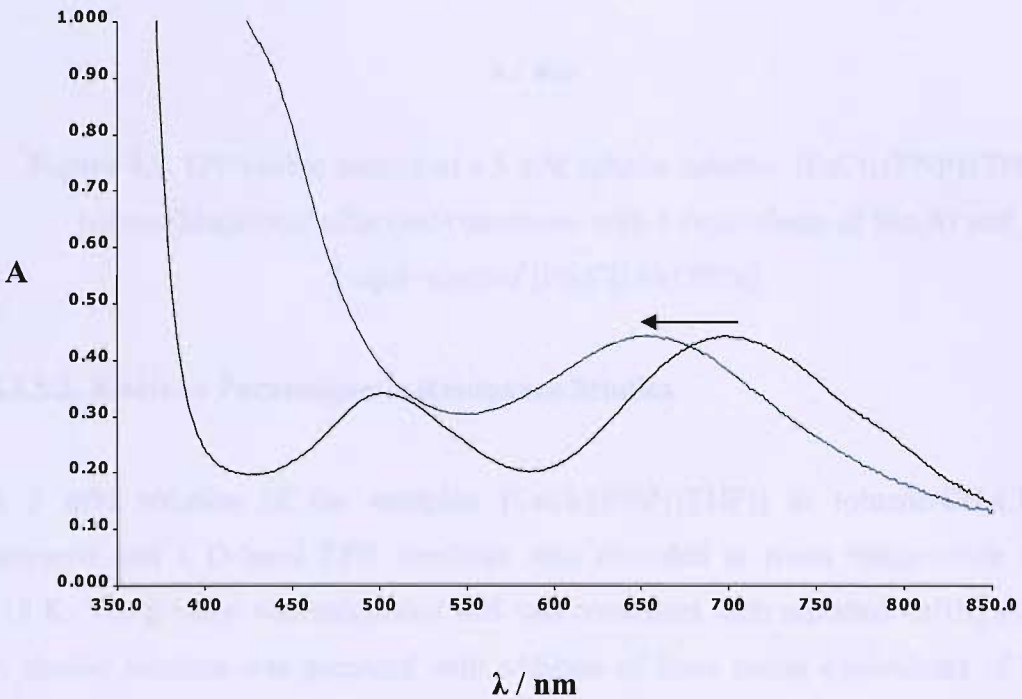

Figure 4.6. UV/visible spectra of a 5 mM toluene solution $[CrCl_3\{PNP\}(THF)]$ before (black) and after (blue) treatment with 5 equivalents of Me_3Al

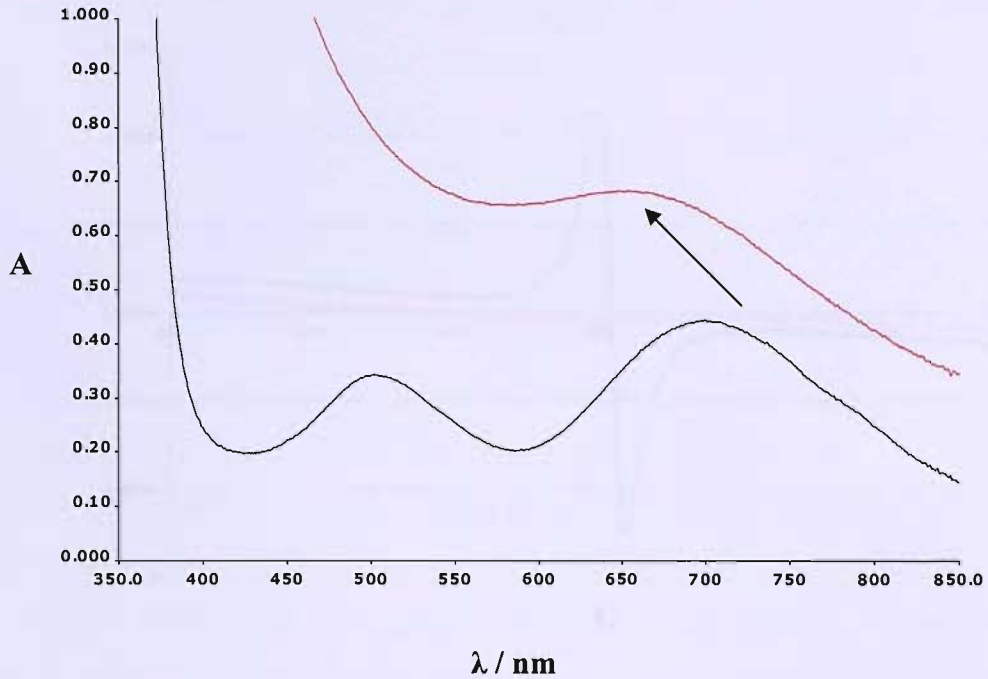

Figure 4.7. UV/visible spectra of a 5 mM toluene solution [$CrCl_3${PNP}(THF)] before (black) and after (red) treatment with 5 equivalents of Me_3Al and 1 equivalent of $[Ph_3C][Al(ORf)_4]$

4.3.5.2. Electron Paramagnetic Resonance Studies

A 5 mM solution of the complex [$CrCl_3${PNP}(THF)] in toluene/CH_2Cl_2 was prepared and a Q-band EPR spectrum was recorded at room temperature and at 115 K. The ***g*** value was calculated and was consistent with reported Cr(III) systems. A similar solution was prepared with addition of three molar equivalents of Me_3Al and the EPR spectrum was measured (Figure 4.8). The disappearance of the broad peak, characteristic of d^3 systems was observed. The experiment was repeated in the presence of one molar equivalent of the aluminate $[Ph_3C][Al(ORf)_4]$ and the disappearance of the signal was also noticed (Figure 4.9). This system behaves like all the chromium(III) complexes studied in this Thesis when treated with Me_3Al and we can then confirm that a change in the oxidation state of the metal centre occurs upon addition of an excess of trimethylaluminum.

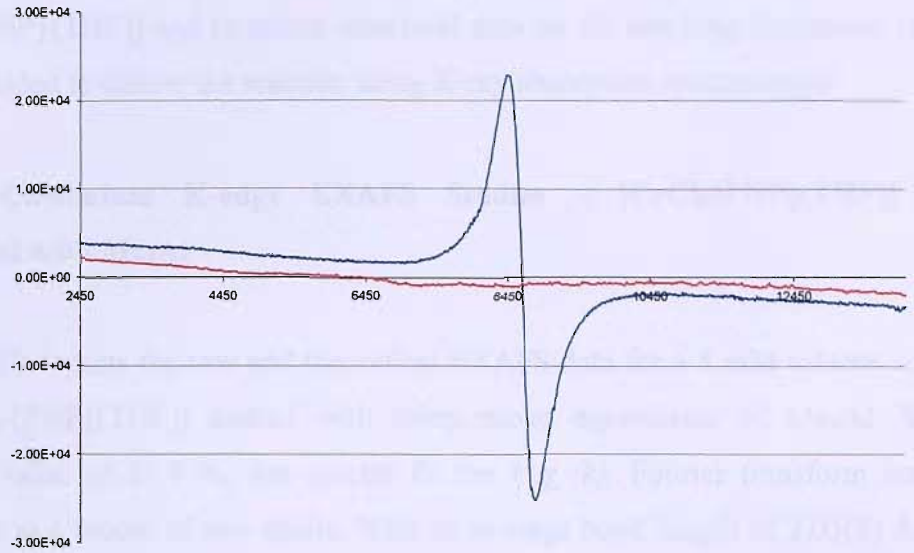

Figure 4.8. EPR spectrum (Q-band) for a toluene/CH_2Cl_2 solution of [$CrCl_3${PNP}(THF)] (blue) treated with 3 equivalents of Me_3Al (red); recorded as a frozen glass at T = 115 K, g = 1.99

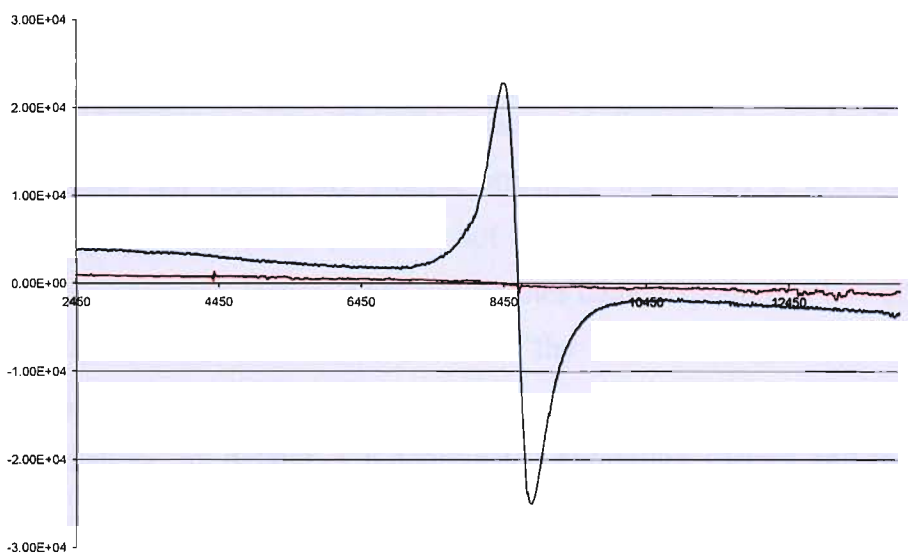

Figure 4.9. EPR spectrum (Q-band) for a toluene/CH_2Cl_2 solution of [$CrCl_3${PNP}(THF)] (blue) treated with 5 equivalents of Me_3Al (red) and 1 equivalent of $[Ph_3C][Al(ORf)_4]$; recorded as a frozen glass at T = 115, g = 1.99

In order to probe further changes occurring upon addition of Me_3Al to $[CrCl_3\{PNP\}(THF)]$ and to obtain structural data on the resulting chromium species, it was decided to follow the reaction using X-ray absorption spectroscopy

4.3.5.3. Chromium K-edge EXAFS Studies – $[CrCl_3\{PNP\}(THF)]$ upon Treatment with Me_3Al

Figure 4.10 depicts the raw and theoretical EXAFS data for a 5 mM toluene solution of $[CrCl_3\{PNP\}(THF)]$ treated with thirty molar equivalents of Me_3Al. With a R-factor value of 27.9 %, the spectra fit the $k^3.\chi\ (k)$, Fourier transform and sine transform to a model of two shells. With an average bond length of 2.03(9) Å and a coordination number of 0.9(4) atom, this first shell can be assigned to the Cr-C shell. The average $Cr\text{-}C_{alkyl}$ bond length ranges from 2.042 to 2.151 Å as seen in Chapter 3. We have to note that a carbon shell and an oxygen shell can not be easily differentiated for EXAFS analysis. Hence, it is important to consider that the active species could bear a THF molecule instead of a methyl group, thus two partial structures can be proposed. The second shell, with an average bond length of 2.46(3) Å and a coordination number of 1.9(2), is likely to correspond to the Cr-P shell. EXAFS data, from a second batch of complex, were recorded and gave similar results. It is important to note that the species studied appears to be 3-coordinate. Literature does not report any similar structure with such a low coordination. However, the EXAFS technique does not enable to see hydrogen atoms directly bonded to the absorber. Hence, a hydride species could explain this low coordination if we consider one or more Cr-H bonds in the structure. Figure 4.11 depicts the proposed partial structure for the complex treated with an excess of Me_3Al. The structures display, by default, a 6-coordinated chromium species and the unknown ligands are represented by a "?" which could, as explained above, be indicative of hydrogen atoms.

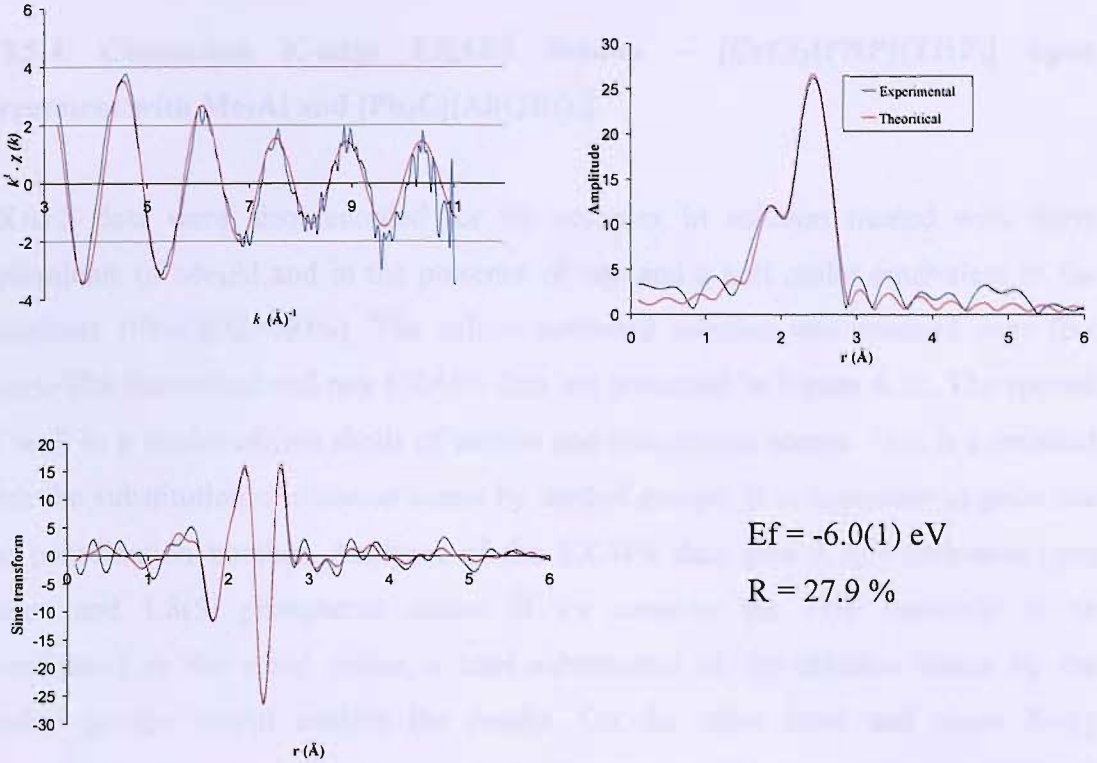

Ef = -6.0(1) eV

R = 27.9 %

Atom	C.N.	R / Å	$2\sigma^2$ / Å^2
C	0.9(4)	2.03(9)	0.009(4)
P	1.9(2)	2.46(3)	0.013(1)

Figure 4.10. The chromium K-edge k^3-weighted EXAFS, Fourier transform and sine transform for a 5 mM toluene solution of [$CrCl_3${PNP}(THF)] treated with 30 molar equivalents of Me_3Al

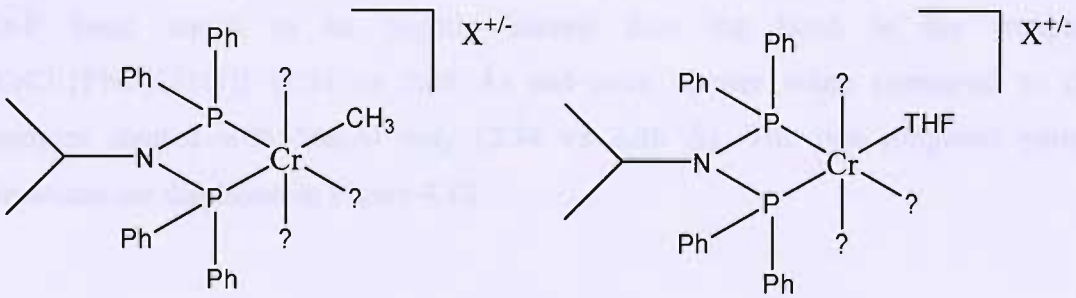

Figure 4.11. Proposed partial structures for the species produced when [$CrCl_3${PNP}(THF)] is treated with 30 molar equivalents of Me_3Al

4.3.5.4. Chromium K-edge EXAFS Studies – $[CrCl_3\{PNP\}(THF)]$ upon Treatment with Me_3Al and $[Ph_3C][Al(ORf)_4]$

EXAFS data were also recorded for the complex in solution treated with thirty equivalents of Me_3Al and in the presence of one and a half molar equivalent of the aluminate $[Ph_3C][Al(ORf)_4]$. The yellow activated solution was scanned over five hours. The theoretical and raw EXAFS data are presented in Figure 4.12. The spectra fit well to a model of two shells of carbon and phosphorus atoms. This is consistent with the substitution of chlorine atoms by methyl groups. It is important to point out the coordination number. Analyses of the EXAFS data give 3.7(5) carbon/oxygen atoms and 1.8(5) phosphorus atoms. If we consider the THF molecule to be coordinated to the metal centre, a total substitution of the chlorine atoms by the methyl groups would explain the results. On the other hand and since X-ray absorption spectroscopy is an average technique, we could be measuring a mixture of two different species. The first one containing the THF molecule, the bidentate PNP ligand and three methyl groups and the second species containing the bidentate PNP ligand and three methyl groups only, leaving a vacant site on the chromium centre to enable coordination of an ethylene molecule during the catalysis reaction. As for the $[CrCl_3\{SNS\}]$ complex treated with the same reagent, we could also expect the formation of a cationic-anionic pair. The average bond length for the carbon shell, 2.00(7) Å, is consistent with the values expected for a chromium-carbon bond. However, the average bond length for the phosphorus shell is shorter than in previous experiments. Literature reports that alkyl groups can cause a marked lengthening of Cr-P bonds in comparison to chlorine as the group *trans* to P [21]. In our case, the Cr-P bond seems to be slightly shorter than the bond in the complex $[CrCl_3\{PNP\}(THF)]$ (2.34 *vs* 2.39 Å) and even shorter when compared to the complex treated with Me_3Al only (2.34 vs 2.46 Å). The two proposed partial structures are displayed in Figure 4.13.

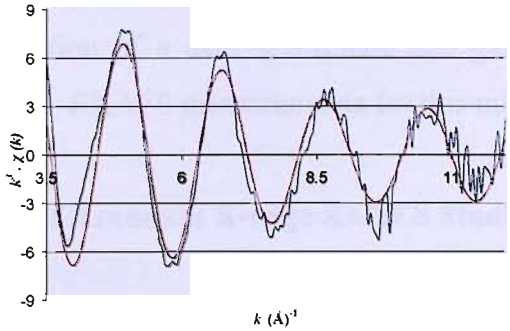

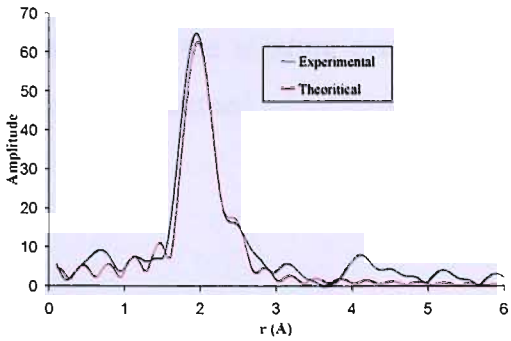

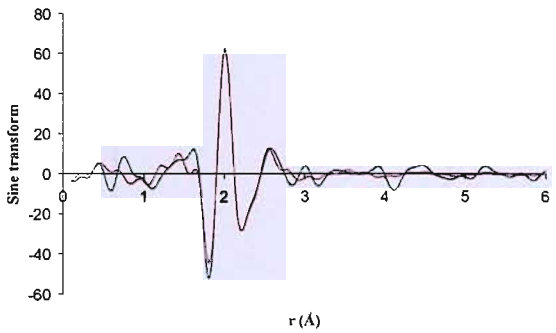

Ef = 4.4(7) eV

R = 35.4 %

Atom	C.N.	R / Å	$2\sigma^2$ / Å^2
C	3.7(5)	2.00(7)	0.002(1)
P	1.8(5)	2.34(4)	0.018(0)

Figure 4.12. The chromium K-edge k^3-weighted EXAFS, Fourier transform and sine transform for a 5 mM toluene solution of [$CrCl_3${PNP}(THF)] treated Me_3Al and [Ph_3C][$Al(ORf)_4$]

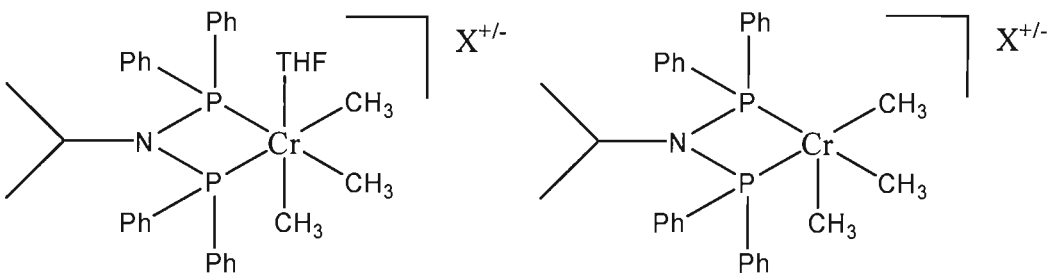

Figure 4.13. Proposed partial structures for [$CrCl_3${PNP}(THF)] treated with 30 molar equivalents of Me_3Al and 1.5 molar equivalent of [Ph_3C][$Al(ORf)_4$]

It is important to note that the presence of 1-hexene in the solution resulted in the formation of a dark precipitate and gas evolution during the mixture preparation. Hence, EXAFS measurements for this mixture were not performed.

4.3.6. Chromium K-edge XANES Studies

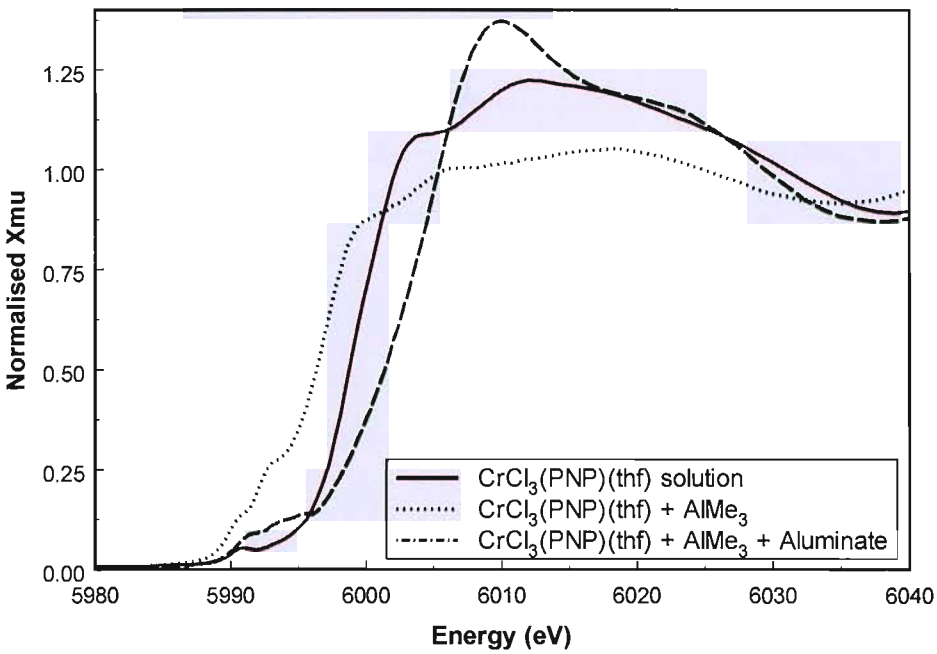

Figure 4.14. Normalised XANES spectra for a 5 mM toluene solution of $[CrCl_3\{PNP\}(THF)]$ treated with Me_3Al and $Me_3Al/[Ph_3C][Al(ORf)_4]$

The XANES spectrum for the complex $[CrCl_3\{PNP\}(THF)]$ in solution treated with thirty molar equivalents of Me_3Al shows a shift of the edge to lower energy, from 6000 eV to 5996 eV (Figure 4.14). EPR suggests that a Cr(II) or Cr(IV) species is formed upon addition of the aluminium reagent. Studies on a range of chromium complexes show that a Cr(IV) complex tends to have an absorption range around 6008 eV (for $Cr(CH_2Si(Me)_3)_4$) [22]. A Cr(II) species can however range between 6007 eV for the dimer $Cr(OAc)_2.H_2O$ and 6001 eV for $CrCl_2(THF)_2$. EXAFS studies show that the chromium centre is at least 3-coordinate and its local symmetry can not be determined. Since the oxidation states and hence, the position of the absorption edge, depend on the local symmetry of the complex, it is therefore very difficult to

favour a Cr(II) species to a Cr(IV) species when the complex is treated with Me_3Al. The second spectrum displayed in Figure 4.14 depicts the XANES for the complex treated with thirty molar equivalents of Me_3Al and one and a half molar equivalent of the aluminate $[Ph_3C][Al(ORf)_4]$. In this case, the absorption edge of the new species shifts to higher energy when compared to the absorption edge for the non-treated complex, from 6000 eV to 6004 eV. EPR studies support a change in the oxidation state, from Cr(III) to Cr(II) or Cr(IV). However, EXAFS studies did not give clear results and a mixture of two species was probably measured. Hence, the oxidation state of the active species when $[CrCl_3\{PNP\}(THF)]$ is treated with Me_3Al and $[Ph_3C][Al(ORf)_4]$ can not be determined.

4.4. Conclusions

In this chapter, we have probed the reaction between the complex $[CrCl_3\{(isoPr)N(PPh_2)_2\}]$ and an aluminium reagent, Me_3Al, using UV/visible, EPR and EXAFS spectroscopy and cyclic voltammetry. UV/visible results revealed that a change in the coordination sphere of the chromium metal centre occurs upon addition of the aluminium reagent involving a substitution of some or all chlorine groups by methyl groups and a change in the oxidation state of the metal centre.

The change in the oxidation state from Cr(III) to Cr(II) or Cr(IV) was also confirmed by EPR spectroscopy with the disappearance of the broad and strong signal, characteristic for d^3 systems. Similar results were obtained by addition of the aluminate species $[Ph_3C][Al(ORf)_4]$.

EXAFS measurements showed unexpected results with the formation of a very low coordinate species when the complex was treated with an excess of Me_3Al. The formation of a hydride intermediate was then suggested since a 3-coordinate chromium(III) complex is unlikely for this reaction. EXAFS measurements were performed for the complex treated with Me_3Al and in the presence of $[Ph_3C][Al(ORf)_4]$. Data analysis revealed the possible formation of a mixture of two species.

XANES data analyses did not enable us to determine the oxidation state of the active species. It is important to note the presence of a big shift in the absorption edge between the species formed by treatment of the complex with Me_3Al only and the complex treated by Me_3Al plus $[Ph_3C][Al(ORf)_4]$. The symmetry of the active species being unresolved by EXAFS analyses, it was therefore impossible to determine their oxidation state.

As explained in Chapter 1, it is thought that the catalytic cycle with the PNP ligand involves a Cr(I)/Cr(III) couple. Our investigation did not give evidence of such a cycle. Therefore, part of our work was focused on a new Cr(I) species, $[Cr(CO)_4\{PNP\}][Al(ORf)_4]$, as a catalyst. The lack of data did not enable us to present this system in this Thesis.

4.5. Experimental

The ligand isoPrN(PPh_2)$_2$ and the chromium complexes [$CrCl_3${isoPrN(PPh_2)$_2$}(THF)] and [$Cr(CO)_4${isoPrN(PPh_2)$_2$}] were prepared by literature methods or modification of those. Bis(phenyl)phosphorus chloride and isopropylamine were purchased from Aldrich and were used as received.

Synthesis of isoPrN(PPh_2)$_2$ [10]: To a solution of bis(phenyl)phosphorus chloride (10 mL, 56 mmol) in dry/degassed toluene (50 mL) and triethylamine (25 mL, 0.180 mol) at 0°C was added isopropylamine (2.4 mL, 0.028 mol). The reaction was stirred for 30 minutes after which the ice bath was removed. The mixture was stirred overnight under N_2. Degassed brine was added and the aqueous phase was extracted with toluene (3 x 30 mL). The organic extracts were combined and dried over $MgSO_4$. The solution was then filtered off and the toluene was removed *in vacuo*. The yellowish product obtained was then washed with methanol (50 mL) to give a white solid. Yield: 18.7 g, 44 mmol (78%). ^{1}H NMR ($CDCl_3$): δ 1.1 (d, 6H, C**H**$_3$), 3.70 (m, 1H, C**H**), 7.35 (m, 20H, Ar) ppm. ^{13}C{^{1}H} ($CDCl_3$): δ 24.36 (**C**H_3), 51.94 (**C**H), 127.96, 128.04, 128.53, 132.74, 133.02 (Ar) ppm. ^{31}P{^{1}H} ($CDCl_3$): δ 48.9 ppm.

Synthesis of [$CrCl_3${isoPrN(PPh_2)$_2$}(THF)] [14]: The procedure was to add the PNP ligand (0.20 g, 0.468 mmol) to a solution of [$CrCl_3(THF)_3$] (0.175g, 0.468 mmol) in dried and degassed dichloromethane (15 mL). The resulting mixture was stirred at room temperature under nitrogen for 1 hour and the solvent was then removed *in vacuo* to afford a blue solid. Yield: 0.194 g, 2.95×10^{-4} mol (63%).

4.6. References

1. Freeman, J. W.; Buster, J. L. and Knudsen, R. D.; *U.S. Patent 5,856,257*, (1999), Phillips Petroleum Company.
2. McGuinness, D. S.; Wasserscheid, P.; Morgan, D. H. and Dixon, J. T.; *Organometallics*, (2005), **24**, 552.
3. McGuinness, D. S.; Wasserscheid, P.; Keim, W.; Morgan, D.; Dixon, J. T.; Bollmann, A.; Maumela, H.; Hess, F. and Englert, U.; *J. Am. Chem. Soc.*, (2003), **125**, 5272.
4. McGuinness, D. S.; Wasserscheid, P.; W, W. Keim; Hu, C.; Englert, U.; Dixon, J. T. and Grove, C.; *Chem. Commun.*, (2003), 334.
5. Carter, A.; Cohen, S. A.; Cooley, N. A.; Murphy, A.; Scutt, J. and Wass, D. F.; *Chem. Comm.*, (2002), 858.
6. Agapie, T.; Schofer, S. J.; Labinger, J. A. and Bercaw, J. E.; *J. Am. Chem. Soc.*, (2004), **126**, 1304.
7. Yu, Z. and Houk, K. N.; *Angew. Chem. Int. Ed.*, (2003), **42**, 808.
8. Blok, A. N. J.; M.Budzelaar, P. H. and Gal, A. W.; *Organometallics*, (2003), **22**, 2564.
9. Kuhlmann, S.; Dixon, J. T.; Haumann, M.; Morgan, D. H.; Ofili, J.; Spuhl, O.; Taccardi, N. and Wasserschied, P.; *Adv. Synth. Catal.*, (2006), **348**, 1200.
10. Bollmann, A.; Blann, K.; Dixon, J. T.; Hess, F. M.; Killian, E.; Maumela, H.; McGuinness, D. S.; Morgan, D. H.; Neveling, A.; Otto, S.; Overett, M.; Slawin, A. M. Z.; Wasserscheid, P. and Kuhlmann, S.; *J. Am. Chem. Soc.*, (2004), **126**, 14712.
11. McGuinness, D. S. and Rucklidge, A. J.; *IPN PCT/IB2006/0053494*, (2006), Sasol Technology UK
12. Overett, M. J.; Blann, K.; Bollmann, A.; Dixon, J. T.; Hess, F.; Killian, E.; Maumela, H.; Morgan, D. H.; Neveling, A. and Otto, S.; *Chem. Commun.*, (2005), 622.
13. Overett, M. J.; Blann, K.; Bollmann, A.; Dixon, J. T.; Haasbroek, D.; Maumela, H.; McGuinness, D. S. and Morgan, D. H.; *J. Am. Chem. Soc.*, (2005), **127**, 10723.
14. Pope, S. J. A.; Champness, N. R. and Reid, G.; *J. Chem. Soc., Dalton Trans.*, (1997), 1639.

15. Gray, L. R.; Hale, A. L.; Levason, W.; McCullough, F. P. and Webster, M.; *J. Chem. Soc., Dalton Trans.*, (1984), 47.

16. Jones, P. J.; Hale, A. L.; Levason, W. and McCullough, F. P.; *Inorg. Chem.*, (1983), **22**, 2642.

17. Ogden, J. S., *Introduction to Molecular Symmetry*, (2001), Oxford, Oxford University Press.

18. Hale, A. L. and Levason, W.; *J. Chem. Soc., Dalton Trans.*, (1983), 2569.

19. Cotton, F. A.; Duraj, S. A.; Powell, G. L. and Roth, W. J.; *Inorg. Chim. Acta*, (1986), **113**, 81.

20. McGuinness, D. S.; www.ip.com; *IPCOM000031729D.*

21. Thaler, E. G.; Folting, K.; Huffman, J. C. and Caulton, K. G.; *J. Organomet. Chem.*, (1989), **379**, 343.

22. Tromp, M.; Moulin J.; Reid G. and Evans J.; AIP Conference Proceedings, Proceedings of the 13th International Conference on X-ray Absorption Fine Structure Spectroscopy, Stanford, 9-13 July 2006, *Accepted for publication.*

Chapter 5

Novel Chromium(III) Complexes for Ethylene Oligomerisation: Effect of Ligand Structure on Activity and Selectivity

5.1. Introduction

5.1.1. Ethylene Oligomerisation and Polymerisation

Over recent years, a phenomenal acceleration in research activity has been experienced on the investigation and development of homogeneous transition metal catalysts in ethylene oligomerisation and polymerisation [1-3]. Only lately, several publications describe chromium catalysts as playing an important role in both ethylene oligomerisation and polymerisation [4, 5]. The chromium based heterogeneous Phillips catalyst for ethylene polymerisation [6] produces polyethylene with broad molecular weight distributions (C_6-C_{20} range) as a unique property. Presently, α-olefins are produced by the Alfen [7] or Shell higher olefin [8] processes. Meanwhile, and as seen in Chapters 3 and 4, Cr-based catalysts play a central role in the ethylene trimerisation and tetramerisation reactions [9-14]. Homogeneous catalysis supported by chromium catalysts has recently drawn much attention for ethylene polymerisation and oligomerisation [15]. Coordinated to a broad range of tridentate ligands bearing a combination of sulfur, nitrogen and phosphorus donor atoms, the chromium(III) complexes have shown great potential in ethylene polymerisation [10, 13, 16-18].

In contrast to the wide range of chromium(III) complexes with hard nitrogen and oxygen donor ligands, few examples of complexes with soft donor ligands such as thioethers are known [19, 20]. Most of all, literature does not report any tridentate chromium(III) complexes ligated with sulfur only donor atoms and used as catalysts for ethylene oligomerisation and polymerisation. On the other hand, chromium(III) complexes coordinated to nitrogen-based acyclic and cyclic ligands show good activities for the combined oligomerisation and polymerisation [4-6].

On a mechanistic point of view, it is believed that a change in the oxidation state of the metal centre occurs upon activation with MAO. Used as a cocatalyst, MAO is normally thought to implicate a cationic active metal centre [21] through the couple Cr(II)→Cr(IV). Even if this route seems more likely than the cycle involving neutral species (couple Cr(I)→Cr(III)), there is still no strong evidence to support that idea (Chapter 3 and Chapter 4). The use of Lewis acids such as *per*-fluoroaryl boranes, along with alkyl metal complexes or alkylating agents, has shown to be an alternative

to the use of MAO, allowing the characterisation of well-defined cationic species [21, 22].

5.2. Aims

With the ultimate goal of gaining useful insight into the catalytic cycle, we describe in this chapter the investigation and the synthesis of novel chromium(III) complexes of the type $[CrCl_3\{L\}]$, with L being a tridentate ligand, for the reaction of ethylene oligomerisation and polymerisation. This chapter focuses on the effect of the ligand structure on the activity and selectivity. The ligands are chosen to cover a wide area of catalytic activity; from the geometry – open-chain, tripod, macrocycle - to the type of donor atoms, hard donor nitrogen and oxygen atoms and soft donor sulfur atoms. Most of the chromium(III) complexes coordinated to ligands bearing methyl groups on their donor atoms appeared to be insoluble in organic solvents (Chapter 6). The alkyl group on the donor atoms (decyl or butyl groups) has then been chosen in order to improve the solubility of the chromium complexes. Moreover, studies show that the nature of the alkyl group on the donor plays a significant role in the activity of the catalyst. A longer alkyl chain seems to afford greater activity due to an enhanced solubility in the reaction solvent. A series of chromium(III) complexes are studied using a range of spectroscopic techniques such as infra-red and UV/visible spectroscopy. Partial structural data were obtained with chromium K-edge EXAFS measurements. Activated catalysts were then employed for ethylene oligomerisation and polymerisation and investigation of the partial structure of the activated complexes by Me_3Al was followed by UV/visible and EPR spectroscopy and EXAFS analysis.

5.3. Results and Discussion

5.3.1. Ligands Synthesis

The series of ligands prepared will probe geometric control (facultative, tripodal and macrocyclic geometries) and ligand donor effects (sulfur, oxygen and nitrogen donor atoms) on the ability of the complexes [$CrCl_3${L}] to promote the oligomerisation and polymerisation of ethylene.

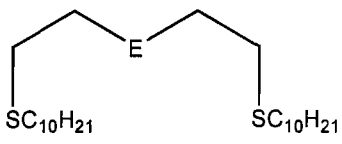

with E = S (L1), O (L2)

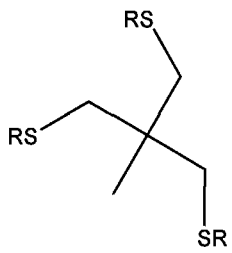

with R = C_4H_9 (L3), $C_{10}H_{21}$ (L4)

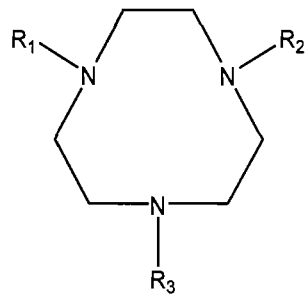

with $R_1 = R_2 = H$, $R_3 = C_{10}H_{21}$ (L5)
$R_1 = R_2 = R_3 = C_{10}H_{21}$ (L6)

a) Synthesis of $S(CH_2CH_2SC_{10}H_{21})_2$

The ligand $S(CH_2CH_2SC_{10}H_{21})_2$ {L1} was prepared from the reaction between bis(2-mercaptoethyl)sulfide with two molar equivalents of iododecane, *via* the disodium salt in ethanol and fractioned *in vacuo* (Scheme 5.1) [23]. The white powder obtained (80% yield) was characterised by a combination of infra-red, ^1H and $^{13}C\{^1H\}$ NMR spectroscopy, mass spectrometry and elemental analysis. The ^1H NMR spectrum of the crude product revealed a multiplet at 2.75 ppm corresponding to the backbone SCH_2CH_2S of the ligand. Four signals at δ 0.88, 1.26, 1.58 and 2.54 ppm also confirmed the presence of the decyl group, $C_{10}H_{21}$. The $^{13}C\{^1H\}$ NMR spectrum of the obtained compound was consistent with the formation of the desired ligand $S(CH_2CH_2SC_{10}H_{21})_2$. Elemental analysis of the ligand was performed and was in excellent agreement with expectations. Therefore no further purifications were necessary.

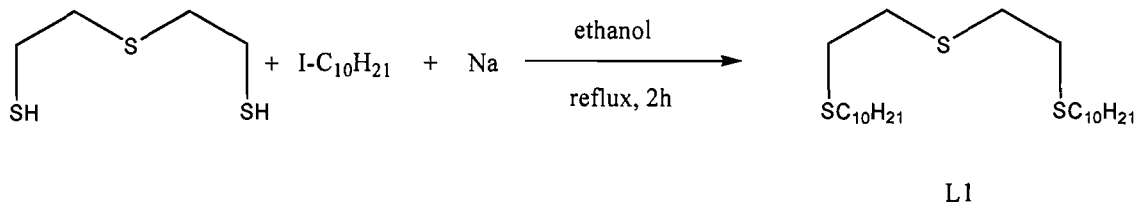

L1

Scheme 5.1. Synthesis of $S(CH_2CH_2SC_{10}H_{21})_2$

b) Synthesis of $O(CH_2CH_2SC_{10}H_{21})_2$

The ligand $O(CH_2CH_2SC_{10}H_{21})_2$ {L2} was prepared using a solution of bis(2-chloroethyl)ether and sodium hydroxide in ethanol, to which two molar equivalents of decanethiol were added (Scheme 5.2). A colourless oil that crystallised upon standing at room temperature was obtained (81% yield). The compound was fully characterised and analyses performed confirmed the nature of the desired ligand.

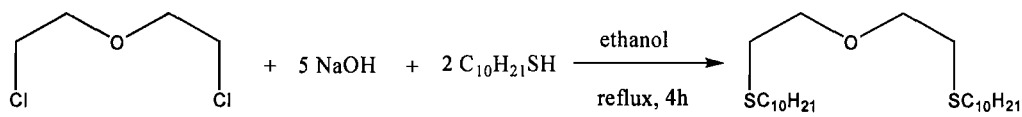

L2

Scheme 5.2. Synthesis of $O(CH_2CH_2SC_{10}H_{21})_2$

c) Synthesis of $MeC(CH_2S^nC_4H_9)_3$

The ligand $MeC(CH_2S^nC_4H_9)_3$ {L3} was synthesised *via* modification of a reported method [24]. The previously prepared starting material $MeC(CH_2Br)_3$ was reacted with three molar equivalents of the salt $Na^+S(^nC_4H_9)^-$. After being refluxed for seventy hours, the reaction mixture was washed and distilled to afford a clear orange oil

(Scheme 5.3). As for the ligands {L1} and {L2}, the compound obtained was fully characterised by ^{1}H, $^{13}C\{^{1}H\}$ NMR spectroscopy, high resolution mass spectrometry and elemental analysis.

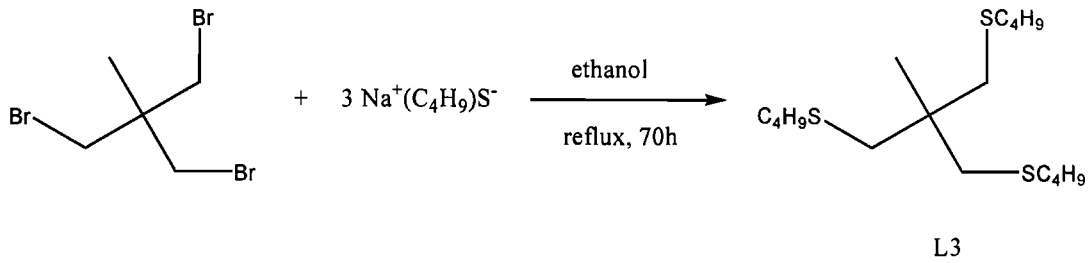

L3

Scheme 5.3. Synthesis of $MeC(CH_2S^nC_4H_9)_3$

d) Synthesis of $MeC(CH_2SC_{10}H_{21})_3$

The synthesis of $MeC(CH_2SC_{10}H_{21})_3$ {L4} was more trivial than the preparation of {L3} and only consisted of reacting $MeC(CH_2Br)_3$ with three molar equivalents of decanethiol in the presence of an excess of sodium hydroxide. The reaction mixture was refluxed under nitrogen for 24 hours to yield an orange oil (Scheme 5.4). Mass spectrometry showed that three fractions corresponding to the mono-, di- and tri-substituted decyl tripod derivatives were obtained. A distillation under nitrogen was performed in order to isolate the desired ligand as a clear oil. The tri-decyl tripod derivative was fully characterised by spectroscopic methods and elemental analysis.

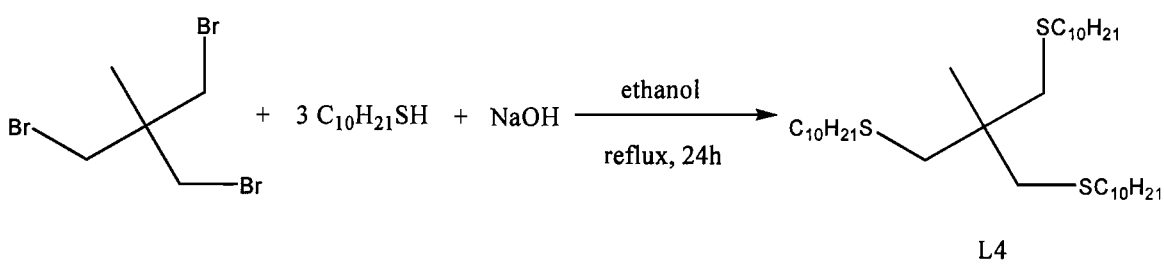

L4

Scheme 5.4. Synthesis of $MeC(CH_2SC_{10}H_{21})_3$

e) Synthesis of $(C_{10}H_{21})$[9]aneN$_3$ and $(C_{10}H_{21})_3$[9]aneN$_3$

Ligands {L5} and {L6} are respectively the mono- and tri-decyl derivatives of the macrocycle [9]aneN$_3$. The 1,4,7-triazacyclononane, [9]aneN$_3$, was synthesised following modified procedures described in the literature (Chapter 6) [25-27]. Direct alkylation of the secondary amino groups of azamacrocycles with simple aliphatic alkyl halides such as decyl chloride or decyl bromide could lead to quaternisation of the nitrogen atoms, producing species with no metaligating properties. To overcome this problem, the two step reaction sequence similar to the one reported by Moore and co-workers for N-alkylated cyclam was adopted [28, 29]. The macrocycle {L6} was produced in 76 % yield based on [9]aneN$_3$ by the reaction of decanoyl chloride with [9]aneN$_3$ in the presence of triethylamine, followed by the reduction of the resulting triamide, $(C_9H_{19}CO)_3$[9]aneN$_3$ with BH_3.THF (Scheme 5.6).

The mono-substituted macrocycle $(C_{10}H_{21})$[9]aneN$_3$ was prepared following a similar method but using the diprotected DiBOC-[9]aneN$_3$. This intermediate was then treated with decanoyl chloride to produce a protected amide $(C_9H_{19}CO)$-DiBOC-[9]aneN$_3$ which was reduced and diprotected with BH_3.THF to yield the desired ligand (49%) (Scheme 5.5). Unlike the waxy solid [9]aneN$_3$, the alkylated ligands $(C_{10}H_{21})$[9]aneN$_3$ and $(C_{10}H_{21})_3$[9]aneN$_3$ were obtained as oils at room temperature. Both ligands were characterised by spectroscopic methods and elemental analysis.

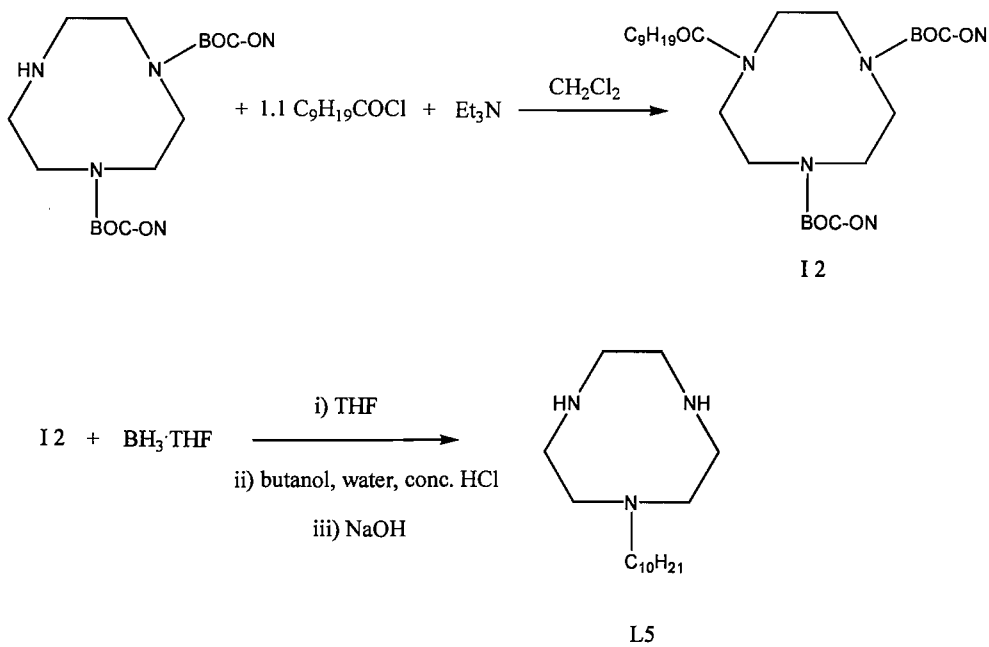

Scheme 5.5. Synthesis of $(C_{10}H_{21})$[9]aneN$_3$

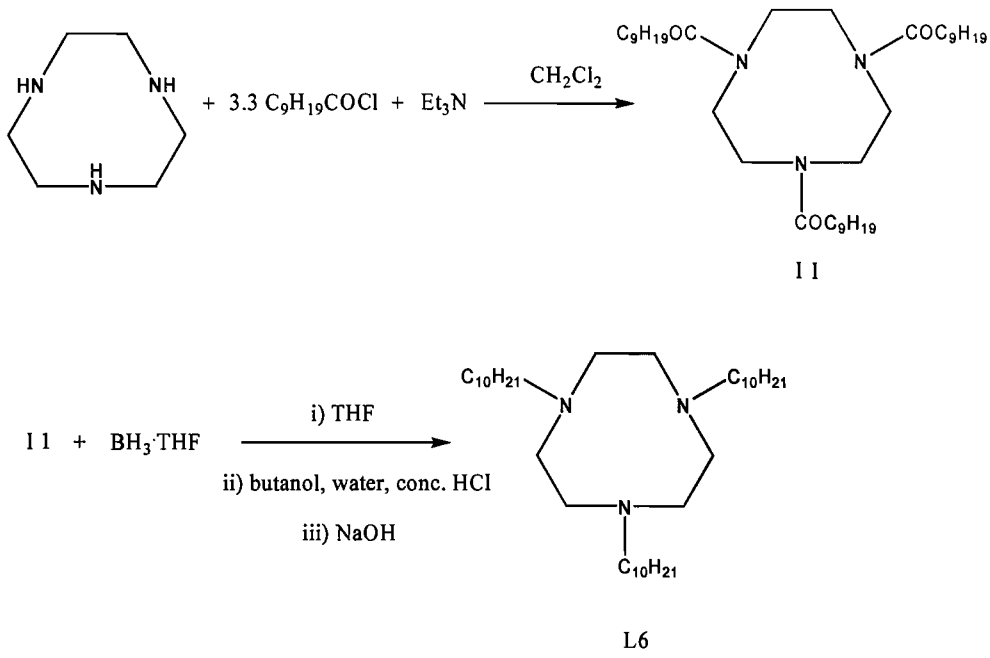

Scheme 5.6. Synthesis of $(C_{10}H_{21})_3$[9]aneN_3

5.3.2. Synthesis of the Chromium(III) Complexes [$CrCl_3${L}] (L = L1-L6)

The distorted octahedral [$CrCl_3${L}] complexes (L = L1-L6) were prepared by reaction of [$CrCl_3(THF)_3$] [30] with one molar equivalent of the ligand {L} in anhydrous CH_2Cl_2 (Scheme 5.7) [19]. The products were isolated in relatively good yields as purple or green coloured solids [$CrCl_3${L}] (L = L1-L5) or oily compounds [$CrCl_3${L6}] by evaporation to dryness.

$$[CrCl_3(THF)_3] + L \xrightarrow[-\ 3\ THF]{CH_2Cl_2} [CrCl_3(L)]$$

with L = L1-L6

Scheme 5.7. Synthesis of [$CrCl_3${L}] (L = L1-L6)

These neutral compounds proved to be soluble in both chlorinated and organic solvents. The complexes [$CrCl_3${L}] (L = L3-L6) are also relatively sensitive to moisture, hence all were stored in a N_2-purged glove-box. Table 5.1 summarises the data supporting the nature of the complexes synthesised.

	Elemental Analysis		Exp. (theor.)
Complex	% C	% H	% E (E = N, S)
[$CrCl_3${L1}]	48.55 (48.59)	8.52 (8.50)	16.22 (16.22)
[$CrCl_3${L2}]	49.87 (49.95)	8.77 (8.73)	-
[$CrCl_3${L3}]	41.17 (41.25)	7.35 (7.33)	-
[$CrCl_3${L4}]	56.36 (56.24)	9.76 (9.71)	-
[$CrCl_3${L5}]	44.82 (44.92)	8.27 (8.25)	9.76 (9.82)
[$CrCl_3${L6}]	61.13 (61.04)	10.75 (10.67)	5.88 (5.93)

Table 5.1. Elemental analysis data for [$CrCl_3${L}] (L = L1-L6) compounds

5.3.3. Characterisation of the Chromium(III) Complexes

5.3.3.1. UV/visible and Infra-red Spectroscopy

An octahedral d^3 system is expected to exhibit three quartet excited states and show three spin-allowed *d-d* transitions in a UV/visible spectrum: $^4A_{2g} \rightarrow {}^4T_{2g}$ (υ_1); $^4A_{2g} \rightarrow {}^4T_{1g}$ (F) (υ_2); $^4A_{2g} \rightarrow {}^4T_{1g}$ (P) (υ_3) [31]. However, the last of these transitions is usually obscured due to a more intense ligand-metal charge-transfer band. The two low energy *d-d* transition are observed for all the chromium(III) complexes studied, and from the low energy transition can be obtained *Dq*. The complexes [$CrCl_3${L1}], [$CrCl_3${L3}], [$CrCl_3${L4}] exhibit a *Dq* value of ~1 440 cm^{-1}. The *Dq* value for [$CrCl_3${L2}] is slightly lower but the difference with the other complexes is not statistically significant. These values are very similar to the ones obtained after extensive studies from Grant, Kuppers and Levason [32, 33, 35] giving *Dq* values of 1 433 cm^{-1} for [$CrCl_3${[9]aneS_3}], 1 420 cm^{-1} for [$CrCl_3${[18]aneS_6}], 1 449 cm^{-1} for [$CrCl_3${$S(CH_3)_2$}$_3$] and 1 470 cm^{-1} for [$CrCl_3${$MeC(CH_2SCH_3)_3$}]. The geometry of the ligand (open-chain and tripodal) does not affect the ligand-field splitting.

The aza-macrocycle complexes $[CrCl_3\{L5\}]$, $[CrCl_3\{L6\}]$, present a higher value with $Dq \sim 1\ 680\ cm^{-1}$. The Dq values for these two complexes is relatively low when compared to similar systems such as $[Cr\{H_2NCH_2CH_2NH_2\}_3]^{3+}$ where $Dq = 2\ 180\ cm^{-1}$ [34], $[Cr\{[9]aneN_3\}_2]^{3+}$, $Dq = 2\ 270\ cm^{-1}$, $[Cr\{[18]aneN_6\}]^{3+}$, $Dq = 2\ 146\ cm^{-1}$, $[Cr\{[20]aneN_6\}]^{3+}$, $Dq = 2\ 190\ cm^{-1}$ and $[Cr\{NH_3\}_6]^{3+}$, $Dq = 2\ 160\ cm^{-1}$. These results allow us to confirm the trend that interactions between the Cr(III) and the soft thioether functions are weak compared to those with the strong nitrogen functions. The relatively low Dq values produced in the Cr(III) cations are due to both electronic and steric factors. The hard Cr(III) centre will bind soft S-donors less strongly than the hard N-donors, and the +3 charge on the cation will cause contraction of the chromium *d* orbitals, increasing the mismatch in size and energy with the S-donor orbitals. This observation is consistent with all the work that has been done on such systems and correlates well with the data obtained with other chromium(III) complexes in the Chapter 6 [35].

The infra-red spectroscopic data for the complexes $[CrCl_3\{L\}]$ (L = L1-L6), presented in Table 5.2, provide evidence of the coordinated thioether and aza-macrocycle ligands. Peaks observed in the region 200-400 cm^{-1} may be assigned to υ(Cr-Cl), hence give structural information on the complexes. However, given that in some cases these peaks were rather weak, and since υ(Cr-S) would also be expected to appear in this region, definitive assignments were not possible.

The steric constraints of the tripodal ligands $MeC(CH_2S^nC_4H_9)_3$ and $MeC(CH_2SC_{10}H_{21})_3$ are such that monomeric complexes must be *facial* isomers [36]. This is borne out by IR spectroscopy and the two bands observed in the 200-400 cm^{-1} region that may be assigned to the ν(Cr-Cl) stretching modes. Moreover, the macrocyclic geometry of the tridentate ligands $(C_{10}H_{21})$[9]aneN$_3$, $(C_{10}H_{21})_3$[9]aneN$_3$ is such that they coordinate *facially* in octahedral complexes. Literature and the infra-red data obtained support this idea [37]. The infra-red spectrum for $[CrCl_3\{(C_{10}H_{21})[9]aneN_3\}]$ depicts a peak at 3189 cm^{-1}, characteristic region of the N-H stretching mode and confirms the coordination of the ligand to the chromium metal centre.

The stereochemistry of the complex $[CrCl_3\{S(CH_2CH_2SC_{10}H_{21})_2\}]$ could not be validated by infra-red spectroscopy. Only a broad band at 342 cm^{-1} was observed. However, extensive work on crown thioether chemistry and the implications of the

ligand design help us to suggest the geometry of the complex. According to Wolf and co-workers [38], 1,4 interactions favour *anti* placements at S-C-C-S bonds. The large size of the sulfur atoms causes greater electron-electron repulsion between them, which destabilises *gauche* placement at the S-C-C-S bonds. On the other hand, even if 1,4 interactions disfavour *gauche* placement at S-C-C-S bonds (repulsive *gauche* effect), they do not disfavour it at C-C-S-C bonds. These conformational effects at C-S and C-C bonds reinforce each other to influence conformation. Hence, the ligand will behave like a cyclic structure and *facially* co-ordinate to the metal centre. We can easily compare the $S(CH_2CH_2SC_{10}H_{21})_2$ with the thioether macrocycle [9]aneS$_3$ which co-ordinates *facially* to form the distorted octahedral [$CrCl_3${[9]aneS$_3$}] (Chapter 6). On the other hand, a *meridional* isomer would be expected for [$CrCl_3\{O(CH_2CH_2SC_{10}H_{21})_2\}$]. 1,4 interactions favour *anti* placements at C-C-O-C bonds. Mark and Flory spectroscopic studies showed that *gauche* placement at C-C-O-C bond is less stable than *anti* and repulsion between the terminal hydrogen atoms result in the favoured *anti* configuration [39]. The *meridional* conformation of the complex is however due to the stabilisation of the attractive *gauche* effect between O and S atoms which favours the *gauche* placement at the O-C-C-S bonds. Analysis of the infra-red spectrum confirmed the stereochemistry of that compound with three bands expected for a *meridional* isomer (C_{2v}) that could be assigned to the ν(Cr-Cl) stretching modes.

Complex	υ_1/cm^{-1}	υ_2/cm^{-1}	Dq/cm^{-1}	ε_1; $\varepsilon_2/M^{-1}.cm^{-1}$	ν (Cr-Cl)/cm^{-1}
[$CrCl_3${L1}]	14 300	19 330	1 430	200, 280	342 (br)
[$CrCl_3${L2}]	13 960	21 050	1 396	250, 400	389, 364, 347
[$CrCl_3${L3}]	14 400	20 320	1 440	185, 220	357, 334
[$CrCl_3${L4}]	14 390	20 280	1 439	-	360, 333
[$CrCl_3${L5}]	16 840	20 620	1 684	-	327, 307
[$CrCl_3${L6}]	16 800	21 790	1 680	104, 179	315, 308

UV/visible spectra recorded in toluene solution. Infra-red spectra recorded as nujol mulls.

Table 5.2. Selected electronic and IR spectroscopic data for [$CrCl_3${L}] (L = L1-L6)

5.3.3.2. Cyclic Voltammetry for [$CrCl_3${L}] (L = L1-L6)

In order to evaluate the effects of the ligands on the oxidation/reduction properties of the chromium(III) complexes [$CrCl_3${L}] (L = L1-L6) we measured cyclic voltammograms. The effectiveness of CV results from its capability for rapidly observing the redox behaviour over a wide potential range. Electrochemical data were recorded at room temperature under an N_2 atmosphere and with a scan rate of 100 mV/s over a range of 1.5 to -1.5V. A 0.2 M [Bu^n_4N]BF_4 electrolyte in anhydrous CH_2Cl_2 was employed with a double platinum working and counter electrode and a standard calomel electrode. Table 5.3 summarises the electrochemical data along with the *Dq* values for the chromium(III) complexes.

Complex	E_{PC} *vs* ferrocene/ferrocenium(V)	*Dq*/cm^{-1}
[$CrCl_3${L1}]	-1.28	1 430
[$CrCl_3${L2}]	-1.25	1 396
[$CrCl_3${L3}]	-1.35	1 440
[$CrCl_3${L4}]	-1.27	1 439
[$CrCl_3${L5}]	-	1 684
[$CrCl_3${L6}]	-	1 680

Table 5.3. Electrochemical data and *Dq* values for the [$CrCl_3${L}] (L = L1-L6) compounds in 0.2 M [Bu^n_4N]BF_4 in CH_2Cl_2, scan rate = 100 mV/s , E_{PC} = reduction potential

As expected, the chromium (III) complexes showed only irreversible reductions. This phenomenon is depicted in Figure 5.1 where a well defined irreversible reduction of [$CrCl_3${L2}] is observed. In other cases the reduction is ill-defined. This could be due to a structural rearrangement in the complex slow in comparison to the electron kinetics of the reaction. When comparing the ligand set with reduction potential we can notice that the complexes with a large *Dq* value (strong field) have a more highly anodic reduction potential value too. From Table 5.3, the complexes containing the all nitrogen macrocycle [$CrCl_3${L}] (L = L5, L6) did not undergo reduction within the potential range, showing the effect of the hard nitrogen donors. The reduction potential for the sulfur complexes [$CrCl_3${L1}], [$CrCl_3${L3}] and [$CrCl_3${L4}] were

very similar, as would be expected for comparable systems containing tridentate S-donor ligand along with chlorines [32, 35].

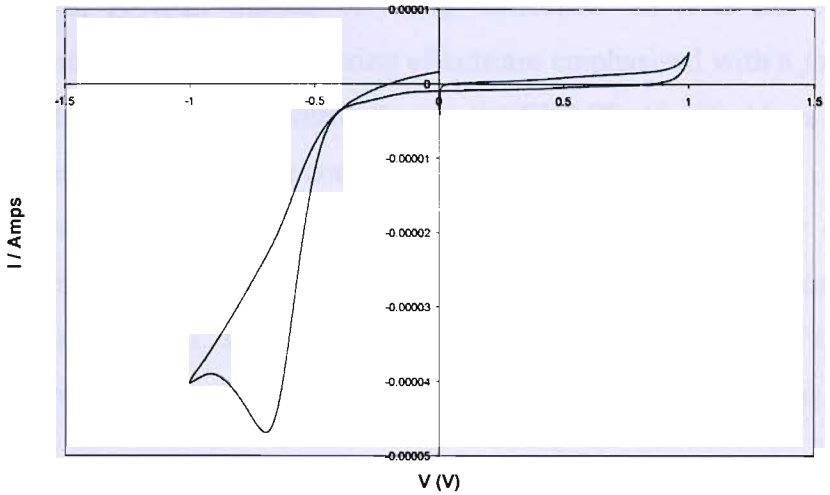

Figure 5.1. Cyclic voltammogram for $[CrCl_3\{O(CH_2CH_2SC_{10}H_{21})_2\}]$ showing an irreversible reduction. 0.2 M $[Bu^n{}_4N]BF_4$ in CH_2Cl_2, scan rate 100 mV/s

5.3.3.3. Chromium K-edge EXAFS Studies for $[CrCl_3\{L\}]$ (L = L1-L6)

Given the lack of structural data on the chromium(III) complexes, we proposed that chromium K-edge EXAFS data would provide useful information regarding the metal-ligand bond lengths of the first coordination sphere, *i.e.* *d*(Cr-S), *d*(Cr-N), *d*(Cr-O) and *d*(Cr-Cl). To some extent, the stereochemistry of the complexes can also be determined using EXAFS. As explained in Chapter 2, the multiple scattering effects can reveal some angular information about the atoms adjacent to the absorbing atom, in our case the chromium metal centre. The phenomenon of multiple scattering occurs if the emitted photoelectron encounters more than one backscattering atom before returning to the absorber. If one atom is behind another, relative to the absorbing atom, this will have a significant contribution to the EXAFS. When a complex appears to be in a *meridional* geometry, three different environments can be encountered for the multiple scattering effects. For a MX_3L_3, where L is a tridentate ligand containing donor atoms of the same nature (in our case, L = S or N, M = Cr and X = Cl), these three environments are X-M-X, L-M-L and X-M-L. It is thought

that they tend to 'cancel' one another and the multiple scattering effects tend to be negligible in the EXAFS studies. However, the opposite appears to occur in presence of a *facial* isomer. In that case, there is only one environment for the multiple scattering effects, X-M-L. Instead of being 'cancelled' as it is the case with a *meridional* isomer, the multiple scattering effects are emphasised with a *facial* isomer and these effects have a large contribution to the EXAFS. Hence this is possible to suggest the stereochemistry of our complexes.

Recording chromium K-edge EXAFS on these species will also allow comparison with the species resulting from the *in situ* reaction between the complexes and the aluminium reagent, Me_3Al. The spectra were recorded for solid pellets of the complex diluted with boron nitride and, when possible, as 5.0 mM toluene solutions.

a) $[CrCl_3\{S(CH_2CH_2SC_{10}H_{21})_2\}]$

Figure 5.2 shows a good fit for a model of 2.7 chlorine and 2.8 sulfur atoms. The errors for the coordination numbers of the two shells are probably due to difficulties resolving them into two discrete shells. The bond lengths *d*(Cr-Cl) and *d*(Cr-S) are consistent with the crystal structures involving similar coordinated atoms to a chromium metal centre. In the complex $[CrCl_3\{S(CH_2CH_2SC_{10}H_{21})_2\}]$ the Cr-Cl bond length is 2.32(6) Å and the Cr-S bond length is 2.45(5) Å. The bond lengths obtained compare very well to those of *fac*-$[CrCl_3\{[18]aneS_6\}]$ where the Cr-S distances are 2.459(3), 2.442(5) and 2.440(5) Å and the Cr-Cl distances are 2.305(5), 2.279(5) and 2.291(5) Å [32]. Values compare also very well to the structural data obtained for the methyl derivative $[CrCl_3\{S(CH_2CH_2SMe)_2\}$ (Chapter 6). The Debye-Waller terms are relatively low, which suggests that each shell is integral to the fit. The second point of interest is that the model proposed gives the best results when the multiple scattering effects are included, to give a fit index value of 5.0, and confirming the expected *facial* configuration.

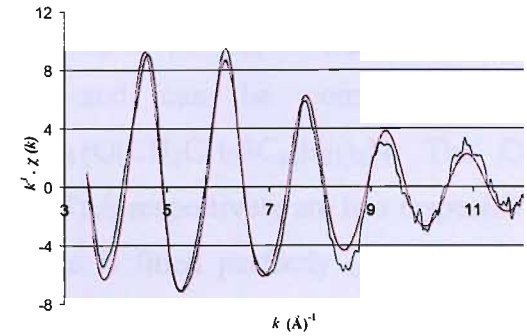

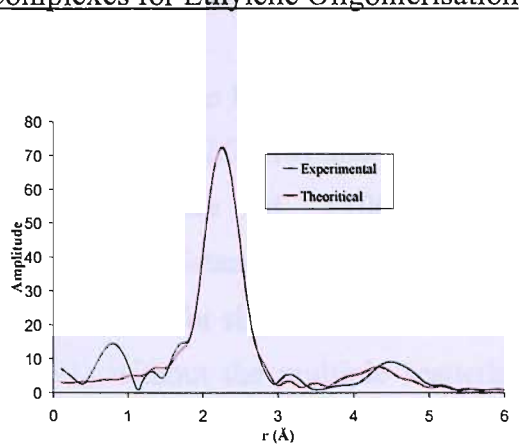

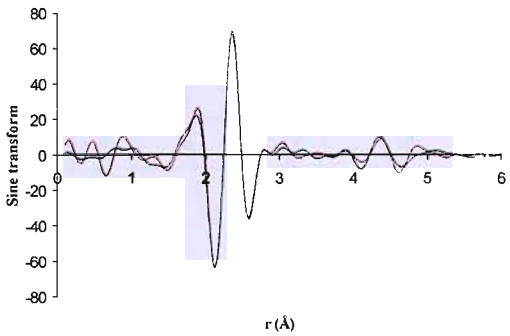

Ef = -6.1(3) eV

R = 23.2 %

Atom	C.N.	R / Å	$2\sigma^2$ / Å^2
Cl	2.7(4)	2.32(6)	0.011(1)
S	2.8(5)	2.45(5)	0.010(2)

Figure 5.2. The chromium K-edge k^3-weighted EXAFS, Fourier transform and sine transform for a solid pellet of $[CrCl_3\{S(CH_2CH_2SC_{10}H_{21})_2\}]$ / boron nitride

b) $[CrCl_3\{O(CH_2CH_2SC_{10}H_{21})_2\}]$

The parameters refined for the complex $[CrCl_3\{O(CH_2CH_2SC_{10}H_{21})_2\}]$ (Figure 5.3) show very sensible values and do not present big errors. With a coordination number of 0.8, the first shell, corresponding to the oxygen shell, is at a distance of 2.10(3) Å. The Debye-Waller factor, with a value of 0.007, shows that the shell is integral to the fit. As for the $[CrCl_3\{S(CH_2CH_2SC_{10}H_{21})_2\}]$ complex, the sulfur and chlorine shells are very difficult to resolve into two distinct shells. That may explain the large Debye-Waller value for the chlorine shell. The bond lengths obtained from EXAFS analysis

stay in a good range when compared to crystal data available for similar systems. In the complex $[CrCl_3(THF)_3]$, the Cr-O distance is 1.994(4), 2.027(4) and 2.077(4) Å [40] and can be compared to the Cr-O distance of 2.10(3) Å in $[CrCl_3\{O(CH_2CH_2SC_{10}H_{21})_2\}]$. The Cr-S and Cr-Cl distances of 2.37(7) and 2.25(3) Å respectively are in a respectable range of values for similar complexes. The feature is fitted perfectly (R = 27.0 %, FI = 5.1) without the multiple scattering effects, which may support the statement that the geometry is *meridional*.

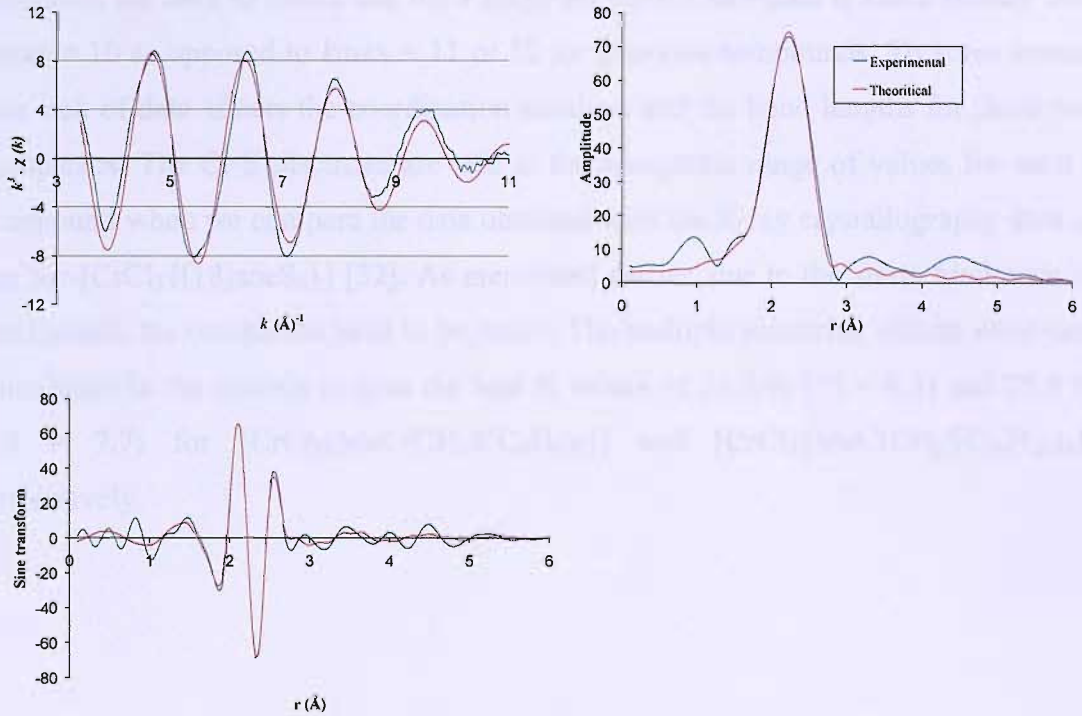

Atom	C.N.	R / Å	$2\sigma^2$ / Å^2
O	0.8(2)	2.10(3)	0.007(7)
Cl	2.7(4)	2.25(3)	0.015(5)
S	2.0(2)	2.37(7)	0.008(0)

Ef = -2.8(8) eV

R = 27.0 %

Figure 5.3. The chromium K-edge k^3-weighted EXAFS, Fourier transform and sine transform for a solid pellet of $[CrCl_3\{O(CH_2CH_2SC_{10}H_{21})_2\}]$ / boron nitride

c) $[CrCl_3\{MeC(CH_2S^nC_4H_9)_3\}]$ and $[CrCl_3\{MeC(CH_2SC_{10}H_{21})_3\}]$

Figures 5.4 shows a good fit for a model of 2.5 chlorine and 2.5 sulfur atoms. We have *d*(Cr-Cl) and *d*(Cr-S) of 2.26(2) Å and 2.43(3) Å respectively for $[CrCl_3\{MeC(CH_2S^nC_4H_9)_3\}]$ while the values for the decyl derivative $[CrCl_3\{MeC(CH_2SC_{10}H_{21})_3\}]$ (Table 5.4) are somewhat shorter with 2.25(3) Å and 2.38(4) Å respectively. Again, these results are in a respectable range of values and can be compared to the methyl derivative $[CrCl_3\{MeC(CH_2SCH_3)_3\}]$ where *d*(Cr-Cl) = 2.32 Å and *d*(Cr-S) = 2.44 Å (Chapter 6).

However, we have to notice that the *k* range for the EXAFS data is much shorter with *k*max = 10 as opposed to *k*max = 11 or 12 for previous compounds. To some extent, this lack of data affects the coordination numbers and the bond lengths for these two complexes. The Cr-S distances are still in the acceptable range of values for such a compound when we compare the data obtained with the X-ray crystallography data of the *fac*-$[CrCl_3\{[18]aneS_6\}]$ [32]. As mentioned earlier, due to the steric hindrance of the ligands, the complexes have to be *facial*. The multiple scattering effects were then introduced in the models to give the best R values of 25.2 % (FI = 6.3) and 25.9 % (FI = 7.7) for $[CrCl_3\{MeC(CH_2S^nC_4H_9)_3\}]$ and $[CrCl_3\{MeC(CH_2SC_{10}H_{21})_3\}]$ respectively.

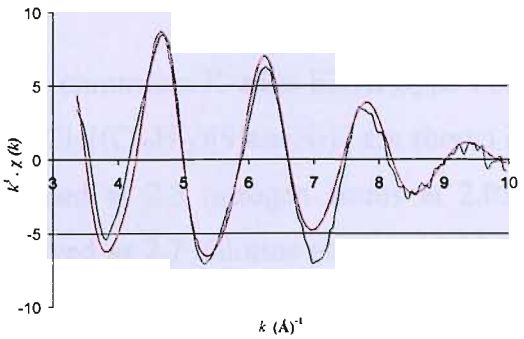

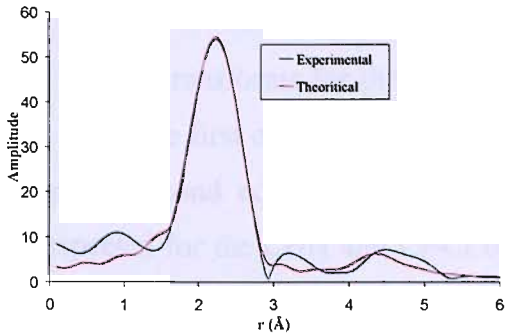

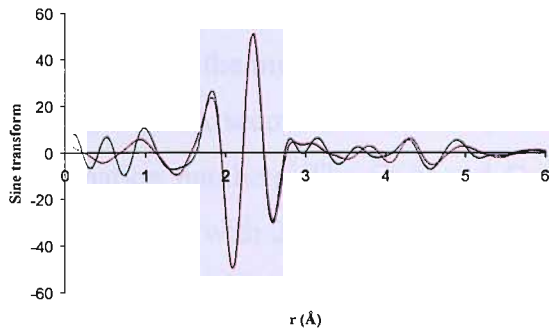

Atom	C.N.	R / Å	$2\sigma^2$ / Å^2
Cl	2.5(3)	2.26(2)	0.011(8)
S	2.5(4)	2.43(3)	0.010(2)

Ef = -5.7(9) eV

R = 25.2 %

Figure 5.4. The chromium K-edge k^3-weighted EXAFS, Fourier transform and sine transform for a solid pellet of $[CrCl_3\{MeC(CH_2S^nC_4H_9)_3\}]$ / boron nitride

Atom	C.N.	R / Å	$2\sigma^2$ / Å^2
Cl	2.5(5)	2.25(3)	0.003(8)
S	2.5(2)	2.38(4)	0.001(7)

Ef = -1.1(7) eV

R = 25.9 %

Table 5.4. The chromium K-edge k^3-weighted structural data for a toluene solution of $[CrCl_3\{MeC(CH_2SC_{10}H_{21})_3\}]$

d) $[CrCl_3\{(C_{10}H_{21})[9]aneN_3\}]$ and $[CrCl_3\{(C_{10}H_{21})_3[9]aneN_3\}]$

The chromium K-edge EXAFS, its Fourier and its sine transforms for the compound $[CrCl_3\{(C_{10}H_{21})[9]aneN_3\}]$ are shown in Figure 5.5a. The first coordination shell was refined at 2.5 nitrogen atoms at 2.01(8) Å, and a second coordination shell was derived as 2.7 chlorine atoms at 2.33(9) Å, as expected for the Cr-N and Cr-Cl bond lengths. The Debye-Waller factor values are sensible and the fit between experimental and theoretical spectral curves is good with these two shells fitted (R = 26.0 %). By introducing the multiple scattering effects to the model, the parameters presented a slight change. A second model was then studied (Figure 5.5b) with similar shells and coordination numbers. The Cr-N and Cr-Cl bond lengths are practically identical to the first model with 2.02(6) Å and 2.33(1) Å. Low Debye-Waller factor values were also obtained within this model. However, an R-factor of 27.4 % was noticed for a fit index of 8.7, as opposed to the fit index of 7.6 for the first model. We can conclude that the multiple scattering effects do not have a big impact on the models proposed but the best parameters are obtained when these effects are not considered in the study. The values obtained are similar to the EXAFS values for $[CrCl_3\{[9]aneN_3\}]$ with d(Cr-N) = 2.05 Å and d(Cr-Cl) = 2.32 Å (Chapter 6). The average bond lengths for $[CrCl_3\{(C_{10}H_{21})[9]aneN_3\}]$ can be compared to those in the literature for the hydroxo-bridged $[Cr_2(OH)_3\{Me_3[9]aneN_3\}_2]^{3+}$ where the reported Cr-N distance is 2.089(4) Å [41]. As seen in the previous complexes, the Cr-Cl distance is similar to the values reported for chromium(III) trichloride complexes.

Table 5.5 shows sensible values for a compound such as $[CrCl_3\{(C_{10}H_{21})_3[9]aneN_3\}]$. The model proposed shows a very good fit with two shells containing respectively 3 nitrogen and 2.5 chlorine atoms. With average Cr-N bond lengths of 2.00 Å and Cr-Cl bond lengths of 2.32 Å, the model gives very good values when compared to the literature and other EXAFS data on similar compounds ($[CrCl_3\{(C_{10}H_{21})[9]aneN_3\}]$ and $[CrCl_3\{[9]aneN_3\}]$).

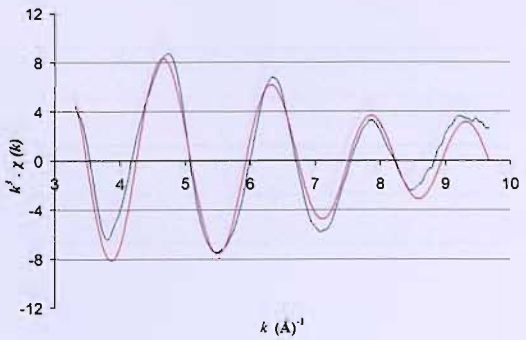

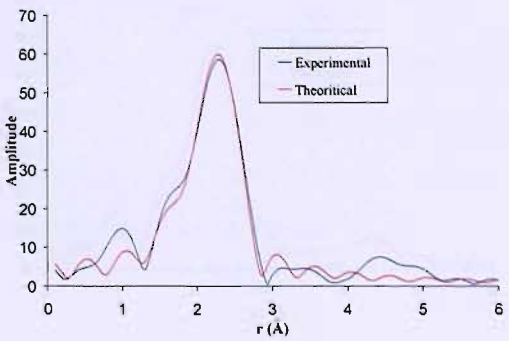

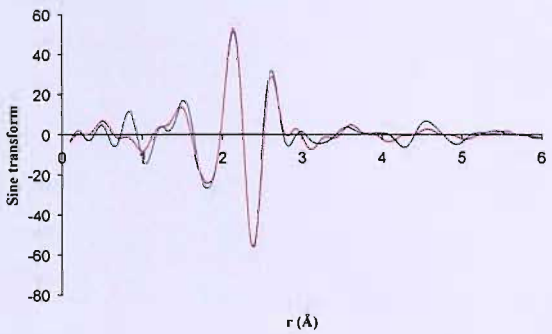

Atom	C.N.	R / Å	$2\sigma^2$ / Å^2
N	2.5(5)	2.01(8)	0.007(6)
Cl	2.7(2)	2.33(9)	0.007(7)

Ef = -3.4(8) eV

R = 26.0 %

Figure 5.5a. The chromium K-edge k^3-weighted EXAFS, Fourier transform and sine transform for solid pellet of $[CrCl_3\{(C_{10}H_{21})[9]aneN_3\}]$ / boron nitride (no multiple scatterings)

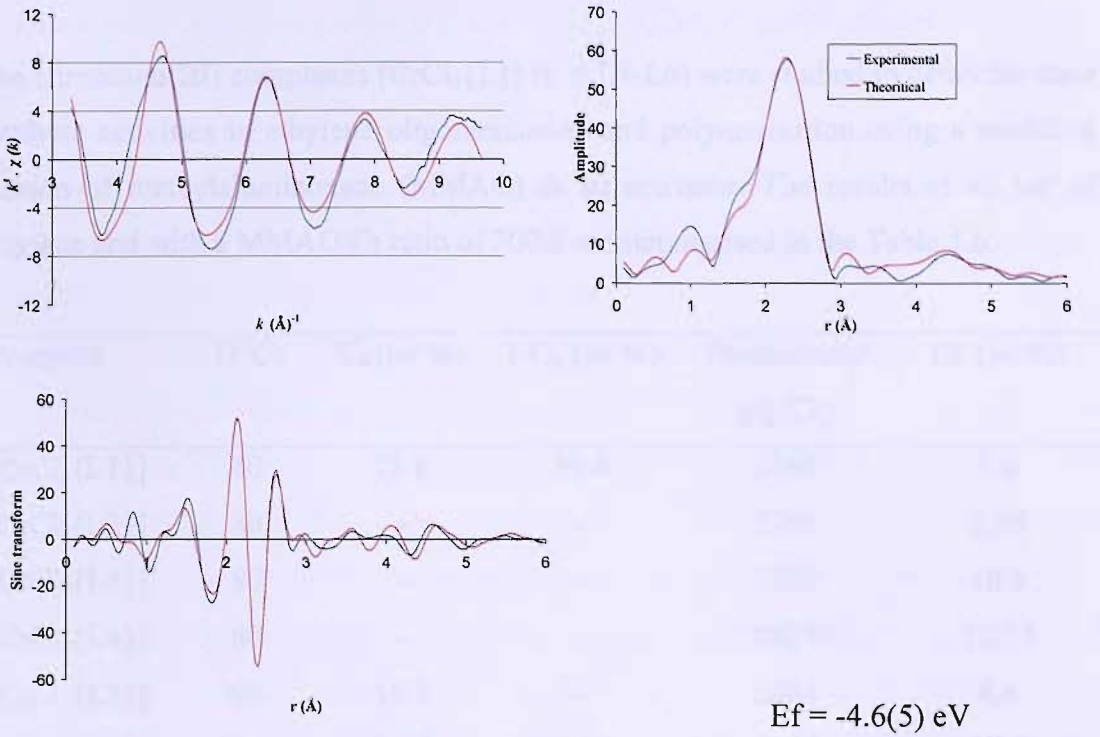

Ef = -4.6(5) eV

R = 27.4 %

Atom	C.N.	R / Å	$2\sigma^2$ / Å^2
N	2.5(6)	2.02(6)	0.009(1)
Cl	2.7(5)	2.33(1)	0.008(8)

Figure 5.5b. The chromium K-edge k^3-weighted EXAFS, Fourier transform and sine transform for a pellet of $[CrCl_3\{(C_{10}H_{21})[9]aneN_3\}]$ / boron nitride (with multiple scatterings)

Atom	C.N.	R / Å	$2\sigma^2$ / Å^2
N	3.0(1)	2.00(6)	0.004(9)
Cl	2.5(4)	2.32(6)	0.011(8)

Ef = 4.8(1) eV

R = 25.2 %

Table 5.5. The chromium K-edge structural data for a pellet of $[CrCl_3\{(C_{10}H_{21})_3[9]aneN_3\}]$ / boron nitride

5.3.4. Ethylene Oligomerisation and Polymerisation

The chromium(III) complexes [$CrCl_3${L}] (L = L1-L6) were studied in detail for their catalytic activities in ethylene oligomerisation and polymerisation using a modified version of methylaluminoxane (MMAO) as an activator. The results at 40 bar of ethylene and with a MMAO/Cr ratio of 300:1 are summarised in the Table 5.6.

Complex	T(°C)	C_6 (wt %)	1-C_6 (wt %)	Productivity g/g(Cr)	PE (wt %)
[$CrCl_3${L1}]	80	71.8	99.4	3165	1.0
[$CrCl_3${L2}]	80	-	-	2295	3.58
[$CrCl_3${L3}]	80	-	-	3109	48.5
[$CrCl_3${L4}]	80	-	-	8827	13.77
[$CrCl_3${L5}]	90	15.7	-	5804	8.4
[$CrCl_3${L6}]	90	14.9	-	3168	10.6

Table 5.6. Ethylene oligomerisation and polymerisation

The complexes [$CrCl_3${L}] (L = L1-L6) exhibit moderate activities for ethylene oligomerisation and polymerisation. The products obtained by [$CrCl_3${L5}] and [$CrCl_3${L6}] are comprised of oligomers with a distribution that closely resembles Schulz-Flory rules [42-44]. The weight of C_8-C_{20} fractions was used to calculate the Schulz-Flory distribution coefficient β by fitting the following simplified Schulz-Flory equation:

$$\chi_\rho = \beta / (1+\beta)^\rho \qquad \textbf{Equation 5.1}$$

where χ_ρ = mole fraction of $C_{2\rho+2}$ olefin.

Calculation of the β factor for [$CrCl_3${L5}] and [$CrCl_3${L6}] gave a value of 0.68 and 0.70 respectively. Extensive literature reports that complexes containing N-H groups show relatively high catalytic activity compared with other analogues (Chapter 3). However, this tendency does not apply for [$CrCl_3${L5}] leading to the suggestion that

the stereochemistry of the complex might significantly influence the catalytic activity and selectivity. It has been shown that the oligomerisation of ethylene and more specifically the preparation of high quality linear α-olefins from ethylene occur when using a catalyst which includes an aluminoxane and a complex containing a sterically demanding tridentate coordinating ligand, such as [9]aneN$_3$ derivatives [45]. Oligomerisation is believed to result from the difficult access of ethylene to the active catalyst sites, which is afforded by such polydentate ligands.

Along with MMAO as activator, [CrCl$_3${L1}] gave an active and selective catalyst for the trimerisation of ethylene to 1-hexene. However the catalyst stayed active for a very short period of time, explaining the low productivity obtained. This is probably due to the possible loss of the ligand upon addition of Me$_3$Al. It is interesting to note that no chromium(III) trichloride complexes bearing a tridentate S-donor ligand in a *facial* geometry has been reported for such a reaction before and this system would need further investigations. The active catalyst of the complex [CrCl$_3${L2}], containing a mixed S- and O-donor atoms set did not trimerise or tetramerise ethylene and the catalysis test only resulted in polyethylene formation. We should note that this complex is the only one of the series with a *meridional* geometry. It is thought that a *meridional* geometry is required for the trimerisation of ethylene to 1-hexene. Catalysis tests of these complexes support the idea of the efficiency of an N-H group for a complex in a *meridional* geometry.

Complexes [CrCl$_3${L3}] and [CrCl$_3${L4}] showed moderate activity but the decyl derivative gave a much higher productivity under the same catalytic conditions. Unlike [CrCl$_3${L1}], these two complexes, also in a *facial* geometry, did not trimerise ethylene. Addition of MMAO probably resulted in the loss of the ligand.

In order to have a better understanding of what is occurring when the complexes [CrCl$_3${L}] (L = L1-L6) are treated with an aluminium reagent, spectroscopic studies were carried out on the active species to try to determine the oxidation state and environment of the chromium metal centre.

5.3.5. Study of the $[CrCl_3\{L\}]$ (L = L1-L6) Complexes Activated by Addition of Me_3Al

5.3.5.1. UV/visible Studies

In an attempt to investigate the nature of the active catalyst, it was decided to probe by UV/visible spectroscopy the catalytic species present in solution after addition of Me_3Al. To a 5 mM toluene solution of the complex $[CrCl_3\{L\}]$ (L = L1-L6) were added five molar equivalents of the aluminium reagent and UV/visible spectra were recorded. The reason for adding an excess of Me_3Al was to allow for possible multiple substitution of the chlorine atoms by methyl groups. Figure 5.6 shows typical UV/visible spectra for a complex in solution when activated with five molar equivalents of Me_3Al.

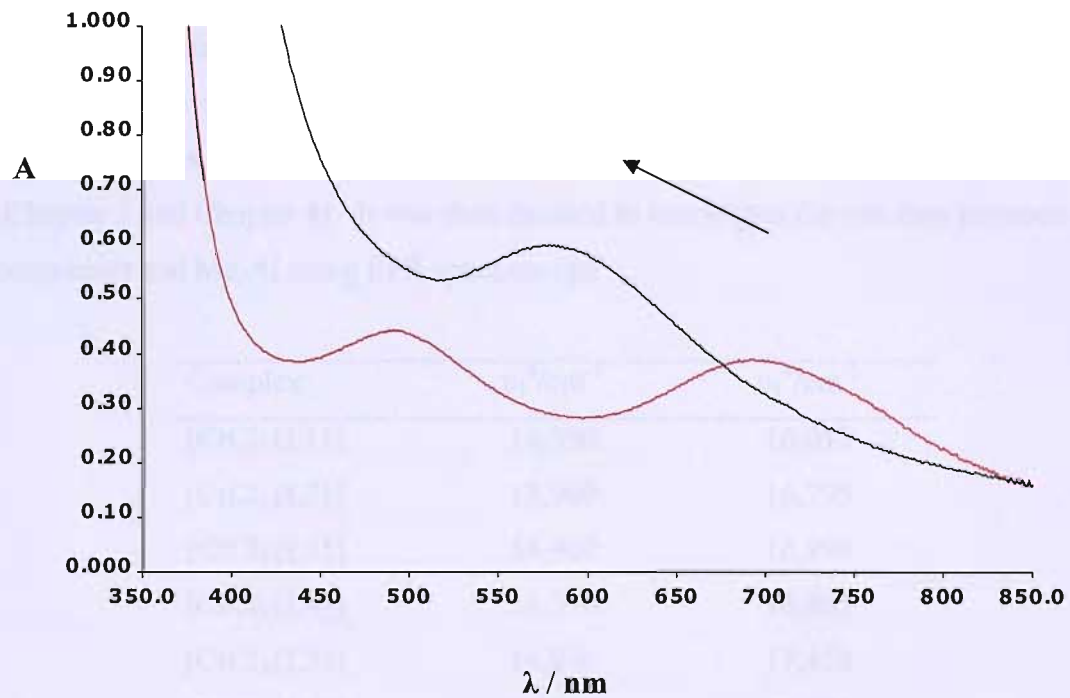

Figure 5.6. UV/visible spectra of a 5 mM toluene solution of $[CrCl_3\{MeC(CH_2S^nC_4H_9)_3\}]$ before (red) and after (black) treatment with 5 equivalents of Me_3Al

It is clear that a considerable change is observed in the UV/visible spectrum upon addition of the aluminium reagent. Only one transition is observed and at a different

energy (Table 5.7). An instantaneous colour change of the complexes in solution to give a yellow/green solution was noticed. Again, either a blue shift is occurring and the peak corresponding to ν_2 is obscured by the charge transfer bands or substitution of the chlorine atoms by methyl groups occurred after addition of Me_3Al. The results obtained for other chromium(III) trichloride complexes (Chapter 3 and Chapter 4) suggest that chlorine atoms substitution is more likely to happen. No discernible energy difference is observed upon addition of five equivalents of Me_3Al for the complexes $[CrCl_3\{L\}]$ (L = L5, L6) which did not undergo reduction by cyclic voltammetry. It should be noted that the shifted peaks were in many cases very broad, hence accuracy of the exact energy of the transition is low. The shifts of the UV/visible bands are summarised in Table 5.7.

The extent of the chlorine atoms substitution is not known. In some cases, addition of a further five equivalents of Me_3Al leads to a further shifting of the UV/visible peak υ_1 which could indicate further substitution of one or more chlorine atoms from the complex by methyl groups present in the aluminium reagent. A change in the oxidation state of the chromium metal centre is also expected and would correlate with the results obtained for the complexes $[CrCl_3\{SNS\}]$ and $[CrCl_3\{PNP\}(THF)]$ (Chapter 3 and Chapter 4). It was then decided to investigate the reaction between the complexes and Me_3Al using EPR spectroscopy.

Complex	$\upsilon_1{}^a/cm^{-1}$	$\upsilon_1{}^b/cm^{-1}$
$[CrCl_3\{L1\}]$	14,300	16,015
$[CrCl_3\{L2\}]$	13,960	16,795
$[CrCl_3\{L3\}]$	14,400	16,990
$[CrCl_3\{L4\}]$	14,390	16,865
$[CrCl_3\{L5\}]$	16,840	17,450
$[CrCl_3\{L6\}]$	16,800	17,375

Table 5.7. Spectroscopic data for a 5 mM toluene solution of $[CrCl_3\{L\}]$ (L = L1-L6) [a]before and [b]after treatment with Me_3Al

5.3.5.2. Electron Paramagnetic Resonance Studies

The reactions between the chromium(III) complexes [$CrCl_3${L}] (L = L1-L6) and the trimethylaluminum have been followed using EPR spectroscopy. The complexes being paramagnetic species are therefore EPR active and a strong and broad signal, characteristic to d^3 systems should be observed. Q- and K-band EPR spectra were recorded for the complexes in a frozen toluene/CH_2Cl_2 glass. The characteristic broad signal was observed for all the chromium(III) complexes and the ***g*** values calculated (Table 5.8).

Complex	***g*** value
[$CrCl_3${L1}]	1.99
[$CrCl_3${L2}]	1.99
[$CrCl_3${L3}]	1.99
[$CrCl_3${L4}]	1.99
[$CrCl_3${L5}]	1.99
[$CrCl_3${L6}]	1.98

Table 5.8. EPR (Q-band and K-band) ***g*** values for a toluene/CH_2Cl_2 glass of [$CrCl_3${L}] (L = L1-L6); recorded at 115 K

Q-band and K-band EPR spectra for the complexes in solution and in presence of three molar equivalents of the aluminium reagent Me_3Al were recorded. Figures 5.7 and 5.8 depict the data obtained from the measurements and for a selected set of complexes. It is easily noticeable that the strong signal disappeared almost totally upon addition of the aluminium reagent. This suggests a change in the oxidation state of the metal centre from Cr(III) to Cr(II) or Cr(IV). The hypothesis emerging from the UV/visible measurements about a possible change in the oxidation state of the chromium metal centre could then be confirmed. Similar changes were observed for the series of chromium(III) complexes.

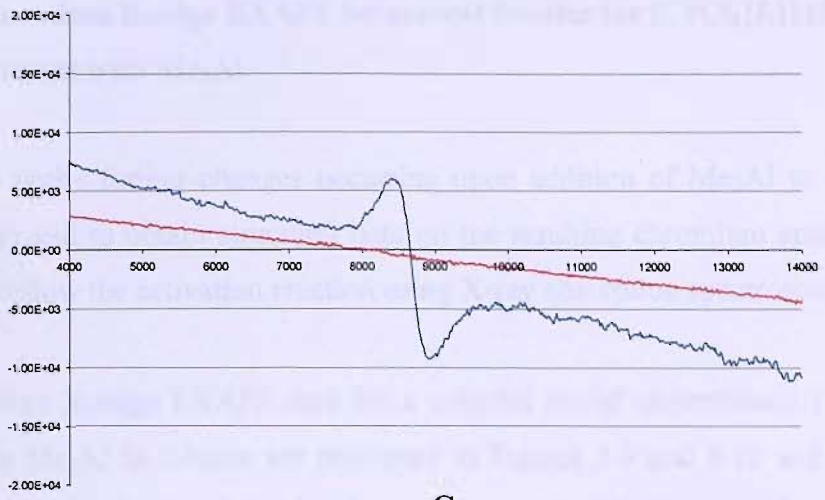

Figure 5.7. K-band EPR spectra for a toluene/CH_2Cl_2 glass of $[CrCl_3\{O(CH_2CH_2SC_{10}H_{21})_2\}]$ (blue) and with 3 equivalents of Me_3Al (red), g = 1.99; recorded at T = 115 K

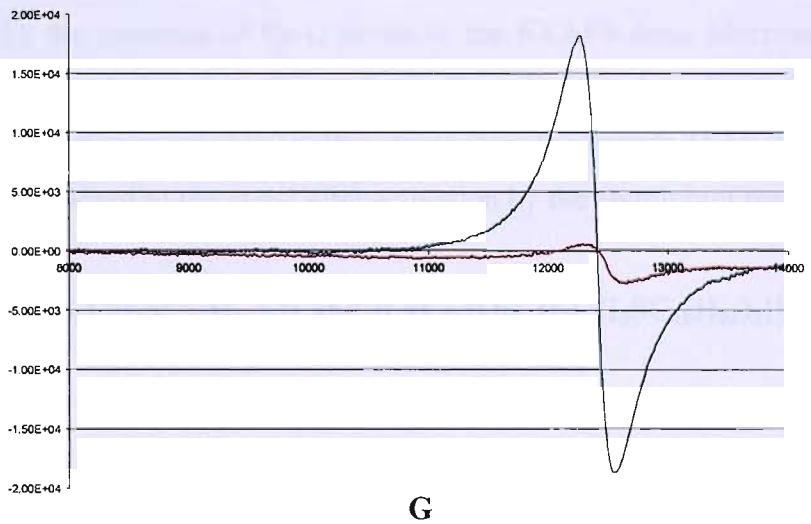

Figure 5.8. Q-band EPR spectra for a toluene/CH_2Cl_2 glass of $[CrCl_3\{(C_{10}H_{21})_3[9]aneN_3\}]$ (blue) and with 3 equivalents of Me_3Al (red), g = 1.98; recorded at T = 115 K

5.3.5.3. Chromium K-edge EXAFS Structural Studies for [$CrCl_3${L}] (L = L1-L6) upon Treatment with Me_3Al

In order to probe further changes occurring upon addition of Me_3Al to [$CrCl_3${L}] (L = L1-L6) and to obtain structural data on the resulting chromium species, it was decided to follow the activation reaction using X-ray absorption spectroscopy.

The chromium K-edge EXAFS data for a selected set of chromium(III) complexes treated with Me_3Al in toluene are presented in Figures 5.9 and 5.10 and Tables 5.9 and 5.10. The analysis of Cr K-edge of the activated systems showed a first coordination shell of ~ three carbon atoms at ~ 2.1 Å. In addition there was one more distant shell evident in the Fourier transform which was modelled by ~ 0.3 sulfur atoms for [$CrCl_3${L}] (L = L1-L4). EXAFS data for [$CrCl_3${L5}] and [$CrCl_3${L6}] were unsatisfactory and did not enable us to investigate on the active species. The results obtained support the UV/visible measurements and confirm a loss of the chlorine atoms after treatment by Me_3Al. The substitution by methyl groups is confirmed by the presence of Cr-C bonds in the EXAFS data. Moreover, it is now clear that the ligands do not tend to stay coordinated to the chromium after addition of Me_3Al. Indeed, an average of 0.3 sulfur atoms from the ligands {L1}, {L2}, {L3} and {L4} remain attached to the metal after activation by the aluminium reagent.

a) [$CrCl_3${$S(CH_2CH_2SC_{10}H_{21})_2$}] and [$CrCl_3${$O(CH_2CH_2SC_{10}H_{21})_2$}] Treated with Me_3Al

Figure 5.9 depicts the EXAFS data for [$CrCl_3${$S(CH_2CH_2SC_{10}H_{21})_2$}] upon treatment with thirty molar equivalents of Me_3Al. The spectra fit the $k^3.\chi\ (k)$, Fourier transform and sine transform to a simple model of two shells. The model proposed has refined coordination numbers of three carbon and 0.3 sulfur atoms. The three carbons confirm the substitution of the chlorine atoms with the methyl groups from the aluminium reagent Me_3Al. The average value of 0.3 sulfur indicate that the ligand tend to be dissociated from the chromium metal centre after treatment with the aluminium reagent. The Debye-Waller terms have values which show they are integral to the fit. Finally, the bond lengths are sensible to the values expected with d(Cr-C) = 2.07 Å and d(Cr-S) = 2.44 Å (d(Cr-S) = 2.45 Å for the solid pellet of

[$CrCl_3\{S(CH_2CH_2SC_{10}H_{21})_2\}$]). As seen in Chapter 3, the average Cr-C(methyl) bond length ranges from 2.042 to 2.151 Å [46, 47].

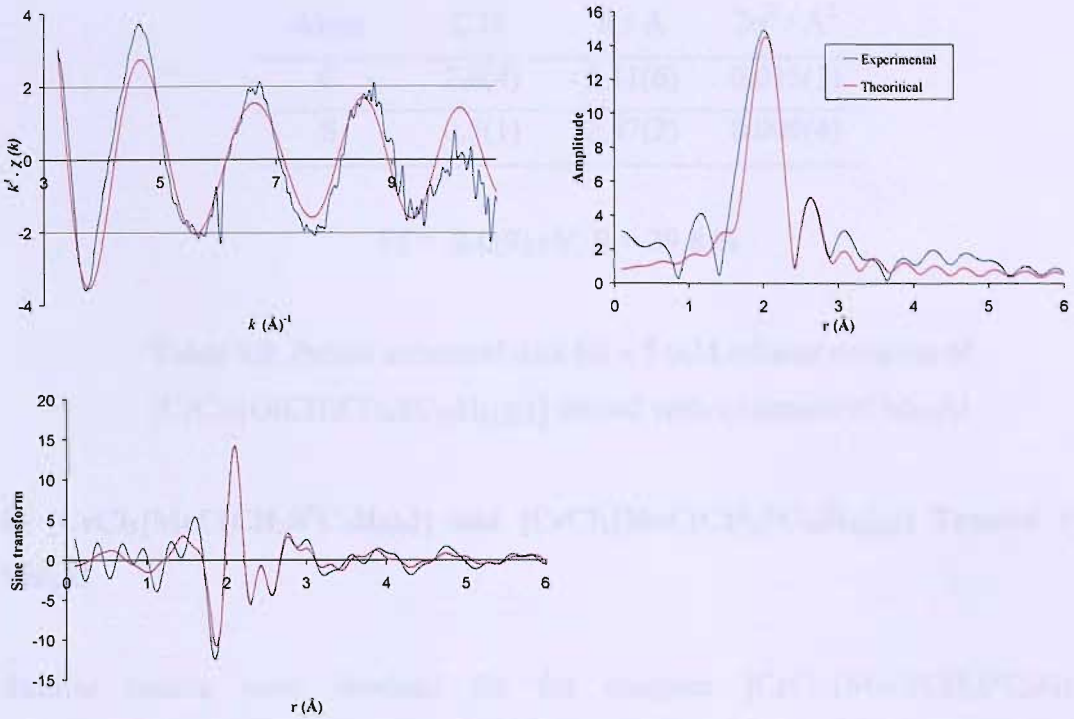

Atom	C.N.	R / Å	$2\sigma^2$ / Å^2
C	3.0(2)	2.07(7)	0.011(4)
S	0.3(3)	2.44(5)	0.007(1)

Ef = -3.1(8) eV

R = 37.6 %

Figure 5.9. The chromium K-edge k^3-weighted EXAFS, Fourier transform and sine transform for a 5 mM toluene solution of [$CrCl_3\{S(CH_2CH_2SC_{10}H_{21})_2\}$] treated with an excess of Me_3Al

Similar results were obtained for $[CrCl_3\{O(CH_2CH_2SC_{10}H_{21})_2\}]$ and the structural data for this complex treated thirty molar equivalents of Me_3Al are presented in Table 5.9.

Atom	C.N.	R / Å	$2\sigma^2$ / Å^2
C	2.6(4)	2.11(6)	0.015(1)
S	0.5(1)	2.47(2)	0.009(4)

Ef = -2.0(9) eV; R = 39.8 %

Table 5.9. Partial structural data for a 5 mM toluene solution of $[CrCl_3\{O(CH_2CH_2SC_{10}H_{21})_2\}]$ treated with an excess of Me_3Al

b) $[CrCl_3\{MeC(CH_2S^nC_4H_9)_3\}]$ and $[CrCl_3\{MeC(CH_2SC_{10}H_{21})_3\}]$ Treated with Me_3Al

Similar results were obtained for the complex $[CrCl_3\{MeC(CH_2S^nC_4H_9)_3\}]$ (Figure 5.14). The model proposed for the species obtained from the reaction between $[CrCl_3\{L4\}]$ and Me_3Al fits well with two shells. The first shell corresponds to the Cr-C bond at 2.09 Å with a coordination number of 2.8 carbon atoms. The second shell at 2.44 Å corresponds to the Cr-S bond with 0.3 sulfur atoms (d(Cr-S) = 2.43 Å for the solid pellet of $[CrCl_3\{MeC(CH_2S^nC_4H_9)_3\}]$. The Debye-Waller terms show that they are integral to the fit. No chlorine atoms could be fitted in the model, supporting the idea that we have a substitution of the chlorine atoms by the methyl groups from Me_3Al.

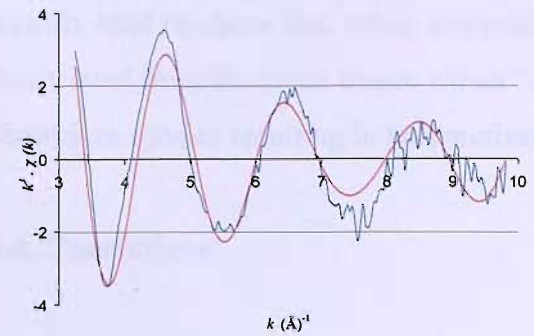

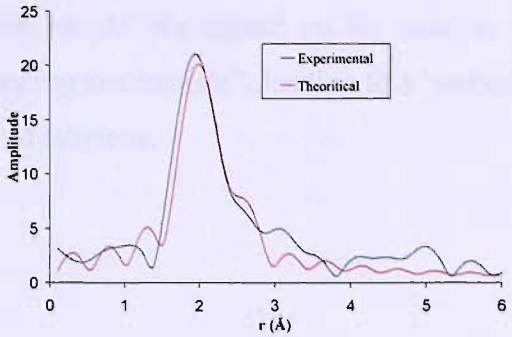

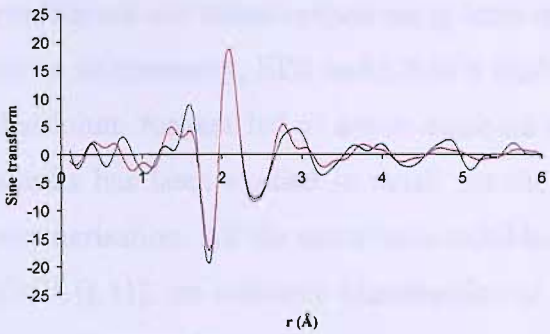

Atom	C.N.	R /Å	$2\sigma^2$ / Å^2
C	2.8(5)	2.09(3)	0.011(9)
S	0.3(7)	2.44(3)	0.003(4)

Ef = -8.2(1) eV

R = 36.2 %

Figure 5.10. The chromium K-edge k^3-weighted EXAFS, Fourier transform and sine transform for a 5 mM toluene solution of $[CrCl_3\{MeC(CH_2S^nC_4H_9)_3\}]$ treated with an excess of Me_3Al

Similar results were obtained for the decyl derivative $[CrCl_3\{MeC(CH_2SC_{10}H_{21})_3\}]$ and the structural data for this complex treated with thirty molar equivalents of Me_3Al are presented in Table 5.10.

Atom	C.N.	R /Å	$2\sigma^2$ / Å^2
C	2.9(7)	2.06(4)	0.013(1)
S	0.2(3)	2.40(7)	0.006(1)

Ef = -4.6(5) eV; R = 36.7 %

Table 5.10. Partial structural data for a 5 mM toluene solution of $[CrCl_3\{MeC(CH_2SC_{10}H_{21})_3\}]$ treated with an excess of Me_3Al

Results tend to show that when activated with Me_3Al, the ligand on the catalyst is dissociated from the metal centre *via* an "unzipping mechanism", leading to a "naked" chromium species resulting in polymerisation of ethylene.

5.4. Conclusions

A range of tridentate ligands and chromium(III) complexes have been successfully synthesised and characterised using infra-red and UV/visible spectroscopy along with cyclic voltammetry, EPR and EXAFS studies. Treatment of these compounds with an aluminium reagent led to active catalytic species. The catalytic ability of the active species has been studied in detail for the reaction of ethylene oligomerisation and polymerisation. All the complexes exhibited capacity for such a reaction. Apart from $[CrCl_3\{L1\}]$, no selective trimerisation or tetramerisation of ethylene took place by using the complexes $[CrCl_3\{L\}]$ (L = L2-L6). Complexes $[CrCl_3(L5\text{-}L6)]$ followed the Schulz-Flory distribution rules of olefins as expected. Based on results obtained by UV/visible and EPR measurements, it is clear that a change in the oxidation state of the chromium metal centre occurs upon addition of an excess of Me_3Al. Investigation of the partial structure of the active species has been followed using EXAFS spectroscopy. It appears that when the chromium(III) complexes are treated with the aluminium reagent, the ligands L1-L6 tend to dissociate from the metal centre *via* an unzipping mechanism. The resulting species involves then the polymerisation of ethylene, which is supported by the catalysis tests.

5.5. Experimental

The ligands and chromium(III) complexes were generally prepared by literature methods or by modifications of those. The reagents were purchased from Aldrich and Acros and were used as received.

Synthesis of $S(CH_2CH_2SC_{10}H_{21})_2$ [23]: Bis(2-mercaptoethyl)sulfide (7.16 g, 46.0 mmol) was dissolved in ethanol (200 mL) under nitrogen, and sodium (2.14 g, 93.0 mmol) was added. When the sodium had dissolved the mixture was heated to reflux and 1-iododecane (25 g, 93.0 mmol) added dropwise. The ethanol was reduced *in vacuo* and water (35 mL) was added. The mixture was extracted with Et_2O (3 x 35 mL) and the organic extracts were dried over $MgSO_4$. After filtration, the solvent was removed *in vacuo* to afford the ligand as a white solid. Yield: 16.28 g, 37.5 mmol (80%). Melting point: 54.5-55.5°C. ^1H NMR ($CDCl_3$): δ 0.88 (t, 6H, $C\underline{H}_3C_9H_{18}S$-); 1.26 (s, 28H, $CH_3C_7\underline{H}_{14}C_2H_4S$-); 1.58-2.54 (m, 8H, $C_8H_{17}C\underline{H}_2C\underline{H}_2S$-); 2.74 (m, 8H, $C_{10}H_{21}SC_2\underline{H}_4S$-) ppm. $^{13}C\{^1H\}$ NMR ($CDCl_3$): δ 14.25 ($\underline{C}H_3C_9H_{18}S$-); 22.81 ($CH_3\underline{C}H_2C_8H_{16}S$-); 28.88, 29.04, 29.38, 29.45, 29.67, 29.70, 29.88 ($C_2H_5\underline{C}_7H_{14}CH_2S$-); 32.0, 32.40, 32.48 ($C_9H_{19}\underline{C}H_2S\underline{C}H_2\underline{C}H_2S$) ppm. $C_{24}H_{50}S_3$ requires C, 66.36; H, 11.52; S, 22.12 %; Found C, 66.25; H, 11.60; S, 22.19 %.

Synthesis of $O(CH_2CH_2SC_{10}H_{21})_2$: To a solution of bis(2-chloroethyl)ether (3.42 g, 24.0 mmol) in ethanol (250 mL) was added sodium hydroxide (2.868 g, 1.25 mol). 1-decanethiol (8.35 g, 48.0 mmol) was added dropwise and the mixture refluxed for 4 hours under nitrogen. The solvent was then removed *in vacuo* and water (35 mL) was added to the remaining oil. The mixture was extracted with diethyl ether (3 x 35 mL). The organic extracts were dried over $MgSO_4$ and filtered off. The solvent was removed *in vacuo* to afford a colourless oil that crystallised upon standing at room temperature. Yield: 8.1 g, 20 mmol (81%). ^1H NMR ($CDCl_3$): δ 0.80 (t, 6H, $C\underline{H}_3C_9H_{18}S$-), 1.17 (m, 28H, $CH_3C_7\underline{H}_{14}C_2H_4S$-), 1.56-2.46 (m, 8H, $C_8H_9C\underline{H}_2C\underline{H}_2S$-), 2.63 (t, 4H, $C_{10}H_{21}SC\underline{H}_2CH_2O$-), 3.55 (t, 4H, $C_{10}H_{21}SCH_2C\underline{H}_2O$-) ppm. $^{13}C\{^1H\}$ NMR ($CDCl_3$): δ 14.48 ($\underline{C}H_3C_9H_{18}S$-), 23.06 ($CH_3\underline{C}H_2C_8H_{16}S$-), 29.28, 29.65, 29.70, 29.95, 30.22, 31.93, 32.29, 33.10

($C_2H_5\underline{C}_8H_{16}S\underline{C}H_2CH_2O$-), 71.16 ($C_{10}H_{21}SCH_2\underline{C}H_2O$-) ppm. $C_{24}H_{50}OS_2$ requires C, 68.83; H, 12.03 %; Found C, 68.78; H, 12.00 %.

Synthesis of $MeC(CH_2S^nC_4H_9)_3$ [24]: Ammonia (100 mL) was condensed onto dry, degassed THF (100 mL) in a 1L flask equipped with a condenser and using a Me_2CO/CO_2 slush bath. A small piece of solid Na was added to the mixture, leading to a dark royal blue solution. ($^nC_4H_9)_2S_2$ (12.82 g, 72.0 mmol) was added slowly to produce a creamy white colour. The remaining Na (3.31 g, 0.144 mol) was added slowly and the NH_3 was then allowed to evaporate. The creamy white mixture was concentrated *in vacuo* in order to remove the THF. A mixture of ethanol and $MeC(CH_2Br)_3$ (7.34 g, 24.0 mmol) was added dropwise to the $Na^+S(^nC_4H_9)^-$ first diluted with 150 mL of ethanol. The resulting mixture was refluxed for 70 hours under nitrogen. The grey reaction mixture was cooled, filtered off and washed with a saturated $NaHCO_3$ solution. Diethyl ether (50 mL) was added and the aqueous layer was extracted. The organic layer was dried over anhydrous $MgSO_4$, filtered off and the solvent was removed *in vacuo* to afford a clear orange oil which was distilled (80°C; 0.5 mm Hg). Yield: 4.1 g, 12.24 mmol (51%). ^1H NMR ($CDCl_3$): δ 0.89 (t, 9H, $C\underline{H}_3C_3H_6S$-), 1.06 (s, 3H, $C\underline{H}_3C$), 1.35 (m, 6H, $CH_3C\underline{H}_2C_2H_4S$-), 1.55 (m, 6H, $C_2H_5C\underline{H}_2CH_2S$-), 2.51 (t, 6H, $C_3H_7C\underline{H}_2S$), 2.63 (s, 6H, $C_4H_9SC\underline{H}_2$) ppm. $^{13}C\{^1H\}$ NMR ($CDCl_3$): δ 13.66 ($\underline{C}H_3C_3H_6S$-), 21.95 ($CH_3\underline{C}H_2C_2H_4S$-), 23.80 ($\underline{C}H_3C$), 32.03 ($C_2H_5\underline{C}H_2CH_2S$-), 33.82 ($C_3H_7\underline{C}H_2S$), 38.88 ($CH_3\underline{C}$), 41.84 ($C_4H_9S\underline{C}H_2$) ppm. $C_{17}H_{36}S_3$ requires C, 60.65; H, 10.78 %; Found C, 60.56; H, 10.81 %. HRMS analysis (ESI): *m/z* calculated $[M+H]^+$: 336.1981; Found: 336.1979.

Synthesis of $MeC(CH_2SC_{10}H_{21})_3$: $MeC(CH_2Br)_3$ (4.0 g, 13.0 mmol) was dissolved in ethanol (200 mL) and NaOH (2.1g, 52.0 mmol) was added to the mixture. Decanethiol (7.5 g, 43.0 mmol) was added dropwise over a period of 30 minutes and the resulting mixture was refluxed under nitrogen for 24 hours. The resulting mixture was cooled, filtered off and washed with saturated $NaHCO_3$ solution (30 mL). The aqueous layer was then extracted with diethyl ether (3 x 50 mL). The organic layer was dried over anhydrous $MgSO_4$, filtered off and the solvent was removed *in vacuo* to afford an orange oil. Yield: 2.75 g, 4.68 mmol (36%). ^1H NMR ($CDCl_3$): δ 0.90 (t, 9H, $C\underline{H}_3C_9H_{18}S$-), 1.08 (s, 3H, $\underline{C}H_3C$), 1.29 (m, 42H, $CH_3C_7\underline{H}_{14}C_2H_4S$-), 1.62 (m, 6H, $C_8H_{17}C\underline{H}_2CH_2S$-), 2.52 (t, 6H, $C_9H_{19}C\underline{H}_2S$-), 2.60 (s, 6H, $C_{10}H_{21}SC\underline{H}_2$) ppm.

$^{13}C\{^1H\}$ NMR ($CDCl_3$): δ 14.07 ($\underline{C}H_3C_9H_{18}S$-), 22.66 ($CH_3\underline{C}H_2C_8H_{16}S$-), 23.80 ($\underline{C}H_3C$), 29.00, 29.26, 29.30, 29.54, 29.96 ($C_3H_7\underline{C}_5H_{10}C_2H_4S$-), 30.83 ($C_8H_{17}\underline{C}H_2CH_2S$-), 31.89 ($C_2H_5\underline{C}H_2C_7H_{14}S$-), 34.06 ($C_9H_{19}\underline{C}H_2S$-), 40.75 ($\underline{C}H_3C$), 41.84 ($C_{10}H_{21}S\underline{C}H_2$) ppm. HRMS analysis (ESI): *m/z* calculated $[M+H]^+$: 588.48; Found: 588.4789.

Synthesis of 1,4,7-triazacyclononane-1,4-dicarboxylic acid di-tert-butyl ester DiBOC[9]aneN$_3$ [48, 49]: To a solution of 1,4,7-triazacyclonane (2.36 g, 18.3 mmol) in $CHCl_3$ (10 mL) was added triethylamine (1.5 mL dried over Na_2SO_4) at room temperature. BOC-ON (9.00 g, 36.6 mmol) dissolved in $CHCl_3$ (10 mL) was added with stirring within 30 minutes. The solution was stirred at room temperature for 2 hours and was then concentrated under reduced pressure. To the obtained residue was added EtOAc (30 mL). The EtOAc solution was successively washed with 4% $NaHCO_3$ (aq) (15 mL), NaCl (aq) (15 mL), and 10% citric acid (aq) (3 x 20 mL), whereupon the desired moved to the aqueous phase. To the aqueous phase was carefully added NaOH (aq) under ice-cooling until the pH was adjusted to 10. The turbid solution was extracted with $CHCl_3$ (3 x 20 mL). The organic phase was dried over Na_2SO_4 and concentrated under reduced pressure to give a yellow oil. Yield: 3.50 g, 10.6 mmol (58%).^1H NMR ($CDCl_3$): δ 1.37 (s, 18H $C\underline{H}_3$ (^{t}Bu)), 2.80-2.82 (m, 4H, [9]aneN$_3$ ring), 3.12-3.17 (m, 4H, [9]aneN$_3$ ring), 3.32-3.38 (m, 4H, [9]aneN$_3$ ring) ppm. $^{13}C\{^1H\}$ NMR ($CDCl_3$): δ 26.1 (^{t}Bu), 43.6, 44.9, 45.3, 45.7, 45.8, 47.1, 47.3, 47.9, 49.2, 49.9, 50.0, 50.6 ([9]aneN$_3$ ring), 74.3, 74.7, 75.2 (^{t}Bu), 153.3, 153.5 ($\underline{C}$=O) ppm. Positive electrospray (CH_2Cl_2): *m/z* = 330 $(M+H)^+$.

Synthesis of 1-decyl-4,7-triazacyclononane (C$_{10}$H$_{21}$)[9]aneN$_3$ [28, 29]: Decanoyl chloride (2.01 g, 10 mmol) was added dropwise at room temperature to a stirred solution containing 1,4,7-triazacyclononane-1,4-dicarboxylic acid di-tert-butyl ester (3.15 g, 9.60 mmol) and triethylamine (2.7 mL) in distilled CH_2Cl_2 (100 mL). The solution was left to stir overnight under nitrogen and then washed with water (3 x 30 mL); the organic layer was dried over $MgSO_4$, and the CH_2Cl_2 was removed with a rotary evaporator. The intermediate 1,4,7-tri(nonylcarbonyl)-1,4,7-triazacyclononane was obtained as a pale yellow oil. Yield: 1.96 g, 6.9 mmol (69%). ^1H NMR ($CDCl_3$): δ 0.94 (t, 3H, $C\underline{H}_3C_8H_{16}CON$-), 1.25-1.30 (m, 12H, $CH_3C_6\underline{H}_{12}CH_2CON$-), 1.32-1.65 (m, 20H, $C(C\underline{H}_3)_3$ and $C_7H_{15}C\underline{H}_2CON$-),

2.22-2.39 (m, 4H, [9]aneN$_3$ ring), 3.10-3.35 (m, 4H, [9]aneN$_3$ ring), 3.43-3.6 (m, 4H, [9]aneN$_3$ ring) ppm. $^{13}C\{^1H\}$ NMR ($CDCl_3$): δ 14.07 ($\underline{C}H_3C_8H_{16}CON$-), 22.63, 24.22, 25.35, 28.85, 29.25, 29.47, 31.85, 33.40, 35.28, 48.18, 49.67, 52.94 ([9]aneN$_3$ ring and $CH_3\underline{C}_8H_{16}CON$-), 155.36 ($\underline{C}$=O BOC), 173.13 ($C_9H_{19}\underline{C}ON$-) ppm. Positive electrospray (CH_2Cl_2): *m/z* = 484 ((C$_9$H$_{19}$CO)-DiBOC-[9]aneN$_3$ + H)$^+$.

The amide ((C$_9$H$_{19}$CO)-DiBOC-[9]aneN$_3$) (3.30g, 6.83 mmol) was dissolved in dry THF (50 mL); a solution of BH_3·THF (48 mL) was added, and the mixture was refluxed overnight under a dinitrogen atmosphere. After being allowed to cool at room temperature, the excess BH_3·THF was quenched by slow addition of methanol, and the colourless solution was evaporated to leave a colourless oil. This was dissolved in 1-butanol (50 mL), water (50 mL), and concentrated HCl (80 mL) and refluxed overnight. After the mixture was cooled, sodium hydroxide was added until pH > 12, and the product was extracted with CH_2Cl_2 (6 x 50 mL). The combined organic extracts were dried over $MgSO_4$, filtered and evaporated *in vacuo* to give the desired product as an orange oil. Yield: 0.9 g, 3.34 mmol (49%). ^1H NMR ($CDCl_3$): δ 0.95 (t, 3H, $C\underline{H}_3C_9H_{18}N$-), 1.12-1.65 (m, 16H, $CH_3C_8\underline{H}_{16}CH_2N$-), 2.38-2.55 (m, 2H, $C_9H_{19}C\underline{H}_2N$-), 2.56-2.75 (m, 4H, [9]aneN$_3$ ring), 2.78-3.04 (m, 8H, [9]aneN$_3$ ring) ppm. $^{13}C\{^1H\}$ NMR ($CDCl_3$): δ 14.08 ($\underline{C}H_3C_9H_{18}N$), 22.66, 27.23, 27.31, 29.28-29.56 ($C_3H_7C_4\underline{H}_8C_3H_6N$-), 31.87 ($CH_3\underline{C}_8H_{16}CH_2N$-), 43.15, 44.72 ([9]aneN$_3$ ring), 49.78 ($C_9H_{19}C\underline{H}_2N$-), 56.55 ([9]aneN$_3$ ring) ppm. Positive electrospray (CH_2Cl_2): *m/z* = 270 ((C$_{10}$H$_{21}$)[9]aneN$_3$ + H)$^+$. $C_{16}H_{35}N_3$ requires C, 71.31; H, 13.09; N, 15.59 %; Found C, 71.24; H, 12.90; N, 15.50 %.

Synthesis of 1,4,7-tris(decyl)-triazacyclononane (C$_{10}$H$_{21}$)$_3$[9]aneN$_3$: Decanoyl chloride (4.87 g, 25.0 mmol) was added dropwise at room temperature to a stirred solution containing TACN (1.0 g, 7.75 mmol) and triethylamine (6.5 mL, 46.6 mmol) in distilled CH_2Cl_2 (100 mL). The solution was left to stir overnight under a dinitrogen atmosphere and then washed with water (3 x 30 mL); the organic layer was dried over $MgSO_4$, and the CH_2Cl_2 was removed with a rotary evaporator. The intermediate 1,4,7-tris(nonylcarbonyl)-1,4,7-triazacyclononane was obtained as a pale yellow solid. Yield: 3.47 g, 5.89 mmol (76%). ^1H NMR ($CDCl_3$): δ 0.8 (t, 9H, $C\underline{H}_3C_8H_{16}CON$-), 1.19 (m, 36H, $CH_3C_6\underline{H}_{12}C_2H_4CON$-), 1.53 (m, 6H, $C_7H_{15}C\underline{H}_2CH_2CON$-) 2.19 (m, 6H, $C_7H_{15}CH_2C\underline{H}_2CON$-), 3.32

(s, 6H, [9]aneN$_3$ ring), 3.61 (s, 6H, [9]aneN$_3$ ring) ppm. $^{13}C\{^1H\}$ NMR ($CDCl_3$): δ 14.01 ($\underline{C}H_3C_8H_{16}CON$-), 22.58 ($CH_3\underline{C}H_2C_7H_{14}CON$-), 25.20 ($C_7H_{15}\underline{C}H_2CH_2CON$-), 29.44-29.46 ($C_3H_7\underline{C}_4H_8C_2H_4CON$-), 31.79 ($C_2H_5\underline{C}H_2C_6H_{12}CON$-), 33.16 ($C_8H_{17}\underline{C}H_2CON$-), 49.16, 51.05 ([9]aneN$_3$ ring), 174.35 ($\underline{C}$=O) ppm. Positive electrospray (CH_2Cl_2): *m/z* = 592.5 $((C_9H_{19}CO)_3$-[9]aneN$_3$ + H$)^+$. Infra-red (C=O): 1637 cm^{-1}.

The triamide ($(C_9H_{19}CO)_3$-[9]aneN$_3$) (3.30 g, 5.58 mmol) was dissolved in dry THF (50 mL); a solution of BH_3·THF (39 mL) was added, and the mixture was refluxed overnight under a dinitrogen atmosphere. After being allowed to cool at room temperature, the excess BH_3·THF was quenched by slow addition of methanol, and the colourless solution was evaporated to leave a colourless oil. This was dissolved in 1-butanol (50 mL), water (50 mL), and concentrated HCl (80 mL) and refluxed overnight. After the mixture was cooled, sodium hydroxide was added until pH > 12, and the product was extracted with CH_2Cl_2 (6 x 50 mL). The combined organic extracts were dried over $MgSO_4$, filtered and evaporated *in vacuo* to give the desired product as a pale yellow oil. Yield: 2.30 g, 4.18 mmol (75%). ^1H NMR ($CDCl_3$): δ 0.88 (t, 12H, $C\underline{H}_3C_9H_{18}N$-), 1.26-1.43 (m, 48H, $CH_3C_8\underline{H}_{16}CH_2N$-), 2.45 (t, 6H, $C_9H_{19}C\underline{H}_2N$-), 2.73 (s, 12H, [9]aneN$_3$ ring) ppm. $^{13}C\{^1H\}$ NMR ($CDCl_3$): δ 14.08 ($\underline{C}H_3C_9H_{18}N$-), 22.67, 27.60, 28.05, 29.33, 29.61-29.68, 31.91 ($CH_3\underline{C}_8H_{16}CH_2N$-), 59.00 ($C_9H_{19}\underline{C}H_2N$-), 55.88 ([9]aneN$_3$ ring) ppm. Positive electrospray (CH_2Cl_2): *m/z* = 550.7 $((C_{10}H_{21})_3$-[9]aneN$_3$ + H$)^+$. $C_{36}H_{75}N_3$ requires C, 78.62; H, 13.74; N, 7.64 %; Found C, 78.53; H, 13.69; N, 7.50%.

Synthesis of [$CrCl_3${$S(CH_2CH_2SC_{10}H_{21})_2$}] [19]: The procedure was to add the ligand $S(CH_2CH_2SC_{10}H_{21})_2$ (0.50 g, 1.15 mmol) previously dissolved in a minimum volume of CH_2Cl_2 to a solution of [$CrCl_3(THF)_3$] (0.43 g, 1.15 mmol) in dried and degassed CH_2Cl_2 (15 mL). The resulting mixture was stirred at room temperature under nitrogen for 1 hour. The solvent was then removed *in vacuo* to afford a purple solid. Yield: 1.02 g, 1.72 mmol (67%). UV/visible (diffuse reflectance): 517, 699 nm.

Synthesis of $[CrCl_3\{O(CH_2CH_2SC_{10}H_{21})_2\}]$: Reaction carried out as above using $[CrCl_3(THF)_3]$ (450 mg, 1.20 mmol) and $O(CH_2CH_2SC_{10}H_{21})_2$ (502 mg, 1.20 mmol) to give a green solid. Yield: 492 mg, $8.52x10^{-4}$ mol (71%). UV/visible (diffuse reflectance): 716, 475 nm.

Synthesis of $[CrCl_3\{MeC(CH_2S^nC_4H_9)_3\}]$: Reaction carried out as above using $[CrCl_3(THF)_3]$ (500 mg, 1.33 mmol) and $CMe(CH_2S^nC_4H_9)_3$ (448 mg, 1.33 mmol) to give a purple solid. Yield: 493 mg, 1.00 mmol (75%). UV/visible (diffuse reflectance): 694, 492 nm.

Synthesis of $[CrCl_3\{MeC(CH_2SC_{10}H_{21})_3\}]$: Reaction carried out as above using $[CrCl_3(THF)_3]$ (127 mg, 0.34 mmol) and $CMe(CH_2SC_{10}H_{21})_3$ (200 mg, 0.34 mmol) to give a dark purple solid. UV/visible (diffuse reflectance): 695, 493 nm.

Synthesis of $[CrCl_3\{(C_{10}H_{21})[9]aneN_3\}]$: Reaction carried out as above using $[CrCl_3(THF)_3]$ (522 mg, 1.39 mmol) and $(C_{10}H_{21})[9]aneN_3$ (269 mg, 1.39 mmol) to give a dark purple solid. Yield: 420 mg, $9.84x10^{-4}$ mol (70%). UV/visible (diffuse reflectance): 594, 485 nm.

Synthesis of $[CrCl_3\{(C_{10}H_{21})_3[9]aneN_3\}]$: Reaction carried out as above using $[CrCl_3(THF)_3]$ (500 mg, 1.33 mmol) and $(C_{10}H_{21})_3[9]aneN_3$ (783 mg, 1.33 mmol) to give a brown oil. Yield: 450 mg, $6.39x10^{-4}$ mol (48%). UV/visible (diffuse reflectance): 595, 459 nm.

5.6. References

1. Britovsek, G. J. P.; Gibson, V. C. and Wass, D. F.; *Angew. Chem. Int. Ed.*, (1999), **38**, 428.
2. Ittel, S. D.; Johnson, L. K. and Brookhart, M.; *Chem. Rev.*, (2000), **100**, 1169.
3. Gibson, V. C. and Spitzmesser, S. K.; *Chem. Rev.*, (2003), **103**, 283.
4. Zhang, W.; Sun, W.; Zhang, S.; Hou, J.; Wedeking, K.; Schultz, S.; Frohlich, R. and Song, H.; *Organometallics*, (2006), **25**, 1961.
5. Groppo, E.; Lamberti, C.; Bordiga, S.; Spoto, G. and Zecchina, A.; *Chem. Rev.*, (2005), **105**, 115.
6. Kohn, R. D.; Haufe, M.; Mihan, S. and Lilge, D.; *Chem. Commun.*, (2000), 1927.
7. Miller, S. A.; *Chem. Proc. Eng.*, (1969), **50**, 103.
8. Peuckert, M. and Keim, W.; *Organometallics*, (1983), **2**, 594.
9. Overett, M. J.; Blann, K.; Bollmann, A.; Dixon, J. T.; Haasbroek, D.; Maumela, H.; McGuinness, D. S. and Morgan, D. H.; *J. Am. Chem. Soc.*, (2005), **127**, 10723.
10. McGuinness, D. S.; Wasserscheid, P.; W, W. Keim; Hu, C.; Englert, U.; Dixon, J. T. and Grove, C.; *J. Chem. Soc., Chem. Commun.*, (2003), 334.
11. McGuinness, D. S.; Wasserscheid, P.; Keim, W.; Morgan, D.; Dixon, J. T.; Bollmann, A.; Maumela, H.; Hess, F. and Englert, U.; *J. Am. Chem. Soc.*, (2003), **125**, 5272.
12. Bollmann, A.; Blann, K.; Dixon, J. T.; Hess, F. M.; Killian, E.; Maumela, H.; McGuinness, D. S.; Morgan, D. H.; Neveling, A.; Otto, S.; Overett, M.; Slawin, A. M. Z.; Wasserscheid, P. and Kuhlmann, S.; *J. Am. Chem. Soc.*, (2004), **126**, 14712.
13. Agapie, T.; Schofer, S. J.; Labinger, J. A. and Bercaw, J. E.; *J. Am. Chem. Soc.*, (2004), **126**, 1304.
14. Dixon, J. T.; Green, M.; Hess, F. M. and Morgan, D. H.; *J. Organomet. Chem.*, (2004), **689**, 3641.
15. Tomov, A. K.; Chirinos, J. J.; Long, R. J.; Gibson, V. C. and Elsegood, M. R. J.; *J. Am. Chem. Soc.*, (2006), Advanced article.
16. Jones, D. J.; Gibson, V. C.; Green, S. M. and Maddox, P. J.; *J. Chem. Commun.*, (2002), 1038.

17. Kohn, R. D.; Haufe, M.; Kociok-Kohn, G.; Grim, S.; Wasserscheid, P. and Keim, W.; *Angew. Chem. Int. Ed.*, (2000), **39**, 4337.
18. Ruther, T.; Cavell, K. J.; Braussaud, N. C.; Skelton, B. W. and White, A. H.; *J. Chem. Soc., Dalton Trans.*, (2002), 4684.
19. Pope, S. J. A.; Champness, N. R. and Reid, G.; *J. Chem. Soc., Dalton Trans.*, (1997), 1639.
20. Champness, N. R.; Jacob, S. R. and Reid, G.; *Inorg. Chem.*, (1995), **34**, 396.
21. Chen, E. Y. and Marks, T. J.; *Chem. Rev.*, (2000), **100**, 1391.
22. Krossing, I. and Raabe, I.; *Angew. Chem. Int. Ed.*, (2004), **43**, 2066.
23. Hartley, F. R.; Murray, S. G.; Levason, W.; Soutter, H. E. and McAuliffe, C. A.; *Inorg. Chim. Acta*, (1979), **35**, 265.
24. Ali, R.; Higgins, S. J. and Levason, W.; *Inorg. Chim. Acta*, (1984), **84**, 65.
25. Richman, J. E. and Atkins, T. J.; *J. Am. Chem. Soc.*, (1974), **96**, 2268.
26. Searle, G. H. and R, J. Geue; *Aust. J. Chem.*, (1984), **37**, 959.
27. Koyama, H. and Yoshino, T.; *Bull. Chem. Soc. Jpn.*, (1972), **45**, 481.
28. Alcock, N. W.; Benniston, A. C.; Grant, S. J.; Omar, H. A. A. and Moore, P.; *J. Chem. Soc., Chem. Commun*, (1991), 1573.
29. Diebold, A.; Elbouadili, A. and Hagen, K. S.; *Inorg. Chem.*, (2000), **39**, 3915.
30. Herwig, W. and Zeiss, H.; *J. Organomet. Chem.*, (1958), **23**, 1404.
31. Lever, A. B. P.; *Inorganic Electronic Spectroscopy, 2nd Edition,* (1984), Amsterdam, Elsevier Science Publisher.
32. Grant, G. J.; Rogers, K. E.; Setzer, W. N. and VanDerveer, D. G.; *Inorg. Chim. Acta*, (1995), **234**, 35.
33. Kuppers, H. J. and Wieghardt, K.; *Polyhedron*, (1989), **8**, 1770.
34. Serpone, N.; Jamieson, M. A.; Hoffman, M. Z.; Bolletta, F. and Maestri, M.; (1979), **101**, 2907.
35. Hale, A. L. and Levason, W.; *J. Chem. Soc., Dalton Trans.*, (1983), 2569.
36. Gray, L. R.; Hale, A. L.; Levason, W.; McCullough, F. P. and Webster, M.; *J. Chem. Soc., Dalton Trans.*, (1984), 47.
37. Kirk, A. D. and Namasivayam, C.; *Inorg. Chem.*, (1988), **27**, 1095.
38. Wolf, R. E.; Hartman, J. R.; Storey, J. M. E.; Foxman, B. M. and Cooper, S. R.; *J. Am. Chem. Soc.*, (1987), **109**, 4328.
39. Mark, J. E. and Flory, P. J.; *J. Am. Chem. Soc.*, (1965), **87**, 1415.

40. Cotton, F. A.; Duraj, S. A.; Powell, G. L. and Roth, W. J.; *Inorg. Chim. Acta*, (1986), **113**, 81.

41. Wieghardt, K.; Chaudhuri, P.; Nuber, B. and Weiss, J.; *Inorg. Chem.*, (1982), **21**, 3086.

42. Flory, P. J.; *J. Am. Chem. Soc.*, (1940), **62**, 1561.

43. Schulz, G. V. Z.; *Phys. Chem., Abt. B*, (1935), **30**, 379.

44. Meurs, M. V.; Britovsek, G. J. P.; Gibson, V. C. and Cohen, S. A.; *J. Am. Chem. Soc.*, (2005), **127**, 9913.

45. Wu, F. J.; *US 5744677*, (1998), Amoco.

46. Gibson, V. C.; Newton, C.; Redshaw, C.; Solan, G. A.; White, A. J. P. and Williams, D. J.; *Eur. J. Inorg. Chem.*, (2001), 1895.

47. Fryzuk, M. D.; Leznoff, D. B. and Retting, S. J.; *Organometallics*, (1995), **14**, 5193.

48. Kovacs, Z. and Sherry, A. D.; *Tetrahedron Lett.*, (1995), **36**, 9269.

49. Kimura, S.; Eckhard, B.; Bothe, E.; Weyhermuller, T. and Wieghardt, K.; *J. Am. Chem. Soc.*, (2001), **123**, 6025.

Chapter 6

Coordination Chemistry of Chromium(III) Complexes: Spectroscopic and Extended X-ray Absorption Fine Structure Studies

6.1. Introduction

6.1.1 Chromium Thioether Complexes

Traditionally, acyclic thioether ligands attracted much less interest than their phosphine analogues, probably because the widely held belief that they were only modest σ donors and therefore weakly coordinating ligands [1]. The bi- and poly-dentate ligands with aliphatic backbones are generally produced by attack of RS^- on the appropriate haloalkane. This is usually the method of choice for $RS(CH_2)_nSR$ (with n = 2, 3) and $MeC(CH_2SR)_3$. Tridentate ligands with donor atoms on the arms of a tripod are commonly used in coordination chemistry [2]. The methyl substituted group 16 tripod ligand $MeC(CH_2SMe)_3$ and its coordination chemistry have been reported in the literature [3]. The use of such a ligand finds its interest in its steric constraints. The ligand typically adopts the 3-coordinate (*facial*) bonding of donor atoms in the majority of the complexes, although other bonding modes involving only one or two of the thioether functions are also known [3]. Coordination chemistry literature reports chromium(III) complexes of acyclic thioethers: $[CrCl_3\{MeC(CH_2SMe)_3\}]$, $[Cr\{S(CH_2CH_2CH_2SMe)_2\}][BF_4]_3$, $[Cr\{MeSCH{=}CHSMe\}_3][BF_4]_3$ [3-5].

Nevertheless, during the past decade, there has been a remarkable increase in activity of the coordination chemistry of thioether ligands, especially research dealing with the nine-membered ring trithioether, 1,4,7-trithiacyclononane [9]aneS_3. Several articles reviewing thioether ligand systems have appeared [6-9]. Although [9]aneS_3 forms stable complexes with nearly every transition metal, only a few examples of the coordination to early transition metals are known [10]. The strong coordination of this macrocycle to the 'late' transition metals comes from both its steric (*endo* conformation) [11] and electronic properties. Most past research efforts have focused on thioether complexation with soft or borderline metal ions. The coordination chemistry of thioethers with hard, trivalent metal ions from the early transition metals remained relatively unexplored [10, 12]. The preparation of $[M\{[9]aneS_3\}]^{3+}$ complexes with trivalent, first row transition metals has been limited to chromium(III), cobalt(III), nickel(III) and iron(III) [10, 13, 14]. Chromium(III) complexes with a range of thioether macrocycles have been prepared and characterised by X-ray crystallography *e.g.* $[CrCl_3\{[18]aneS_6\}]$ [4]. Owing to the

limited solubilities displayed by many of the thioether complexes and their sensitivity to moisture, in most cases crystals suitable for an X-ray study could not be obtained. Hence, chromium K-edge EXAFS has been a good alternative technique and partial structural data on a series of chromium(III) complexes are now available: $[CrCl_3\{[9]aneS_3\}]$, $[CrBr_3\{[9]aneS_3\}]$, $[CrCl_3\{[10]aneS_3\}]$, $[CrBr_2\{[14]aneS_4\}][PF_6]$, $[CrCl_2\{[14]aneS_4\}][PF_6]$. $[Cr_2Cl_6\{[18]aneS_6\}]$ [15, 16].

6.1.2 Chromium(III) Aza-Macrocyclic Complexes

1,4,7-triazacyclononane based ligands have been widely used in the synthesis of high- and low-valent organometallics as well as for the preparation of models of metalloprotein active sites [17]. Because of the kinetic and thermodynamic stability which these macrocycles impart upon their complexes, they have become valued as supporting ligands. Simple alkyl groups (*e.g.* methyl [18], isopropyl [19] or benzyl [20]) as well as a variety of functionalised substituents such as phenolate [21] or alkoxide [22] have been added to the $[9]aneN_3$ ring resulting in the formation of N,N',N''-trisubstituted ligands.

The coordination chemistry of various Cr(III) species with $[9]aneN_3$ has been investigated over the last decade [23] and $[9]aneN_3$ complexes present relatively stable products, the hard N-donor atoms being compatible with the hard Cr(III) ion. A wide range of $[Cr\{[9]aneN_3\}X_3]$ have been reported (with X = F, Br, CN, NCS) and investigated in the early 1980s [23-26]. However, studies on the complex $[CrCl_3\{[9]aneN_3\}]$ have not been described in detail. Nevertheless the chromium complex $[Cr\{[9]aneN_3\}_2]^{2+/3+}$ has been much more studied [25, 27]. The synthesis and coordination chemistry of the $[9]aneN_3$ derivatives have also been of interest in the last few decades (Figure 6.1).

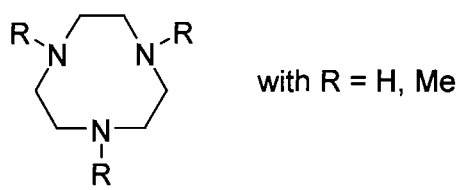

Figure 6.1. Representation of a tri-substituted $[9]aneN_3$ [17, 18]

Wieghardt and co-workers [17, 18] reported the preparation of $Me_3[9]aneN_3$ coordinated with a series of transition metals (Cr, Co, Rh). In the same way, the synthesis of the mono-derivatives $E[9]aneN_3$ and their coordination chemistry have been investigated with E = CH_2CO_2H, $CH_2PO(OH)_2$, $CH_2CO_2{}^tBu$, $CH_2PO(OEt)_2$ [28, 29]. The selective alkylation of only one or two $[9]aneN_3$ nitrogen atoms received attention over the last decade and extensive work on $[9]aneN_3$ di- and tri-derivatives has been reported [30-32].

6.2. Aims

This chapter investigates the coordination chemistry of soft sulfur and hard nitrogen donor atoms to the hard chromium(III) metal ion. The ultimate goal is to have a better understanding of these complexes using techniques such as UV/visible, Infra-red and electron paramagnetic resonance spectroscopy and EXAFS measurements. The ligands are chosen to cover a wide area, from the geometry – facultative, tripodal and macrocyclic – to the set of donor atoms – soft sulfur and hard nitrogen. All the spectroscopic and structural data obtained from these chromium(III) complexes allow for comparison with the chromium(III) complexes studies for the study of the homogeneous catalysis reactions of trimerisation, tetramerisation and oligomerisation of ethylene (Chapters 3, 4 and 5).

6.3. Results and Discussion

6.3.1. Ligands Synthesis

The ligands were generally prepared by literature methods or by modifications of those.

a) Synthesis of $S(CH_2CH_2SMe)_2$

The ligand $S(CH_2CH_2SMe)_2$ was prepared from reaction of bis(2-mercaptoethyl) sulfide with sodium in EtOH and two molar equivalents of an alkyl halide, iodomethane, *via* the disodium salt in ethanol and fractioned *in vacuo* (Scheme 6.1) [33], to afford a clear and colourless oil with a yield of 66%. The ligand was characterised by combination of IR spectroscopy, ^1H and $^{13}C\{^1H\}$ NMR, mass spectroscopy and elemental analysis. The ^1H NMR spectrum of the crude product revealed a multiplet at 2.75 ppm corresponding to the backbone SCH_2CH_2S of the ligand. One signal at 2.15 (singlet) ppm confirmed the presence of the methyl group, CH_3. The $^{13}C\{^1H\}$ DEPT NMR spectra of the obtained compounds were consistent with the formation of the desired ligand $S(CH_2CH_2SMe)_2$. Elemental analysis of the ligand was obtained and was in excellent agreement with expectations. Therefore, no further purification was necessary.

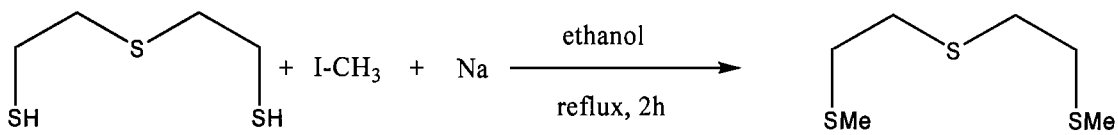

Scheme 6.1. Synthesis of $S(CH_2CH_2SMe)_2$ [33]

b) Synthesis of $MeC(CH_2SCH_3)_3$

The ligand $MeC(CH_2SCH_3)_3$ was synthesised following a reported method [2]. The previously prepared starting material $MeC(CH_2Br)_3$ [34] was reacted with three molar equivalents of the salt $Na^+S(Me)^-$. After being refluxed for 70 hours, the reaction mixture was washed, the organics extracted, dried and distilled to afford a clear orange oil (Scheme 6.2). The compound obtained was fully and successfully characterised by spectroscopic methods (^1H and $^{13}C\{^1H\}$ NMR spectroscopy, high resolution mass spectrometry) and by elemental analysis.

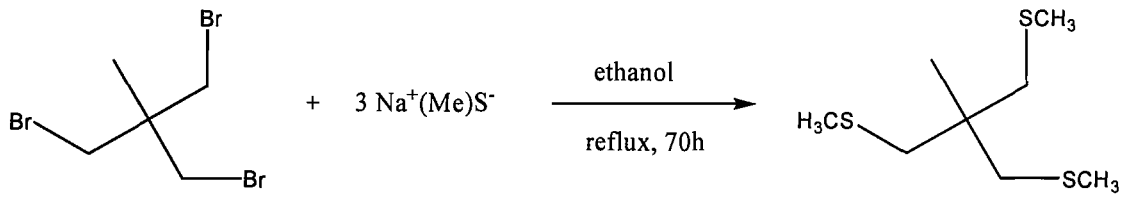

Scheme 6.2. Synthesis of $MeC(CH_2SCH_3)_3$ [2]

c) Synthesis of $[9]aneN_3$

The macrocycle 1,4,7-triazacyclononane $[9]aneN_3$ was prepared following a modified method reported by Richman and Atkins for the synthesis of cyclic polyamines [35-37]. The preparation of the macrocycle $[9]aneN_3$ is a 4-step reaction and consists of the cyclisation of two tosylated parent compounds *via* a high dilution process.

The first step of this synthesis is the preparation of the two starting materials, 1,2-*bis*[(*p*-tolylsulfonyl)oxy]ethane and N,N',N''-*tris*(*p*-tolylsulfonyl)diethylene triamine. 1,2-*bis*[(*p*-tolylsulfonyl)oxy]ethane (1) was prepared as depicted in Scheme 6.3 by reaction of ethylene glycol with tosyl chloride in dry pyridine and at 0°C. The cold mixture was then added to hydrochloric acid. After work-up and recrystallisation from CH_2Cl_2/MeOH, (1) was obtained as a white solid in good yield (~70%) and successfully characterised (Scheme 6.3) [38].

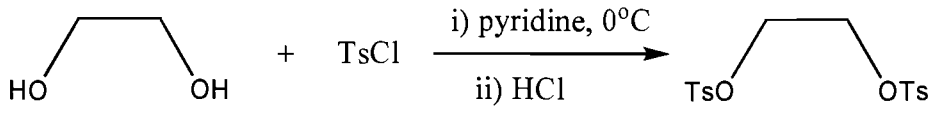

(1)

Scheme 6.3. Synthesis of 1,2-*bis*[(*p*-tolylsulfonyl)oxy]ethane (1) [38]

N,N',N''-*tris*(*p*-tolylsulfonyl)diethylene triamine (2) was prepared by the reaction of diethylene triamine and NaOH with tosyl chloride in diethyl ether. Methanol was then added to the reaction mixture to afford the desired compound as a white powder in very good yield (99%). NMR spectra were consistent with the reported literature values [38]. Scheme 6.4 illustrates the reaction described above for the formation of (2).

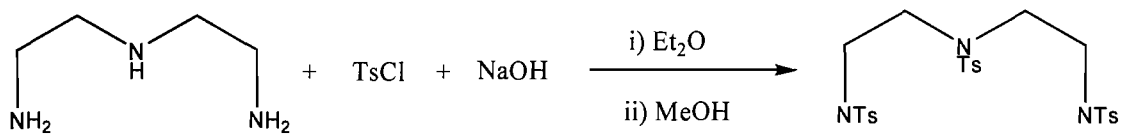

(2)

Scheme 6.4. Synthesis of N,N',N''-*tris*(*p*-tolylsulfonyl)diethylene triamine (2) [38]

The second step of the [9]aneN$_3$ synthesis is the cyclisation (Scheme 6.5). This reaction is performed *via* a high-dilution process. This direct synthetic procedure involves the reaction, in equimolar concentrations, of the two precursor species (1) and (2) incorporating the required fragments for the target macrocycle such that a 1:1 condensation occurs. The overnight reaction between (1) and (2) in the presence of K_2CO_3 and after work-up led to the desired product, obtained as a white powder (3) [36].

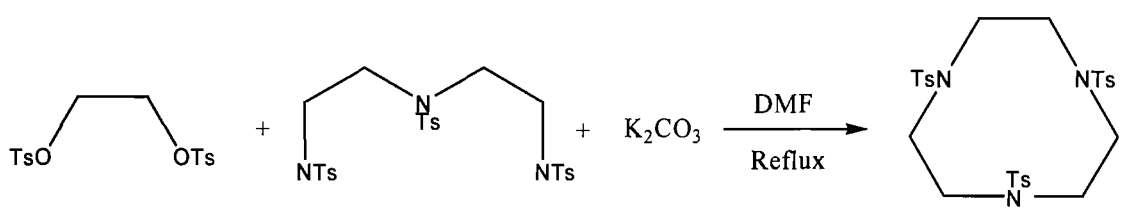

(3)

Scheme 6.5. Synthesis of 1,4,7-*tris*(*p*-tolylsulfonyl)-1,4,7-triazacyclononane (3) [36]

The following stage consists of synthesising the trihydrobromide salt (4). This species was obtained by heating (3) overnight in degassed concentrated sulfuric acid. The resulting black solution was added to cold methanol and the grey solid obtained was then dissolved in hot water and precipitation of the salt occurred after addition of HBr (Scheme 6.6).

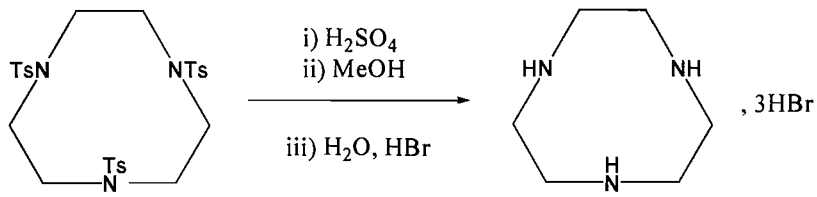

(4)

Scheme 6.6. Synthesis of 1,4,7-triazacyclonane trihydrobromide (4)

The last stage of the synthesis consists of isolating the free base from the trihydrobromide salt (4). The desired final compound was obtained by using a Dean and Stark trap and refluxing a solution mixture of the salt (4) / water / toluene and NaOH. After complete removal of the solvent, a pale yellow crystalline solid was obtained (Scheme 6.7). The ligand was successfully characterised by combination of ^{1}H, $^{13}C\{^{1}H\}$ NMR spectroscopy, mass spectrometry and elemental analysis.

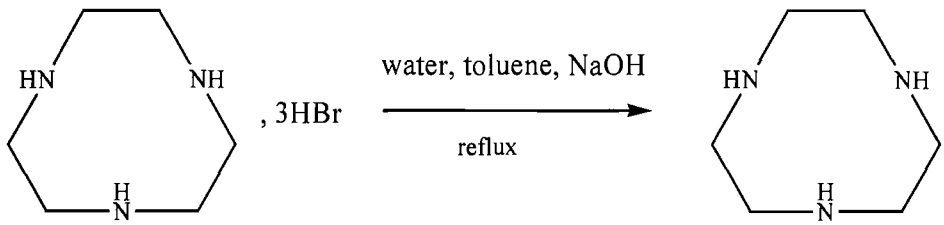

Scheme 6.7. Synthesis of 1,4,7-triazacyclononane

A crystal structure of [9]aneN_3.0.5H_2O was obtained. The compound crystallises in the high symmetry trigonal space group P-3*c*1 (hexagonal symmetry cell), the asymmetric unit containing one-third of a [9]aneN_3 molecule and one-sixth of a water molecule. The [9]aneN_3 molecule contains the three nitrogen atoms oriented *facially*, suitable for binding to metal ions. The structure obtained is very similar to the one recently reported in the literature [39].

d) Synthesis of $Me_3[9]aneN_3$

The trimethyl [9]aneN$_3$ derivative was synthesised *via* modification of method reported by Barefield and Wagner (Scheme 6.8) [40] and Wieghardt [18]. The reaction consisted of refluxing [9]aneN$_3$, paraformaldehyde, formic acid and water for 24 hours. The pH of the resulting mixture was then adjusted to 12 using a sodium hydroxide solution. The mixture was then extracted with chloroform, dried over anhydrous sodium sulfate, filtered off and reduced to an oily and yellow residue successfully characterised.

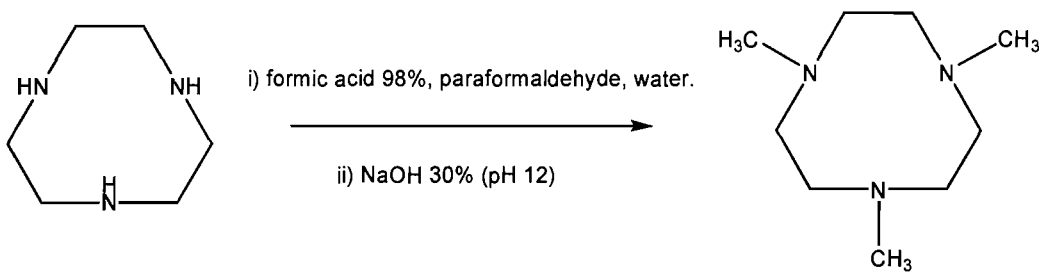

Scheme 6.8. Synthesis of 1,4,7-trimethyl-1,4,7-triazacyclononane, $Me_3[9]aneN_3$ [18, 40]

e) Synthesis of $(isoPr)_2[9]aneN_3$

The [9]aneN$_3$ derivative 1,4-diisopropyl-1,4,7-triazacyclononane was synthesised *via* a three-step reaction and following two methods reported by Bulkowski [38] and Cramer [30].

The first intermediate compound, 1-(*p*-toluenesulfonyl)-1,4,7-triazacyclononane (5) was obtained by treating 1,4,7-(*p*-toluenesulfonyl)-1,4,7-triazacyclononane with phenol in a solution of 33% HBr/AcOH (Scheme 6.9). After refluxing the mixture for 36 hours, the white precipitate was filtered and dissolved in 1 M NaOH before being extracted with chloroform. The white product was successfully characterised by ^1H, $^{13}C\{^1H\}$ NMR spectroscopy and mass spectrometry.

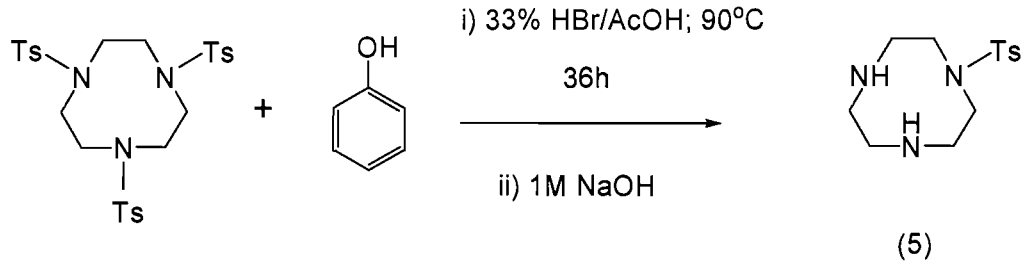

(5)

Scheme 6.9. Synthesis of 1-(*p*-toluenesulfonyl)-1,4,7-triazacyclononane (5)

The second intermediate species, 1,4-diisopropyl-7-(*p*-toluenesulfonyl)-1,4,7-triazacyclononane (6) was obtained by combining 1-(*p*-toluenesulfonyl)-1,4,7-triazacyclononane (5) and 2-bromopropane in degassed acetonitrile (Scheme 6.10). After adding Na_2CO_3 and refluxing the resulting mixture for 18 hours under a N_2 atmosphere, the solvent was removed under vacuo. The resulting oil was dissolved in $CHCl_3$ and washed with a NaOH solution. The product was obtained as a tan solid and successfully characterised by NMR spectroscopic methods.

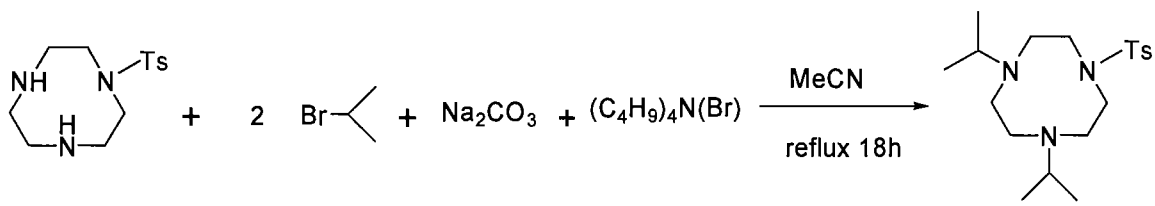

(6)

Scheme 6.10. Synthesis of 1,4-diisopropyl-7-(*p*-toluenesulfonyl)-1,4,7-triazacyclononane (6)

The final species, 1,4-diisopropyl-1,4,7-triazacyclononane, was synthesised by treatment of 1,4-diisopropyl-7-(*p*-toluenesulfonyl)-1,4,7-triazacyclononane (6) with H_2SO_4 for 18 hours at 120°C (Scheme 6.11). After extraction in $CHCl_3$, the compound was obtained as an amber oil. Spectroscopic analyses were performed on the product and confirmed the expected nature of the ligand with values similar to the ones reported in the literature [30, 38].

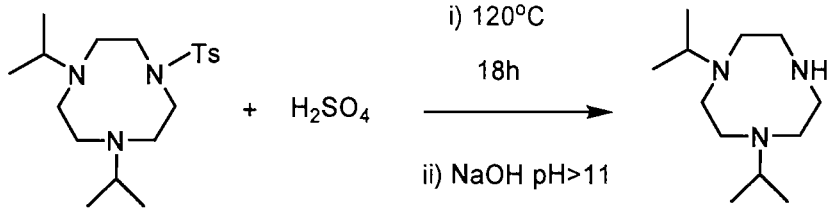

Scheme 6.11. Synthesis of 1,4-diisopropyl-1,4,7-triazacyclononane

6.3.2. Synthesis of the Chromium(III) Complexes [$CrCl_3${L}]

The polymeric and insoluble nature of $CrCl_3$ makes it an unsuitable starting material for coordination chemistry and hence, the readily soluble [$CrCl_3(THF)_3$] was used. The purple [$CrCl_3(THF)_3$] is prepared in essentially quantitative yield by continuous soxhlet extraction of anhydrous $CrCl_3$ with THF and zinc dust catalyst (Scheme 6.12) [41]. The zinc behaves as a reducing agent, solubilising the chromium in its divalent form which subsequently reduces more Cr^{3+} and at the same time is itself oxidised with concurrent formation of [$CrCl_3(THF)_3$] [41].

$$[CrCl_3] \xrightarrow[\text{Zn cat.}]{\text{THF}} [CrCl_3(THF)_3]$$

Scheme 6.12. Synthesis of [$CrCl_3(THF)_3$] [41]

The distorted octahedral [$CrCl_3${L}] complexes (L = [9]aneS_3, $S(CH_2CH_2SMe)_2$, $MeC(CH_2SMe)_3$, [9]aneN_3 and $(isoPr)_2$[9]aneN_3) were prepared by reaction of [$CrCl_3(THF)_3$] with one molar equivalent of the ligand {L} in anhydrous and degassed CH_2Cl_2 (Scheme 6.13) [15]. The products were isolated in relatively high yield as solid compounds by precipitation with diethyl ether or petroleum ether and by evaporation to dryness. It has been found that in order to promote coordination through the S- and N-donors it was necessary to remove the THF from the reaction mixture, otherwise the harder O-donor would bind preferentially [3].

$$[CrCl_3(THF)_3] + L \xrightarrow[\text{ii) } Et_2O^a \text{ or Pet. ether}^b]{\text{i) } CH_2Cl_2} [CrCl_3\{L\}]$$

$$\xrightarrow{\text{- 3 THF}}$$

with L = $[9]aneS_3$[a]
$S(CH_2CH_2SMe)_2$[a]
$MeC(CH_2SMe)_3$[b]
$[9]aneN_3$[a]
$(isoPr)_2[9]aneN_3$

Scheme 6.13. Synthesis mechanism for the $[CrCl_3\{L\}]$ compounds [15].

The chromium(III) complex $[CrCl_3\{Me_3[9]aneN_3\}]$ was prepared following a reported method [18]. In methanolic solutions of $Me_3[9]aneN_3$ and $CrCl_3.6H_2O$, the green monomeric complex $[CrCl_3\{Me_3[9]aneN_3\}]$ is formed (Scheme 6.14). The ligand $Me_3[9]aneN_3$ was added to chromium trichloride hexahydrate in methanol in the presence of granulated zinc, the mixture was refluxed for two hours to afford a green solid which was filtered *in vacuo*.

$$[CrCl_2(H_2O)_4]Cl.2H_2O + Me_3[9]aneN_3 \xrightarrow[\text{gran. Zn}]{\text{methanol}} [CrCl_3\{Me_3[9]aneN_3\}]$$

$$\xrightarrow{\text{reflux 2h}}$$

Scheme 6.14. Synthesis mechanism for $[CrCl_3\{Me_3[9]aneN_3\}]$ [18]

The neutral, coloured compounds proved to be poorly soluble in both chlorinated and unchlorinated organic solvents. Some are also relatively sensitive to moisture, hence all were stored in a N_2-purged glove-box. Table 6.1 summarises the analytical data that support the identity of the complexes synthesised.

Complex	Elemental Analysis % C	% H	Exp. (theor.) % N
$[CrCl_3\{[9]aneS_3\}]$	21.18 (21.28)	3.60 (3.57)	-
$[CrCl_3\{S(CH_2CH_2SMe)_2\}]$	21.11 (21.14)	3.94 (4.11)	-
$[CrCl_3\{MeC(CH_2SMe)_3\}]$	26.00 (26.06)	5.01 (4.92)	-
$[CrCl_3\{[9]aneN_3\}]$	24.95 (25.05)	5.30 (5.22)	14.57 (14.61)
$[CrCl_3\{Me_3[9]aneN_3\}]$	32.65 (32.79)	6.45 (6.42)	12.79 (12.75)
$[CrCl_3\{(isoPr)_2[9]aneN_3\}]$	38.67 (38.77)	7.25 (7.32)	11.18 (11.30)

Table 6.1. Elemental analysis data for $[CrCl_3\{L\}]$ compounds

6.3.3. Characterisation of the Chromium(III) Complexes.

6.3.3.1. UV/visible and Infra-red Spectroscopy

Table 6.2 presents the selected spectroscopic data for $[CrCl_3\{L\}]$ compounds. The chromium(III) complexes $[CrCl_3\{[9]aneS_3\}]$, $[CrCl_3\{S(CH_2CH_2SMe)_2\}]$, $[CrCl_3\{MeC(CH_2SMe)_3\}]$ exhibit a *Dq* value of ~1 450 cm^{-1}. These values are identical or very similar to those for other chromium(III)-thioether species known, *e.g.* $[CrCl_3\{MeC(CH_2SCH_3)_3\}]$, *Dq* = 1 470 cm^{-1} [3] and $[CrCl_3\{[9]aneS_3\}]$, *Dq* = 1 433 cm^{-1} [4]. Values obtained for the chromium(III)-thioether complexes generally compare well with other soft donor sets such as phosphines *e.g.* $[CrCl_3\{MeC(CH_2PPh_2)_3\}]$, *Dq* = 1 600 cm^{-1} [3]. The geometry of the ligand does not affect the ligand-field splitting since the *Dq* values are similar with any of the ligand sets: macrocyclic, facultative and tripodal.

The aza-macrocycle complexes $[CrCl_3\{[9]aneN_3\}]$, $[CrCl_3\{Me_3[9]aneN_3\}]$ and $[CrCl_3\{(isoPr)_2[9]aneN_3\}]$ present slightly higher *Dq* values with 1 690, 1 680 and 1 570 cm^{-1} respectively. However, these values are smaller than those reported for $[Cr\{NH_3\}_6]^{3+}$ where *Dq* = 2 160 cm^{-1} [10] or the chromium(III)-open chain ligand species $[Cr\{H_2NCH_2CH_2NH_2\}_3]^{3+}$ where *Dq* = 2 180 cm^{-1} [42] or even for the dimeric species $[Cr\{[9]aneN_3\}_2]^{3+}$ where *Dq* = 2 270 cm^{-1} [10]. Nevertheless, these results allow us to confirm the trend that interactions between the Cr(III) and the soft thioether functions are weak.

Complex	υ_1/cm^{-1}	υ_2/cm^{-1}	Dq/cm^{-1}	ν(Cr-Cl)/cm^{-1}
$[CrCl_3\{[9]aneS_3\}]$	14,560	20,120	1 450	290, 349
$[CrCl_3\{S(CH_2CH_2SMe)_2\}]$	14,500	19,700	1 450	344 (br)
$[CrCl_3\{MeC(CH_2SMe)_3\}]$	14,700	21,150	1 470	357, 326
$[CrCl_3\{[9]aneN_3\}]$	16,900	22,600	1 690	331, 346
$[CrCl_3\{Me_3[9]aneN_3\}]$	16,780	22,400	1 680	324, 348
$[CrCl_3\{(isoPr)_2[9]aneN_3\}]$	15, 670	21,550	1 570	344, 328

UV/visible spectra recorded for solid samples diluted with barium sulfate. Infra-red spectra recorded as nujol mulls.

Table 6.2. Selected spectroscopic data for $[CrCl_3\{L\}]$ compounds

A complex of the type MX_3L_3 (in our case, X = Cl and L = S or N) can exist in two isomeric forms, *mer* (C_{2v}) or *fac* (C_{3v}). Theory predicts three infra-red active metal-halogen stretches for *mer* isomers ($2A_1 + B_1$) and two for *fac* ($A_1 + E$), based upon local symmetry. It is thus possible, in theory, to distinguish between, *fac* and *mer* MX_3L_3 complexes by examination of their low infra-red spectra which should show two or three bands respectively, attributable to metal-halogen stretching vibrations. The extensive literature on chromium complexes shows that usually one isomer is favoured [43]. If we assume that all the THF molecules are substituted, the steric constraints of the tripodal ligand $MeC(CH_2SMe)_3$ are such that the monomeric complex must be *facial* isomer.

The macrocyclic geometry of the tridentate ligands $[9]aneS_3$, $[9]aneN_3$, $Me_3[9]aneN_3$ and $(isoPr)_2[9]aneN_3$ is such that they coordinate *facially* in octahedral complexes [23]. The facultative ligand $S(CH_2CH_2SMe)_2$ is also expected to coordinate *facially* (Chapter 5).

The infra-red spectra of these species, presented in Table 6.2, provide evidence of the coordinated thioether and aza-macrocycle ligands. Peaks observed in the region 200-400 cm^{-1} may be assigned to ν(Cr-Cl) hence give structural information on the complexes. Given that in some cases these peaks were rather weak, and since ν(Cr-S) would also be expected to appear in this region, definitive assignments were not possible. This is notably the case for $[CrCl_3\{S(CH_2CH_2SMe)_2\}]$ which depicts a broad band in the 344 cm^{-1} region and does not allow us to determine the stereochemistry of

this complex. However, extensive work on S-C-C-S torsions angles show that the complex is expected to be *facial* [44, 45] (Chapter 5).

Figure 6.2 displays the infra-red spectrum for a nujol mull of $[CrCl_3\{S(CH_2CH_2SMe)_2\}]$ and the broad peak associated with the Cr-Cl stretching mode.

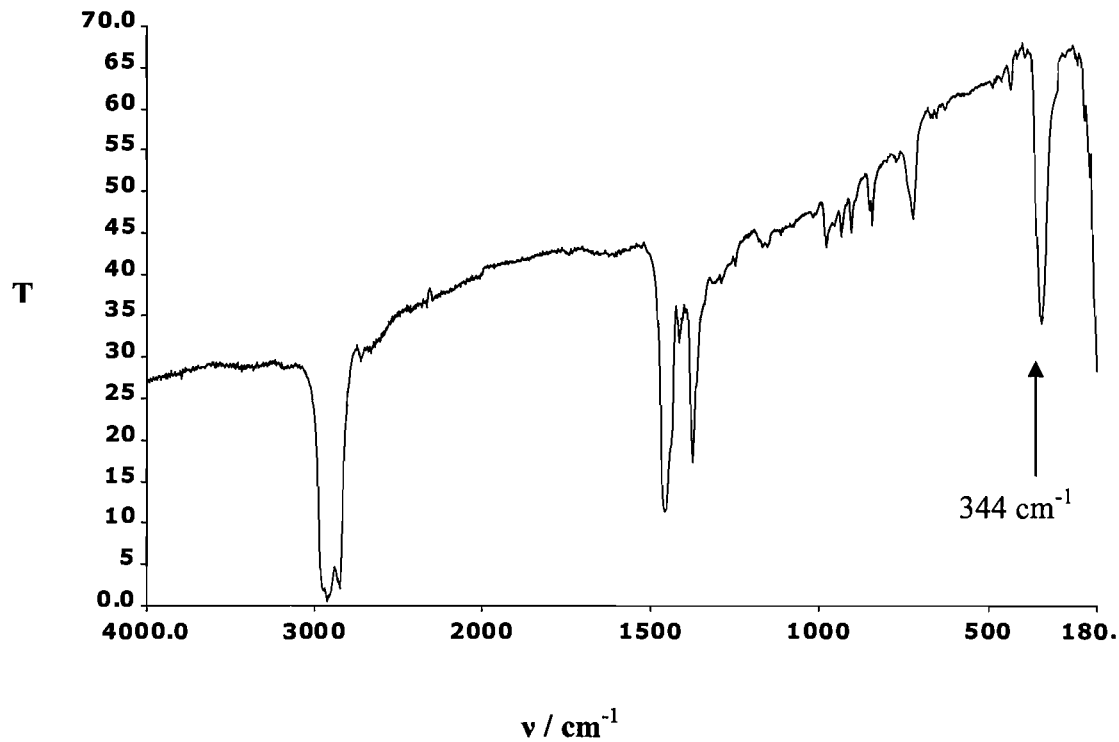

Figure 6.2. Infra-red spectrum for a nujol mull of $[CrCl_3\{S(CH_2CH_2SMe)_2\}]$

6.3.3.2. Chromium K-edge EXAFS Studies for $[CrCl_3\{L\}]$

Owing to the limited solubilities displayed by the compounds isolated, and their sensitivity to moisture, in most cases crystals suitable for X-ray study could not be obtained. However, given the lack of structural data on compounds of this type, we proposed that chromium K-edge EXAFS data would provide useful information regarding the metal-ligand bond lengths for the first coordination sphere, *i.e.* *d*(Cr-S), *d*(Cr-N) and *d*(Cr-Cl). Chromium K-edge EXAFS was also recorded for the $[CrCl_3(THF)_3]$ model compound. EXAFS structural data for this series of chromium(III) complexes would also serve as excellent model compounds for the different studies carried out in this Thesis (Chapter 5).

a) $[CrCl_3(THF)_3)]$

Figure 6.3 depicts the raw and theoretical EXAFS data for a solid pellet of $[CrCl_3(THF)_3]$. The experimental data were satisfactorily modelled to a first shell of 3.3 oxygen atoms, with an average Cr-O distance of 2.06(5) Å, and to a second shell of 2.8 chlorine atoms, with a Cr-Cl distance of 2.31(7) Å. With a R-factor of 27.5 %, these results correlate very well with the average Cr-O and Cr-Cl distances derived from X-ray crystallographic studies. Literature reports for $[CrCl_3(THF)_3]$, Cr-O distances of 1.994(4), 2.027(4) and 2.077(4) Å and Cr-Cl distances of 2.312(2), 2.307(2) and 2.283(2) Å [46]. EXAFS studies previously performed on this system also give consistent data with an average Cr-O bond length of 2.009(13) Å and a Cr-Cl bond of 2.295(4) Å [15].

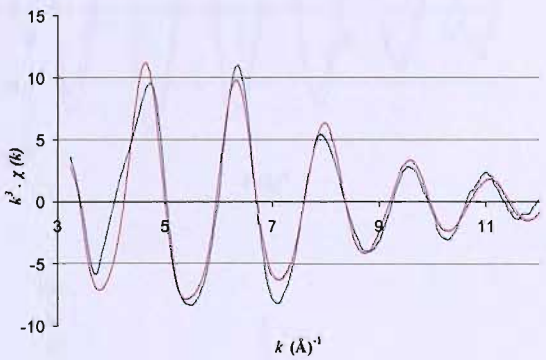

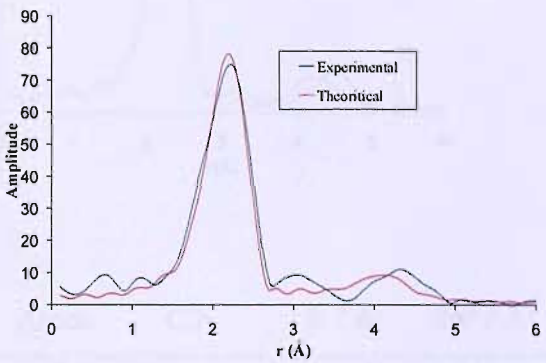

Atom	C.N.	R / Å	$2\sigma^2$ / Å^2
O	3.3(1)	2.06(5)	0.011(2)
Cl	2.8(7)	2.31(7)	0.010(5)

Ef = -8.5(0) eV

R = 27.5 %

Figure 6.3. The chromium K-edge k^3-weighted EXAFS and Fourier transform for a solid pellet of $[CrCl_3(THF)_3]$ / boron nitride

b) $[CrCl_3\{[9]aneS_3\}]$

Figure 6.4 displays the EXAFS data for a solid pellet of $[CrCl_3\{[9]aneS_3\}]$. The theoretical spectra fit the experimental $k^3.\chi\ (k)$, Fourier transform and sine transform very well (FI = 2.8) to a simple model of two shells. The model proposed has refined coordination numbers close to the expected values of 3 chlorine and 3 sulfur atoms

with 2.8(2) and 2.8(2) atoms respectively. The Debye-Waller terms have values which indicate they are integral to the fit. The values obtained compare very well to the chromium K-edge EXAFS structural data available in the literature for this compound, where Cr-S is 2.396(11) Å and Cr-Cl is 2.306(9) Å [15]. X-ray crystallography data for the analogue complex $[CrCl_3\{[18]aneS_6\}]$ also gives similar bond lengths with Cr-Cl distances of 2.305(5), 2.279(5) and 2.291(5) Å and Cr-S distances of 2.459(3), 2.442(5) and 2.440(5) Å [4].

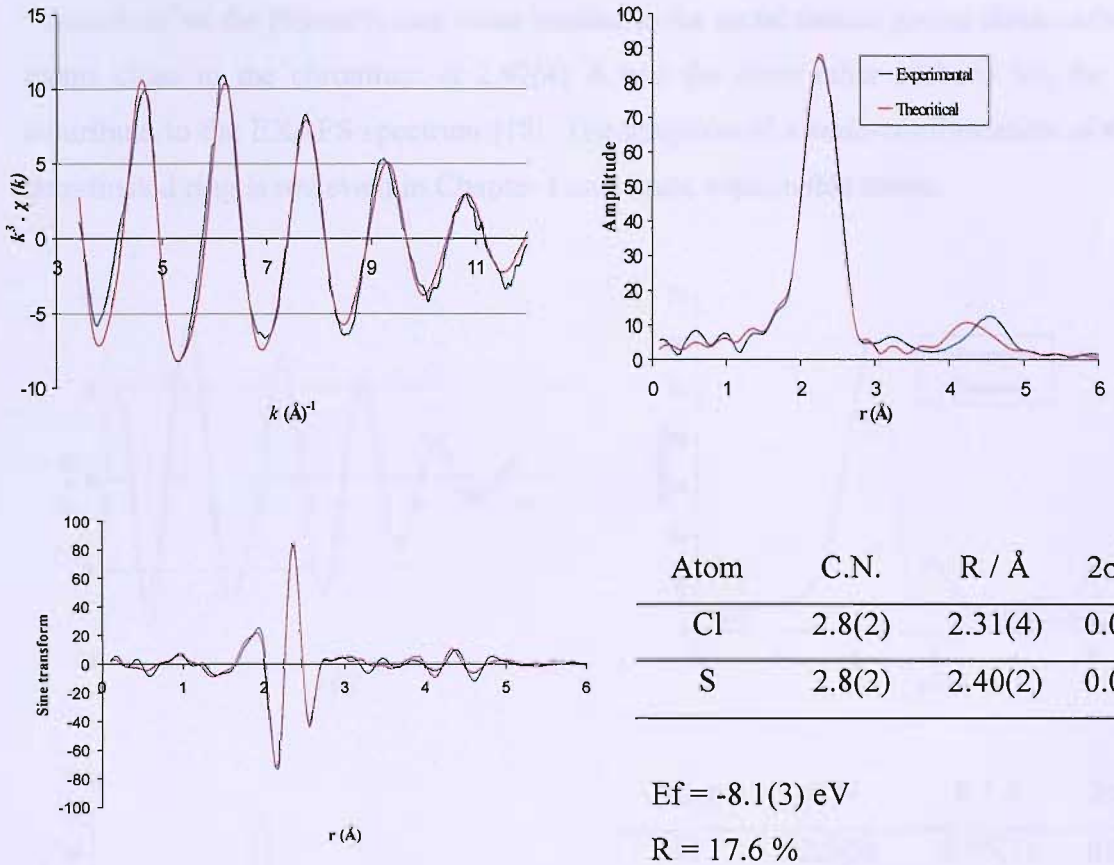

Atom	C.N.	R / Å	$2\sigma^2$ / Å^2
Cl	2.8(2)	2.31(4)	0.013(5)
S	2.8(2)	2.40(2)	0.012(3)

Ef = -8.1(3) eV

R = 17.6 %

Figure 6.4. The chromium K-edge k^3-weighted EXAFS, Fourier transform and sine transform for a solid pellet of $[CrCl_3\{[9]aneS_3\}]$ / boron nitride

c) $[CrCl_3\{[9]aneN_3\}]$

The model proposed for $[CrCl_3\{[9]aneN_3\}]$ (Figure 6.5) fits very well with a model of 2.5(5) nitrogen and 2.5(4) chlorine atoms, which is very close to the expected values of 3 nitrogen and 3 chlorine atoms. The bond lengths of 2.05(1) Å and 2.32(6)

Å for Cr-N and Cr-Cl respectively are close to the literature values for similar compounds. A X-ray crystal structure for the triply OH-bridged binuclear complex of chromium(III), $[\{Me_3[9]aneN_3\}_2Cr_2(OH)_3]^{3+}$ gives a Cr-N bond length of 2.089(4) Å [18]. The Cr-Cl distances are also similar to the expected range of values (as seen for the above examples). The model was extended to establish if improvements could be introduced to the fit. As well as introducing the multiple scattering effects to the model, a third shell consisting of carbon atoms (from the $[9]aneN_3$ ring) was added at 3.00 Å to fit the non-bonded chromium carbon distances. The best fit obtained gives a coordination number for the third shell of 2.9. This value could be explained by a "distortion" of the $[9]aneN_3$ ring when bonded to the metal centre, giving three carbon atoms close to the chromium at 2.97(4) Å and the three other carbons too far to contribute to the EXAFS spectrum [18]. The adoption of a *endo*-conformation of the coordinated ring is reviewed in Chapter 1 and could explain this result.

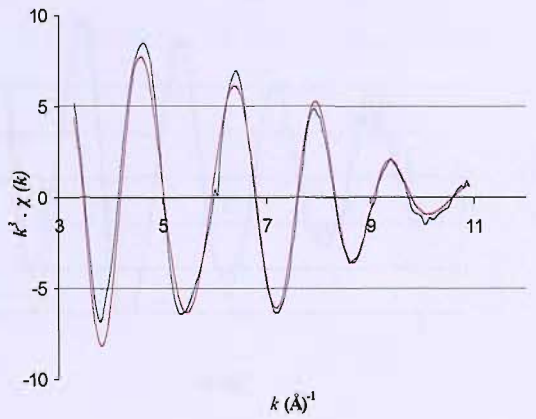

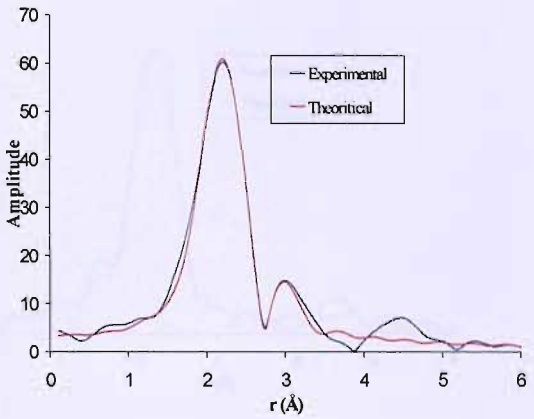

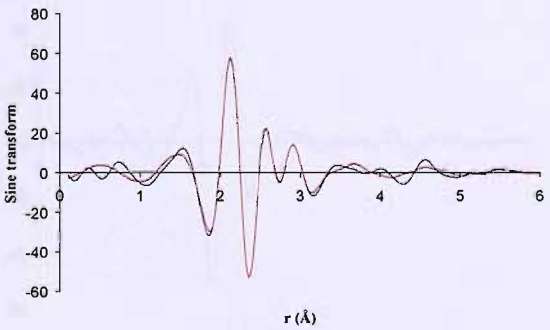

Atom	C.N.	R / Å	$2\sigma^2$ / Å^2
N	2.5(5)	2.05(1)	0.008(2)
Cl	2.5(4)	2.32(6)	0.010(1)
C	2.9(4)	2.97(4)	0.006(3)

Ef = -7.7(6) eV

R = 18.2 %

Figure 6.5. The chromium K-edge k^3-weighted EXAFS, Fourier transform and sine transform for a solid pellet of $[CrCl_3\{[9]aneN_3\}]$ / boron nitride

d) $[CrCl_3\{MeC(CH_2SMe)_3\}]$

The model proposed, including the multiple scattering effects, for $[CrCl_3\{MeC(CH_2SMe)_3\}]$ (Figure 6.6) fits well with relatively low fit index and R factor (FI = 7.5 and R = 25.81 %). The model consists of a shell of 3.2(4) chlorine atoms and a shell of 2.7(4) sulfur atoms. The errors for the coordination numbers of the two shells are probably due to difficulties resolving them into two discrete shells. The Debye-Waller values are quite low suggesting that each shell is integral to the fit. The bond lengths, Cr-Cl = 2.32(2) Å and Cr-S = 2.44(3) Å, are consistent with the expected values for such a set of atoms. The values obtained compare well with the chromium K-edge EXAFS data for the butyl and decyl derivatives (Chapter 5) where the average Cr-Cl distance is 2.26(2) Å and 2.25(3) Å while the Cr-S distance is 2.43(3) Å and 2.38(4) Å for the butyl and decyl derivatives respectively.

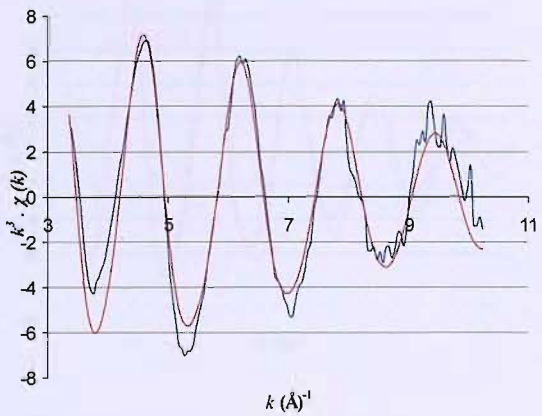

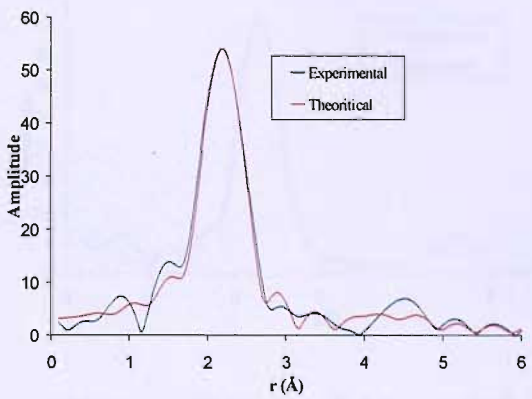

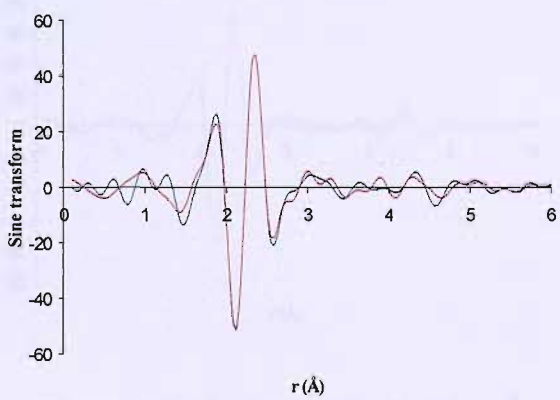

Atom	C.N.	R / Å	$2\sigma^2$ / Å^2
Cl	3.2(4)	2.32(2)	0.011(4)
S	2.7(4)	2.44(3)	0.011(2)

Ef = -7.4(1) eV

R = 25.8 %

Figure 6.6. The chromium K-edge k^3-weighted EXAFS, Fourier transform and sine transform for a solid pellet of $[CrCl_3\{MeC(CH_2SMe)_3\}]$ / boron nitride

e) $[CrCl_3\{S(CH_2CH_2SMe)_2\}]$

The picture emerging from Figure 6.7 shows a good fit for a model of 2.8 chlorine and 2.7 sulfur atoms. The errors for the coordination numbers of the two shells are probably due to difficulties resolving them into two discrete shells. In $[CrCl_3\{S(CH_2CH_2SCH_3)_2\}]$, the Cr-Cl bond is 2.32(1) Å long and the Cr-S bond is 2.45(1) Å. The bond lengths Cr-Cl and Cr-S are consistent with the crystal structures involving similar coordinated atoms to a chromium metal centre (examples above) and also compare well with the chromium K-edge EXAFS data for the decyl derivative $[CrCl_3\{S(CH_2CH_2SC_{10}H_{21})_2\}]$ (Chapter 5) where *d*(Cr-Cl) = 2.32(6) Å and *d*(Cr-S) = 2.45(5) Å. The multiple scattering effects were included to the model to give a FI value of 6.0.

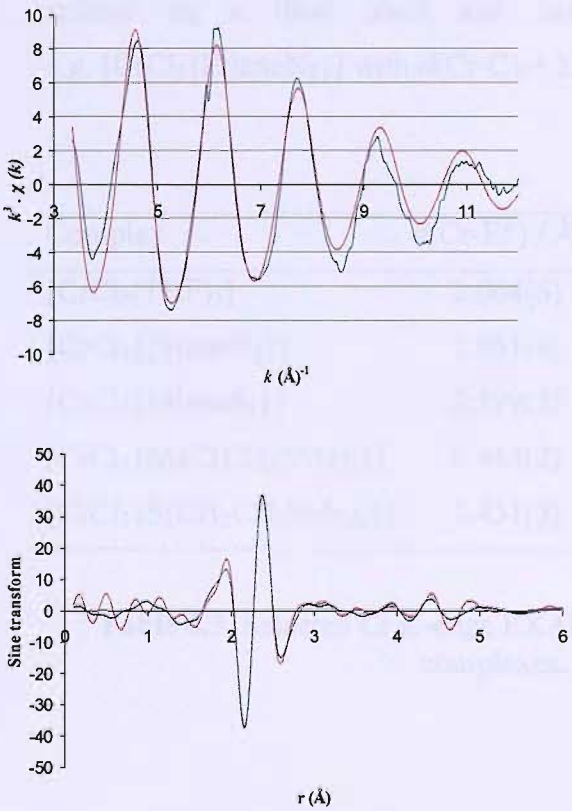

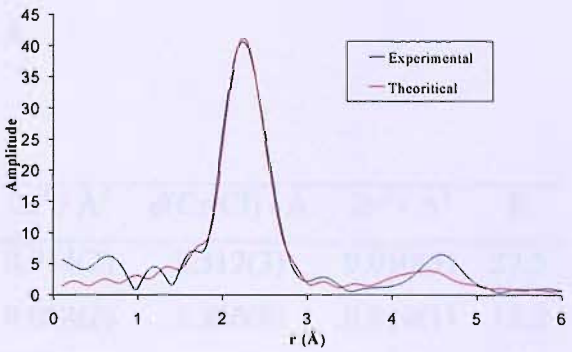

Atom	C.N.	R / Å	$2\sigma^2$ / Å^2
Cl	2.8(4)	2.32(1)	0.011(2)
S	2.7(5)	2.45(1)	0.018(1)

Ef = -7.4(9) eV

R = 27.2 %

Figure 6.7. The chromium K-edge k^3-weighted EXAFS, Fourier transform and sine transform for a solid pellet of $[CrCl_3\{S(CH_2CH_2SMe)_2\}]$ / boron nitride.

f) Structural Information

Table 6.3 summarises thee structural data for selected chromium(III) complexes. The values derived from the EXAFS measurements compare very well with those available in the literature ($[CrCl_3(THF)_3]$, $[CrCl_3\{[9]aneS_3\}]$ [15]) and the X-ray crystallographic studies for similar compounds [46]. With an averaged value of ~ 2.43 Å, the Cr-S bonds are independent of the geometry of the ligands and consistent with the reported data. The weak interactions between the hard chromium(III) and the soft thioether functions are, along with the *Dq* values, confirmed. In the same way, the Cr-Cl bonds are identical for every chromium(III) complex studied by EXAFS spectroscopy with a averaged value of 2.31 Å. The multiple scattering effects support the predicted *facial* geometry of the complex $[CrCl_3\{S(CH_2CH_2SCH_3)_2\}]$. In some cases, carbons of the ligand backbone were refined as a third shell and helped to obtain a well defined model *e.g.* $[CrCl_3\{[9]aneN_3\}]$ with d(Cr-C) = 2.97 Å.

Complex	d(Cr-E*) / Å	$2\sigma^2$ / Å^2	d(Cr-Cl) / Å	$2\sigma^2$ / Å^2	R
$[CrCl_3(THF)_3]$	2.064(6)	0.014(2)	2.312(3)	0.010(5)	27.5
$[CrCl_3\{[9]aneN_3\}]$	2.051(4)	0.008(2)	2.326(8)	0.010(1)	18.2
$[CrCl_3\{[9]aneS_3\}]$	2.399(2)	0.012(3)	2.310(3)	0.013(6)	17.6
$[CrCl_3\{MeC(CH_2SMe)_3\}]$	2.443(2)	0.011(2)	2.322(3)	0.011(4)	25.8
$[CrCl_3\{S(CH_2CH_2SMe)_2\}]$	2.451(5)	0.018(1)	2.321(1)	0.011(2)	27.2

Table 6.3. Selected Cr K-edge EXAFS structural data for some chromium(III) complexes. (*E = S, O or N)

6.3.3.3. Electron Paramagnetic Resonance Spectroscopy for [$CrCl_3${L}]

Characterisation of the chromium(III) complexes was completed by EPR spectroscopy. X-band (9.4 GHz) EPR measurements were performed on the solid complexes at room temperature and 115 K. In both temperature conditions, the strong and broad signal, characteristic to d^3 systems was observed for each complex. Table 6.4 shows the ***g*** values for X-band EPR spectra of the chromium(III) complexes recorded at 115 K. The values obtained are characteristic of Cr(III) ions (***g*** ~ 1.98) [47] and also compare well with the values obtained for similar compounds in Chapter 5.

Complex	***g*** values
$[CrCl_3(THF)_3]$	1.99
$[CrCl_3\{[9]aneS_3\}]$	1.99
$[CrCl_3\{S(CH_2CH_2SMe)_2\}]$	1.99
$[CrCl_3\{MeC(CH_2SCH_3)_3\}]$	1.99
$[CrCl_3\{[9]aneN_3\}]$	1.98
$[CrCl_3\{Me_3[9]aneN_3\}]$	1.99
$[CrCl_3\{isoPr_2[9]aneN_3\}]$	1.98

Table 6.4. EPR (X-band) ***g*** values for $[CrCl_3\{L\}]$ compounds at 115 K.

6.4. Conclusions

A series of chromium(III) thioether and amine complexes of the form $[CrCl_3\{L\}]$ have been synthesised and characterised by infra-red, UV/visible, EPR spectroscopy and X-ray absorption spectroscopy. The ligands were chosen to probe geometry and donor set control. The results obtained confirm that, despite the anticipated incompatibility between hard chromium(III) metal centres and soft thioether functions, the relatively stable but insoluble complexes involving S_3Cl_3 donor sets has been successfully synthesised. On the other hand, the donor set N_3Cl_3 confirmed its strong interaction with the hard chromium(III) centre. Chromium K-edge EXAFS studies have proved to be extremely useful for the structural characterisation of such complexes. This unusual series of compounds show very sensible Cr-S, Cr-N and Cr-Cl bond lengths when compared to X-ray crystallographic studies or EXAFS structural data available for similar compounds. It is also clear that the Cr(III)-S (thioether) weak interaction is independent of the geometry of the ligands – facultative, tripodal, macrocyclic – since similar Cr-S bond lengths were obtained with the three geometries.

All the spectroscopic and structural data obtained from these chromium(III) complexes will allow for comparison with the chromium(III) complexes studies for the study of the homogeneous catalysis reactions of trimerisation, tetramerisation and oligomerisation of ethylene (Chapters 3, 4 and 5).

6.5. Experimental

The ligands and chromium(III) complexes were generally prepared by literature procedures or by modifications of those. The reagents were purchased from Aldrich and Acros and were used as received.

Synthesis of $S(CH_2CH_2SMe)_2$ [33]: 2-mercapto-ethyl sulfide (5.0 g, 32.5 mmol) was dissolved in ethanol (150 mL) under nitrogen and sodium (1.5 g, 65 mmol) was added. When the sodium had dissolved, the mixture was heated to reflux and iodomethane (9.23g, 65 mmol) was added dropwise. The mixture was refluxed for one hour. The ethanol was reduced *in vacuo*. A clear solution with a white precipitate (NaI) remains in the flask. Water (35 ml) was added to dissolve the solid. The mixture was placed in a separating dropping funnel and extracted with diethyl ether (3 x 35 mL). The organic layer was dried over $MgSO_4$ and filtered off. The solvent was removed under vacuo, leading to a clear and colourless oil. Yield: 3.92 g, 215 mmol (66%). ^1H NMR ($CDCl_3$): δ 2.15 (s, 6H, $C\underline{H}_3S$), 2.75 (m, 8H, $SC\underline{H}_4S$) ppm. $^{13}C\{^1H\}$ NMR ($CDCl_3$): δ 15.77 (s, $\underline{C}H_3$), 31.85 ($CH_3SCH_2\underline{C}H_2S$) 34.35 ($CH_3S\underline{C}H_2$) ppm. $C_6H_{14}S_3$ requires C, 39.52; H, 7.74 %; Found C, 39.56; H, 7.74 %.

Synthesis of $MeC(CH_2Br)_3$ [34]: 1,1,1-trishydroxy(methyl)ethane (25 g, 0.208 mol) was placed in a 250 mL three neck flask equipped with a thermometer, a condenser and a dropping funnel containing PBr_3 (84.46 g, 0.312 mol). A bubbler filled with water was connected to the condenser. PBr_3 was added dropwise over 2 hours and at 100^0C. The 1,1,1-tris-hydroxy(methyl)ethane dissolved with a considerable effervescence to produce a viscous orange mixture. This mixture was heated at 100^0C for 30 minutes following the addition of PBr_3. The orange mixture was then heated at 180^0C for 24 hours. After standing at room temperature for 5 hours, distilled water (250 mL) was added and the hard black material was broken up with a spatula. The mixture was filtered off and washed with water (200 mL). The water washing was placed in a separating funnel, forming two layers: a yellow one on the bottom and a brown one on the top. The lower layer was removed and the upper one was extracted with toluene (3 x 100 mL). The three organic extracts and the yellow layer, previously removed, were combined and washed with a saturated $NaHCO_3$ solution (3 x 200 mL)

and water (40 mL). The organic extracts were dried over $MgSO_4$. Filtration of the mixture was followed by removal of the solvent on a rotary evaporator. The final product was obtained as a brown solution. Yield = 52.6 g, 0.173 mol (83%). ^{1}H NMR ($CDCl_3$): δ 1.20 (s, 3H, C**H**$_3$C), 3.40 (s, 6H, C**H**$_2$Br) ppm. ^{13}C{^{1}H} NMR ($CDCl_3$): δ 21.59 (**C**H$_3$C), 39.02 (**C**H$_2$Br), 39.55 (CH$_3$**C**) ppm.

Synthesis of MeC(CH$_2$SCH$_3$)$_3$ [2]: Ammonia (100 mL) was condensed onto dry, degassed THF (200 mL) in a 1L flask equipped with a condenser. A small piece of solid Na was added to the mixture, leading to a dark royal blue solution. Me_2S_2 (16.16 g, 0.172 mol) was added slowly to produce a creamy white colour. The remaining Na was added slowly and the NH_3 was then allowed to evaporate. The creamy white mixture was concentrated under vacuo in order to remove the THF. Then a mixture of ethanol (100 mL) and MeC(CH$_2$Br)$_3$ (17.45 g, 0.057 mol) was added dropwise to the Na^+SMe^- first diluted with ethanol (150 mL). The resulting mixture was refluxed for 70 hours under nitrogen. The grey reaction mixture was cooled, filtered off and washed with a saturated $NaHCO_3$ solution (30 mL). The aqueous layer was then extracted with diethyl ether (3 x 50 mL). The organic layer was dried over anhydrous $MgSO_4$, filtered off and the solvent was removed *in vacuo* to leave an orange clear oil which was distilled (52°C; 0.5 mm Hg). Yield: 7.49 g, 0.0356 mol (62.2%). ^{1}H NMR ($CDCl_3$): δ 1.12 (s, 3H, C**H**$_3$C), 2.15 (s, 9H, SC**H**$_3$), 2.63 (s, 6H, C**H**$_2$SCH$_3$) ppm. ^{13}C{^{1}H} NMR ($CDCl_3$): δ 17.78 (S**C**H$_3$), 23.81 (S**C**H$_2$), 41.28 (**C**CH$_3$), 44.31 (C**C**H$_3$) ppm. $C_8H_{18}S_3$ requires C, 45.66; H, 8.62 %; Found C, 45.55; H, 8.58 %.

Synthesis of 1,4,7-triazacyclononane [9]aneN$_3$ [35-38]

a) Synthesis of 1, 2-*bis*[(*p*-tolylsulfonyl)oxy]ethane [38]: Ethane-1,2-diol (32.5 g, 0.524 mol) was dissolved in dry pyridine (300 mL) and 5 equivalents of tosyl chloride (250.0 g, 1.31 mol) was added at 0^{0}C. After refrigeration overnight, the reaction mixture was added to hydrochloric acid (750 mL, 1 mol.L^{-1}) and the precipitate which formed was filtered off, washed with water and dried. Recrystallisation from CH_2Cl_2/MeOH afforded the product as a white solid. Yield: 137.85 g, 0.372 mol (71.0%). ^{1}H NMR ($CDCl_3$): δ 2.50 (s, 6H, ArC**H**$_3$), 4.24 (s, 4H, C**H**$_2$), 7.30-7.80 (dd, 8H, Ar**H**) ppm.

b) Synthesis of N,N',N''-*tris*(*p*-tolylsulfonyl)diethylene triamine [38]: Diethylene triamine (50.0 g, 0.484 mol) and NaOH (60.0 g, 1.5 mol) were dissolved in 2 L of water in a 5 L beaker equipped with a dropping funnel. This solution was stirred vigorously whilst a solution of tosyl chloride (277.2 g, 1.454 mol) in diethyl ether (2 L) was added dropwise over a period of 2 hours. After stirring for a further 1 hour, most of the ether had evaporated and the reaction mixture had begun to solidify. Methanol (750 mL) was added, the mixture was stirred for a further 15 minutes and then the solid product was filtered off and washed with copious volumes of water. The material was washed further with methanol, then ether and dried *in vacuo*. Yield: 272.98 g, 0.483 mol (99%). ^{1}H NMR ($CDCl_3$): 2.40 δ (s, 6H, ArC**H**$_3$), 2.60 (s, 6H, ArC**H**$_3$), 3.0 (m, 4H, NC**H**$_2$), 3.1 (m, 4H, NC**H**$_2$), 7.50-7.80 (dd, 12H, Ar**H**) ppm.

c) Synthesis of the N,N',N''-*tris*(*p*-tolylsulfonyl)-1,4,7-triazacyclonane [36]: 1, 2-*bis*[(*p*-tolylsulfonyl)oxy]ethane (60.0 g, 0.162 mol) was dissolved in DMF (500 mL) and placed in a pressure equalising dropping funnel. N,N',N''-*tris*(*p*-tolylsulfonyl)diethylene triamine (90.5 g, 0.162 mol) and K_2CO_3 (53.0 g, 0.384 mol) were dissolved in DMF (1.5 L) in a 2 L flask equipped with a mechanical stirrer. This solution was stirred vigorously whilst the 1,2-*bis*[(*p*-tolylsulfonyl)oxy]ethane solution was added dropwise at 100^{0}C overnight. After addition, the mixture was then cooled and DMF (1.5L) was removed from the reaction mixture by distillation under atmospheric pressure. The solution was then cooled and poured into 2 L of iced water with vigorous stirring. The white precipitate which was formed was filtered off and washed with water. The solid was dissolved in a minimum volume of CH_2Cl_2 and 5 volume equivalents of methanol were added. The mixture was kept in the fridge overnight, filtered off, washed with cold methanol and dried with the water pump. Yield: 40.0 g, 0.0676 mol (41.7%). ^{1}H NMR ($CDCl_3$): δ 2.40 (s, 9H, ArC**H**$_3$), 3.35 (s, 12H, NC**H**$_2$), 7.20-7.75 (dd, 12H, Ar**H**) ppm.

d) Synthesis of the 1,4,7-triazacyclonane trihydrobromide: Concentrated sulfuric acid (120 mL) was purged with nitrogen and heated to 70°C. N,N',N''-*tris*(*p*-tolylsulfonyl)-1,4,7-triazacyclonane (40.0 g, 0.0677 mol) was added carefully to the hot mixture. The temperature was raised further to 100°C and the mixture was heated and stirred overnight. After being allowed to cool, the black

solution was added dropwise to methanol (360 mL), previously cooled in the fridge. The addition should be done slow enough to keep the mixture below 20°C. Then ether (240 mL) was added. The mixture was filtered off, giving a grey/black solid. This solid was dissolved in a minimum of hot water (80°C). The solution was left to cool and 2 volumes of HBr were added. The mixture was then cooled and filtered off and dried with the water pump. Yield: 17.51 g, 0.047 mol (69.5%). ^{1}H NMR (D_2O): δ 3.42 (s, 12H, C**H**$_2$) ppm.

e) Isolation of 1,4,7-triazacyclononane [9]aneN$_3$: 1,4,7-triazacyclonane trihydrobromide (17.05 g, 0.047 mol), toluene (255 mL), water (17 mL) and NaOH (11.05 g, 0.282 mol) were placed in a 500 mL round bottomed flask fitted with a Dean and Stark trap. The mixture was then refluxed for 12 hours. The water was extracted and the toluene was decanted off. A further 100 mL of toluene was added and heated at 70°C to extract any remaining product from the NaBr crust which had formed. This was also decanted. The toluene/[9]aneN$_3$ extracts were combined and the toluene was removed by distillation under atmospheric pressure, leading to a pale yellow crystalline solid. Yield: 3.25g, 0.025 mol (54%). ^{1}H NMR ($CDCl_3$): δ 2.79 (12H, s, C**H**$_2$) ppm. ^{13}C{^{1}H} NMR ($CDCl_3$) 46.79 (**C**H$_2$) ppm. HRMS analysis (ESI): *m/z* calculated $[M+H]^+$: 129.1267; Found: 129.1273.

Synthesis of 1,4,7-trimethyl-1,4,7-triazacyclononane Me$_3$[9]aneN$_3$ [18, 40]: A solution consisting of [9]aneN$_3$ (0.5 g, 3.87 mmol) in formic acid 98% (4.1 mL), paraformaldehyde (3.0 g, equiv. to 0.1 mol of CH_2O) and water (0.5 mL) was refluxed for 24 hours. The reaction mixture was then transferred with 5 mL of water in a 25 mL beaker and cooled to 0°C. The pH was adjusted to 12 with a concentrated solution of sodium hydroxide 30%. The temperature of the solution was kept below 20°C during the addition. The solution was then extracted with chloroform (5 x 10mL). The extracts were combined and dried over anhydrous sodium sulfate. The extracts were then filtered and reduced in volume to an oily residue. The residue was transferred to a small round bottom flask. A small amount of chloroform was used to wash the remaining oil from the evaporation flask and then added to the flask containing the bulk of oil. The solvent was removed *in vacuo*, leading to a yellow oil.

Yield: 0.310g, 1.82 mmol (47%). ^{1}H NMR (CD_3OD): δ 2.32 (s, 9H, C**H**$_3$), 2.65 (s, 12H, C**H**$_2$) ppm. ^{13}C{^{1}H} NMR (CD_3OD): δ 46.68 (**C**H_2), 57.66 (**C**H_3) ppm. HRMS analysis (ESI): *m/z* calculated $[M+H]^+$: 171.1737; Found: 171.1558.

Synthesis of 1,4-diisopropyl-1,4,7-triazacyclononane (isoPr)$_2$[9]aneN$_3$ [30, 38]

a) Synthesis of 1-(*p*-toluenesulfonyl)-1,4,7-triazacyclononane: 1,4,7-tris(*p*-toluenesulfonyl)-1,4,7-triazacyclonane (37 g, 62.6 mmol) and phenol (44 g, 0.47 mol) were dissolved in 500 mL of 33% HBr/AcOH. The solution was heated at 90°C for 36 hours. The white precipitate that formed was filtered off and washed with Et_2O. This solid was dissolved in 1M NaOH (pH>12) and extracted from chloroform. The organic extracts were combined and dried over $MgSO_4$. The mixture was filtered off and the solvent removed *in vacuo* to afford the product as a white solid. Yield: 10.48 g, 37 mmol (59%). ^{1}H NMR ($CDCl_3$): δ 2.09 (2H, s, N**H**), 2.43 (3H, s, C**H**$_3$Ar), 3.00 (4H, m, [9]aneN$_3$ ring), 3.19 (4H, m, [9]aneN$_3$ ring), 3.44 ([9]aneN$_3$ ring), 7.30 (2H, d, Ar), 7.65 (2H, d, Ar) ppm. ^{13}C{^{1}H} NMR ($CDCl_3$): δ 21.40 (**C**H_3Ar), 46.60 ([9]aneN$_3$ ring), 49.57 ([9]aneN$_3$ ring), 53.19 ([9]aneN$_3$ ring), 127.24 (Ar), 130.00 (Ar), 134.26 (Ar), 144.26 (Ar) ppm. Positive electrospray (CH_2Cl_2): *m/z* = 284 ((**i**) + H)$^+$.

b) Synthesis of 1,4-diisopropyl-7-(*p*-toluenesulfonyl)-1,4,7-triazacyclononane: 1-(*p*-toluenesulfonyl)-1,4,7-triazacyclononane **(i)** (3.0 g, 0.10 mol) and 2-bromopropane (5.2 g, 0.042 mol) were combined in degassed acetonitrile (20 mL). Na_2CO_3 was added as a solid to the above colourless solution and the resultant mixture was heated to reflux under N_2 for 18 hours. Then the yellow mixture was filtered from excess Na_2CO_3 and the solid washed with fresh acetonitrile. The combined extracts were evaporated under reduced pressure to yield a yellow oil with a small amount of a white solid. The residue was dissolved in $CHCl_3$ (20 mL) and the washed with a NaOH solution. The organic layer was removed and the aqueous phase was extracted with $CHCl_3$ (3 x 10 mL). The combined organic extracts were dried over $MgSO_4$ and the solvent removed under reduced pressure to afford the product as a tan solid. Yield: 5.14 g, 14 mmol (14%). ^{1}H NMR ($CDCl_3$): δ 0.92 (d, 12H, (C**H**$_3$)$_2$CH), 2.41(s, 3H, C**H**$_3$Ar), 2.45 (s, 4H, [9]aneN$_3$ ring), 2.75 (m, 2H, (CH$_3$)$_2$C**H**), 2.81-2.87 (m, 4H, [9]aneN$_3$ ring), 3.30 (m, 4H, [9]aneN$_3$ ring),

7.26 (d, 2H, Ar), 7.66 (d, 2H, Ar) ppm. $^{13}C\{^1H\}$ NMR ($CDCl_3$): δ 18.27 ($\underline{C}H_3)_2CH$), 21.44 ($\underline{C}H_3Ar$), 50.33 ([9]aneN_3 ring), 52.34 ([9]aneN_3 ring), 53.70 $(CH_3)_2\underline{C}H$), 53.74 ([9]aneN_3 ring), 127.16 (Ar), 129.47 (Ar), 136.70 (Ar), 142.64(Ar) ppm. Positive electrospray (CH_2Cl_2): m/z = 368.5 $(M+H)^+$.

c) Synthesis of 1,4-diisopropyl-1,4,7-triazacyclononane: A mixture of 1,4-diisopropyl-7-(*p*-toluenesulfonyl)-1,4,7-triazacyclononane (4 g, 0.010 mol) and 18M H_2SO_4 (20 mL) was heated at 120°C for 18h under N_2. After cooling to room temperature, the dark mixture was poured into crushed ice and the resultant mixture brought to pH>11 with aqueous NaOH 2M. The heterogeneous mixture was extracted with $CHCl_3$ until the organic extracts were colourless (500 mL total). The $CHCl_3$ solution of the product was dried over $MgSO_4$ and the solvent removed to yield an amber oil. Yield: 0.34 g, 1.6 mmol (16%). ^1H NMR ($CDCl_3$): δ 0.96 (d, 12H, $(C\underline{H}_3)_2CH$), 2.43(s, 4H, [9]aneN_3 ring), 2.50-2.58(m, 4H, [9]aneN_3 ring), 2.62-2.68 (m, 4H, [9]aneN_3 ring), 2.80 (heptet, 2H, $(CH_3)_2C\underline{H}$), 4. 55 (s, 1H, $N\underline{H}$) ppm. $^{13}C\{^1H\}$ NMR ($CDCl_3$): δ 18.64 ($\underline{C}H_3)_2CH$), 47.00 ([9]aneN_3 ring), 47.82 ([9]aneN_3 ring), 48.96 $(CH_3)_2\underline{C}H$), 52.89 ([9]aneN_3 ring) ppm. Positive electrospray (CH_2Cl_2): m/z = 214 $(M + H)^+$.

Synthesis of $[CrCl_3(THF)_3]$ [41]: The procedure was to add anhydrous chromium trichloride (3.0 g, 0.019 mol) to zinc dust (0.04 g). The mixture was placed in the thimble of a Soxhlet tube and extracted overnight with boiling anhydrous THF (50 mL). After complete extraction, concentration, cooling and filtration of the pink-purple crystalline form of chromium trichloride tris-tetrahydrofuran was obtained. Yield: 5.2g, 14 mmol (73%). UV/Visible (diffuse reflectance): 712, 684, 488 nm. Infra-red (Cr-Cl stretches) Nujol mull: 315, 345, 375 cm^{-1}.

Synthesis of $[CrCl_3\{[9]aneS_3\}]$ [15]: The procedure was to add [9]aneS_3 (0.250 g, 1.40 mmol) to a solution of $[CrCl_3(THF)_3)]$ (0.520 g, 1.40 mmol) in dried and degassed dichloromethane (15 mL). The resulting mixture was stirred at room temperature under nitrogen for 2 hours. Diethyl ether (15 mL) was then added to afford a purple solid which was filtered off and dried *in vacuo*. Yield: 0.450 g, 1.33 mmol (95%).

Synthesis of $[CrCl_3\{S(CH_2CH_2SMe)_2\}]$: Reaction carried out as above using $[CrCl_3(THF)_3]$ (0.62 g, 1.65 mmol) and $S(CH_2CH_2SMe)_2$ (0.3 g, 1.65 mmol) to give a violet solid. Yield: 0.394 g, 1.16 mmol (70%).

Synthesis of $[CrCl_3\{[9]aneN_3\}]$: Reaction was carried out as above using $[CrCl_3(THF)_3]$ (0.87 g, 2.32 mmol) and $[9]aneN_3$ (0.30 g, 2.32 mmol) to give a blue-green solid. Yield: 0.494 g, 1.72 mmol (74%).

Synthesis of $[CrCl_3\{MeC(CH_2SMe)_3\}]$: The procedure was to add $CMe(CH_2SMe)_3$ (1.0 g, 4.76 mmol) to a solution of $[CrCl_3(THF)_3)]$ (1.76 g, 4.76 mmol) in dried and degassed dichloromethane (15 mL). The resulting mixture was stirred at room temperature under nitrogen for 2 hours. Pet. ether (15 mL) was then added to afford a pink solid which was filtered off and dried *in vacuo*. Yield: 1.08 g, 2.95 mmol (62%).

Synthesis of $[CrCl_3\{(isoPr)_2[9]aneN_3\}]$: The procedure was to add and $(isoPr)_2[9]aneN_3$ (0.29 g, 1.36 mmol) to a solution of $[CrCl_3(THF)_3)]$ (0.51 g, 1.36 mmol) in dried and degassed dichloromethane (15 mL). The resulting mixture was stirred at room temperature under nitrogen for 2 hours. And the solvent was pumped to dryness to afford a blue-green solid which was filtered off and dried *in vacuo*. Yield: 0.216 g, 5.85×10^{-4} mol (43%).

Synthesis of $[CrCl_3\{Me_3[9]aneN_3\}]$ [18]: To a solution of chromium trichloride hexahydrate (27 mg, 1.02×10^{-4} mol) in methanol (10 mL) was added a single piece of granulated zinc. To this mixture was added $Me_3[9]aneN_3$ (17 mg, 1.02×10^{-4} mol) in methanol (2 mL), and it was heated under reflux for 2 hours. After cooling, the green solid was collected, washed with water (5 mL), acetone (2 x 5 mL) and ether (5mL) and air-dried. Yield: 10.02 mg, 3.0×10^{-5} mol (29%).

6.6. References

1. Levason, W. and Reid, G.; *Comprehensive Coordination Chemistry II*, (2004), Amsterdam : London, Elsevier Pergamon, **1**, 391.
2. Ali, R.; Higgins, S. J. and Levason, W.; *Inorg. Chim. Acta*, (1984), **84**, 65.
3. Gray, L. R.; Hale, A. L.; Levason, W.; McCullough, F. P. and Webster, M.; *J. Chem. Soc., Dalton Trans.*, (1984), 47.
4. Grant, G. J.; Rogers, K. E.; Setzer, W. N. and VanDerveer, D. G.; *Inorg. Chim. Acta*, (1995), **234**, 35.
5. Hale, A. L. and Levason, W.; *J. Chem. Soc., Dalton Trans.*, (1983), 2569.
6. Schroder, M.; *Pure Appl. Chem.*, (1988), **60**, 517.
7. Blake, A. J. and Schroder, M.; *Advances in Inorganic Chemistry*, Vol. 35. (1990), New York, Academic Press.
8. Cooper, S. R. and Rawle, S. C.; *Struct. Bonding (Berlin)*, (1990), **72**, 1.
9. Cooper, S. R.; *Acc. Chem. Res.*, (1988), **21**, 141.
10. Kuppers, H. J. and Wieghardt, K.; *Polyhedron*, (1989), **8**, 1770.
11. Glass, R. S.; Wilson, G. S. and Setzer, W. N.; *J. Am. Chem. Soc.*, (1980), **102**, 5068.
12. Ashby, M. T. and Lichtenberger, D. L.; *Inorg. Chem.*, (1985), **24**, 636.
13. Kuppers, H. J.; Neves, A.; Pomp, C.; Ventur, D.; Wieghardt, K.; Nuber, B. and Weiss, J.; *Inorg. Chem.*, (1986), **25**, 2400.
14. Blake, A. J.; Holder, A. J. and Schroder, M.; *J. Chem. Soc., Chem. Commun*, (1989), 1433.
15. Pope, S. J. A.; Champness, N. R. and Reid, G.; *J. Chem. Soc., Dalton Trans.*, (1997), 1639.
16. Champness, N. R.; Jacob, S. R. and Reid, G.; *Inorg. Chem.*, (1995), **34**, 396.
17. Chaudhuri, P. and Wieghardt, K.; *Prog. Inorg. Chem.*, (1987), **35**, 329.
18. Wieghardt, K.; Chaudhuri, P.; Nuber, B. and Weiss, J.; *Inorg. Chem.*, (1982), **21**, 3086.
19. Haselhorst, G.; Stoetzel, S.; Strassburger, A.; Walz, W.; Wieghardt, K. and Nuber, B.; *J. Chem. Soc., Dalton Trans.*, (1993), 83.
20. Beisel, T.; Della-Vedova, B. S. P. L.; Wieghardt, K. and Boese, R.; *Inorg. Chem.*, (1990), **29**, 1736.

21. Auerbach, U.; Eckert, U.; Wieghardt, K.; Nuber, B. and Weiss, J.; *Inorg. Chem.*, (1990), **29**, 938.
22. Bossek, U.; Hanke, D.; Wieghardt, K. and Nuber, B.; *Polyhedron*, (1993), **12**, 1.
23. Kirk, A. D. and Namasivayam, C.; *Inorg. Chem.*, (1988), **27**, 1095.
24. Chaudhuri, P.; Wieghardt, K.; Tsai, Y. H. and Kruger, C.; *Inorg. Chem.*, (1984), **23**, 427.
25. Wieghardt, K.; Schmidt, W.; Herrmann, W. and Kuppers, H.; *Inorg. Chem.*, (1983), **22**, 2953.
26. Wieghardt, K.; Tolksdorf, I. and Hermann, W.; *Inorg. Chem.*, (1985), **24**, 1230.
27. Pedersen, E.; *Acta. Chem. Scand.*, (1970), **24**, 3362.
28. Lin, G.; Reid, G. and Bugg, T. D. H.; *J. Am. Chem. Soc.*, (2001), **123**, 5030.
29. Kovacs, Z. and Sherry, A. D.; *Tetrahedron Lett.*, (1995), **36**, 9269.
30. Mahapatra, S.; Halfen, J. A.; Wilkinson, E. C.; Pan, G.; Wang, X.; Young, V. G.; Cramer, C. J.; Que, L. and Tolman, W. B.; *J. Am. Chem. Soc.*, (1996), **118**, 11555.
31. Alcock, N. W.; Benniston, A. C.; Grant, S. J.; Omar, H. A. A. and Moore, P.; *J. Chem. Soc., Chem. Commun*, (1991), 1573.
32. Diebold, A.; Elbouadili, A. and Hagen, K. S.; *Inorg. Chem.*, (2000), **39**, 3915.
33. Hartley, F. R.; Murray, S. G.; Levason, W.; Soutter, H. E. and McAuliffe, C. A.; *Inorg. Chim. Acta*, (1979), **35**, 265.
34. Doering, W. Von E. and Levy, L. K.; *J. Am. Chem. Soc.*, (1955), **77**, 509.
35. Richman, J. E. and Atkins, T. J.; *J. Am. Chem. Soc.*, (1974), **96**, 2268.
36. Searle, G. H. and R, J. Geue; *Aust. J. Chem.*, (1984), **37**, 959.
37. Koyama, H. and Yoshino, T.; *Bull. Chem. Soc. Jpn.*, (1972), **45**, 481.
38. Martin, A. E.; Ford, T. M. and Bulkowski, J. E.; *J. Org. Chem.*, (1982), **47**, 412.
39. Battle, A. R.; Johnson, D. L. and Martin, L. L.; *Acta Cryst.*, (2005), **E61**, 330.
40. Barefield, K. E. and Wagner, F.; *Inorg. Chem.*, (1973), **12**, 2435.
41. Herwig, W. and Zeiss, H.; *J. Organomet. Chem.*, (1958), **23**, 1404.
42. Serpone, N.; Jamieson, M. A.; Hoffman, M. Z.; Bolletta, F. and Maestri, M.; *J. Am. Chem. Soc.*, (1979), **101**, 2907.
43. House, D. A. and Garner, C. S.; *Trans. Met. Chem.*, (1970), **6**, 1.

44. Mark, J. E. and Flory, P. J.; *J. Am. Chem. Soc.*, (1965), **87**, 1415.

45. Wolf, R. E.; Hartman, J. R.; Storey, J. M. E.; Foxman, B. M. and Cooper, S. R.; *J. Am. Chem. Soc.*, (1987), **109**, 4328.

46. Cotton, F. A.; Duraj, S. A.; Powell, G. L. and Roth, W. J.; *Inorg. Chim. Acta*, (1986), **113**, 81.

47. Abragam, A. and Bleaney, B.; *Electron Paramagnetic Resonance of Transition Ions*, (1970), Oxford, Clarendon Press.

Chapter 7

Conclusion

Chromium K-edge XAFS technique was used in conjunction with other spectroscopic methods such as UV/visible, Infra-red and EPR as well as cyclic voltammetric measurements, to characterise the active species when a chromium(III) complex is treated with an aluminium reagent.

The work started with the synthesis of the chromium(III) complex $[CrCl_3\{HN(CH_2CH_2SC_{10}H_{21})_2\}]$. After characterisation, the complex was tested for the catalytic reaction of trimerisation of ethylene to 1-hexene. In order to validate a previously proposed catalytic cycle, involving a change in the oxidation state of the metal centre via a Cr(II)/Cr(IV) couple and the formation of a metallacycle species, the reaction of the complex with Me_3Al, in the absence and in the presence of an aluminate species $[Ph_3C][Al(ORf)_4]$ and of 1-hexene, was investigated by UV/visible and EPR spectroscopy. Along with the substitution of chlorine atoms by methyl groups, the results obtained showed that a change in the oxidation state of the chromium metal centre occurs upon addition of the aluminium reagent occurs. This was borne out by the disappearance of the strong and broad EPR signal, suggesting an oxidation process from Cr(III) to Cr(IV) or a reduction process from Cr(III) to Cr(II). Different partial structures of the activated species were proposed after analysis of EXAFS data. EXAFS data analysis tends to support the retention of the Cr-N link, probably via the formation of an amido bond, a result of a possible deprotonation of the amine. The presence of one Cr-S bond confirms coordination of the ligand and suggests that the Cr-amido bond is the key to avoid an "unzipping mechanism" of the ligand, as seen for other complexes studied in this thesis. One of the proposed structures involved the formation of a metallacycle, supporting reported hypotheses and extensive deuterium studies. XANES studies enabled us to suggest the oxidation state of the activated species but more calculations are required in order to have a better insight of the active system.

Similar measurements were performed on the complex $[CrCl_3\{PNP\}(THF)]$. The activated catalyst appeared to be efficient for the selective tetramerisation and trimerisation of ethylene to 1-octene and 1-hexene. The change in the oxidation state of the chromium centre was also probed by spectroscopic methods. However, the partial structures of the active species by EXAFS spectroscopy did not enable us to determine a partial structure of the activated species, which is probably a

chromium-hydride species. Formation of a mixture of active species is likely to occur, giving species-averaged EXAFS data. Similarly, the oxidation state of the chromium could not be properly investigated since the local symmetry of the catalyst was not fully determined.

The oligomerisation and polymerisation of ethylene was then investigated with a series of chromium(III) complexes bearing a wide range of donor atom ligands and geometries. All the complexes studied appeared to be efficient for the catalysis reaction. However, EXAFS data analysis suggested an "unzipping mechanism" of the ligand (facultative and tripodal geometries) following the addition of Me_3Al. The complexes bearing macrocyclic ligands appeared to be highly active for the polymerisation of ethylene, confirming extensive studies on such systems.

Finally, our work was focused on the coordination chemistry of a series of chromium(III) complexes. The insoluble nature of these complexes makes them unsuitable species for X-ray crystallography. Spectroscopic measurements such as UV/visible, Infra-red and EXAFS were then performed in order to have a better insight of their coordination modes. Results obtained were in accordance with similar systems reported in the literature.

Experimental techniques

All procedures involving air sensitive materials were performed under an inert atmosphere of N_2 and using standard Schlenk techniques. Solvents were dried using standard techniques (THF, Et_2O, hexane, petroleum ether spirits over sodium benzophenone; toluene over Na; CH_2Cl_2 over CaH_2; CH_3CN over P_2O_5; DMF over $MgSO_4$) and distilled under nitrogen prior to use or store in Young's ampoules over dry molecular sieves under a nitrogen atmosphere.
Unless stated, commercial reagents were used as received from Aldrich, Acros and Fluorochem.

Instrumentation

^1H NMR spectra, $^{13}C\{^1H\}$ NMR spectra and $^{31}P\{^1H\}$ NMR spectra were recorded on a Bruker AV300 spectrometer. ^1H NMR and $^{13}C\{^1H\}$ NMR spectra were referenced internally from the residual protio solvent (^1H) or the signals of the solvent (^{13}C). $^{31}P\{^1H\}$ NMR spectra were referenced externally relative to 85% H_3PO_4 in D_2O. ^{27}Al NMR spectra were recorded on a Bruker DPX400 spectrometer and referenced relative to $Al(NO_3)_3$ in H_2O/D_2O. ^7Li NMR spectra were recorded on a Bruker DPX400 spectrometer and referenced relative to LiCl in H_2O/D_2O.
Mass spectra were on electrospray mode (positive or negative) using a VG Biotech Platform.
Microanalyses were obtained from the University of Strathclyde microanalytical service and from the London Metropolitan University elemental analysis service.
Infra-red spectra were recorded as Nujol mull between CsI plates, using a Perkin Elmer 983 IR spectrometer over the range 4000 – 180 cm^{-1}.
UV/visible spectra were recorded on a Perkin Elmer Lambda 19 spectrometer in toluene or CH_2Cl_2 solutions or by diffuse reflectance.
Electron paramagnetic resonance spectra were obtained from the EPSRC EPR National Service, University of Manchester. Data were collected by Dr J. Wolowska and Dr E. McInness. K-band (~ 24.0 GHz) and Q-band (~ 34.00 GHz) spectra were recorded using an ESP 300 spectrometer. X-band (~ 9.4 GHz) spectra were recorded using an EMX spectrometer.

Cyclic voltammetry measurements were performed using an Eco Chemie PGSTAT20. Platinum beads were used as both working and auxiliary electrodes and a calomel reference electrode was used with 0.2 M tetrabutylammonium tetrafluoroborate $[Bu^n_4N]BF_4$ as base electrolyte. All experiments were performed in degassed CH_2Cl_2 and standardised against the ferrocene/ferrocenium couple.

Catalysis testings were carried out at Sasol Technology (UK) Ltd St. Andrews Laboratory by Dr D. McGuinness and Dr A. Rucklidge, according to the procedure below.

Procedure for catalysis

The reactor was prepared by filling/venting with ethylene (5 x 10 bar). Toluene was added and the reactor heated to 80°C or 90°C. To activate the complexes $[CrCl_3\{L\}]$, MMAO (1.9 M in heptane) or Et_3Al / $[Ph_3C][Al(ORf)_4]$ were added to the complexes previously dissolved in toluene. The solution was mixed and immediately added to the reactor. Ethylene (40 bar) was added and fed as required to keep at a constant pressure. The reactor was kept allowed to run until ethylene uptake ceased. The reactor was then cooled with ice to ~10°C and the ethylene slowly vented. Nonane (1000 μL) was added followed by MeOH and HCl (10 %) to destroy the MMAO. The reactor was opened and the polymer collected, dried, weighed and when possible a liquid fraction was collected for GC-MS analysis.